REPORT DOCUMENTATION PAGE

FORM APPROVED
OMB No. 0704-0188

1. AGENCY USE ONLY (Leave blank)	2. REPORT DATE	3. REPORT TYPE AND DATES COVERED
	5 DEC 95	FINAL: 1 June 94 - 1 Aug. 95

4. TITLE AND SUBTITLE OF REPORT
Intelligent PRocessing of Ferroelectric Thin Films

5. FUNDING NUMBERS
N00014-91-J-1508

6. AUTHOR(S)
Gene H. Haertling and William Paradise

7. PERFORMING ORGANIZATION NAME(S) AND ADDRESS(ES)
Clemson University
Clemson, SC 29634-0907

8. PERFORMING ORGANIZATION REPORT NUMBER:

9. SPONSORING/MONITORING AGENCY NAME(S) AND ADDRESS(ES)
Office of Naval Research
Arlington, VA 22217-5660

10. SPONSORING/MONITORING AGENCY REPORT NUMBER:

11. SUPPLEMENTARY NOTES:

12a. DISTRIBUTION AVAILABILITY STATEMENT
No restrictions

12b. DISTRIBUTION CODE

13. ABSTRACT (Maximum 200 words)

This report details work that was performed at Clemson University over the fourth year of a four-year program involving intelligent processing of ferroelectric thin films. Since ferroelectric and electrooptic materials are known to possess properties that can vary widely due to form factor and processing method, studies were carried out by producing electrooptic thin films and bulk ceramics from the same acetate precursors via a liquid chemical MOD (metal organic decomposition) process and then characterizing their chemical, electrical, physical and electrooptic properties. It was desirable that a processing method compatible with both spin and dip-coated thin films as well as bulk ceramics made from coprecipitated powders be used in order to quantitatively compare their respective properties. The dielectric properties of electrooptic thin films were varied by mechanically altering the stresses placed upon the films. Comparisons were made among thin films under applied bending stresses of different magnitude. Properties measured were dielectric constant, saturation polarization, remanent polarization, coercive field and unit cell d-spacing.

14. SUBJECT TERMS	15. NUMBER OF PAGES:
Ferroelectrics, Thin Films, Thin Film Processing, Electrooptics, Electrooptic Films	165
	16. PRICE CODE

17. SECURITY CLASSIFICATION OF REPORT:	18. SECURITY CLASSIFICATION OF THIS PAGE	19. SECURITY CLASSIFICATION OF ABSTRACT	20. LIMITATION OF ABSTRACT
Unclassified	Unclassified	Unclassified	UL

DISCLAIMER NOTICE

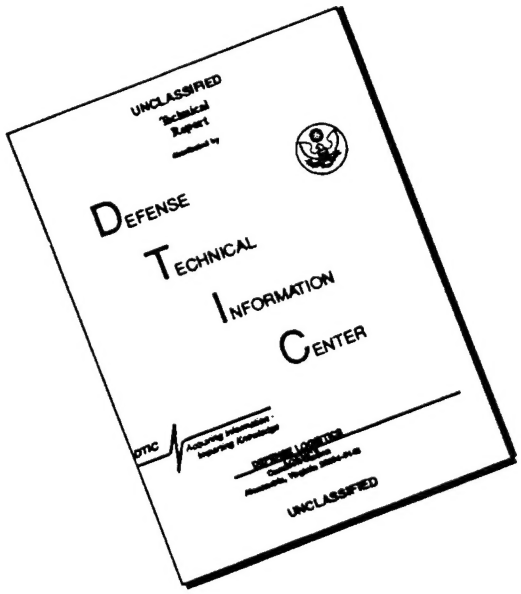

THIS DOCUMENT IS BEST QUALITY AVAILABLE. THE COPY FURNISHED TO DTIC CONTAINED A SIGNIFICANT NUMBER OF PAGES WHICH DO NOT REPRODUCE LEGIBLY.

INTELLIGENT PROCESSING OF FERROELECTRIC THIN FILMS

Final Report

Period: June 1, 1994 to August 1, 1995

OFFICE OF NAVAL RESEARCH
Arlington, VA 22217-5660

Contract No. N00014-91-J-1508

Principal Investigator: Gene Haertling

Supporting Investigators: William Paradise

December 5, 1995

CLEMSON
UNIVERSITY

The Gilbert C. Robinson
Department of Ceramic Engineering

College of Engineering

Table of Contents

SUMMARY

This report details work that was performed in the Ceramic Engineering Department of Clemson University over the period from June 1, 1994 to August 1, 1995 under ONR contract No. N0014-91-J-1508. The work described in this report covers the fourth year of a four-year program involving intelligent processing of ferroelectric electrooptic thin films. This fourth year essentially involved the final year of the EPSCOR add-on program to the 3-year parent work on intelligent processing of ferroelectric thin films. As such, this final year only included the work of one doctoral graduate student; however, all of the external publications which resulted from the total 4-year program are included for the reader's benefit.

Electrooptic ceramics have properties that can vary widely due to thickness, shape and processing method. These materials have conventionally been produced by a variety of deposition processes. These processes include the bulk ceramic techniques (sintering, hot pressing and tapecasting) along with chemical (sol-gel, CVD and MOD) and physical (evaporation, sputtering and laser ablation) processes used in producing films. The goals of the ONR program on "Intelligent Processing of Electrooptic Thin Films" were to determine the similarities and differences in material properties produced by various processes. Part of these goals were carried out by producing electrooptic thin films and bulk ceramics from the same acetate precursors and then characterizing the chemical, electrical, physical and electrooptic properties of these materials. It was desirable that a processing method compatible with both thin films and bulk ceramics be used in order to better compare their respective properties. An acetate precursor system was employed to produce both acetate solutions for spin and dip coated thin films as well as coprecipitated powders for bulk ceramics.

In another study, the dielectric properties of electrooptic thin films were varied by altering the stresses placed upon the films. Selected thin films in the PLZT system were produced by using the dip-coating process and applying various stresses. Comparisons were made among thin films under mechanically applied stresses of different magnitude. Properties measured were dielectric constant, saturation polarization, remanent polarization, coercive field and unit cell d-spacing. The effects of the applied stresses on the physical and electrical properties of the films were determined.

Part I.

Electrooptic Thin Films

INTRODUCTION

The perovskite lanthanum-modified lead zirconate titanate system (PLZT), because of its combined dielectric, pyroelectric, piezoelectric and electrooptic properties, has created new possibilities for their use in electronic and photonic devices. Electrooptic ceramics have been a topic of interest due to the desirable properties they possess. The importance of electrooptic thin films is evident in their many applications ranging from sensors to light modulators.[1] These thin film uses come from the electrooptic bulk ceramics developed over the years. Thin films possess some advantages over bulk ceramics such as easier integration with silicon technology, lower operating voltage, higher speed and lower cost which make them more desirable for many devices. The research for new materials with unique and improved properties has continued as new modifications and compositions of the PLZT system are constantly developed.

Electrooptic thin films have properties that can vary widely due to their differences in thickness, processing method and substrate type.[2] The effects of applying mechanical stress to electrooptic ceramics, known as strain-biasing, has been used in image storage and display applications.[3] It has also been shown that under compressive stress a transition in ceramics from a rhombohedral to a tetragonal symmetry can occur.[4] It is believed that through the study of these materials, an optimization of their properties can be achieved. In order to understand and optimize thin film electrooptic behavior, a comparison is necessary between the thin film and bulk ceramics properties. The understanding of the correlation between stresses and the changes within thin-film properties is also needed.

Direct correlation between the bulk and thin film materials is difficult since typically the precursors and processing techniques of each are different. Within this research this problem was eliminated by using the same acetate precursor solutions in the manufacturing of the PLZT bulk ceramics and thin films. It is believed that this process allows for a close comparison of PLZT bulk and thin film electrooptics by minimizing or eliminating differences in the processing of these materials induced by precursor impurities, batching variations and differences in mixing of the precursor materials. This

allows us to characterize similarities and differences in the properties of bulk ceramics produced from chemically coprecipitated powders and dip coated thin films produced by a metallorganic decomposition process without having variations in starting materials as a factor.

Research on quenched PLZT 9.5/65/35 ceramics showed that internal stresses induced in samples can enhance polar region ordering which would produce a more ferroelectric-like response by the material.[5] This response would produce higher remanent polarizations in quenched samples than in annealed samples. A compressive stress in the thin films will align the domains parallel with the applied electric field, enhancing the ferroelectric properties of the thin films. Tensile stresses will align the domains perpendicular to the applied field and the effect will be a decrease in the remanent polarization, shown in Figure 1.[6] Watanabe et al. [7] proposed that differences in lattice constant between bulk and thin film PZT ceramics can be caused by the mechanical stress present within the thin films. When a polycrystalline ceramic is deformed in such a way that the strain is uniform over a relatively large distance, the lattice plane spacing in the constituent grains changes from a stress-free value to some new value corresponding to the magnitude of the applied stress. The new spacing is essentially constant from one grain to another for any particular set of planes that are similarly oriented with respect to the stress.

It has been shown that mechanical stresses altered the properties of several electrooptic bulk devices and resulted in materials for new applications. Wang et al. [8] described a thin film light modulator that utilizes the interference of multiple reflections of light between the bottom and the top electrode to obtain a high contrast ratio. The primary role of electrooptic thin film materials in integrated optical and electrooptic devices is to modulate light waves. Since the materials are electrooptic, such modulations can be achieved by electrically controlling the indices of refraction in the thin film materials. The characterization of the electrooptic properties of the thin film materials is of obvious importance. While several investigations on the effects of stress on the properties of bulk electrooptic ceramics have been reported, it is believed that

systematic investigation of stress effects on electrooptic thin films has not been conducted.

By producing electrooptic thin films from acetate precursors and characterizing the electrical and physical properties of these materials an optimization of the thin films properties may be reached. The principal interests now under examination are the electrooptic properties of the thin films and the manner in which stresses acting on and within these films can effect their properties.

EXPERIMENTAL PROCEDURE

Processing

PLZT bulk ceramics and dip coated thin films were produced using a water soluble acetate precursor method.[9] The chemical coprecipitation process which was used to produce PLZT powder from acetate precursors is shown in Figure 2.[10] This processing method produces bulk and thin film samples from the same batches. This allowed for a unique comparison of properties between bulk ceramics and thin films since it reduced or removed any variations between batches and precursor histories. All the elements needed to produce PLZT were placed into an acetate form and mixed together. The acetate precursors were chosen primarily for their low cost, insensitivity to moisture, and chemical stability. The starting precursors were titanium acetyl acetonate, zirconium acetate, lanthanum acetate and lead subacetate powder. The lead subacetate was mixed into solution by the addition of acetic acid and methanol so that all of the acetate precursors were in a liquid form in order to promote a more homogeneous and intimate mixing. Incomplete mixing would produce compositional fluctuations between bulk and thin film solutions. A portion of this solution was then taken off to be used for the thin film productions.

The bulk portion of the solution was coprecipitated in a high speed blender by adding oxalic acid and methanol during blending in order to bring about precipitation of the PLZT powder. As stated earlier, this process produces a more homogeneous mixture

of precursors and therefore produces a more intimately mixed PLZT powder with a smaller particle size than the mixed oxide process. This powder was then vacuum dried at 70°C to produce a solid cake. The cake was crushed, calcined at 500°C for 8 hours and milled in trichloroethylene for 6 hours to produce a PLZT oxide powder. The powder was then either pressed into disks at 3000 psi and sintered at 1250°C in a lead-rich atmosphere for 4-6 hours or hot pressed for 4-6 hours at 1250°C and 2000 psi. Typically, 110g of powder was produced for hot pressing. The sintered and hot pressed parts were sliced on a diamond saw and lapped to 20 mils thickness. Electroless nickel electrodes were plated onto the ceramics through a series of chemical baths. The samples were electroded for measurement of their dielectric and hysteresis loop properties.

Thin films were produced by the automatic dip coating process shown in Figure 3.[6] These films were produced to determine if the firing temperature could be reduced without affecting the film's properties. For thin film production, the small portion (usually 5g) of the decanted acetate solution was diluted with methanol at a 4:1 ratio by weight. This improves solution stability and reduces cracking during heat treatments. The films were dipped onto silver foil substrates, allowed to dry for 30 seconds and pyrolyzed at 500°C or 700°C for 3 minutes. Some of the films had their firing temperature changed after the first and/or before the last layer was applied. Therefore, a "575" film had the first layer fired on at 500°C, the middle 22 layers fired on at 700°C and the remaining layer fired on at 500°C. All of the films had 24 layers and were approximately 1 μm thick. The films were electroded by vacuum evaporation of copper and measured for dielectric constant, electrical resistivity and hysteresis loop characteristics.

In another experiment the chemical coprecipitation process was used again to produce PLZT acetate precursors. Incomplete mixing would produce compositional fluctuations within the thin film's structure. Thin films were produced by the automatic dip coating process. The films were dipped onto silver foil substrates, allowed to dry for a minute and then pyrolyzed at 700°C for three minutes. Three compositions (2/55/45, 9/65/35 and 28/0/100) were used, and of each of these compositions, three film thicknesses were produced. The three films of each composition had 24, 36 and 72 layers

and were approximately 1, 2 and 3 microns thick respectively. The films were then electroded for measurement of their dielectric and hysteresis loop properties

Stressing

To induce a stress within the thin films, the films were placed within a three point bender and flexed as shown in Figure 4a. The applied stress in the films were correlated to the curvature of the films. The electrical properties were measured at various stress levels by measuring them at different film curvatures. Compressive versus tensile stress effects on properties were compared simply by taking measurements at concave versus convex curvatures.

MEASUREMENTS

Bulk and thin film samples were measured for dielectric constants, electrical resistivities and hysteresis loops. The capacitance and dissipation factor were measured on bulk and thin film samples using a Leader LCR meter at a measuring frequency of 1 kHz. Resistance was measured using a Keithley electrometer. Hysteresis loops were also measured for both materials to determine their polarization versus an electric field. The bulk samples were measured using a Sawyer-Tower circuit with a dc applied voltage of $\pm$1400 V, and the hysteresis loops were plotted with a Goerz Metrawatt X-Y plotter. Hysteresis loops of the thin film samples were measured at 1 kHz using a Sawyer-Tower circuit with an oscilloscope readout shown in Figure 5. The coercive fields and remanent polarizations were calculated for all of the samples from their hysteresis loops. X-ray diffraction analysis was performed on the thin films using a Scintag XDS 2000 diffractometer with Cu Kα radiation at a scan rate of 2^{o}/min.

The strain induced within the thin films was calculated by Equation 1

$$\text{Strain} = \frac{(t/2)}{R} \qquad (1)$$

where t is the total thickness of the film and substrate, and R is the radius of curvature of the film.[11] Some assumptions need to be made before this equation can be used though. First, it is assumed that the axes of symmetry lie through the center of the film. Second, the film must have a constant radius of curvature. And third, the substrate must be rigid enough not to plastically deform so as not to relieve any of the stress applied to the film. Radius of curvature can be found by using the following equation

$$(2R-d)*d = L^2 \qquad (2)$$

where d is the deflection of the substrate and film, and L is the length of the deflection from the center as shown in Figure 4b.[12] The stress is obtained by multiplying the strain value with the Young's modulus of the material. The sign agrees with the convention that it is positive for tension and negative for compression.

A film residing on a rigid substrate of much greater thickness is unable to move freely. Therefore, after the fabrication process, the film is usually strained in a way corresponding to the induced tensile or compressive stress imposed by the substrate. The substrate should also experience an opposite stress exerted by the film and deform accordingly, which may lead to a distribution or a relaxation of the induced stresses within the film.[13] This effect is neglected here since for the dip coating process the two sides of the substrate are evenly coated and the bending moments from the films on the opposite sides are thus expected to cancel each other.

Should there exist any difference in the thermal expansion behavior between the thin film and the substrate, development of intrinsic stresses within the film during the cooling stage will occur. Since most ferroelectric materials possess large electromechanical coupling effects, the presence of an intrinsic stress in a ferroelectric

film will affect its dielectric properties. This intrinsic stress tends to be compressive for PLZT thin films produced on silver substrates due to PLZT's lower thermal expansion than that of the silver substrate. The compressive induced stress on the films due to thermal expansion mismatch is not taken into account within this paper. It is the addition of the applied stresses to the thin films that is measured. The effect of the total stress acting on the films is not analyzed, only the effects of the applied portion of the total stress within the films, therefore, the thin films are taken to be stress free after fabrication.

RESULTS AND DISCUSSION

Bulk and Thin Film Comparison

Hot pressed bulk ceramics and dip coated thin films on Ag foil substrates were fabricated, and a comparison of properties was established. Sintered and hot pressed ceramics along with dip coated thin films (on silver foil) for the 9/65/35 composition were compared as shown in Table 1. These values showed that the hot pressed ceramics had very little remanent polarization and reached a lower saturation level than the other two; while the thin films had a large amount of remanent polarization with a lower dielectric constant than either of the bulk ceramics. These effects have been reported to be due to differences between bulk and thin film configurations. The fact that the thin film dielectric constants were generally lower could be attributed to the small grain size of the thin films, mechanical clamping effects or, due to the high electric field applied to the thin films, the voltage sensitivity of the measurement. This could imply that the hot pressed ceramics had better properties due to larger grain growth and fewer defects, which would be expected with hot pressed materials. These differences could also be seen when comparing the hysteresis loops as in Figure 6. Internal stresses induced in samples, as stated earlier, can enhance polar region ordering producing a more ferroelectric-like response by the material. This response would produce higher remanent polarizations. These findings could explain the memory behavior found in the thin films used in this experiment. Residual stresses may have caused these films to retain

ferroelectric memory hysteresis loops that were not observed in the bulk materials. More batches are being produced and analyzed in an attempt to further explain differences and similarities in properties between the bulk and thin film electrooptics.

The coercive fields and remanent polarizations were calculated for all the films in the temperature dependence test and are listed along with dielectric constants and dissipation factors in Table 2. The highest poled dielectric constants were found to be in the "777" thin film. In comparison to the "777" sample, the hysteresis loop of the "555" sample was more conductive and electrically shorted more readily. The ac loop of the "777" sample reached much better saturation and looked similar to a bulk hysteresis loop. The ac hysteresis loops are shown in Figure 7. The hysteresis loops also became slimmer as the temperature used increased. All this indicated that films fired at higher temperatures had better nucleation and grain growth. As anticipated, the properties of the thin films were found to be highly dependent on firing schedule. Graphs of the improvements in properties with firing temperatures are shown in Figures 8 and 9. These graphs clearly show the increase in dielectric constant and remanent polarization as the firing temperature is increased from 500^{o}C to 700^{o}C.

Stress Effects

Dielectric Constant

The composition 2/55/45 was chosen for study because it lies near the morphotropic phase boundary in the PLZT system. This phase boundary composition regularly exhibits a ferroelectric memory behavior. The material exhibits both a rhombohedral and tetragonal symmetry since the 2/55/45 composition lies near this boundary. It is observed from the experiment that the general trend of the dielectric constant for this composition is to increase with an increasing tensile stress, as shown in Figure 10. It is believed that a transition in symmetry is taking place within the 2/55/45 thin film upon stressing. This change in symmetry toward a more rhombohedral symmetry would account for an increase in the dielectric constant.

The 9/65/35 composition is near the paraelectric phase region and tends to have a slim-loop hysteresis with very little memory behavior. The dielectric constant for this composition is observed to not be affected by the addition of either a compressive or tensile stress as shown in Figure 11.

The 28/0/100 composition lies within a cubic region and also tends to exhibit slim-loop properties. Due to its pseudo-cubic nature and limited number of domains, this compositions properties should not vary much under stress. This composition showed a slight change in the dielectric constant under different stresses with a maximum being reached when a compressive stress was placed on the film as shown in Figure 12. The addition of a further compressive stress caused the dielectric constant to decrease. This decrease is also evident with the addition of a tensile stress.

Hysteresis Properties

Compressive stresses within the thin films will align the domains parallel with the applied electric field. This type of ordering will increase the ferroelectric properties of the thin films. A tensile stress will align the domains perpendicular to the applied field, and the effect will be a decrease in the ferroelectric properties. Both the 9/65/45 and the 28/0/100 showed this effect to some degree, but the 2/55/45 thin films had a decrease in remanent polarization under a compressive stress as shown in Figure 13. This response is not yet fully understood, but it most likely is a combination of factors affecting these properties under the stresses applied. The effects of having the sample clamped during measurement is now being investigated as a possible explanation along with understanding the thermodynamics involved.

The coercive fields of all the compositions increased under a compressive stress and decreased under tensile. The 28/0/100 thin films did not show much of a change within any of the properties measured. This can again be related to the composition's pseudo-cubic structure producing a very stable material with very few domains present.

Lattice Spacing

X-ray diffraction patterns of the 2μm 2/55/45 thin film were taken at different stress levels. In analyzing the lattice spacings of the different levels of applied stress, it was observed that the compressive stress produced slightly larger d-spacings than in the tensile stress. As shown previously, mechanical stress present in PZT thin films can cause differences in the lattice constant between bulk and thin film materials. When a polycrystalline ceramic is deformed in such a way that the strain is uniform over a relatively large distance, the lattice plane spacing in the grains change to a new value corresponding to the magnitude of the applied stress, as shown in Figure 14. A uniform strain over the thin film will cause a shift of the diffraction lines to new 2θ positions. The new spacing is essentially constant from one grain to another for any particular set of planes that are similarly oriented with respect to the stress. A smaller lattice constant perpendicular to the film corresponds to a tensile stress. A graph of the (211) d-spacings at the various stress levels is shown in Figure 15. From this figure it can be seen that the d-spacing does decrease from compressive to tensile stress as expected.

SUMMARY AND CONCLUSIONS

Sintered and hot pressed ceramics along with dip coated thin films (on silver foil) for the 9/65/35 composition were compared. PLZT bulk ceramics and thin films were fabricated from the same acetate precursor solutions in order to minimize batching variations and accurately compare properties between bulk and thin film samples of the same compositions. The bulk materials produced slim hysteresis loops, but this was never completely achieved in the thin films. It has been suggested that these differences may be attributed to the induced stresses built up within the thin films. This comparison of bulk and thin film electrooptics is believed to be an accurate comparison of properties versus differences in processing since both used the same starting precursors. Therefore, the only variables between the bulk ceramics and thin films were their physical differences. It is believed that the complete mixing of precursors and accurate batching

of materials which was used for both bulk and thin film production provided a minimization of differences that could cause serious variations in their composition and properties. It is believed this process provided a true correlation between these materials.

The properties of the thin films were found to be highly dependent on the firing schedule used. It is believed that at higher firing temperatures the films had better nucleation and grain growth which would account for the increase in measured properties.

As anticipated, the properties of the thin films were found to be dependent on the type and amount of stress applied. A compressive stress on the thin films will align the domains. This aligning will produce slightly larger d-spacings within the material and, if parallel with the applied electric field, increases in the dielectric properties. It is also believed that the increase in dielectric constant within the 2/55/45 thin films, upon applying a tensile stress, may be caused by a change in symmetry. The 28/0/100 composition's properties did not vary much under stress which may be due to its pseudo-cubic structure.

AUTOMATIC SPIN-COATER

Thin films can now be produced by an automatic spin coat reactor/analyzer which is shown in Figure 16. The automatic spin coat reactor/analyzer, produced by Digital Controls, Inc. in Rolla, MO, is controlled by an IBM compatible, 80386DX computer with software to operate the ellipsometer and set parameters for atmospheric gas control, deposition, spinning, heating and cooling. It will be utilized for spin coating and rapid thermal processing of thin films from liquid precursors. Computer control provides hands-off fabrication and flexibility in processing of the films. Samples may be prepared without exposure to the outside environment.

The fluid dispense system has the capability of depositing one of three precursor solutions onto 1/2" to 4" diameter substrates. A nitrogen dusting step can also be inserted through the dispense arm before fluid deposition. Spinning is executed with an ac brushless servo motor and controller with programmable time, speed and acceleration. Six water-cooled parabolic strip heaters with infrared quartz lamps containing tungsten

filaments comprise the rapid thermal processing unit. This RTP unit allows the sample to be heated to 700°C within 5 to 10 seconds. Variable atmospheric gases (N_2, O_2, Ar) and low pressures as well as vacuum capability are possible in the atmosphere control system. In-situ thickness measurements are taken before and after heating by a Gaertner Scientific laser ellipsometer. A typical run would proceed as follows:

1. Chamber was pumped down to vacuum pressures
2. Chamber was vented with set gas mixture and pressure
3. Dispense arm moved over substrate, blew off surface with nitrogen gas and fluid injected onto substrate
4. Sample stage spin initiated
5. Dispense arm moved back and heater (water cooled quartz infrared lamps) moved forward over sample stage
6. Heater ramped and soaked at set parameters using a rapid thermal annealing process
7. Heater moved back and laser ellipsometer used to measure film thickness

This cycle can be repeated for any number of layers or with a change in composition of layers. A cooling stage is placed in between layers to allow the film to cool before the next deposit of solution.

FUTURE WORK

As stated earlier, there maybe a strong correlation between the amount of stress a film has placed upon it and the properties the film exhibits. This correlation will be researched further to determine if the properties within a film can be optimized or enhanced. The whole study is composed of three portions, and they are:

(a) Choosing an appropriate film-substrate system.

(b) Measure and characterize the stress distribution in the thin films and the effects of this distribution on the films dielectric and electrooptic properties. Analyze and evaluate the stress-related parameters in the

dielectric and electrooptic coefficients of several representative PLZT ceramics.

(c) Develop a phenomenological model to explain the experiments and to predict the properties of thin film ferroelectrics under applied stress.

This proposed research will focus on the effects of mechanically stressing thin films. Thin film ceramics in the PLZT system will be used for this experiment. Several films will be produced for improvement of dielectric and electrooptic properties and for use in optical devices such as memories and sensors. By stressing these materials possibilities exist for improved properties and possibly new devices. To achieve this goal, strains are artificially created in PLZT samples of selected compositions by imposing the samples to various kinds of stresses under appropriate mechanical boundary conditions. Measurements and characterizations will be made of the stress distribution in the thin films as well as the effects of the stresses on the dielectric and electrooptic properties.

The linear and nonlinear dielectric and electrooptic properties of these devices will be modeled in order to understand the interactions between the applied stresses and the properties of the thin films. Modeling of the linear and nonlinear dielectric and electrooptic behavior of these films under different stresses is important in order to understand the interactive behavior between the stress and the film properties. These models will then be compared to the experimentally measured dielectric and electrooptic properties of the thin films. Comparisons of these results with those found in the non-stressed films will be made so as to evaluate the characteristics of the stresses on the properties in the films.

Experimental Procedure

PLZT thin films will be produced by computer-controlled spin and dip coating equipment.[14] Successive layers will be deposited from the acetate solutions onto substrates and pyrolyzed. The automatic dip coater, which employs automated deposition, pyrolyzes films in a conventional furnace. The spin coater, which has automatic deposition and spinning, uses rapid thermal processing. Evaporated copper

will be deposited for measurement of the dielectric and hysteresis loop properties, while indium tin oxide will be used in the electrooptic measurements. To induce a stress within the thin films, the films will be placed within the three point bender and flexed.

Measurements

Capacitance and dissipation factors will be measured using an LCR meter. Resistance will be measured using a Keithley electrometer and the hysteresis loops will be measured using a Sawyer-Tower circuit with an oscilloscope readout. The coercive fields and remanent polarizations will be calculated for all the films from their hysteresis loops. The electrooptic response of the thin films will be manipulated by varying the stresses placed upon the films. Electrooptic properties of thin films on opaque substrates will be measured with reflective differential ellipsometry, as shown in Figure 17. The measurement involves the detection of a phase shift in a probing light beam reflected from the film. The changes in the extraordinary and ordinary indexes can then be determined by measuring the phase shift at various incident angles, since the extraordinary and ordinary index calibration coefficients are dependent on the angle.

The effects of the stresses on the properties of the thin films, such as polarization vs. electric field and strain vs. electric field relationships, dielectric constant and so on, will be determined for the comparison with theoretical modeling. The films will be flexed to induce a stress. The applied stress in the films will then be measured by two techniques:

(a) The strain induced within the thin films will be calculated by measuring the radius of curvature the film exhibits while being stressed.

(b) Film strain measured in a direction normal to the film plane will also be calculated based on the interplanar d-spacings obtained from X-ray diffraction data.

Comparisons will be made between mechanically applied stresses and stresses from thermal expansion mismatch between the substrate and the film. These measurements

along with the measurements already obtained should help us understand the differences and similarities that exist between bulk materials and thin films.

Modeling

Modeling of thin films is important in understanding and predicting any changes within a structures properties so that suitable materials can be chosen for device manufacturing. Dielectric and electrooptic properties do not behave linearly as functions of the electric field. The modeling of nonlinear dielectric properties can be accomplished through phenomenological free energy expressions. Beige and Schmidt [15] derived a dielectric displacement equation for a piezoelectric element under a constant stress. The linear and nonlinear dielectric and electrooptic properties of the stressed thin films will be modeled. Polarization can be described by nonlinear effects, whereas, electric field strength can be described as a nonlinear function of polarization. These properties will then be measured experimentally and compared to the models to determine the accuracy of the model. In this study, two aspects of modeling will be conducted:

(a) Simulate the preferential domain orientation resulting from the stress and the influence of this domain orientation on the thin film properties. The argument here is: a special domain pattern corresponding to the stress applied will be produced. Domains are oriented as to release the internal stresses, making the energy of the thin films minimum.

(b) Analyze and evaluate the stress-related parameters in the dielectric and electrooptic coefficients of several representative PLZT ceramics. These parameters will then be used in the theoretical modeling.

REFERENCES

[1] G. H. Haertling, Engineered Materials Handbook, 1124-1130 vol. 4 (Ceramics and Glasses), ASM International, (1991).

[2] K. D. Preston and G. H. Haertling, "Comparison of Electro-Optic Lead-Lanthanum Zirconate Titanate Films on Crystalline and Glass Substrates," *Appl. Phys. Lett.* 60 [23], 2831-33 (1992).

[3] Juan R. Maldonado and Allen H. Meitzler, "Strain-Biased Ferroelectric-Photoconductor Image Storage and Display Devices," Proc. IEEE 59 [3], 368 (1971).

[4] A. H. Meitzler and A. H. O'Bryan, Jr., "Ferroelectric Behavior of PLZT Ceramics When Subjected to large Tensile Strains," *Appl. Phys. Lett.* 19 [4], 107 (1971).

[5] W. Y. Gu, E. Furman, A. Bhalla and L. E. Cross, *Ferroelectric,* 89, 221 (1989).

[6] K. K. Li, "A Study of PLZT Ferroelectric Thin Films Chemically Derived From Acetate Precursors," Ph.D. Thesis, Clemson University, Clemson, SC (1993).

[7] H. Watanabe, T. Mihara and C. A. Paz De Araujo, "Device Effects of Various Zr/Ti Ratios of PZT Thin-Films Prepared by Sol-Gel Method," Proceeding of the 3rd International Symposium on Integrated Ferroelectrics, 139-50, 1991.

[8] F. Wang and G. H. Haertling, "Thin Film Ferroelectric Reflection Spacial Light Modulator with Fabry-Perot Etalon," Intelligent Processing of Ferroelectric Thin Films, Annual Report, submitted to The Office of Naval Research, 1994.

[9] G. H. Haertling, "PLZT Thin Films Prepared From Acetate Precursors," *Ferroelectric* 116, 51 (1991).

[10] D. Dausch, "An Investigation of the Dielectric and Hysteresis Properties of PLZT Ferroelectric and Multilayer Composite Thin Films," Ph.D. Thesis, Clemson University, Clemson, SC (1995).

[11] C. H. Hsueh and A. G. Evans, "Residual Stresses in Metal/Ceramic Bonded Strips," *J. Am. Ceram. Soc.*, [3] 241-8, (1985).

[12] S. Timoshenko, "Analysis of Bi-Metal Thermostats," *J. Optical Soc. Am.*, [11] 233-56, (1925).

[13] R. W. Hoffman, Physics of Nonmetallic Thin Films, ed. by C. H. S. Dupuy and A. Cachard, 273-353, Plenum Press, New York (1976).

[14] D. Dausch and G. H. Haertling, "Spin Coated Thin Films and Bulk Ceramics," Intelligent Processing of Ferroelectric Thin Films, Annual Report, presented to The Office of Naval Research, 1994.

[15] H. Beige and G. Schmidt, "Electromechanical Resonances for Investigating Linear and Nonlinear Properties of Dielectrics," *Ferroelectrics*, 41, 39-49 (1982).

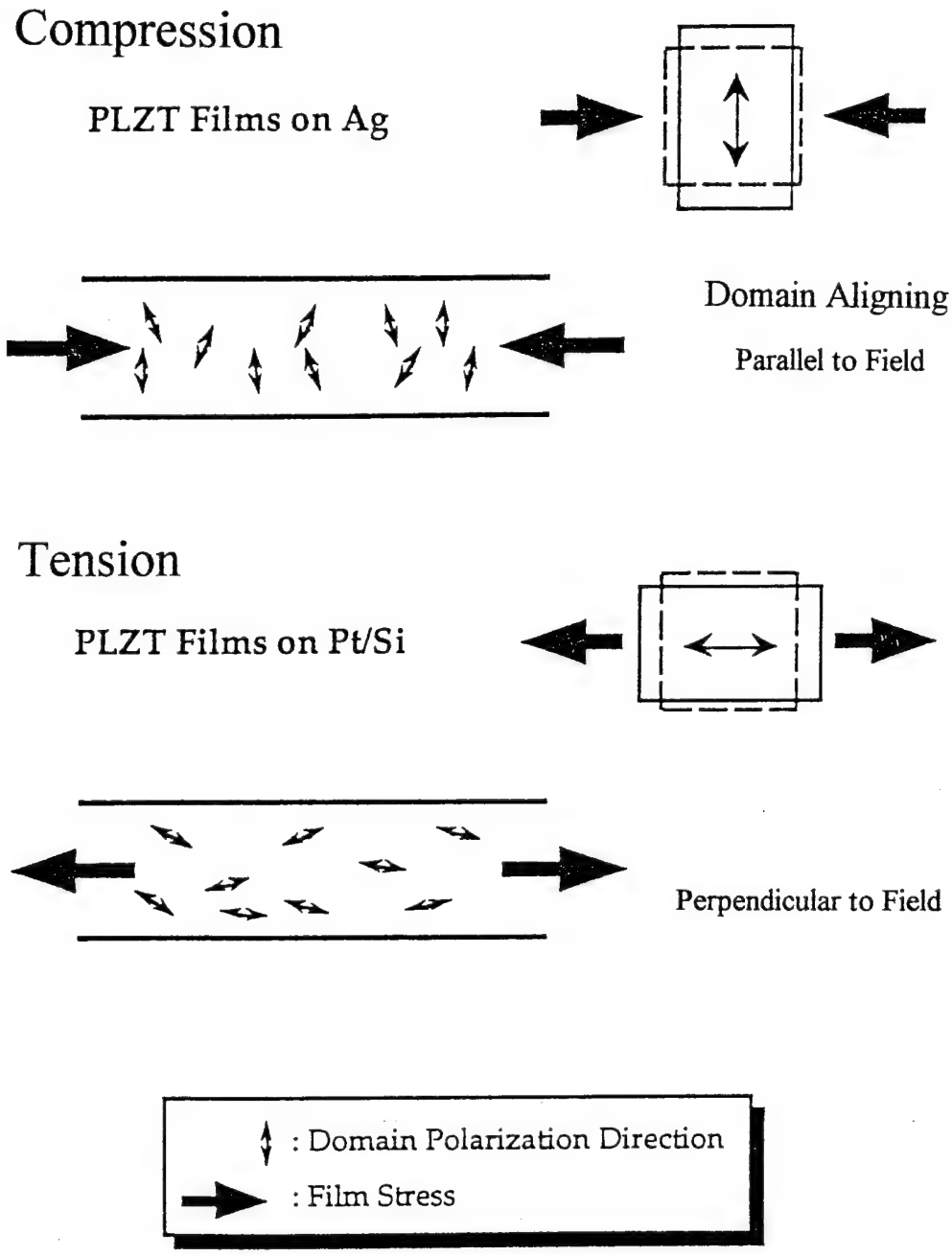

Figure 1. Effects of compression and tensile stresses on domain orientation.

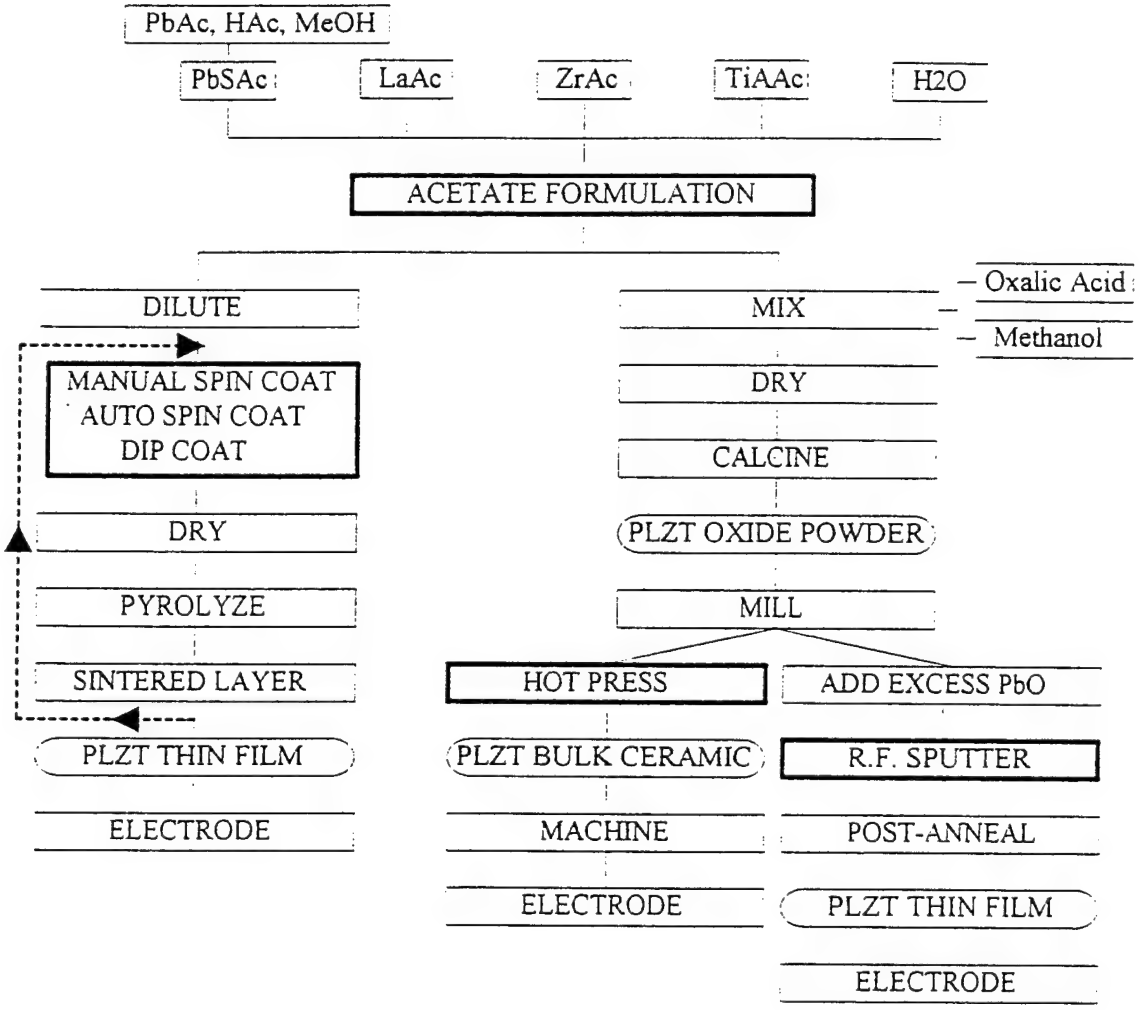

Figure 2. Acetate precursor coprecipitation process for producing PLZT thin film solutions and bulk powders.

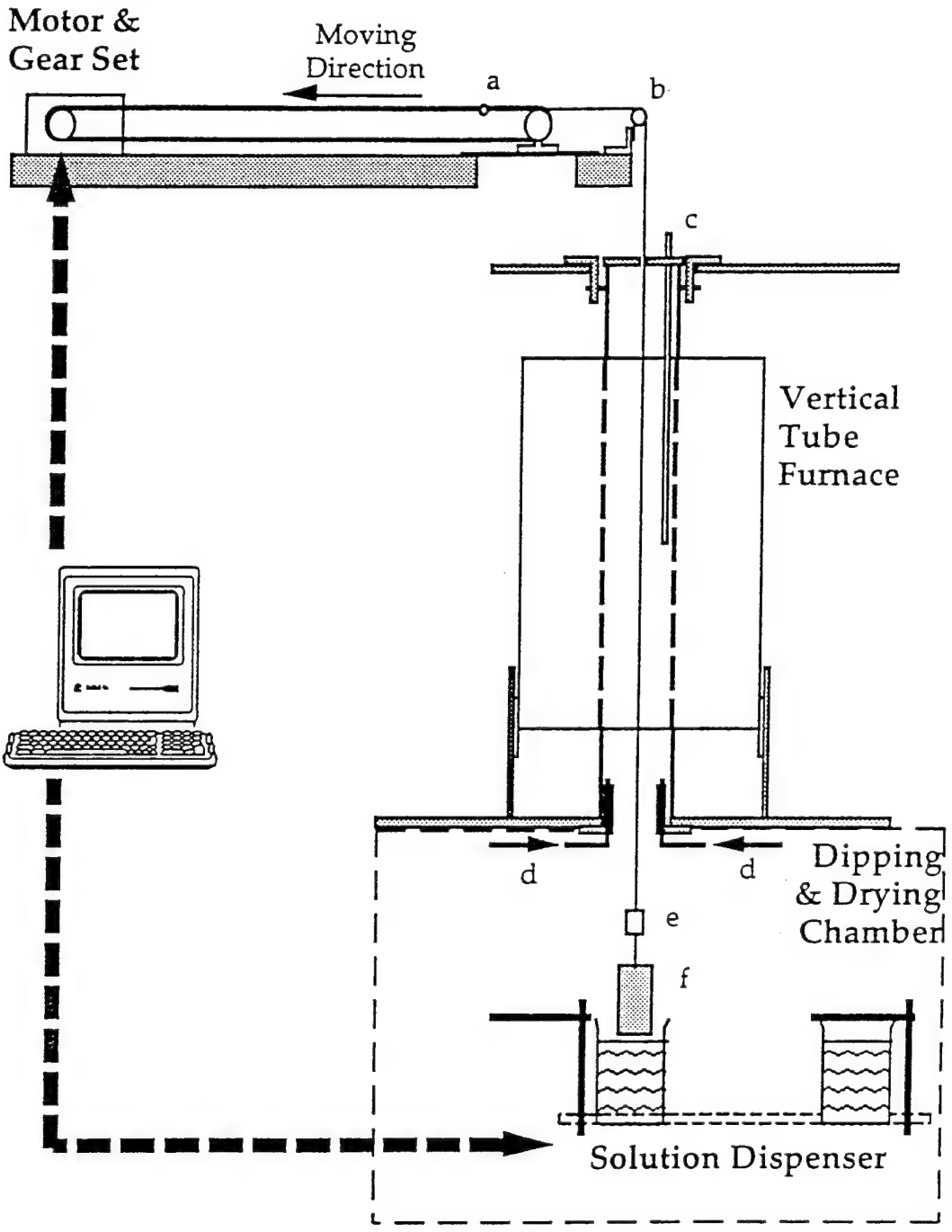

Figure 3. The automatic dip coating apparatus. The motion of the substrate and the selection of the dipping solution are monitored by a computer. (a: connecting pin; b: positioning wheel; c: thermocouple; d: furnace atmosphere inlets; e: ceramic weight; f: substrate.)

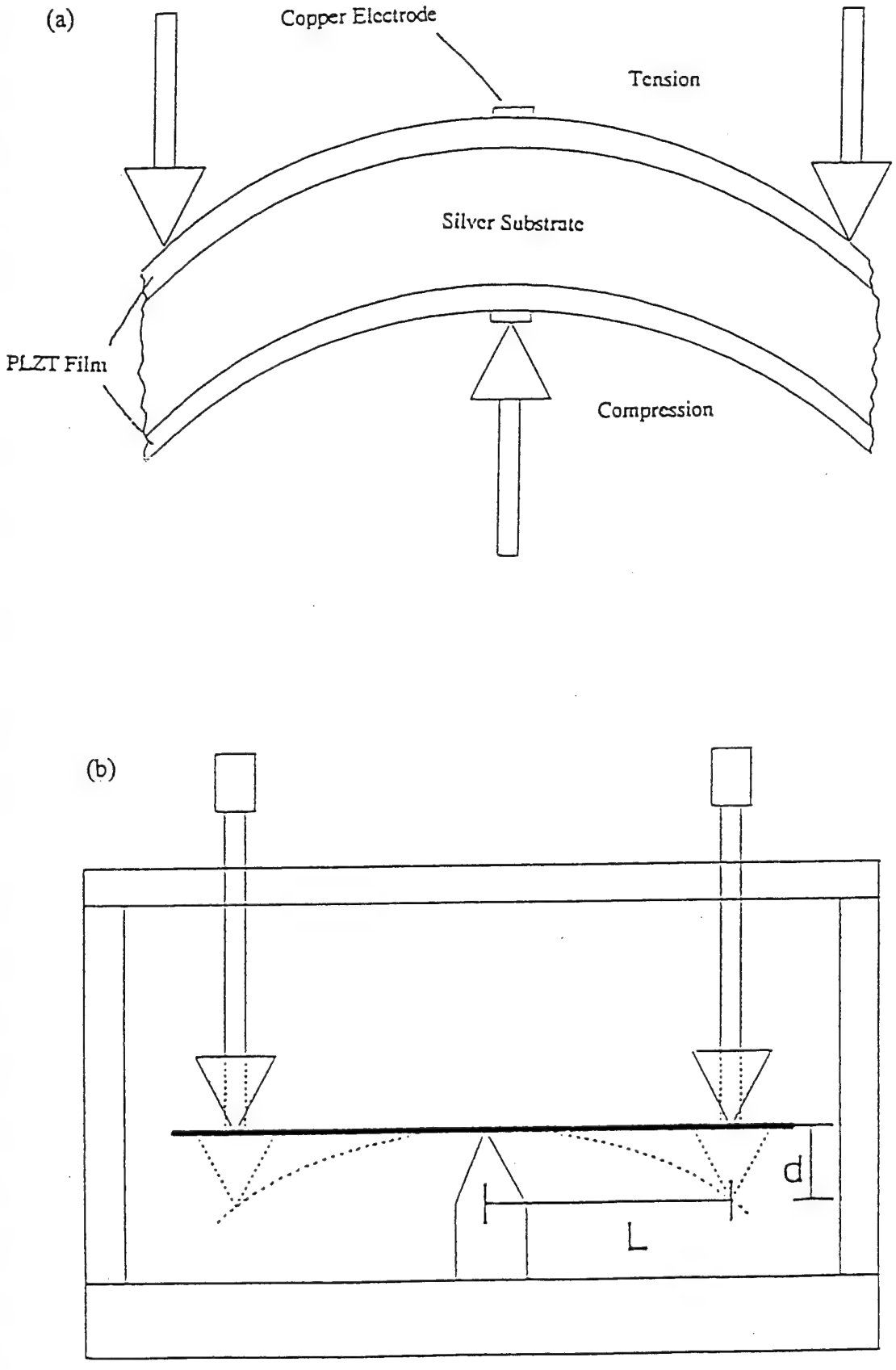

Figure 4. Three point bender showing a) applied stresses and b) measurements needed for the calculation of the radius of curvature.

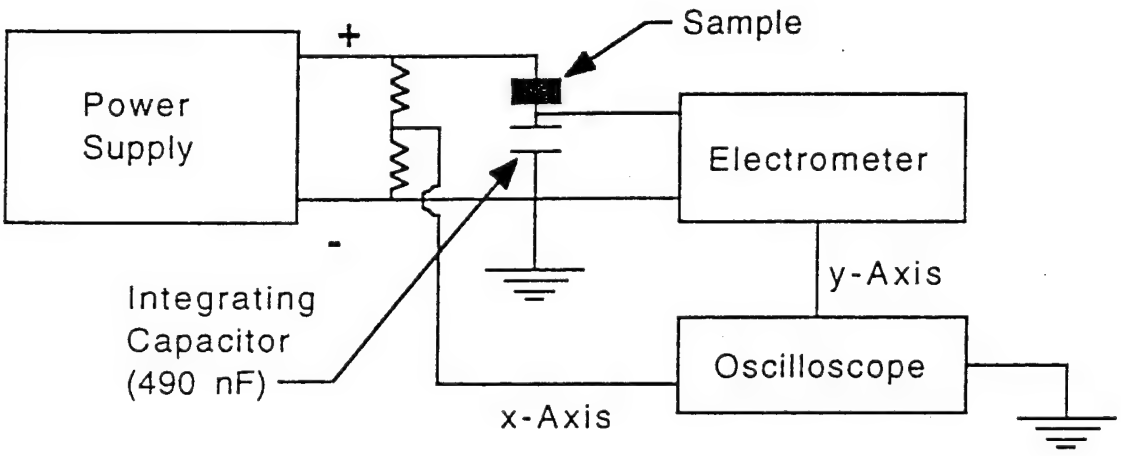

Figure 5. Electrical schematic of hysteresis looper set-up.

Table 1. Electrical properties of sintered, hot pressed and dip coated PLZT (9/65/35) thin films.

	tan δ (pol)	K (pol)	E_C [kV/cm]	P_R [μC/cm^2]	P10 [μC/cm^2]	P20 [μC/cm^2]
Sintered	.035	4205	1.77	3.27	26.2	29.6
Hot pressed	.033	4317	.958	1.45	20.57	27.13
Thin film	.151	3194	23	19.7	------	-----

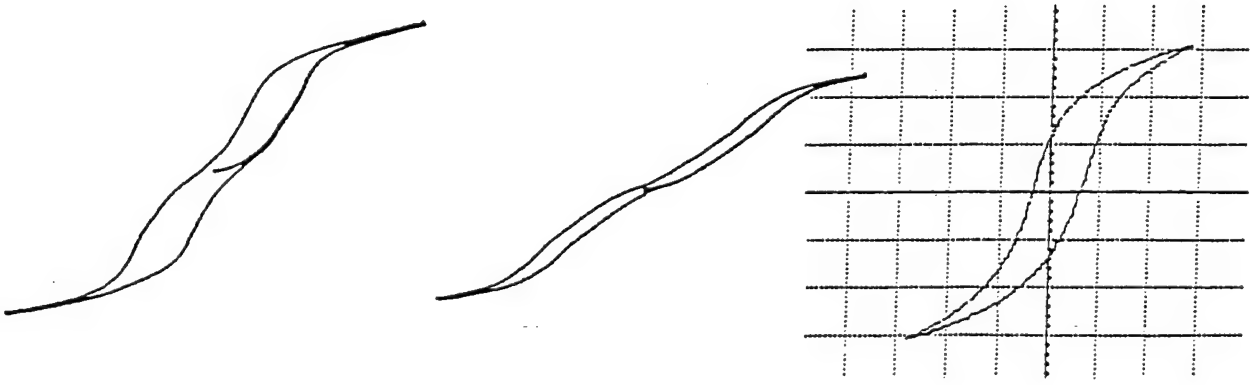

Figure 6. Hysteresis loops for sintered and hot pressed bulk materials and dip coated thin films (PLZT 9/65/35).

Table 2. Electrical properties of PLZT (9/65/35) thin films with various firing schedules.

	P_R [$\mu C/cm^2$]	E_C [kV/cm]	tan δ (pol)	K (pol)
555	----	----	.035	----
755	----	----	.034	----
575	14.1	38	.094	1174
775	15.4	24	.116	2014
557	9	19	.119	1833
757	14.1	21	.162	2414
577	11.8	23	.138	1901
777	19.7	23	.151	3194

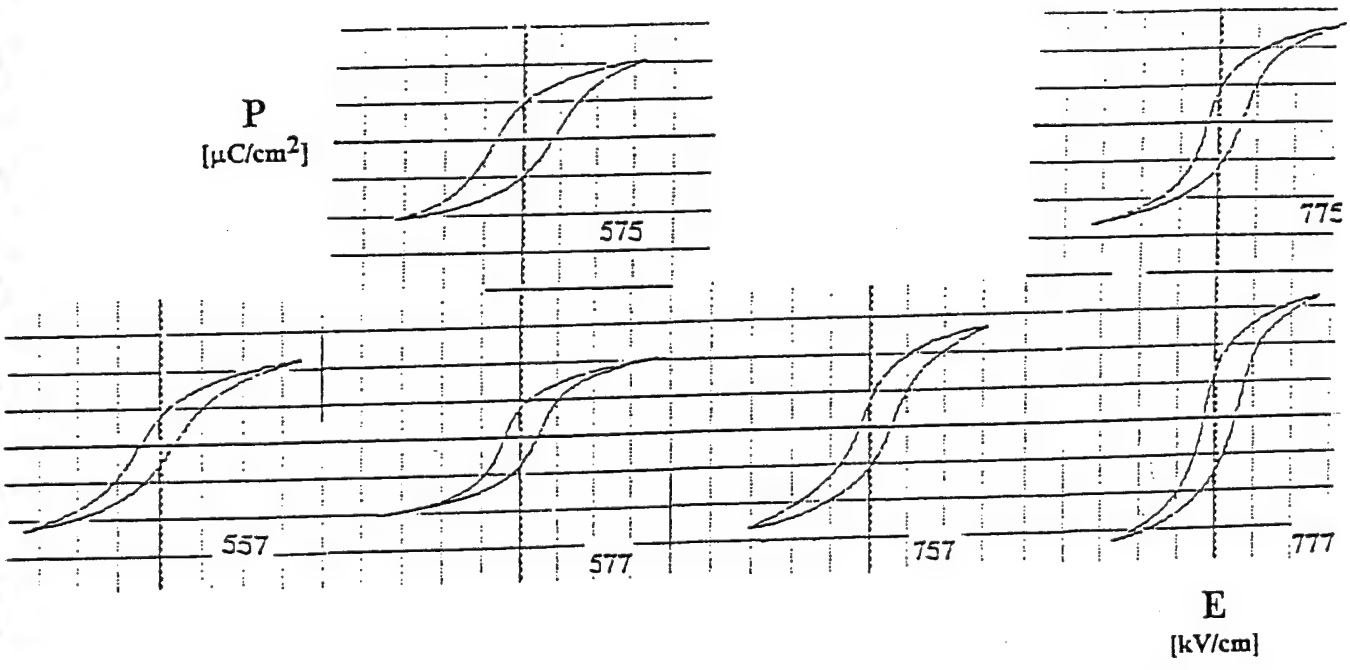

Figure 7. Ac hysteresis loops of PLZT 9/65/35 thin films with various firing schedules. Vertical scale = 15 $\mu C/cm^2$ per div. Horizontal scale = 50 kV/cm per div.

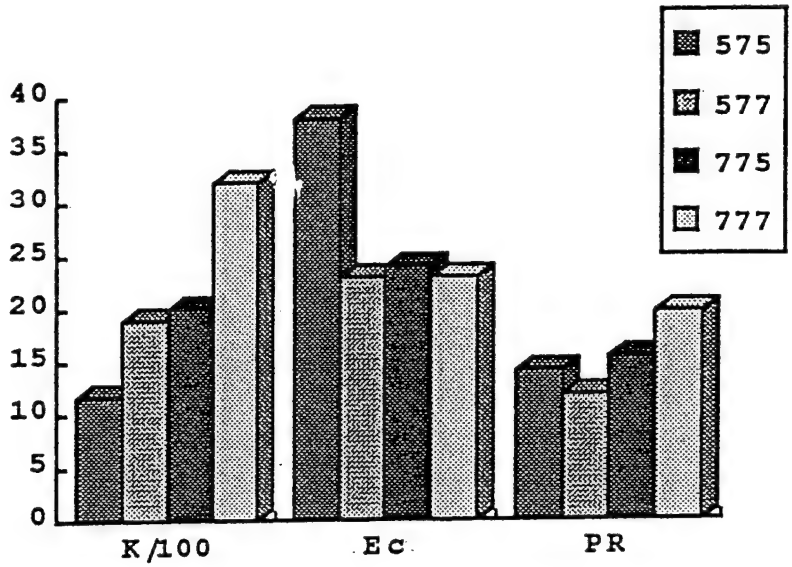

Figure 8. Thin film electrical measurements arranged according to increasing temperature within firing schedule.

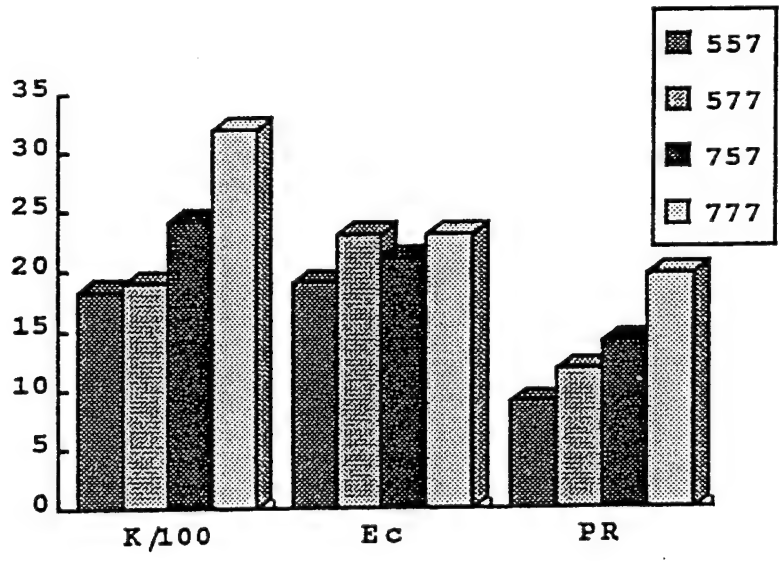

Figure 9. Thin filn electrical measurements arranged according to increasing temperature within firing schedule.

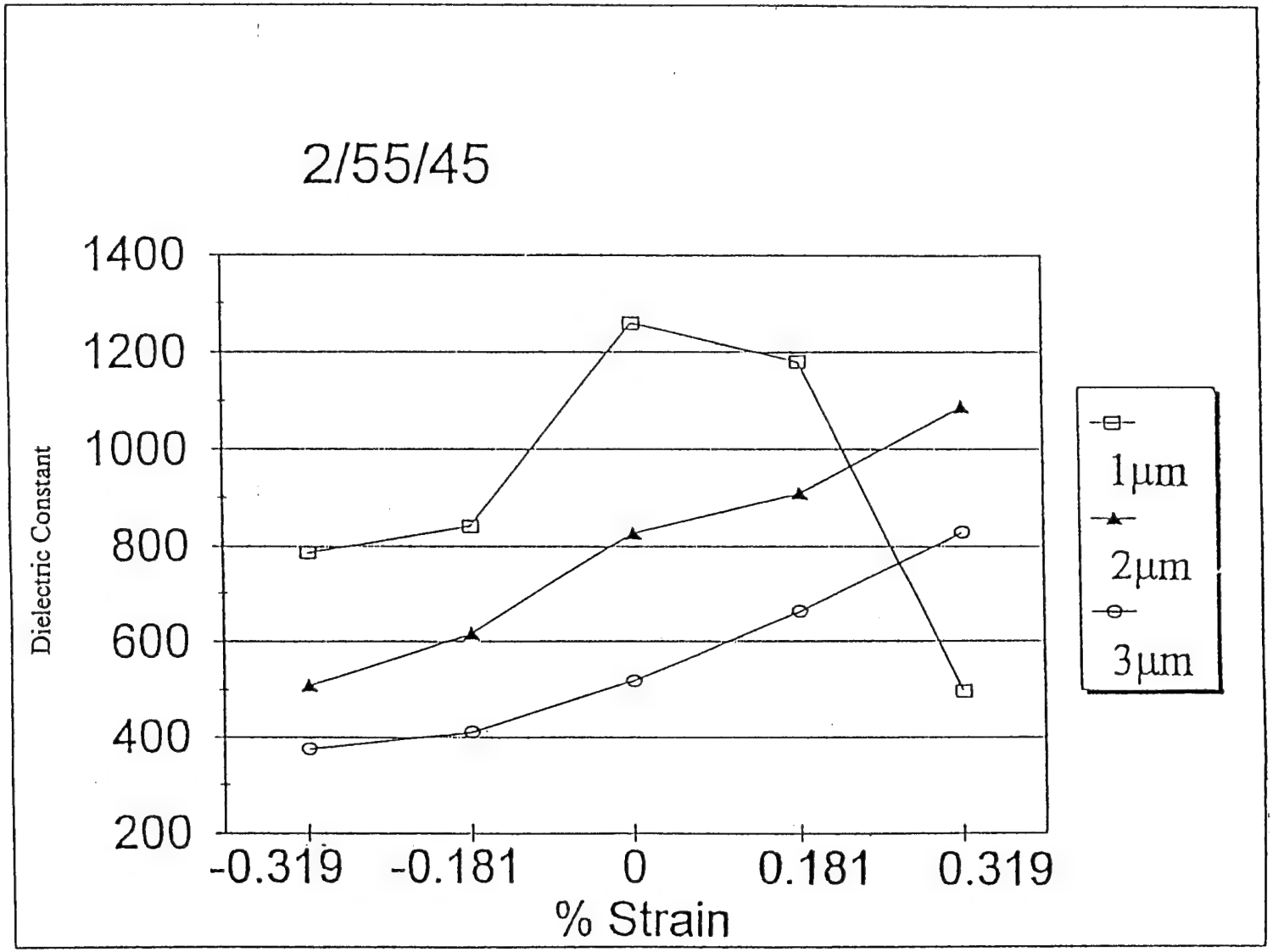

Figure 10. Change in dielectric constant for 2/55/45 thin film PLZT on Ag foil.

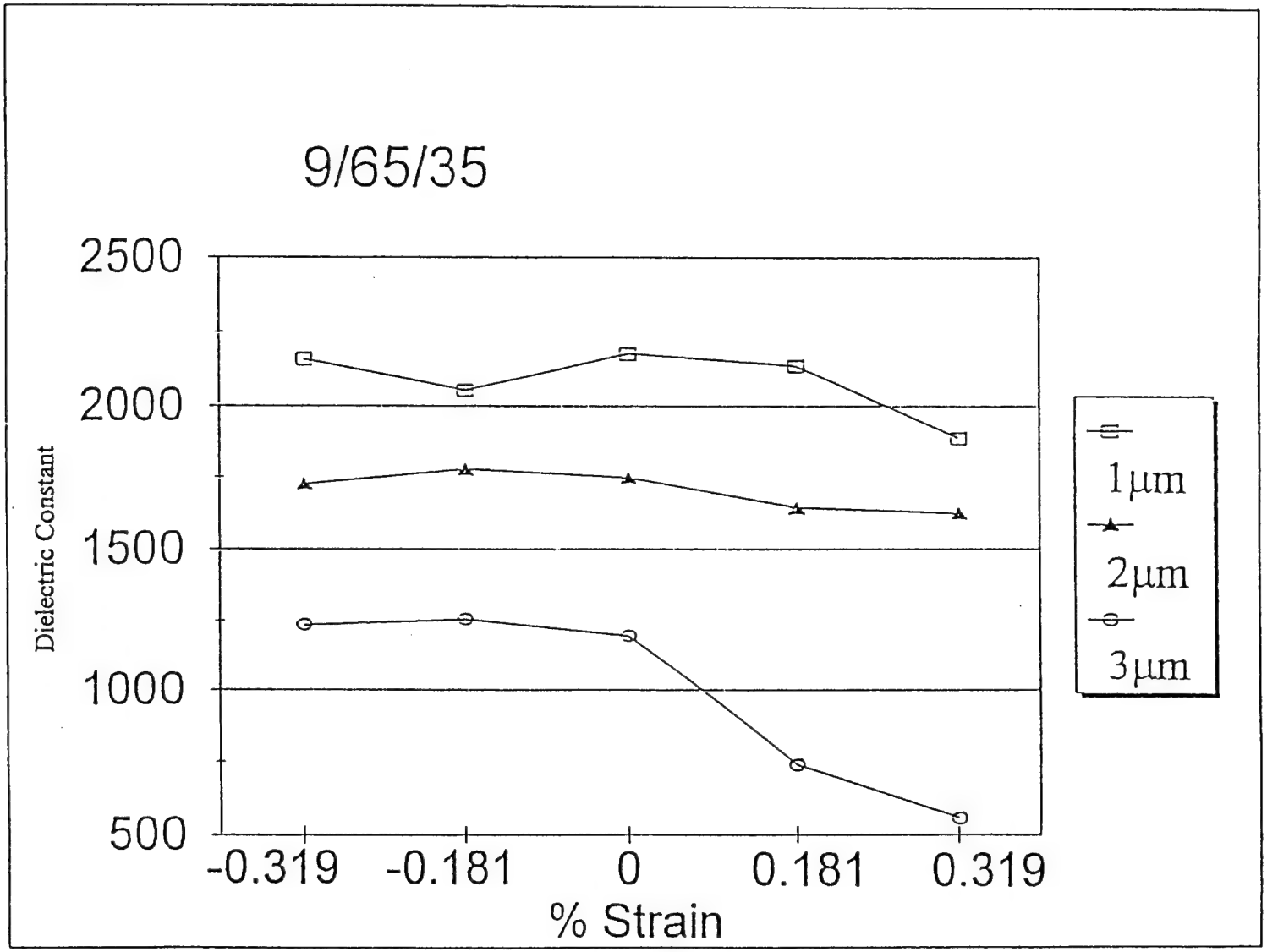

Figure 11. Change in dielectric constant for 9/65/35 thin film PLZT on Ag foil.

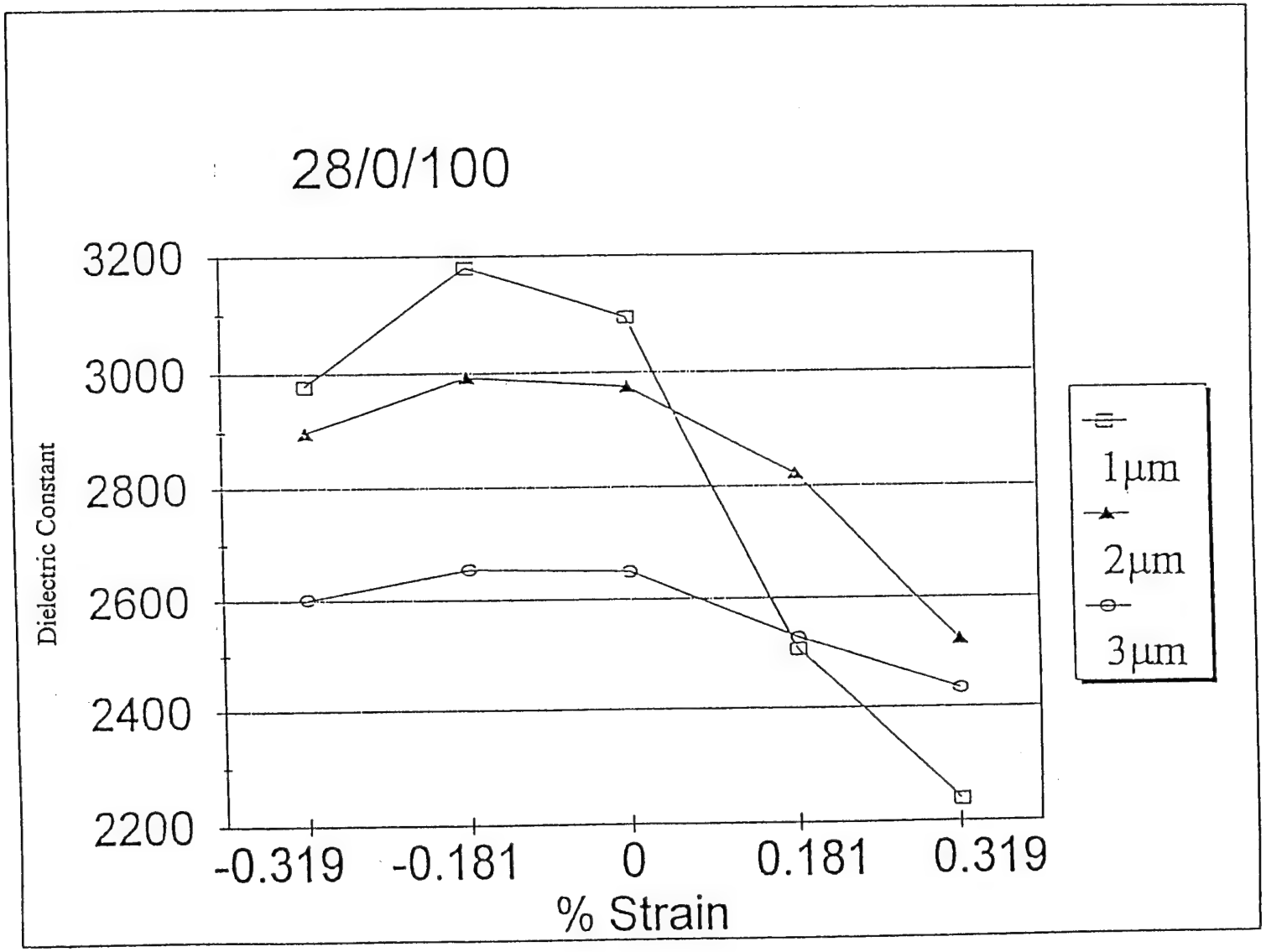

Figure 12. Change in dielectric constant for 28/0/100 thin film PLZT on Ag foil.

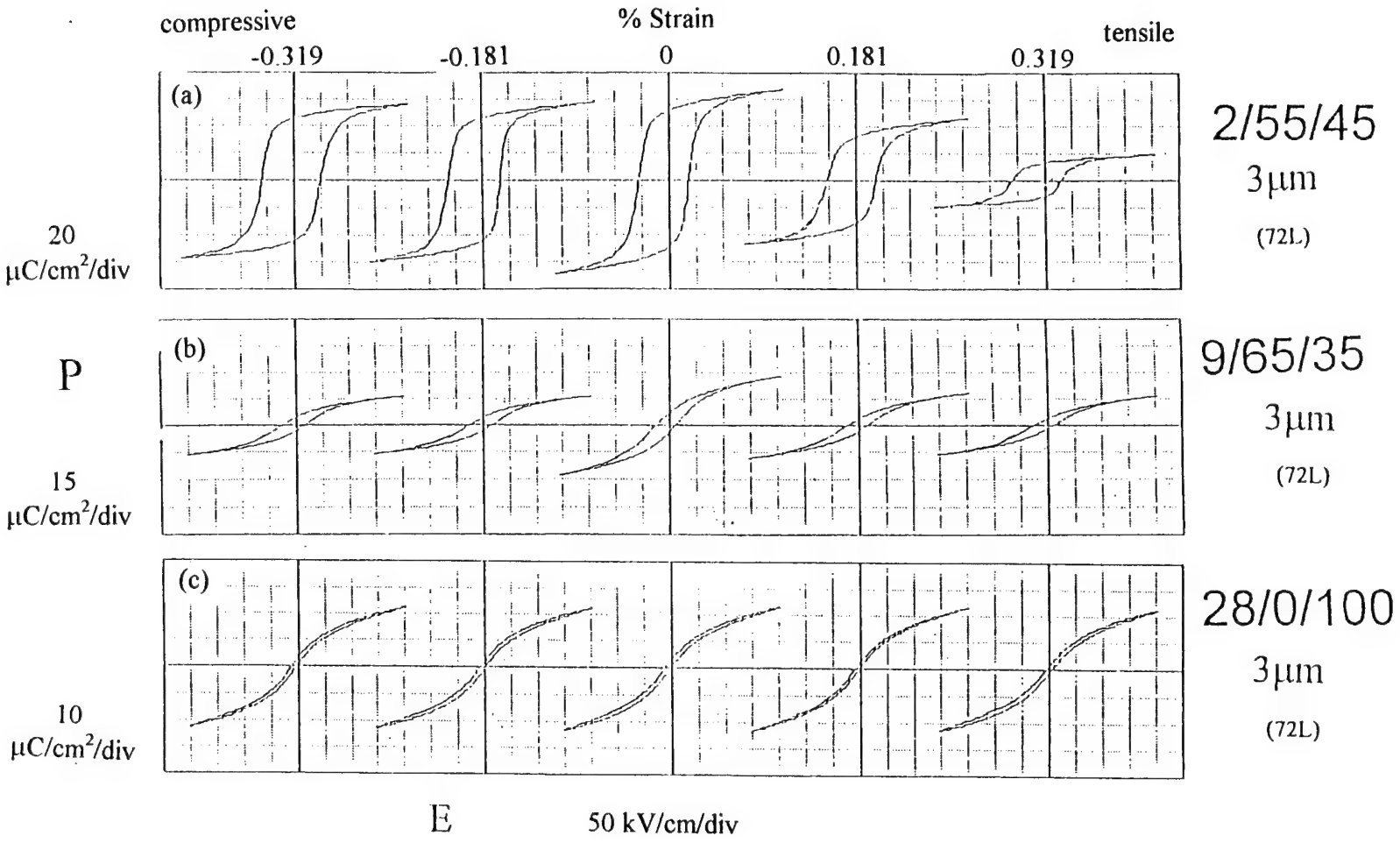

Figure 13. Hysteresis loops for 3μm thin films of different compositions on Ag foil measured at various stress levels.

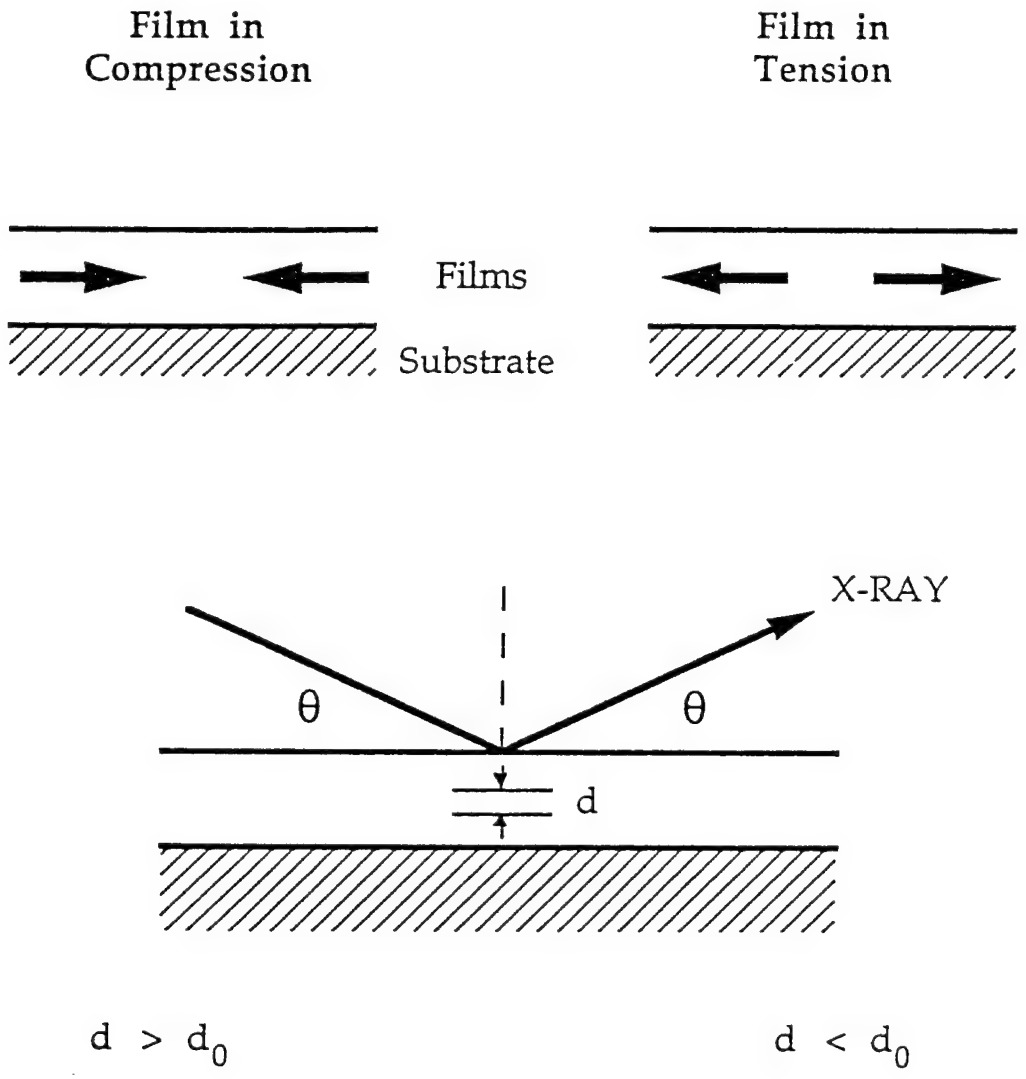

Figure 14. Types of thermal stresses, and the strained lattice constant (d) measured by XRD, compared with the stress-free value (d_o).

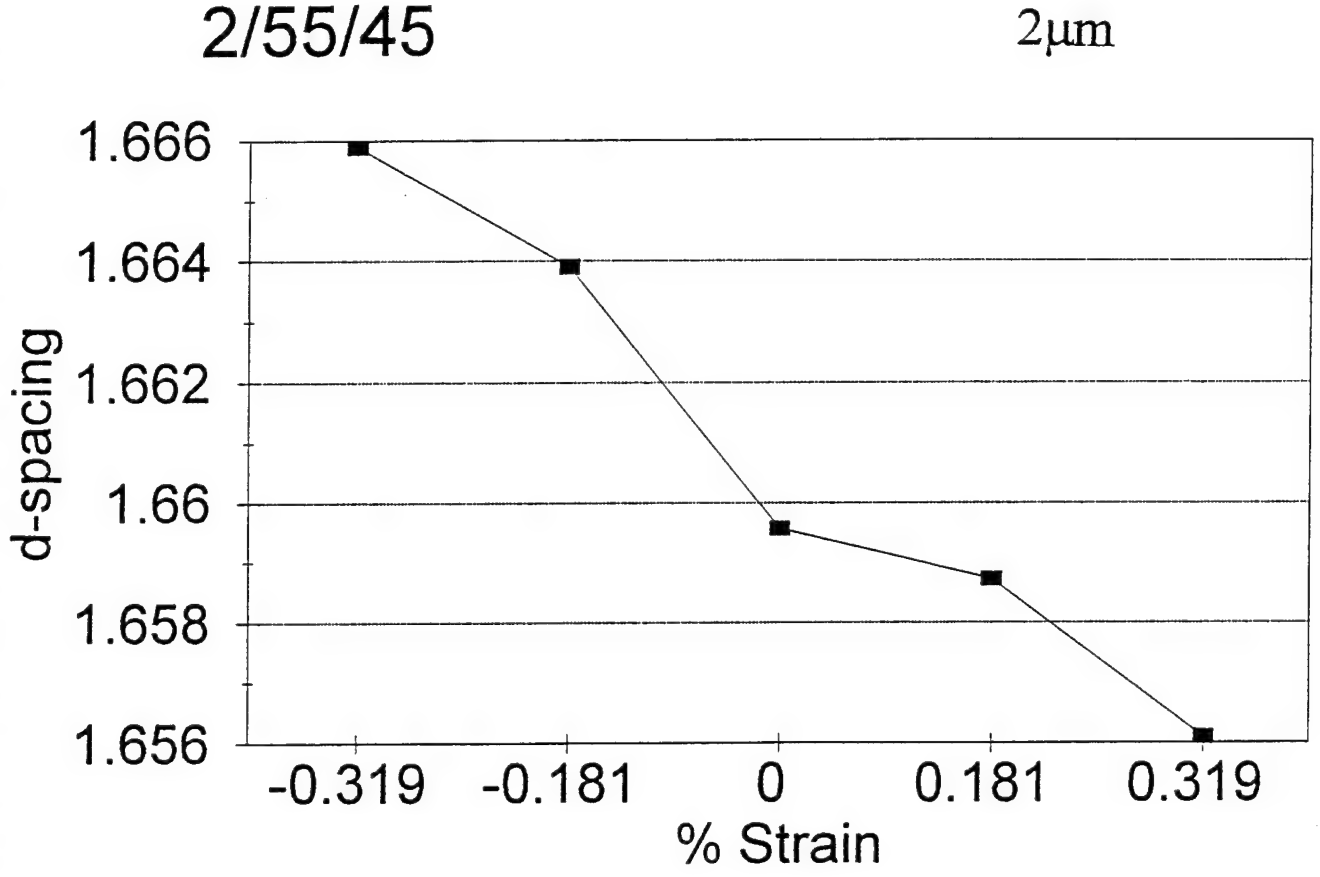

Figure 15. Lattice constant from X-ray diffraction patterns of a 2μm PLZT 2/55/45 thin film on Ag foil at various applied stresses.

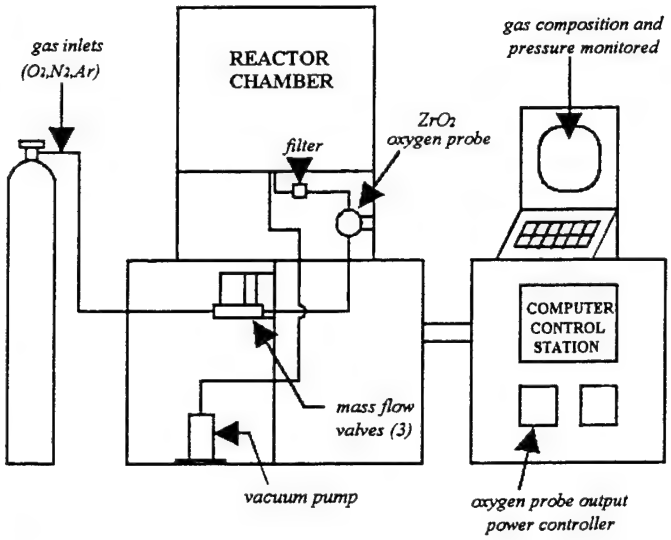

ATMOSPHERE CONTROL SYSTEM

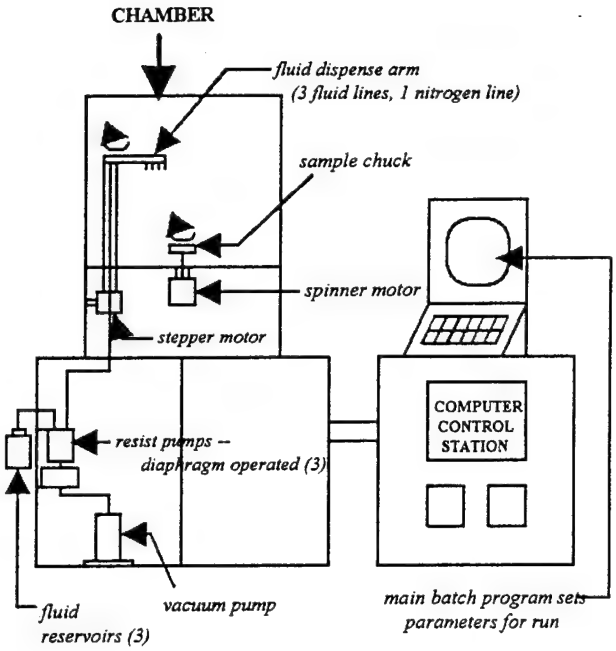

FLUID DISPENSE SYSYTEM

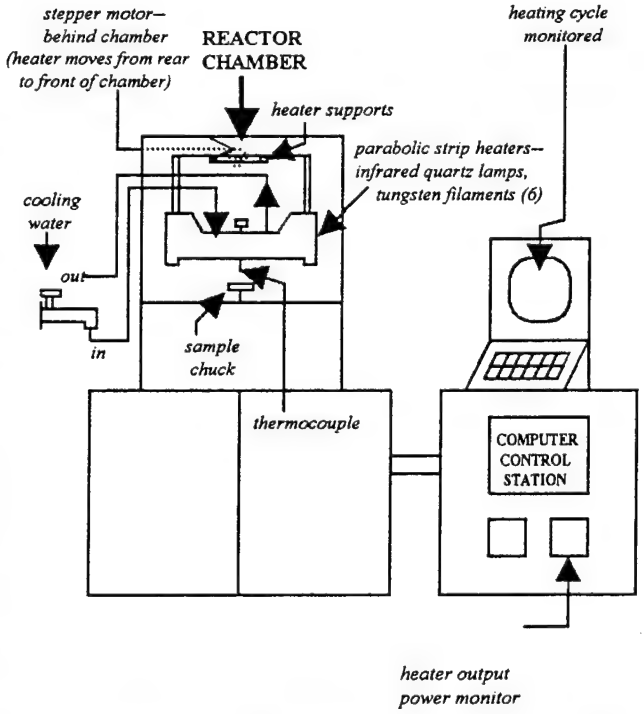

RAPID THERMAL PROCESSING UNIT

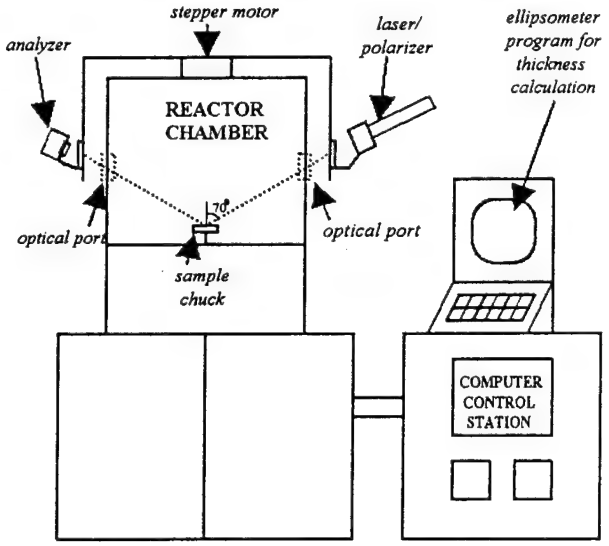

IN SITU LASER ELLIPSOMETER

Figure 16. Automatic spin coat reactor/analyzer.

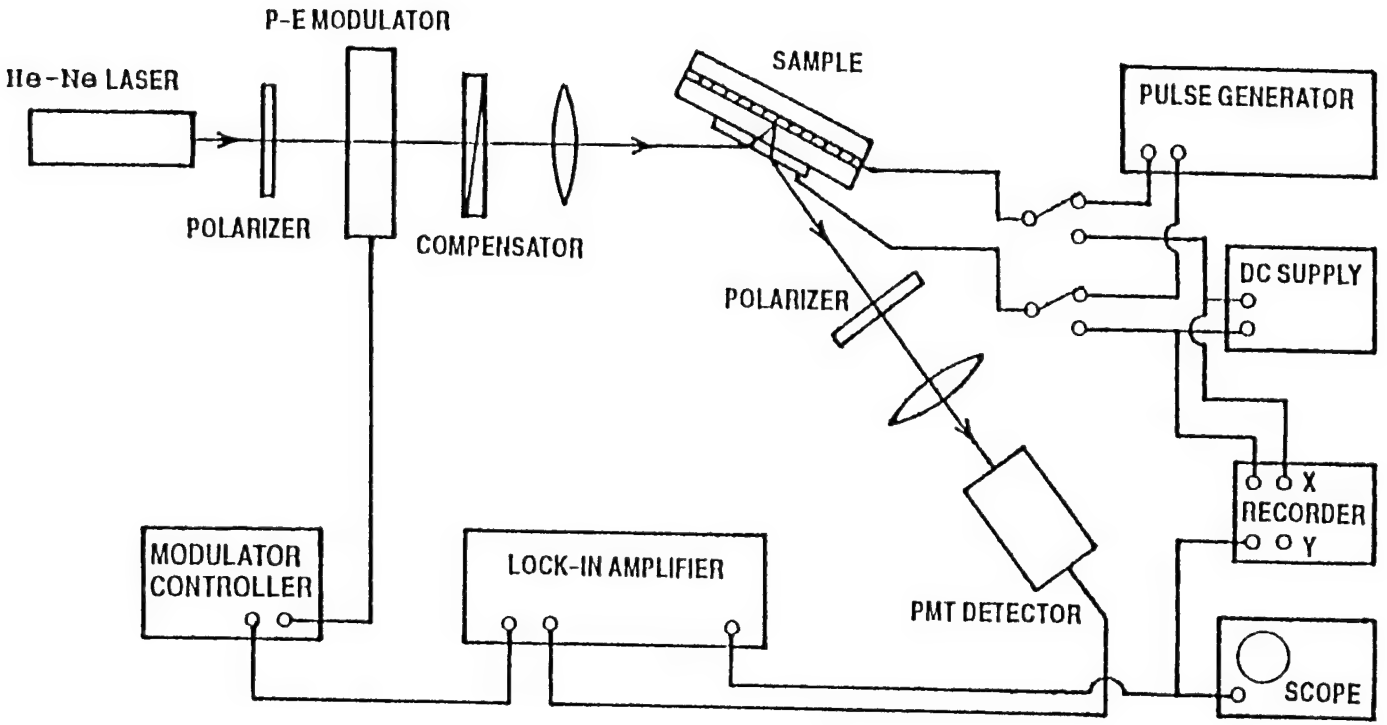

Figure 17. Instrumental set-up for electrooptic measurements in the reflection mode.

Part II.

Publications

Photoactivated birefringence in antiferroelectric thin films via a structural transition

Feiling Wang, Kewen K. Li, and Gene H. Haertling
Gilbert C. Robinson Department of Ceramic Engineering, Clemson University, Clemson, South Carolina 29634-0907

(Received 24 June 1994; accepted for publication 1 September 1994)

A photoactivated birefringence has been observed in an antiferroelectric lead zirconate titanate (PZT) thin film material bounded by an indium-tin oxide (ITO) electrode. This phenomenon stemmed from the ultraviolet (UV) assistance to an antiferroelectric-to-ferroelectric structural transition which otherwise was inhibited by an effect of the lead zirconate titanate (PZT)-ITO interface. The UV-assisted structural transition was accompanied by a significant change in the birefringence of the PZT thin films. Using this phenomenon, an UV-addressed visible-light modulation was demonstrated with an ITO/PZT/Pt thin film structure on silicon substrates. © *1994 American Institute of Physics.*

The use of ferroelectric (FE) materials for optical processing is mainly based on two distinct properties, i.e., optical nonlinearity and photorefraction. Photorefraction, being an electro-optic effect by nature, requires much lower light intensity than processes relying solely on optical nonlinear susceptibilities. The search for new media with novel or enhanced nonlinear optical and electro-optical capabilities has continued to draw intense effort. Antiferroelectric (AFE) thin film materials, emerging recently, exhibited unique and promising electro-optic properties, i.e., a birefringent bistability manifested during a field-induced AFE-to-FE structural transition.[1,2] Prior study of bulk AFEs in regard to their electro-optic properties was conducted by Land *et al.*[3,4] Recently, there has been growing interest in AFE thin film materials.[5–7] To date, however, little is known as to whether thin film AFEs possess significant value for all-optical processes. The purpose of this letter is to report a newly observed photoactivated birefringence in an AFE thin film material. Unlike previously known effects in FEs, the photoactivated birefringence is associated with a photoassisted AFE-to-FE structural transition.

AFE thin films of lead zirconate titanate (PZT) (96/4 Zr/Ti ratio) were deposited on Pt/Ti-coated silicon substrates by using an automatic dip-coating technique.[8] The thickness of the films was approximately 700 nm. An indium-tin oxide (ITO) layer approximately 240 nm thick was deposited on the PZT films by means of sputtering. With the introduction of the lead titanate, the field threshold for the AFE-to-FE transition was reduced from 50 kV/mm for lead zirconate to approximately 20 kV/mm for the PZT composition while maintaining the AFE structure of the films under zero external field.

The field-induced birefringence of the PZT thin films was characterized by means of differential ellipsometry in a reflection mode.[2] The arrangement of the electrodes and the light sources are depicted in Fig. 1. A phase-modulated helium-neon laser beam of 543.5 nm was obliquely incident on the thin film sample. An incident angle of approximately 52° was used in the experiments. A short-arc mercury vapor lamp was utilized as the UV source for the experiments described later in the letter. The phase-sensitive detection scheme allowed the direct measurement of the relative phase shift of the p-polarized light (component parallel to the incident plane) with respect to s-polarized light (component perpendicular to the incident plane) as a function of a low frequency voltage signal. The relative phase shift, as measured, was directly related to the field-induced ellipticity of the indicatrix (birefringence) of the PZT thin films. Being a polycrystalline material, the PZT thin films were macroscopically uniaxial defined by the external electric field in a normal direction of the substrate.

It was found that, in the dark, the phase shift versus voltage loop was severely asymmetric with respect to the polarity of the applied voltage. While the material exhibited a digital electro-optic response in the negative half-cycles of the voltage (the Pt bottom electrode being the reference for the electric potential), the digital electro-optic response was absent in the positive half-cycles of the voltage, as shown in Fig. 2(a). A corresponding dielectric hysteresis loop of the thin film material was taken with a Sawyer–Tower circuit and shown in Fig. 2(b). It was clear from Fig. 2 that the

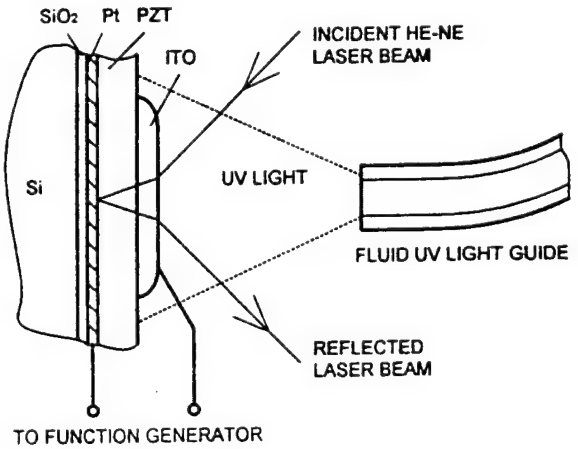

FIG. 1. Arrangement of the electrodes and the light sources in measuring the electro-optic and dielectric properties of the thin film material with UV illumination.

 0003-6951/94/65(20)/2507/3/$6.00

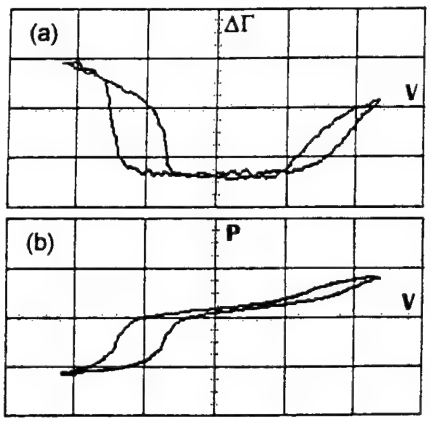

FIG. 2. (a) Relative phase shift of the reflected light beam, $\Delta\Gamma$ taken in the dark, as a function of the cyclic voltage. (b) Polarization of the thin film material as a function of the cyclic voltage taken in the dark. The horizontal scale is 7.5 V per division. The vertical scales for (a) and (b) are 0.21 per division and 27 $\mu C/cm^2$ per division, respectively.

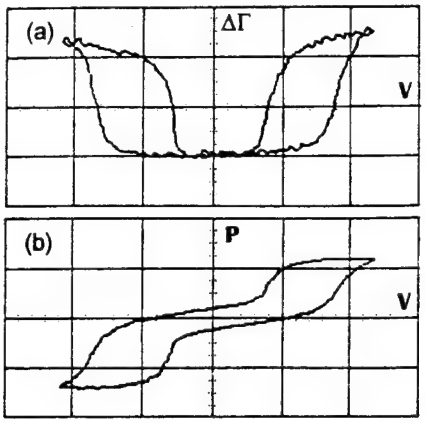

FIG. 3. (a) Relative phase shift of the reflected light beam, taken with UV illumination, as a function of the cyclic voltage. (b) Polarization of the thin film material as a function of the cyclic voltage taken with UV illumination. The scales of the plots are identical to those for Fig. 2.

field-induced AFE-to-FE structural transition in the PZT thin films was repressed in the positive half-cycles of the voltage. In contrast to the films with ITO electrodes, PZT thin films with copper top electrodes showed normal double hysteresis loop, typical for AFE materials under field-induced structural transition. This experimental evidence strongly suggested that because of the existence of the ITO-PZT interface the field-induced AFE-to-FE structural transition of the PZT thin film materials was suppressed in the positive half-cycles of the voltage. Consequently, the digital electro-optic response of the PZT thin films was absent in the positive half-cycles of the voltage.

The photoactivated birefringence change in the ITO-electroded PZT thin films was observed when the films were illuminated with low intensity near-UV light. Filtered radiation from the UV lamp, peaked at 365 nm wavelength, was brought to the thin film samples through a fluid filled light guide. The intensity of the UV radiation at the sample was estimated to be less than 100 mW/cm^2. The UV light was switched on and off manually using a shutter. Under the UV illumination, the electro-optic response of the PZT thin films exhibited a characteristic change. As shown in Fig. 3(a) for a phase shift versus voltage loop recorded by a digital oscilloscope, the electro-optic response of the material became characteristically symmetric. Withdrawal of the UV illumination restored the asymmetric electro-optic response of the material shown in Fig. 2(a). A corresponding change in the hysteresis loop of the materials with the UV illumination was also observed, as shown in Fig. 3(b). Comparing Figs. 2 and 3, it was clear that the UV illumination released the ITO-PZT interfacial suppression to the field-induced AFE-to-FE structural transition in the positive half-cycles of the voltage.

The amplitude of the field-induced birefringence with the UV illumination was estimated to be 0.02, similar to that of lead zirconate thin films under a normal AFE-to-FE transition. The thin film structure shown in Fig. 1 behaved like a Fabry–Pérot etalon, where the air-ITO and PZT-Pt interfaces were the primary reflection surfaces. The large field-induced phase shift measured in the reflected light beam, shown in Figs. 2(a) and 3(a), was obtained by taking advantage of the Fabry–Pérot peak. At a Fabry–Pérot peak, greatly enhanced phase retardation can be achieved; approximately 30° was obtained when the AFE-to-FE structural transition occurred. Because the experimentally convenient incident angles were close to the Brewster angle for p-polarized light incident on the ITO layer, the thin film Fabry–Pérot etalon possessed a higher finesse for the s-polarized light component than the p-polarized light. As a consequence, near a Fabry–Pérot peak, the measured relative phase retardation was attributed mainly to the phase shift of the s-polarized light component.

In the absence of the UV light, the suppression of the AFE-to-FE structural transition during the positive voltage half-cycles may be understood through the semiconductor nature of the ITO electrode. The ITO material is known to be an n-type semiconductor. In the negative voltage half-cycles, the positive surface charges at the ITO-PZT interface due to the termination of the PZT polarization can be completely compensated for by the accumulation of the majority carries. In the positive voltage half-cycles, however, the negative surface charges have to be compensated for by the accumulation of the minority carries and the depletion of the majority carries. Such a mechanism may not be adequate for compensating the large polarizations associated with the field-induced FE state of the PZT material; the AFE-to-FE transition in the positive voltage half-cycles is thus suppressed. The UV assistance to the field-induced AFE-to-FE transition may be explained through the photogeneration of free charge carries that provide additional compensation to the surface charges; the AFE-to-FE transition in the positive voltage half-cycles is thus ignited and sustained. The effects of polarity-sensitive charge compensation are known to exist for semiconductor-ferroelectric interfaces.[9] A related phenomenon was observed with an ITO-PLZT junction where the polarity-sensitive charge compensation resulted in the bistable remanent birefringence in the PLZT thin films.[10]

Among possible applications of the observed phenomenon, an UV-addressed visible light modulation has been

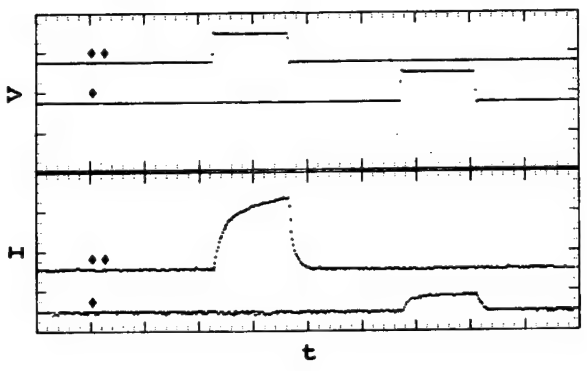

FIG. 4. Modulation of the reflected helium-neon laser beam from a PZT thin film with and without UV illumination. Upper traces: electric pulses (20 V per vertical division). Lower traces: light intensity. The horizontal scale is 5 ms per division. Traces marked with "◆◆" were taken with UV illumination; traces marked with"◆" were taken without UV illumination.

realized using the PZT films. The arrangement of the light sources was similar to that for electro-optical characterization, as shown in Fig. 1, except that the incident helium-neon laser beam was linearly polarized in a direction of 45° with respect to the incident plane. A light sensor (photomultiplier tube) was located in the direction of the reflected light behind a polarizer. The orientation of the polarizer was adjusted so that the reflected light beam was blocked from the light sensor when the film was not activated. In order to observe the UV-addressed switching of the visible laser beam, positive electric pulses, 15 V in peak height and 7 ms in width, were fed to the thin film device. Shown in Fig. 4 was the light intensity recorded along with the electric pulses in an oscilloscope, with and without the UV illumination to the device. It was observed that the intensity of the switched light increased by a factor of 4 in the UV-addressed state as compared with the nonaddressed state. The switching speed of the thin film material under the UV-addressed condition appeared to be around 1 ms.

The observed phenomenon possesses an apparent analogy to the photorefraction in ferroelectric materials. Yet the UV-activated birefringent change in the AFE thin films is currently unparalleled by any nonlinear optical or photorefractive processes. Using the AFE films as holographic recording media, significantly higher diffraction efficiency may be expected. With a suitable coherent UV source, two-dimensional holograms may be recorded in the AFE thin films; nondestructive readout may be realized by means of a visible light beam.

The authors are indebted to E. Furman for many helpful discussions regarding this subject. This study was sponsored by the U.S. Office of Naval Research under Contract No. N00014-19-J-508.

[1] F. Wang, K. K. Li, and G. H. Haertling, Opt. Lett. **17**, 1122 (1992).
[2] F. Wang, K. K. Li, E. Furman, and G. H. Haertling, Opt. Lett. **18**, 1615 (1993).
[3] C. E. Land, IEEE Trans. Electron. Devices **ED-26**, 1143 (1979).
[4] C. E. Land, J. Am. Ceramic Soc. **71**, 905 (1988).
[5] G. R. Bai, H. L. M. Chang, and D. L. Lam, Appl. Phys. Lett. **62**, 1754 (1993).
[6] J.-F. Li *et al.*, J. Appl. Phys. **75**, 442 (1994).
[7] T. Tani *et al.*, J. Appl. Phys. **75**, 3017 (1994).
[8] K. K. Li, F. Wang, and G. H. Haertling, J. Mater. Sci. (in press).
[9] D. Wurfel and I. P. Batra, Phys. Rev. B **8**, 5126 (1973).
[10] F. Wang and G. H. Haertling, Appl. Phys. Lett. **63**, 1730 (1993).

TRANSVERSE ELECTROOPTIC PROPERTIES OF MAGNETRON SPUTTERED PLZT THIN FILMS

F. WANG and G.H. HAERTLING
Department of Ceramic Engineering,
Clemson University,
Clemson, SC 29634 , USA

ABSTRACT. Ferroelectric thin films of (Pb,La)(Zr,Ti)O_3 ceramics were deposited on various substrates by magnetron sputtering. With the use of a phase-detection technique, the transverse electrooptic properties of the films were characterized. It was found that the electrooptic response of the films is strongly dependent on the grain orientation of the thin film materials.

1. Introduction

Lead lanthanum zirconate titanate (PLZT) thin films have been deposited onto various substrates by means of solution coating techniques using acetate precursors [1-3]. In search of the optimum coating technique for producing high quality PLZT thin films for various applications, PLZT powders derived from the acetate precursors have been used as target materials in a radio-frequency (RF) magnetron sputter deposition technique designed to complement the solution coating methods.

Recently, increasing attention has been paid to the choice of substrates in obtaining thin films of desired properties [2]. It was reported that the thermal expansion mismatch between a ferroelectric thin film and its substrate significantly influences the orientational preference of ferroelectric domains, thus their dielectric properties. This paper is mainly concerned with the observed divergence of the transverse electrooptic properties in PLZT thin films deposited on various substrates by the RF magnetron sputtering.

2. Experimental Method

A high vacuum RF magnetron sputter unit was used to deposit PLZT thin films. The target material was a PLZT powder of composition 2/55/45 (La/Zr/Ti) produced by a coprecipitation method from a water soluble acetate precursor [1]. A post-deposition annealing process was utilized to obtain perovskite PLZT films. Typical deposition and annealing parameters are listed below:

RF power:	70 watt	Annealing temperature:	650°C
Total pressure:	10 micron	Annealing time:	40 min.
Oxygen percentage:	40%		
Substrate temperature:	350°C		
Deposition rate:	250 nm/hour		

O. Auciello and J. Engemann (eds.): Multicomponent and Multilayered Thin Films for Advanced Microtechnologies: Techniques, Fundamentals and Devices, 375–379.

Thin films were deposited onto three types of substrates, i.e. Pt/Ti-coated silicon, randomly oriented sapphire and fused silica substrates.

The transverse electrooptic properties of the PLZT thin films on sapphire and fused silica substrates were measured by a phase-detection technique [4] in a transmission mode using a He-Ne laser as the light source. Planar copper electrodes with a gap width of 50 mm were fabricated on top of the thin film by a photolithography process.

3. Results and Discussion

3.1 GRAIN ORIENTATION

With the identical deposition and annealing processes mentioned previously, the thin films deposited on the three types of substrates exhibited significant differences in grain orientation as revealed by x-ray diffraction patterns.

By comparing to the diffraction pattern of the powder, it was found that peak heights for (100) and (110) orientations in thin films on Pt/Ti-coated silicon were reversed, as shown in Figure 1(a). In contrast to the films on Pt/Ti-coated silicon, films on sapphire substrates, shown in Figure 1(b), exhibit a strengthening of the (110) peak, indicating a preferred (110) grain orientation. The most drastic preferential orientation of crystal grains was observed in the thin films deposited on fused silica substrate with (100) being the dominant orientation, as shown in Figure 1(c). Summarized in Table 1 are the types of preferential grain orientation for 2/55/45 PLZT thin films deposited on the three different substrate along with their thermal expansion coefficients.

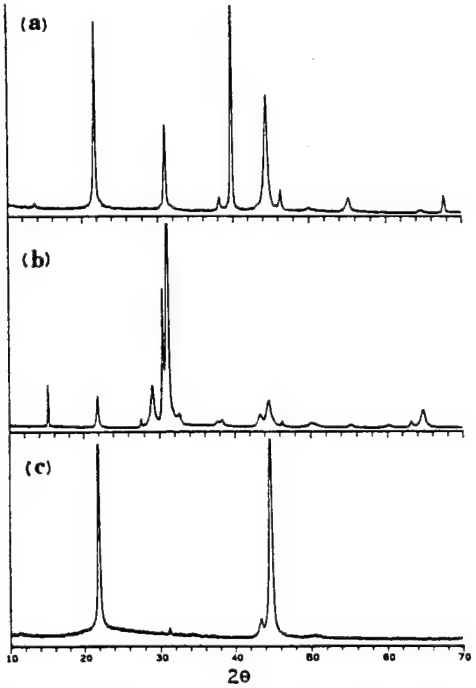

Figure 1. X-ray diffraction patterns for 2/55/45 PLZT thin films deposited on (a) Pt/Ti-coated silicon, (b) sapphire and (c) fused silica substrates.

TABLE 1. Orientation of 2/55/45 PLZT thin films

Substrate	thermal expansion coef. (ppm/^{o}C)	film orientation
fused silica	0.5	dominant (100)
silicon	2.5	preferred (100)
sapphire	8.0	preferred (110)

Noticing that the thermal expansion coefficient of PLZT materials (approximately 5 ppm/^{o}C) is intermediate between those of silicon and sapphire, the results strongly suggest that there is a correlation between the grain orientation and the thermal expansion property of the substrates in sputter deposited thin films. As shown in Table 1, thin films deposited on substrates with smaller thermal expansion coefficients exhibited dominant or preferred (100) orientation while thin films deposited on substrate with larger expansion coefficient exhibits preferred (110) grain orientation. It is not clear at present whether the preferred grain orientations are formed during the low temperature deposition or during the annealing procedure.

3.2. ELECTROOPTIC PROPERTIES

The field-induced birefringence of soft ferroelectric materials generally exhibit butterfly loops. In order to quantitatively describe this hysteretic electrooptic effect, three quantities are proposed to characterize a butterfly loop in the following discussion. These quantities are: the optical coercive field E_{oc} where two birefringence minima occur, the birefringence at the crossover point of a loop Δn_c (measured from the bottom of a curve) and the birefringence at the tip of a loop Δn_t. The value of Δn_t is meaningful only when the corresponding electric field at the tip E_t is given.

A series of butterfly loops for the electrooptic effect of a sputtered 2/55/45 PLZT film on a sapphire substrate is shown in Figure 2, created by a series field scans from a small range to a large range. Compared to the films on sapphire substrate, the 2/55/45 PLZT thin films deposited on the fused silica substrate exhibit much poorer electrooptic response as shown in Figure 3. The Δn_t for the film on fused silica is approximately one fourth of that for the film on sapphire substrate, taken under the same E_t. Table 2 lists the three characteristic quantities for films on both sapphire and fused silica substrates.

TABLE 2. Electrooptic properties of 2/55/45 PLZT thin films

Substrate	Thickness (nm)	E_{oc} (kV/mm)	Δn_t 10^{-3}	Δn_c 10^{-3}
f. silica	620	2.0	1.5	0.2
sapphire	620	1.6	6.2	1.3

Δn_t values were taken at E_t=8 kV/mm for both samples.

Being a rhombohedral material, the polar direction of a 2/55/45 PLZT crystal grain is along a three-fold direction of a oxygen-octahedra, i.e. a (111) crystal direction. When the external electric field is parallel to the substrate surface in the phase-detection measurement in the transmission mode, there is virtually no chance for the external field to encounter the (111) crystal direction of the grains in films on fused silica with (100) dominant orientation. Films of this type of orientation, therefore, are unfavorable for utilizing the transverse electrooptic effect of the films in the transmission mode.

In contrast to the films on fused silica, sputtered films on sapphire substrate possess (110) preferred grain orientation, which enhances the possibility for the external electric field to encounter the (111) crystal direction. This preferred grain orientation, therefore,

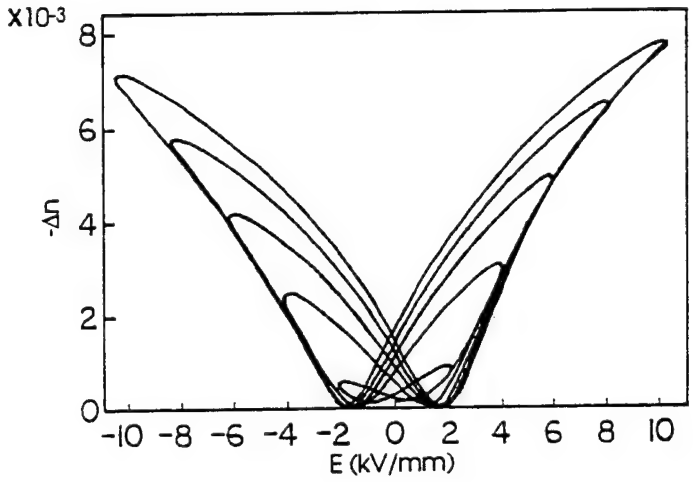

Figure 2. The evolution of the electrooptic response from a small to a large field scan range for a 2/55/45 PLZT film of thickness of 0.62 μm on a sapphire substrate.

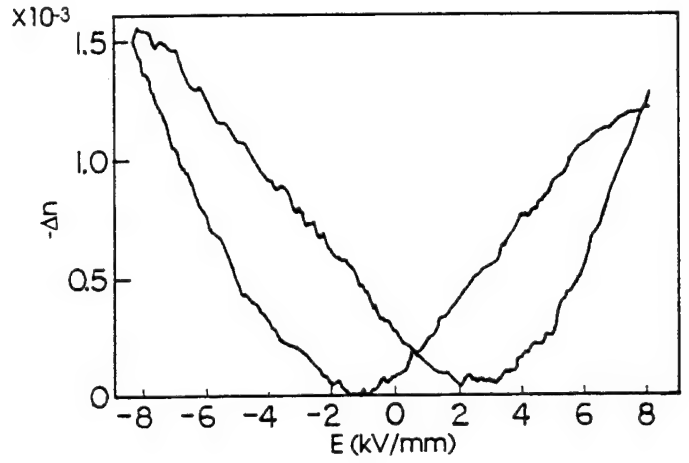

Figure 3. The electrooptic response of a 2/55/45 PLZT film of 0.62 μm thickness on a fused silica substrate.

favors the polarization, which in turn produces a large field-induced birefringence in the materials. As shown in Table 2, films deposited on sapphire substrates with preferred (110) grain orientation indeed exhibited superior electrooptic response.

4. Conclusions

PLZT thin films of composition 2/55/45 were deposited on various substrate with a RF magnetron sputtering technique using powders derived from an acetate precursor.

The electrooptic characterization shows that the films on sapphire with preferred (110) orientation exhibits superior electrooptic response over the films on fused silica with dominant (100) grain orientation. The difference is attributed to the fact that (110) orientation favors the polarization in rhombohedral thin film materials when the external electric field is along a planar direction.

5. Acknowledgements

This research was supported by the Office of Naval Research under contract No. N00014-91-J-508.

6. References

1. G.H. Haertling, Ferroelectrics **116** (1991) 51.
2. K.D. Preston and G.H. Haertling, Appl. Phys. Lett. **60** (1992) 2831.
3. K.K. Li, G.H. Haertling and W.Y. Howng, Integrated Ferroelectrics vol.**3**, No.1 (in print, 1992)
4. F. Wang, C.B. Juang, C. Bustamante, and A.Y. Wu, in Proc. of 4th International SAMPE Electronic Conference, Albuquerque, New Mexico, June 12-14, 1990, p.712.

TRANSVERSE ELECTROOPTIC PROPERTIES OF ANTIFERROELECTRIC LEAD CONTAINING THIN FILMS

Feiling Wang, Kewen K. Li and Gene H. Haertling
Department of Ceramic Engineering
Clemson University
Clemson, South Carolina 29634-0907

The transverse electrooptic effect was observed in solution coated lead zirconate thin films. The electric-field-induced birefringent shift exhibited a characteristic response which differed from the normal butterfly-like loops for ferroelectric materials. The observed unique response in lead zirconate thin films was related to their antiferroelectric nature and the electric-field-induced antiferroelectric-ferroelectric phase transition. The possible applications of the materials for optical memory are discussed.

Introduction

Ferroelectric (FE) thin films, owing to their high dielectric constant and two electrically switchable remanent states, have attracted great interest for the development of nonvolatile memory devices and other applications[1,2]. A variety of ferroelectric materials are also known to possess transverse electrooptic properties, i.e. the electric-field-controlled birefringence; however, ferroelectric switching (polarization reversal with an electric field) has not proved equally useful in integrated optical and/or optoelectronic devices. To facilitate an optical memory function in optoelectronic devices, it is desirable for the waveguide materials to possess two electrically switchable birefringent states. However, the two remanent polarization states are not distinguishable for the index ellipsoid in ferroelectric materials. Therefore, it is not feasible to realize optical memory in ferroelectric materials by switching between the two remanent polarization states.

Recently the transverse electrooptic effects in antiferroelectric (AFE) lead zirconate ($PbZrO_3$) thin films were observed[3]. The electric-field-induced birefringent shift in the lead zirconate thin films showed a characteristic response not exhibited in ferroelectric materials. The unique electrooptic response in the antiferroelectric thin films was found to stem from the electric-field-induced antiferroelectric-ferroelectric phase transition. Besides its importance as a fundamental material property, the transverse electrooptic effect in the antiferroelectric thin films may also furnish a mechanism for optical memory in optoelectronic devices. In this report the latest measurements of the transverse electrooptic properties in antiferroelectric lead zirconate thin films are presented.

Experimental Method

Lead zirconate thin films were deposited onto fused silica and Pt/Ti coated silicon substrates by a solution coating technique from an acetate precursor[4,5]. The antiferroelectric crystal structure of the resultant thin films was confirmed by the appearance of the X-ray diffraction peak at $2\theta^{o} = 16.9$, characterizing the antiferroelectric double cell structure. For the measurement of the dielectric properties of the materials, copper dots were evaporated onto the thin films deposited on the Pt/Ti-coated silicon substrate. For the detection of the transverse electrooptic properties, copper intedigitated electrodes with gap widths ranging from 5 to 40 μm were deposited on top of the thin films grown on the fused silica substrates.

The electric-field-induced birefringent shift of the thin film was measured by means of a phase-detection technique[6], using a He-Ne laser of wavelength of 632.8 nm as the light source. The phase modulation of the incident light was provided by means of a modulator. The measurements were performed with a transmission mode. In the phase detection scheme, the amplitude of the output signal (from a lock-in amplifier) at the modulating frequency was directly proportional to the phase retardation of the sample, provided that the total phase retardation of the sample was sufficiently small. A slow varying dc voltage was applied to the interdigitated electrodes during the measurement. An optical compensator was used to calibrate the measuring system.

Results and Discussion

A typical electrooptic response of the lead zirconate thin film is shown in Figure 1 where the birefringent shift of the thin film is plotted as a function of the slow varying dc electric field. The thickness of the film was 1 μm. Interdigital electrodes with a gap width of 10 μm was used in the measurement. As shown in the figure, the electrooptic response of the antiferroelectric thin film exhibits a number of features different from that of ferroelectric materials. For the purpose of comparison, a typical birefringence verses E-field curve for a ferroelectric thin film, i.e. PLZT[7] of composition 2/55/45, is shown in Figure 2. The birefringence verses E-field curve for the lead zirconate thin film is characterized by (1) enhanced hysteretic

CH3080-0-7803-0465-9/92$3.00 ©IEEE

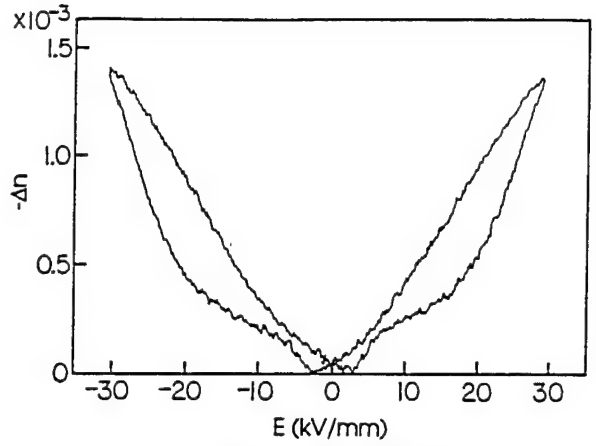

Figure 1 Measured birefringent shift as a function of the external dc electric field for a lead zirconate thin film deposited on a fused silica substrate.

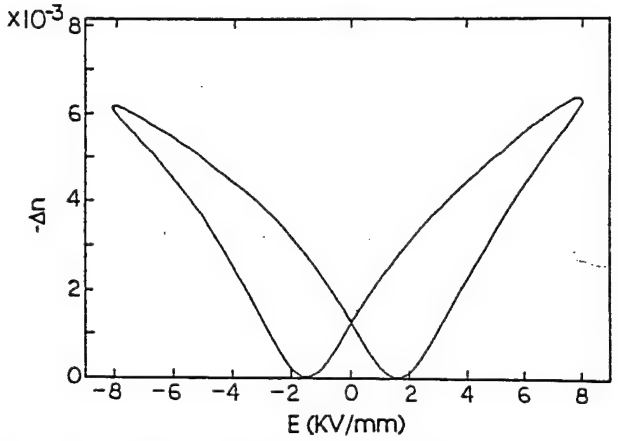

Figure 2 Measured birefringent shift as a function of the external dc electric field for a ferroelectric PLZT thin film deposited on a sapphire substrate.

behavior in the region of field strength above 10 kV/mm, (2) diminished hysterestic behavior in the region of field strength below 5 kV/mm and (3) rapid increase of the slope when the increasing electric field exceeds 20 kV/mm. It was found that the characteristic response of the lead zirconate thin films was attributed to the electric-field-induced AFE-FE structural transition[3].

With the help of a phenomenological model, the correlation between the field-induced birefringent shift of a material and electric polarization P(E) can be described by the following relation:

$$\Delta n \propto [\, E + \beta P(E)]^2, \qquad (1)$$

where β is a constant dependent on the crystal structure of the material ($4\pi/3$ for cubic structure). The main features for the electrooptic response of the lead zirconate thin films shown in Figure 1 are consistent with those predicted from the dielectric properties (double hysteresis loop) by using relation (1).

To better understand the nature of the antiferroelectric lead zirconate thin films, a static bias electric field was applied to the thin film material in both the dielectric and electrooptic measurements. Thin films deposited on the Pt/Ti coated silicon substrates were used for the measurement of the dielectric behavior. With the increase of the dc bias, the polarization versus E field curve of the lead zirconate thin film gradually evolves from a double hysteresis loop to a single hysteresis loop. As shown in Figure 3, under an appropriate bias field, the shape of the biased single hysteresis loop very much resembles the normal hysteresis loop for ferroelectric materials. Unlike the ferroelectric materials, however, the two remanent states in the biased single hysteresis loop (denoted by P_A and P_B in Fig.3) possess polarizations of different magnitude, which produce two distinguished birefringent states in the thin films. These two birefringent states are clearly represented in the biased birefringence verses E-field curve, as shown in Fig.4, measured from a lead zirconate thin film grown on a fused silica substrate. A static bias field of approximately 17 kV/mm was applied during the measurement. It is obvious that the two distinguished remanent birefringent states Δn_A and Δn_B are associated with the two remanent polarization states P_A and P_B in the biased single hysteresis loop shown in Figure 3. It should be noted, however, that to avoid the breakdown of the electrodes through the air, the bias electric field and the scan range are lower in the measurement of the electrooptic properties than in the measurement of the dielectric property. In addition, because these two measurements involve thin films deposited on two different types of substrates with different directions of applied electric field, quantitative correlation between these two measurements is not possible.

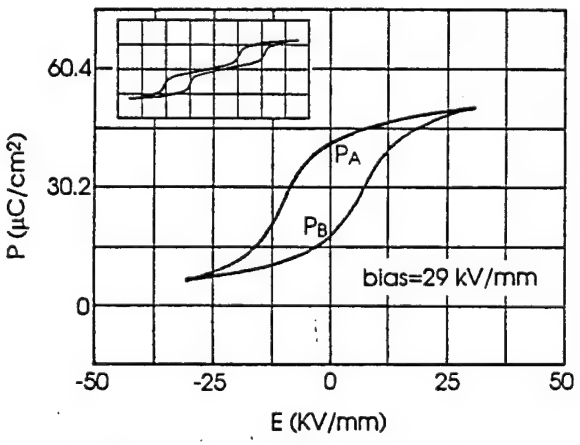

Figure 3 Dielectric properties of a lead zirconate thin film grown on a Pt/Ti-coated silicon substrate, taken under a static bias field of 29 kV/mm. The insert is a hysteresis loop of the same sample taken with zero bias field. The horizontal and vertical scales for the insert plot are 25 kV/mm per division and 30.2 $\mu C/cm^2$ per division, respectively.

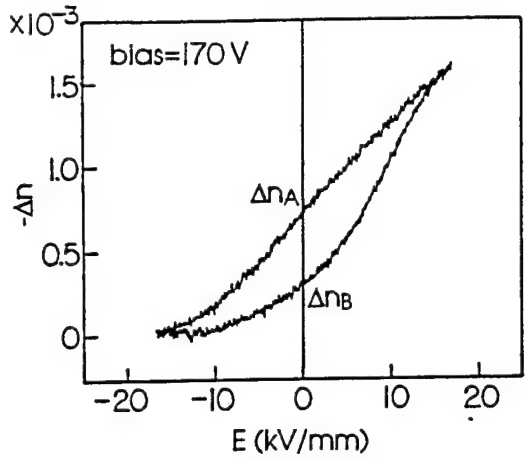

Figure 4 Birefringent shift as a function of the slow varying external field measured with a dc bias field of 17 kV/mm for a lead zirconate thin film on a fused silica substrate.

It was found that the lead zirconate thin films acquired a permanent birefringence once an initial electric field of sufficient magnitude was applied. Shown in Figure 5 is the birefringent shift of a lead zirconate thin film as a function of the slow varying external electric field recorded during the first few cycles of the field scan. In the first half cycle of the field scan, the birefringence of the material drastically increased when the increasing electric field exceeded approximately 16 kV/mm. When the external electric field was reduced to zero, the material retained a significant remanent birefringent shift. During the next few scan cycles, this remanent birefringence kept increasing yet the increment was smaller and smaller after each cycle. A stable remanent birefringence (permanent birefringence) was finally reached as shown previously in the birefringence versus E-field curve of Figure 1. The stable remanent birefringent state, under zero external electric field, was chosen as the zero-

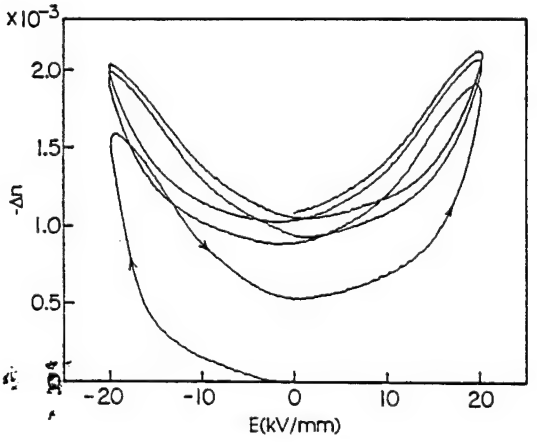

Figure 5 The evolution of the electrooptic response of a lead zirconate thin film on a fused silica substrate during the first few cycles of the electric field scan.

birefringence point in plotting both Figure 1 and Figure 4. After testing a few lead zirconate thin film samples, it was found that this initiating process of the material was reproducible.

The observed permanent birefringence in the antiferroelectric thin films mentioned above may be related to other types of memory behavior previously observed in antiferroelectric lead zirconate materials[8]. A possible explanation for this birefringence memory is that when the AFE-FE phase transition occurred under a sufficiently high electric field the ferroelectric domains are forced to align along the direction of the E-field; although the structure of antiparallel dipoles was restored after the withdrawal of the external E-field, the antiferroelectric dipoles remained preferentially aligned in the direction along which the E-field was previously applied. Such an explanation for the birefringence memory is supported by an optical study of the lead zirconate crystal which showed that the index of refraction is the smallest for the light polarized along the a axis of the antiferroelectric unit cell[9]. This mechanism of birefringence memory is distinguished from that of ferroelectric materials where birefringence memory is mainly caused by the remanent polarization.

The characteristic electrooptic response of the lead zirconate thin films may furnish a means of realizing optical memory in optoelectronic devices. Two different mechanisms may be utilized in optical memory devices. In the first type of memory, the information may be stored in a virgin material by applying a sufficiently high electric field. After the withdrawal of the electric field, as shown in Figure 5, the thin film material becomes permanently oriented and possesses a permanent birefringence of approximately 1.3 10^{-3}. The second type of memory is associated with the two distinguished birefringent states of the thin film materials in the presence of a bias electric field as shown in Figure 4. Because these two birefringent states, Δn_A and Δn_B, are produced by the two remanent states of polarization, P_A and P_B, of the material, they are stable under the bias field. The merit of the second type of memory is that the two birefringent states are electrically switchable. For example, a TIR switch[10] made of the antiferroelectric thin film would allow the inter-switching of the light between the two waveguide channels by electric pulses of opposite polarities, operated under a static bias field. Such a switch is not possible with ferroelectric materials in which the two remanent polarization states are optically equivalent.

Conclusions

The transverse electrooptic property of the solution coated lead zirconate thin film exhibits a characteristic response which is attributed to the electric-field-induced antiferroelectric-ferroelectric phase transition. Under an appropriate static bias electric field, the material possess two distinguishable birefringent states

associated with the two remanent polarization states of the material. The thin films were also found to acquire a permanent birefringence once a sufficiently high electric field was applied to the virgin materials.

Two types of mechanisms are proposed for utilizing the antiferroelectric thin films for optical memory in optoelectronic devices. The first type of memory makes use of the permanent orientation of the material induced by an initial electric field. The second type of memory involves the inter-switching between the two distinguishable birefringent states of the material under a bias field with electric pulses.

Acknowledgment

This study was partially sponsored by the Office of Naval Research under contract No. N00014-91-J-508.

References

[1] G.H. Haertling, "Ferroelectric Thin Film for Electronic Applications," J. Vac. Sci. Technol. A, 9, 414(1991)

[2] D. Bonsurant and F. Gnadinger, "Ferroelectrics for Nonvolatile RAMs," IEEE Spectrum, July 1989, p.30

[3] F. Wang, K.K. Li, and G.H. Haertling, "Transverse Electro-Optic Effect of Antiferroelectric Lead Zirconate Thin Films," Optics Lett. 17, 1122(1992)

[4] K.K. Li, F. Wang, and G.H. Haertling, "Antiferroelectric Lead Zirconate Thin Films Derived from an Acetate Precursor System," J. Mater. Sci. (to be published)

[5] G.H. Haertling, "PLZT Thin Film Prepared from Acetate Precursors," Ferroelectrics, 116, 51(1991)

[6] F. Wang, C.B. Juang, C. Bustamante, and A.Y. Wu, "Electro-optic Properties of (Pb, La)(Zr, Ti)O_3, $BaTiO_3$, (Sb, Ba)Nb_2O_6 and $BaNaNb_5O_{15}$ Thin Films," in Proc. of 4th International SAMPE Electronic Conference, p.712

[7] G. H. Haertling and C.E. Land, "Hot-pressed (Pb, La)(Zr, Ti)O_3 Ferroelectric Ceramic for Electronic Applications," J. Am. Ceram. Soc. 54, 1(1971)

[8] K. Uchino, "Digital Displacement Transducer Using Antiferroelectrics," Japan. J. Appl. Phys. 24, suppl., 24(1985)

[9] F. Jona, G. Shirane, and R. Pepinsky, "Optical Study of $PbZrO_3$ and $NaNbO_3$ Single Crystals," Phys. Rev. 97, 1585(1955)

[10] H. Higashino, T. Kawaguchi, H. Adachi, T. Makino and O. Yamazaki, "High Speed Optical TIR Switchs Using PLZT Thin Film Waveguides on Sapphire," Jap. J. Appl. Phys. 24, suppl., 284(1985)

A PLZT OPTICAL PHASE MODULATOR AND ITS APPLICATIONS

Feiling Wang and Gene H. Haertling
Department of Ceramic Engineering
Clemson University
Clemson, South Carolina 29634-0907

An electrooptic phase modulator was designed and fabricated by using the quadratic electrooptic effect of PLZT ceramic of composition 10/65/35. The modulator can be operated at either the fundamental or double frequency of the AC signal driver. The modulator proved effective as a phase modulation device in a phase-detection measurement of small birefringent shift of thin film materials. The principles for such usage are discussed.

Introduction

Relaxor ceramic materials in the (Pb,La)(Zr, Ti)O_3 (PLZT) system are known to possess strong quadratic or slim-looped transverse electrooptic effects[1]. The applications of the materials in optical area have been found in light shutters, spatial light modulators, second harmonic generation as well as waveguide devices such as total internal reflection switches[2,3]. Although single crystal materials that possess linear electrooptic effects such as $LiNbO_3$ and KDP have traditionally been the primary material group for optical phase modulation, polycrystalline PLZT ceramics which possess quadratic electrooptic effects can also be used as optical phase modulation media. In this report, an optical phase modulator made from a hot-pressed PLZT ceramic is presented. The application of the modulator in a phase-detection technique for the measurements of small optical phase retardation in thin film materials is discussed.

Design and Operation

A bulk 10/65/35 PLZT wafer was chosen as the modulating medium. The material was made with a hot pressing process using stoichiometric powder derived from a water-soluble precursor. The material was transparent and showed typical dielectric properties for the material in this composition, i.e. high dielectric constant and very slim hysteresis loop. The electrooptic characterization showed that the dependence of the birefringence shift on the external electric field was primarily quadratic, as presented in Figure 1. The thickness of the PLZT wafer was 0.5 mm (20 mil) with both sides being optically polished. To accommodate the ac driving signal, copper planar electrodes were fabricated on one side of the material by a photolithography technique. The electrode gap width was 50 μm, which allowed a light beam to pass the device without a special focusing effort. An ac electric signal of adjustable amplitude was fed to the electrode pair to drive the modulator. In addition, an adjustable dc bias was also applied to the modulator.

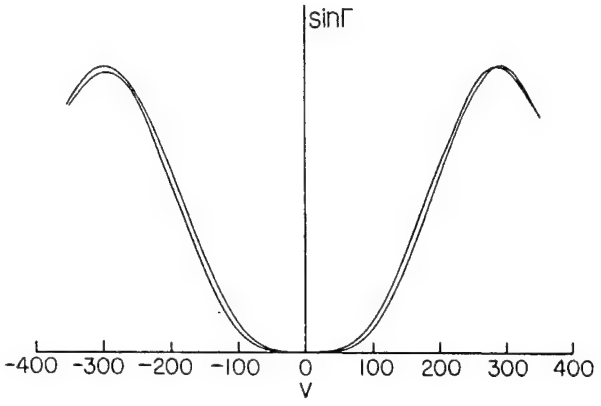

Figure 1 The electrooptic response of a 10/65/35 PLZT ceramic, measured by means of a phase-detection scheme. The Y axis is proportional to sinΓ with Γ being the optical phase shift due to the birefringence of the material.

Under sufficiently small external field, the field-induced birefringent shift of the material can be expressed as a quadratic function of the applied field:

$$\Delta n = \text{constant}\,(E_b + E\sin\Omega t)^2\,, \qquad (1)$$

where E_b is the field strength of the dc bias, Ω is the frequency of the ac driving electric field. It is obvious that under a non-zero bias field, the phase shift generated by the modulator contains both Ω and 2Ω components. By adjusting the bias field E_b, the relative amplitude of Ω and 2Ω components can be altered. The function of the bias field in changing the primary modulating frequency is illustrated in Figure 2 where function Γ(t) is the phase retardation produced by the modulator.

To visualize the phase modulating function of the modulator and the interchange of the modulating frequency with the bias electric field, the modulator was sandwiched between two crossed polarizers with the modulation axis, the direction of the applied electric field, being oriented at 45 degree angle with respect to the polarization direction of the polarizer. With such a arrangement the polarization state of the originally linearly polarized light beam was periodically changed due to the phase shift Γ(t) imposed by the modulator. The intensity of the light output I(t) is given by:

$$I(t) = B\sin^2[\Gamma(t)/2] = B\sin^2[A(E_b + E\sin\Omega t)^2]\,, \qquad (2)$$

CH3080-0-7803-0465-9/92$3.00 ©IEEE

where A and B are two system constants. The waveform of the light intensity given by Equation (2) is graphically analyzed in Figure 2. As shown by the figure, the modulation is purely 2Ω in frequency at zero bias and gradually becomes dominated by the Ω component with the increase of the bias electric field.

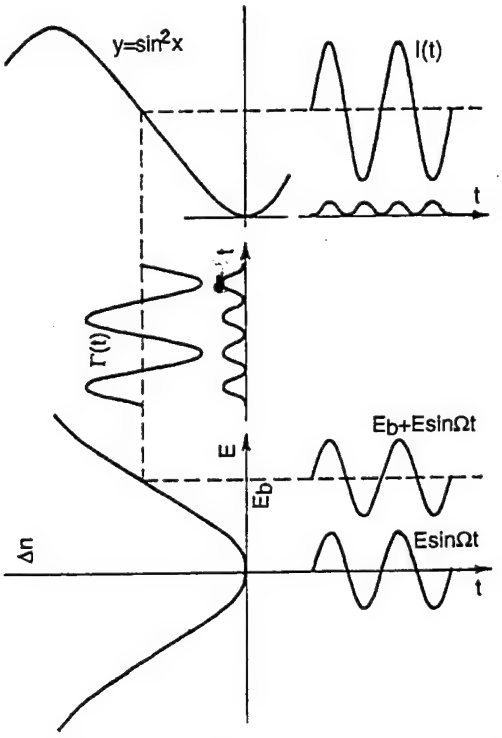

Figure 2 A graphic analysis of the operation modes of the PLZT phase modulator with and without dc bias field.

According to Equation (1), the modulation always contains a 2Ω component although its relative magnitude becomes very small compared to the Ω component when a sufficient bias field is applied. A pure Ω modulation mode can actually be achieved by using the saturation behavior in the electrooptic response of the material. The saturation behavior of the electrooptic response in PLZT materials have been observed[4,5]. In the presence of such saturation, the quadratic relation for the field-induced birefringence is no longer adequate; higher order terms or entirely new functional dependence needs to be used. In the electrooptic response curve that shows saturation behavior, there must be a point where the second derivative of the curve is zero. If a bias electric field is applied to this point, the modulation will be purely Ω in frequency.

In practice, only a iairly low bias field is needed in order for the modulation at 2Ω frequency to become insignificant compared to the Ω component. Figure 3 shows the waveforms of the light output, recorded by an oscilloscope, from the second polarizer with the PLZT modulator driven by a 1kHz ac signal operating under various dc bias voltage. The square waves in the pictures are the trigger signal synchronized with the ac driving voltage. As expected, the modulation was purely 2Ω in frequency under zero bias and eventually became dominated by Ω frequency components under a bias voltage of 150 volts. Components of both frequencies are clearly represented under an intermediate bias, as shown by Figure 3(b). The relative amplitude of modulation at both frequencies as functions of the dc bias was measured by a lock-in amplifier synchronized with the driving function generator. As shown in Figure 4, with the increase of the dc bias voltage, the amplitude of the 2Ω component decreased while the Ω component increased. Under a bias voltage of approximately 120 volts the 2Ω component becomes zero while the Ω component approaches a maximum. Under this bias voltage, the PLZT modulator provides

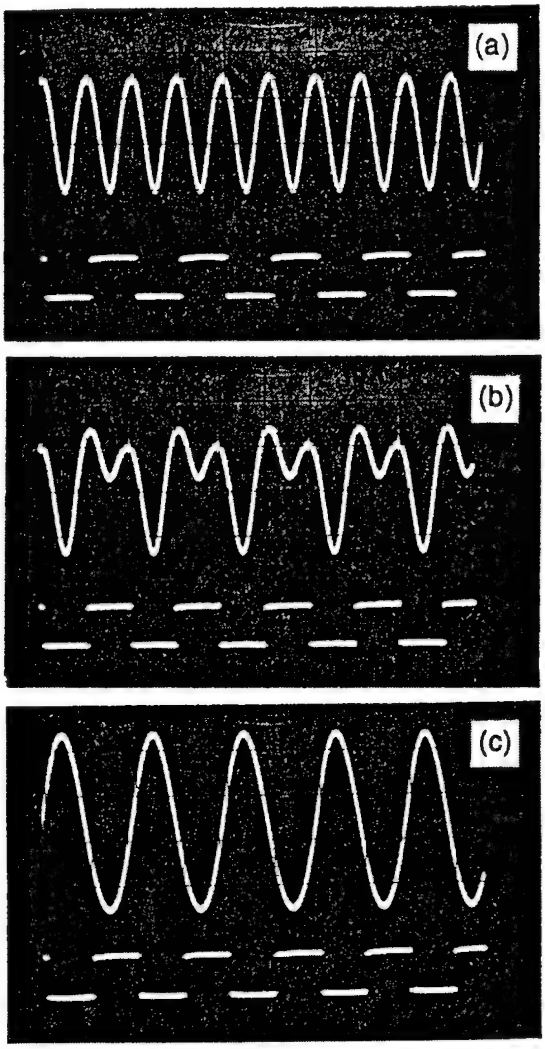

Figure 3 The waveforms of the output light modulated by the PLZT phase modulator operated under (a) bias=0V, (b) bais=20V and (c) bias=150V.

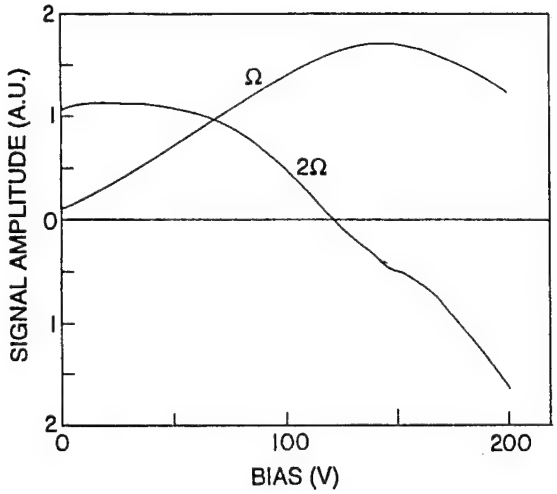

Figure 4 The Ω and 2Ω frequency components in the light modulated by the PLZT phase modulator plotted as functions of the bias voltage.

the same modulation as that from a traditional modulator utilizing the linear electrooptic effect of single crystals, except that there is a constant phase shift. The constant phase shift can be compensated with an optical compensator in applications where it is not desirable. Much lower ac driving voltages are needed to achieve the same phase modulation depth for the PLZT modulator than for traditional modulators because of the strong quadratic electrooptic effect in the PLZT ceramic.

Applications

The PLZT phase modulator has been successfully used as a phase modulation device in a phase-detection scheme for the measurement of small birefringences of thin film materials. The optical arrangement for such application is shown in Figure 5. The PLZT compensator together with an optical compensator and the sample to be measured are sandwiched between two crossed polarizers. The modulating axis of the modulator is oriented 45 degrees with respect to the polarizer but parallel (or perpendicular) to the principle optical axes of the sample determined by the direction of the external electric field. The purpose of the compensator is to compensate the constant phase shift generated by the modulator and to calibrate the system.

With the PLZT phase modulator being driven by an ac signal of frequency Ω under zero bias, the total phase retardation for the light polarized along the modulating axis consists of contributions from all three components, namely, modulator, compensator and sample:

$$\Gamma = \Gamma_{mod.} + \Gamma_{comp.} + \Gamma_{samp.} \qquad (3)$$

As been previously pointed out, the electrooptic effect of PLZT materials exhibits high order field dependence and saturation behavior in some circumstances. The phase modulation produced by the PLZT modulator, therefore, should be expressed by the following Fourier series:

$$\Gamma_{mod.}(t) = \text{constant} + \sum_{m=1}^{\infty} C_m \sin 2m\Omega t\,, \qquad (4)$$

where coefficient C_1 is proportional to the quadratic electrooptic coefficient of the PLZT modulating medium; C_2 is proportional to the quartic electrooptic coefficient, etc. Although in most instances only C_1 needs to be considered, the whole summation in Equation (4) is retained for the strictness of the following discussion.

By adjusting the compensator, the constant in Equation (4) can be eliminated; therefore we have

$$\Gamma(t) = \sum_{m=1}^{\infty} C_m \sin 2m\Omega t + \Gamma_{samp.} \qquad (5)$$

The light intensity detected by the photomultiplier tube (PMT) is therefore given by

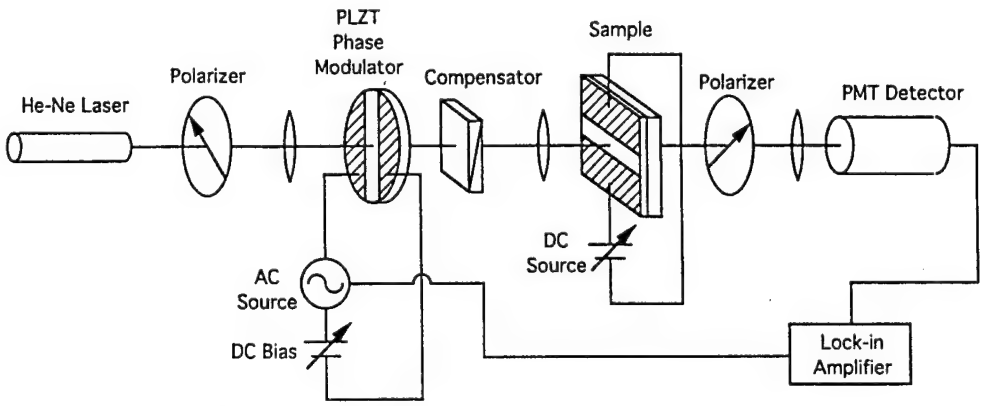

Figure 5 The optical arrangement in a phase-detection scheme using the PLZT modulator as a phase modulating device.

$$I(t) = I_o \sin^2(\Gamma/2)$$

$$= (I_o/2)[1 + \cos(\sum_{m=1}^{\infty} C_m \sin 2m\Omega t + \Gamma_{samp.})]. \quad (6)$$

If the reference signal of the lock-in amplifier is chosen as $\sin 2\Omega t$, the output signal of the lock-in amplifier, S, is proportional to the amplitude of the $\sin 2\Omega t$ term in the Fourier expansion of Equation (6), that is

$$S = D \int_0^t I(t) \sin 2\Omega t \, dt$$

$$= D \int_0^t \cos(\sum_{m=1}^{\infty} C_m \sin 2m\Omega t + \Gamma_{samp.}) \sin 2\Omega t \, dt \quad (7)$$

where D is a system constant. It can be shown that the above integration is approximately given by

$$S = D \, J_1(C_1) \sin\Gamma_{samp.} \quad (8)$$

where J_1 is the Bessel function of the first order. With a fixed driving signal amplitude, C_1 is a constant; the output signal from the lock-in amplifier therefore is proportional to the phase retardation generated by the sample, namely, $\Gamma_{samp.}$. Moreover, in detecting the electrooptic effect of thin film materials, the phase retardation of the sample is usually very small so that the output from the lock-in amplifier becomes directly proportional $\Gamma_{samp.}$ while the proportional constant can be determined by the compensator.

With the PLZT phase modulator, the above scheme has proven an effective way of detecting very small phase retardations produced by electrooptic effects in thin film materials. As an example, Figure 6 shows the birefringence versus E-field curve of a 2/55/45 thin film of 0.5 μm thick grown on a fused silica substrate, measured with the above phase-detection system under zero-bias mode.

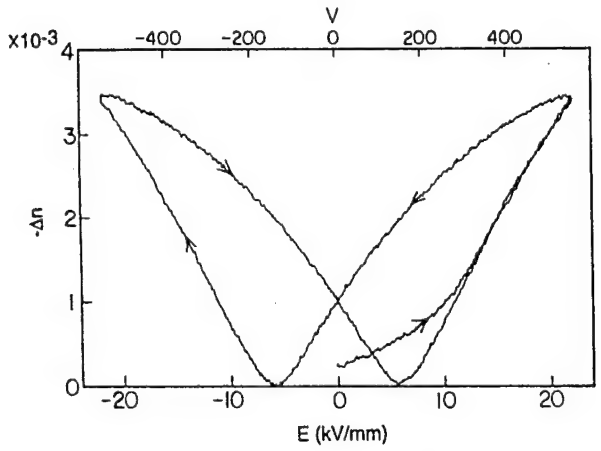

Figure 6 The birefringence versus E-field curve for a 2/55/45 PLZT thin film of 0.5 μm thickness sputter-deposited on a fused silica substrate, measured with the phase-detection scheme using the PLZT phase modulator.

When an appropriate bias field is applied, the modulation becomes predominated by the Ω component. With the reference signal of the lock-in amplifier set at $\sin\Omega t$, the above measuring system functions similarly as in the zero-bias mode.

Conclusions

An optical phase modulator was made by using the quadratic electrooptic effect of a hot-pressed PLZT ceramic. The device can be operated in a zero-bias mode which provides a modulation at double the frequency of the driving signal. When an appropriate bias is applied, the modulator provides a modulation dominated by the component at the frequency of the driving signal. Application of the PLZT modulator has been found in the phase-detection scheme for the measurement of very small birefringence in thin film materials.

References

[1] G.H. Haertling and C.E. Land, "Hot-pressed $(Pb,La)(Zr,Ti)O_3$ Ferroelectric Ceramic for Electronic Applications," J. Am. Ceram. Soc. 54, 1(1971)

[2] G.H. Haertling, "PLZT Electrooptic Materials and Applications-A Review," Ferroelectrics, 75, 25(1987)

[3] H. Higashino, T. Kawaguchi, H. Adachi, T. Makino and O. Yamazaki, "High Speed Optical TIR Switches Using PLZT Thin Film Waveguides in Sapphire," Japan. J. Appl. Phys. 24 suppl., 284(1985)

[4] F. Wang and A.Y. Wu, "Electro-optical and Nonlinear Optical Properties of Thin Film Materials Containing Oxygen-Octahedra under High DC Electric Field," Proc. 7th Intern. Symposium on the Application of Ferroelectrics, pp.131-134, Urbana, IL, June 6-8, 1990.

[5] G.H. Haertling, unpublished results.

AUTOMATED SYSTEM FOR PROCESSING OF PLZT POWDERS DERIVED FROM ACETATE PRECURSORS

J. R. Barrett and E. C. Skaar
Department of Ceramic Engineering, Clemson University
Clemson, S. C. 29634-0907

Abstract

An IBM-PC based system to produce and control the production of PLZT powders from acetate precursors is described. Problems with the development of appropriate sensing systems and algorithms are discussed. A proposed prototype system is presented.

Introduction

The increasing need for better manufacturing methods for new (and old) materials has been the purpose for this study. In advanced materials systems, it is often necessary to very closely monitor a process, which can be very expensive if the procedure is too complicated or too abstract to be overseen by conventional sensors and computer equipment. The development of advanced sensors can enable the reduction of labor-intensive procedures. [1] The use of advanced sensors in conjunction with high-level control methods, such as artificial intelligence, can result in a cheaper, yet higher quality product in processes that may involve complicated processing steps. This study examines the use of software and hardware combined in an automated process to produce PLZT powders from water soluble acetate precursors.

Intelligent Processing of Materials

The purpose of the method of Intelligent Processing of Materials (IPM) is to reduce the period between materials development and the production of those materials while at the same time increasing the quality of the product. The quality that is achieved through the IPM process is built-in during production and not the result of an inspection after manufacture. [1] IPM is desirable because it can improve the quality, reliability, and the yield of processed materials. [2] IPM combines the expertise of the process engineer and the knowledge of the materials scientist through the use of an expert system. [2] The expert system is a computer's software that is an application of artificial intelligence which utilizes efficient and effective data handling and retrieval to analyze and predict processing events. [3] The system is designed in such a way that corrections and/or compensations may be made instantaneously in a process so that the result is a high-quality product. This system monitors all processing steps from raw material characteristics to the final product during the manufacturing so that changes can be made in each step and in future steps to achieve the highest quality product. Process models and real-time sensors are heavily relied upon in the IPM strategy so that higher levels of control and awareness than in conventional processes can be attained. In-situ sensors can monitor complex characteristics such as microstructure in real time and combine this data with conventionally sensed data, such as temperature or viscosity, and the resulting combination is used by the expert system to make process judgements. [1] It is through these judgements that the process is improved continually to compensate for process and raw material variability.

To implement IPM in the production of powders from PLZT acetate solutions, a production process that is compatible with the requirements of an automated process is needed. The production process must be completely defined. The entire process for this system includes: the making of PLZT acetate solutions, the precipitation of a solid, the separation of the solid from the liquid, and the processing of the solid into a powder. As the process is defined, process variables are defined and assessed. These variables must be isolated and treated in a manner that is consistent with the IPM process. It is also important that the equipment that makes up the system be compatible so that it can be linked efficiently and effectively. The hardware, such as mixing equipment, valves, and sensors must be linked to the software (computer) that runs the system. The hardware and software are the two major components of any IPM system, and each has its own purpose.

Sensors

One of the common measurements in a coprecipitation process is the pH of the solution. However, pH measurements have been found to be impractical and not suited for automated processes for this particular material system. The presence of acetic acid, either from addition or from the bulk raw materials, and the high methanol concentration of the water soluble solutions prohibits an accurate and reliable measurement of pH because the glass bulb of the pH probe is strongly attacked under these conditions. [4] The pH measurement is based on the Nernst equation, which assumes that the hydrogen ion activity is equal to the hydrogen ion concentration. However, the Nernst equation is not valid for low hydrogen ion concentrations, and that is the condition that exists with this system. In addition, the ammonium hydroxide used as a precipitating agent destroys the hydrated layer that is used to generate the potential difference for a pH reading. The potential difference is the signal that is converted to a pH value. It is possible to take pH measurements in this system in a laboratory environment, but it is not possible to implement this sensing method in an automated process because of the constant maintenance that is required to keep the pH electrode in operating condition. A long stabilization time for a pH reading also contributed to the decision that pH is not suitable for this IPM procedure.

A method of sensing material properties that has been found to be useful for automated processes is the measurement of resistivity/conductivity. A two-conductor probe was constructed and tested for reading stabilization (response) time and stability of the reading over extended time periods with no probe maintenance. The first attempts to use the probe were made using direct current as the electrical source. It was found that DC measurements would not stabilize or would stabilize only after a long period of time. Because the solutions are polar in nature, it is believed that a polarization of the solution was taking place, causing the readings to drift. As a result, alternating current was used as the electrical source. Using the same probe, as shown in Figure 1, the AC measurement resulted in a quick reading response time, in the range of two to five seconds. The stabilization of the reading was also satisfactory, as the readings stabilized almost immediately. The probe was left in a variety of raw material, solvent, and batch solutions for periods of hours to days, and the readings were extremely stable.

The voltage measurement of the solution, V_2, was used to

CH3080-0-7803-0465-9/92$3.00 ©IEEE

find the resistance of the solution after the current, I, was found using Ohm's Law for the known resistor in the probe system and measuring the voltage across it, V_1. The change in resistance of the solution as the constituents were added to make a 9/65/35 PLZT acetate solution batch for coprecipitation was plotted against the weight of the total batch, as shown in Figure 2. An order of addition of constituents was chosen to best suit the homogeneity of the batch.

Generally, the resistance of the total batch solution increased as each constituent was added. This result is encouraging evidence that an AC resistance probe can be used in an IPM process for PLZT acetate solutions when an expert system has "learned" the characteristics of the batching process with respect to change in solution resistance vs weight of addition. The constituent that shows a possible exception for the upward trend is lead subacetate, for which the resistance decreased after a point. However, the neural network that runs the system can be "trained" to compensate for this result. Naturally, the weight of the batch must be monitored and the process model for this procedure must be available to the network, so that the computer can tailor the batching additions and other parameters to fit the model. At this point in the development of the system, it is believed that the lead subacetate data may actually not be much cause for concern. Because of the difficulty in keeping the material dissolved during this particular test and other conditions, such as the high evaporation rate in this open-air test, there is reason to believe that a test of a larger batch size in a closed container should solve the problem.

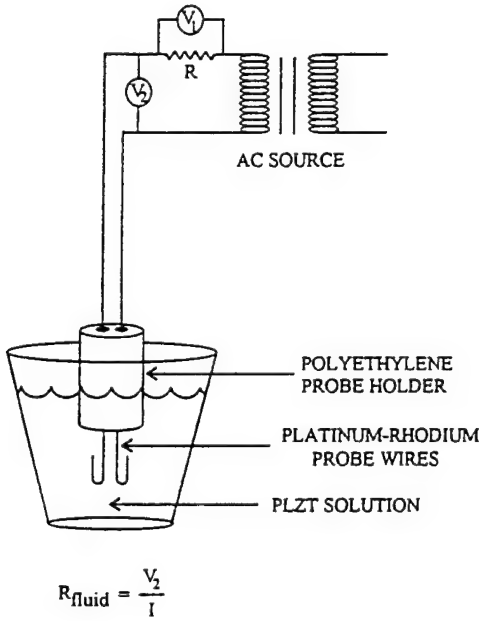

Figure 1. Method of measuring resistance of PLZT acetate solution using alternating current.

Algorithm Development

The control algorithm for this process is a two part algorithm. The first part is a normal weighing or batching algorithm. It contains a database of recipes for the solutions required to make powders of various compositions. As long as the process does not vary, and all the settings remain constant, the process is capable of running with this section of the algorithm alone. The second part of the algorithm (currently under development) is designed to sense problems and make corrections to the process.

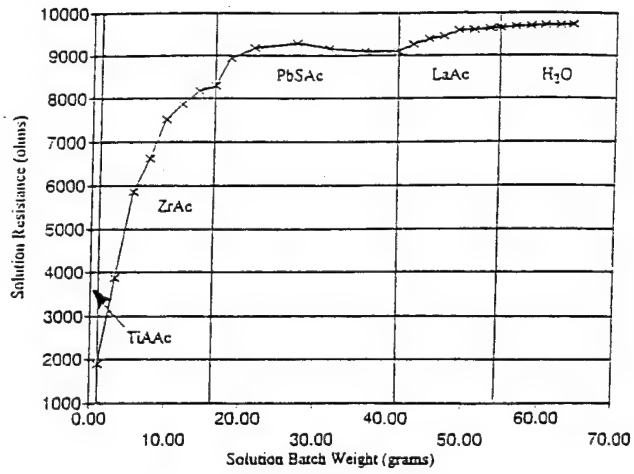

Figure 2. Solution resistance (AC measurement) for the total PLZT acetate batch as constituents were added.

This second section is an artificially intelligent program based on a neural network. It is designed to sense "out of control" conditions and make appropriate corrections to the weighing or batching algorithm.

Neural networks excel at pattern recognition, diagnosis, and decision making. [5] The idea behind this section of the algorithm is to recognize an assignable problem as it develops, and compensate. In a sense, the computer is programmed to utilize statistical process control.

For example, suppose the metering mechanism for one of the constituents became partially clogged. The result would be a variance from normal with respect to the weight and the resistance measurements for the batch. The pattern of these measurements would change. The neural network would be taught to recognize this pattern, and effect the appropriate compensation. Other types of assignable problems would also present their unique patterns which the neural network would be taught to recognize.

The unique beauty of using neural network technology for this application is that the teaching of the network is not a function of programming, but rather simulation. For the network to function, it has to be taught the patterns that specific problems create. We accomplish this by actually simulating the problem in the process. The network is programmed to learn and recognize the resulting sensor patterns. Once the network recognizes the pattern, it is programmed to compensate for the deficiency. A properly designed network, therefore, does not depend upon an exhaustive database of every problem. Rather, as experience is gained with a process, the problems and solutions can be taught to the network. The algorithm improves with operating experience and thus the process can proceed toward optimization.

Automated Batching System

The entire automated process for the production of PLZT acetate powders that is being developed has many parts that need to be both optimized and automated. The section of the process that has received the greatest attention to this point in the development of the total process is the automated batching system. Figure 3 shows this system, which utilizes manually filled reservoirs containing the liquified constituents of the PLZT acetate system which supply smaller, computer-controlled reservoirs that are used to dispense batch amounts. A switch system that consists of two stainless steel screws and a low current is used as a liquid-contact switch such that when the valve from the larger, manually controlled reservoirs is opened, the fluid will flow until the liquid

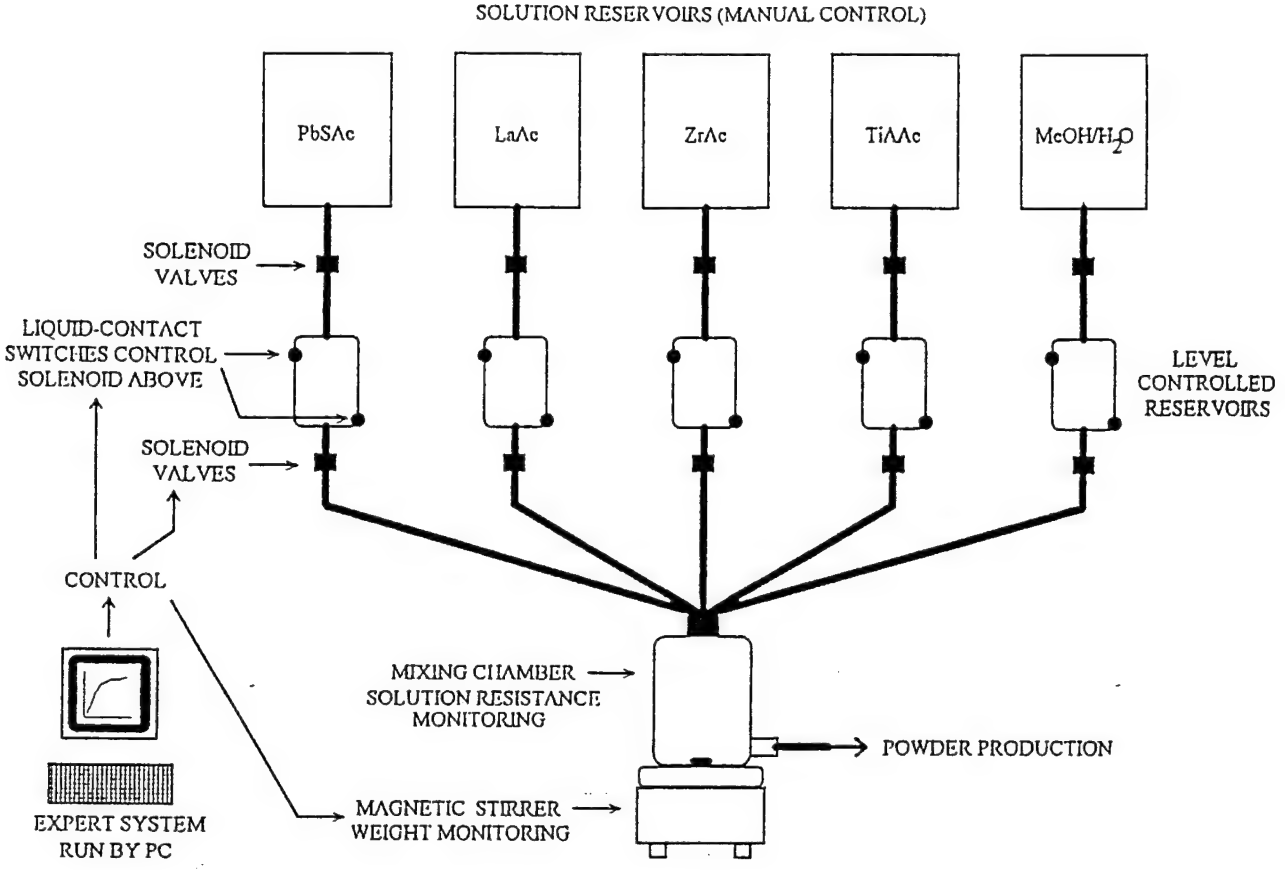

Figure 3. Automated solution batching system controlled by IBM PC.

completes the circuit between the two contacts. The contacts are positioned at the top and at the bottom of the reservoir. The flow of fluid in the system is controlled by sets of solenoid valves that are run by the computer. Once the circuit is completed, as the fluid fills the reservoir, the switch will be activated and the solenoid valve will be closed by the computer to stop the fluid flow. Then, the valves of the smaller dispensing reservoirs are opened for a time period that has been previously determined, based on material characteristics, to a larger mixing reservoir. The longer the time that the valve is opened, the more fluid is added to the batch.

The weight of the constituent is checked and recorded by the computer to check the accuracy of the system. The AC resistance probe will also be used here to detect any changes and be a part of the control in the batching procedures. The system is designed to be able to compensate for clogging of the valves and changes in viscosity by taking in data on the raw materials and the trends in the process. The expert system can then execute an order to make a change in the process parameters if it is necessary to keep the process at the correct level, such as leaving the valve open a longer or shorter period of time. The next step is the mixing of the constituents. After mixing, a valve is opened and the constituents will flow into the precipitation reactor for the coprecipitation process.

The automated batching system will be run by the expert system in a manner in which it will be possible to enter the desired composition of the PLZT acetate solution to be made, and then the process will be changed to yield the correct amounts of each constituent needed.

Summary

The requirements for the use of better manufacturing methods in the production of materials that normally require labor-intensive procedures have been the reason for this study. The reduction of labor hours and the susbstantial improvement in quality of the materials that is possible are the integral in the theory of Intelligent Processing of Materials. An expert system can be used to develop algorithms to control the system if sensors and sensing methods can be improved or developed to suit the needs of such a data intensive system. The next step in the automation of this process is the linking of the system to the other components that are needed in the process, a coprecipitation step and a calcination/powder production step.

Acknowledgement

This work was supported by the Office of Naval Research under contract number N00014-91-J-1508.

References

[1] H. T. Yolken, "Intelligent Processing of Materials," Materials Research Society Bulletin, April 1988, p. 17.

[2] B. G. Kushner and P. A. Parrish, "The Intelligent Processing of Advanced Materials, " Intelligent Processing of Materials and Advanced Sensors, 1987, pp. 173-184.

[3] P. A. Parrish, "Design and Manufacturing of Advanced Materials and Structures," Intelligent Processing of Materials, 1990, pp. 3-15.

[4] Private Communication, Fisher Scientific, Pittsburgh, February 1992.

[5] NeuroWindows, Ward Systems Group, July 1991, pp. 1-3.

PLZT POWDERS FROM ACETATE PRECURSORS VIA COPRECIPITATION

C. Lin, B. I. Lee, and G. H. Haertling
Department of Ceramic Engineering
Clemson University, Clemson, S.C. 29634

Abstract: Various chemical coprecipitation techniques used for the production of PLZT 2/55/45 (La/Zr/Ti) powders were investigated. The coprecipitation condition corresponding to 0.5 M oxalic acid at a titration rate of 24 cc/min and at a temperature of 21°C yielded the largest surface area calcined powders, hence this condition was selected as the optimum in regard to sinterability of the powders. The characteristics of the PLZT 2/55/45 powders under the best precipitation condition were observed and evaluated. It was found by means of FTIR and XRD that the perovskite phase formation occurred at 550°C .

Introduction

There has been great interest in lead-based perovskite ferroelectric compounds within the $(Pb_{1-x},La_x)(Zr_y,Ti_{1-y})_{1-x/4}\ O_3$ system owing to their distinct electrooptic properties and their utilization for transparent ferroelectric ceramics[1, 2] . The purpose of the present work was to observe the characteristics of PLZT 2/55/45 powders obtained from some specific precipitation conditions. Before selecting the final precipitation condition, some important factors relating to the precipitation process were selected i.e., (1) type, (2) concentration, (3) rate of titration and (4) temperature of precursors. These coprecipitation conditions were then screened in regard to the specific surface area of powders obtained from these conditions. Finally, the condition for the formation of PLZT phase was investigated by heat treatment.

Experimental Procedure

Selection of Experimental Conditions

The system of the experimental design[3] is given as in Table 1.

Table 1. PLZT Coprecipitation Conditions

Type	C	K	T	R
1	0.35M	ox	21°C	12 cc/min
2	0.35M	amc	50°C	24 cc/min
3	0.50M	ox	21°C	24 cc/min
4	0.50M	amc	50°C	12 cc/min
5	0.65M	ox	50°C	12 cc/min
6	0.65M	amc	21°C	24 cc/min
7	0.80M	ox	50°C	24 cc/min
8	0.80M	amc	21°C	12 cc/min

C: Concentration (unit: Molarity).
T: Temperature of precursors.
R: Rate of titration of precipitating agent.
K: Kind of precipitating agents.
(for brevity, ox: oxalic acid solution ; amc: $(NH_4)_2CO_{3(aq)}$)

Powder Preparation

The starting precursor chemicals used in this study were lanthanum acetate (LaAc), zirconium acetate (ZrAc), lead subacetate (PbsubAc) and Titanium acetylacetonate (Tiacac). The oxide content (wt%) of each precursor and the stoichiometric batch proportions are given in Table 2.

The flowchart representation for the overall preparation process is shown in Figure 1.

Table 2. Precursor and Batch Weight Proportions for PLZT 2/55/45

Oxide	PbO	La2O3	ZrO2	TiO2
mole ratio	0.98	0.01	0.547	0.448
Precursor (oxide wt %)	78.6	6.78	22.61	16.96
Precursor	PbsubAc	LaAc	ZrAc	Tiacac
Batch (0.0307 mole)				
Batch weight	8.537g	1.474g	9.144g	6.742g

Powder Production

Type 1 Coprecipitation Process The conditions for this process were C=0.35M, K=ox., T=21°C, and R=12 cc/min. A clear solution of 9.305 g ZrAc, 1.474 g LaAc, 6.970 g Tiacac and 8.536 g PbsubAc was prepared in 75 ml of methanol . The solution was titrated at the rate of 12 ml/min with 100 ml 0.35M oxalic acid solution under constant stirring and a constant temperature of T=21°C by means of a water bath. The precipitate suspension was stirred for 5 additional minutes after the titration was completed. Then, the entire precipitate suspension was poured into a stainless pan and was dried in an oven at 70°C. The dried powder was calcined for 7 hours in air at 550°C. The specific surface area of the powders obtained above was measured using the BET multi-point method (Model: Micromeritics, Gemini 2360).

Types 2-8 Coprecipitation Processes The conditions were the same as Type 1 except concentration, kind, temperature and rate were changed according to Table 1.

Direct Pyrolyzation Process The conditions were the same as that of Type 1 except no precipitating agent was involved.

Spray Pyrolysis Process The conditions were the same as Type 3. After titration, drying was performed by spraying the colloidal precipitate suspension into a tube furnace at 450°C. The powders were collected at the exit of the furnace.

CH3080-0-7803-0465-9/92$3.00 ©IEEE

Characterization of PLZT 2/55/45 Powders

Five samples obtained from the optimum coprecipitation condition Type 3 were processed separately with five different heat treatment conditions: (1) 220°C/2 hrs, (2) 400°C/4 hrs, (3) 500°C/7 hrs, (4) 550°C/4 hrs and (5) 550°C/7 hrs. The properties of the PLZT powders were measured using FTIR (Perkin-Elemer 1600 on KBr pellet absorbance mode), X-ray diffraction (Scintag XDS 2000, Cu Kα-radiation) and electron microscopy SEM (JEOL, JSM-848).

Results and Discussion

Selection of the best coprecipitation condition

The Type 3 coprecipitation condition was evaluated as the best condition in regard to the results of the specific surface area as shown in Table 3.

In Table 3, it was noted that the low surface area of uncalcined powders in Types 2, 4, and 6 resulted from aggregation of powders during degasing (200°C/2 hrs) in the BET test, while the low surface areas of uncalcined powders in Types 7 and 8 were mainly due to supersaturation. Also, as shown in Table 4, it indicates that a higher titration rate (comparison between Types 1 and 3 in oxalates) enhances larger number of nuclei of a new phase as well as more rapid precipitation[4]. This results in finer particles with higher surface area in both uncalcined and calcined powders. The effect of temperature as shown in Table 5 indicates that low temperature was favorable for forming powders with higher surface area. This was interpreted that high temperature affects nucleation and hence larger particles due to growth. The effect of kind of precipitant as shown in Table 6 indicates that oxalic acid was a better precipitant.

Table 3. Specific Surface Area of PLZT Powders.

Type	Uncalcined	Calcined (550°C/7 hrs)
1	67.15 (m^2/g)	4.67 (m^2/g)
2	1.65	4.24
3	79.64	16.21
4	1.89	3.50
5	31.11	4.96
6	2.65	2.96
7	2.75	10.60
8	2.02	1.72
MOD	1.82	2.04

Table 4. Mean Effect of Titration Rate on Surface Area of PLZT Powders via oxalate precipitation.

Rate	Uncalcined	Calcined (550°C/7 hrs)
12 cc/min	49.13 (m^2/g)	4.82 (m^2/g)
24 cc/min	41.20	13.48

Table 5. Mean Effect of Temperature on Surface Area of PLZT Powders via oxalate precipitation.

Temperature	Uncalcined	Calcined (550°C/7 hrs)
50°C	15.93(m^2/g)	7.73 (m^2/g)
21°C	73.40	10.44

Table 6. Mean Effect of Kind of Precipitant on Surface Area of PLZT Powders.

Kind	Uncalcined	Calcined (550°C/7 hrs)
ox	45.18 (m^2/g)	9.11 (m^2/g)
amc	2.05	3.11

As shown in Figure 1 , the various processes involve liquid state mixing at the molecular level. The mixed solutions of Pb, La, Zr, and Ti precursors was coprecipitated as the oxalates or carbonates. The selection of the best coprecipitation condition was based on the largest specific surface area of the resulting PLZT 2/55/45 powder. It was found that the conditions of Type 3 coprecipitation (i.e., 0.5M oxalic acid titrated at 24 cc/min at 21°C) were optimum for producing submicron PLZT 2/55/45 powders.

The FTIR spectra of powders prepared under different calcining conditions are shown in Figure 2. The spectra show reduction in the absorbance peaks at ~1700 cm^{-1}, which is due to C-O vibration, as the calcination temperature and/or time increased. On the other hand, the peak at ~575 cm^{-1} is due to metal-oxygen bond, more specifically ZrO_6/TiO_6 octahedra vibrational mode. The increase in the peak size as the degree of calcination increased indicates the formation of crystalline PLZT powder. The small peaks at ~1600 - 1700 cm^{-1} are believed to be originated from the impurities in KBr and at ~1490 cm^{-1} from acetate . The spectra show that calcination at 550°C for 4 hrs is nearly sufficient to calcine PLZT powder for the given coprecipitated powders. There are always absorbance peaks around 2920 cm^{-1} which correspond to the residual carboxylic acid functional groups, i.e., oxalic acid.

The X-ray diffraction pattern shown in Figure 3 indicates that the Type 3 coprecipitated PLZT powder is a mixed phase which is composed of a perovskite PLZT phase and lesser pyrochlore phase ($2\theta=27.93^0$ only) with an approximate mean particle size[5, 6] of 18 nm. This approximation is a calculated value based on the Scherrer relationship of the X-ray diffraction broadening. Improved results for achieving the perovskite phase were obtained by spray pyrolysis as shown in Figure 4. The reason is that spray pyrolysis provides a looser agglomeration of the uncalcined powders which is favorable to forming a better diffusivity environment for the gaseous products during thermal decomposition.

SEM micrographs in Figures 5-6 show the morphologies of the submicron particles.

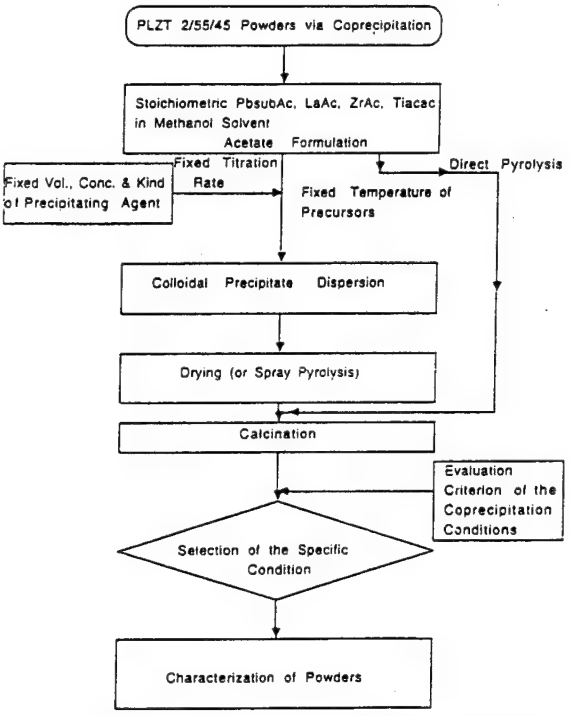

Figure 1. Flowchart of Coprecipitation Processes for PLZT 2/55/45 Powders.

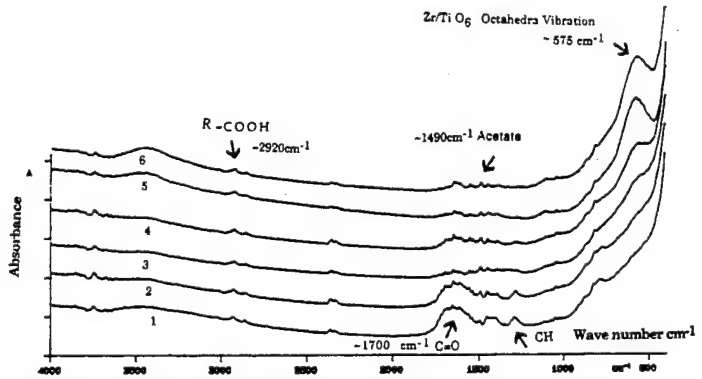

Figure 2. FTIR spectra of PLZT powders: (1) no calcination, (2) 220°C/2 hrs, (3) 400°C /4 hrs, (4) 500°C /7 hrs, (5) 550°C /4 hrs and (6) 550°C /7 hrs.

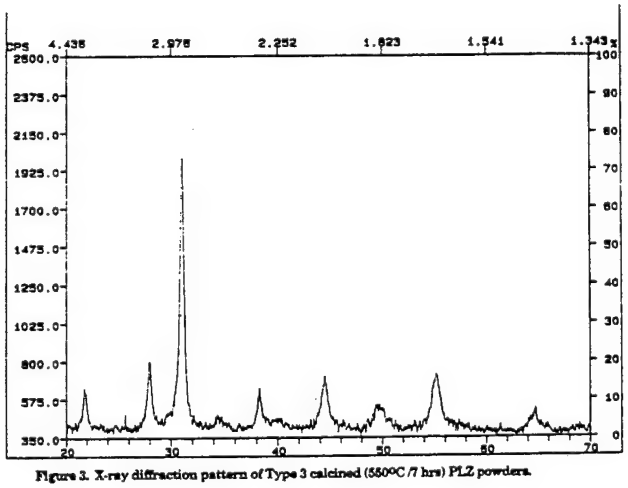

Figure 3. X-ray diffraction pattern of Type 3 calcined (550°C /7 hrs) PLZ powders.

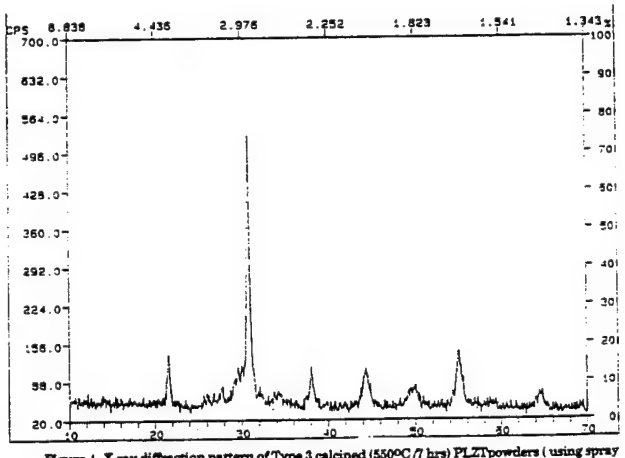

Figure 4. X-ray diffraction pattern of Type 3 calcined (550°C /7 hrs) PLZTpowders (using spray pyrolysis instead of drying).

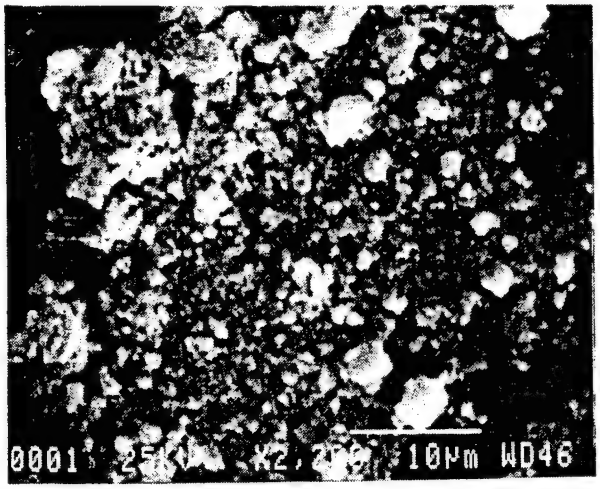

Figure 5. SEM micrograph of Type 3 uncalcined PLZT powder.

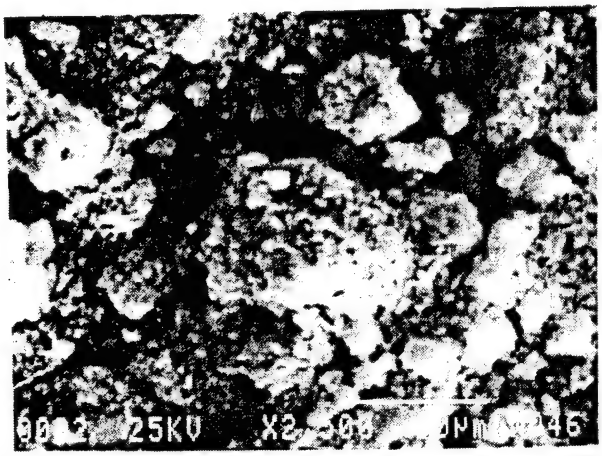

Figure 6. SEM micrograph of Type 3 calcined (550°C/7 hrs) PLZT powder.

Conclusions

There were totally eight coprecipitation processes evaluated in the production of PLZT powders. The oxalates yielded powders with larger specific surface areas (mean value 9.11 m^2/g after calcination) than that of the ammonium carbonates (mean value 3.11 m^2/g).

Under the oxalate conditions, the calcined powders prepared at a lower temperature of precursors yielded higher specific surface area than those at a higher temperature. For the lower temperature cases, the faster titration rate produced calcined powders with higher surface areas than that at the slower rate. Single phase perovskite PLZT powders were produced by using a spray pyrolysis technique for preparing the calcined powders.

Acknowledgement

The project is sponsored by the Office of Naval Research under contract No. N00014-91-J-1508

References

[1] C. E. Land, P. D. Thatcher, and G. H. Haertling, Electrooptic Ceramics, Appl. Solid State Sci. Vol. 4, R. Wolfe, Ed. Academic Press, New York, 1974.

[2] A. E. Krumins and V. Y. Fritsberg, "Semiconductor Properties and General Applications of Optical Ceramics," Ferroelctrics, vol. 35 pp. 149-154, 1981.

[3] G. Taguchi, System of Experimental Design, Unipub/Kraus International Publications, New York, 1988.

[4] M. L. Salutsky and W. R. Grace, Precipitates, Treatise on Analytical Chemistry, Part I, Vol. 1, pp 737-764, I. M. Kolthoff, Ed. The Interscience Enclopedia, New Yotk, 1959.

[5] C. R. Veale, Fine Powders, Applied Science Publishers Ltd. London, 1972.

[6] H. P. Klum and L. P. Alexander, X-ray Diffraction Procedures, Wiley, New york, 1954.

BULK VS. THIN FILM PLZT FERROELECTRICS

D.E. Dausch and G.H. Haertling
Department of Ceramic Engineering, Clemson University
Clemson, SC 29634-0907

Abstract: Lead lanthanum zirconate titanate (PLZT) ferroelectrics were produced in bulk ceramic and thin film form in order to compare their electrical and physical properties. Both bulk and thin film samples of selected compositions were produced from the same acetate precursor solutions. Properties examined were dielectric permittivity, dissipation factor, remanent polarization, coercive field, Curie temperature and crystallinity. Bulk ceramics were hot pressed from chemically coprecipitated powders, and chemically derived thin films were fabricated by spin coating. Typical conditions for hot pressing were 1200°C for 4 hours at 14 MPa (2000 psi), whereas the thin films were sintered at 700°C for 4 minutes per layer. The similarities and differences between the materials are described.

Introduction

Ferroelectric thin films have been the subject of years of ongoing research in the study and optimization of their processing and properties. The importance of ferroelectric thin films is evident in their many applications ranging from nonvolatile memories to electrooptic devices.[1] These thin film applications stem from the many ferroelectric bulk ceramic components successfully developed over the years. In some instances, however, thin films possess advantages over bulk ceramics which make them more desirable for many devices and broaden the range of applications for ferroelectric materials. Lower operating voltage, higher speed, easier integration with silicon technology and lower cost are among the advantages favoring thin film ferroelectrics.

In order to more fully understand and optimize thin film ferroelectric behavior, a comparison is necessary to bulk ferroelectric phenomena. Direct correlation between the bulk and thin film materials is difficult since the precursors and processing techniques of each are typically so dissimilar; however, a study is presented here that diminishes this disparity. This research focuses on the fabrication and characterization of PLZT bulk ceramics and thin films produced from the same acetate precursor solutions. It is believed that this process allows for a close comparison of PLZT bulk and thin film ferroelectrics by minimizing or eliminating differences in the processing of these materials induced by batching variations, precursor impurities and differences in mixing, reactivity and chemical composition of the precursor materials. A study of several PLZT compositions is presented to explore similarities and differences in the behavior of hot pressed bulk ceramics produced from chemically coprecipitated powders and spin coated thin films produced by a metallorganic decomposition (MOD) process.

Experimental Procedure

Processing

PLZT hot pressed ceramics and spin coated thin films were fabricated using a process similar to previously reported processes using a water soluble acetate precursor system.[2] The acetate precursors were chosen primarily for their chemical stability, insensitivity to moisture and low cost. The starting precursors included lead subacetate (PbAc) powder, lanthanum acetate (LaAc), zirconium acetate (ZrAc) and titanium acetylacetonate (TiAAc) solutions. For processing simplicity and accuracy, PbAc was mixed into solution by the addition of acetic acid and methanol so that all of the acetate precursors were in liquid form. This ensured that the beginning acetate formulation was readily and completely mixed into solution. This step becomes important since only a small portion of the total acetate formulation is used for spin coating. Incomplete mixing would produce compositional fluctuations between bulk and thin film solutions. It should be noted that all of the precursors were assayed before experimentation, and the same stock solution of each precursor was used throughout these experiments. These precautions were taken to reduce the possibility of batching variations between bulk and thin film materials so that similarities and differences in their properties were not a result of these variations.

After initial acetate formulation, the solution was separated into bulk and thin film portions. The bulk portion was coprecipitated in a high speed blender with oxalic acid and methanol and then vacuum dried at 70°C to produce a solid, friable cake. The cake was crushed, calcined at 500°C for 8 hours and milled in trichloroethylene for 6 hours to produce a PLZT oxide powder. Typically, 100g of powder was produced for hot pressing. Hot pressing conditions were 1200°C for 4 hours at 14 MPa. To prepare samples for electrical measurement, the hot pressed parts were sliced on a diamond saw and lapped to 0.5 mm (20 mil) thickness. Electroless nickel electrodes were plated onto the samples.

For thin film production, a small portion (usually 5g) of the acetate solution was decanted and diluted with methanol at a 2:1 ratio by weight. The solution was spun onto silver foil substrates using a photoresist spinner at 2000 rpm for 15 seconds, allowed to dry for 15 seconds and pyrolyzed at 700°C for 4 minutes. Repeating this process for 10 layers produced a PLZT thin film approximately 0.9 um thick. For measurement of electrical properties, copper electrodes were applied to the surface of the films via vacuum evaporation. This process allowed for the fabrication of both bulk and thin film materials from the same batch.

Measurements

Bulk and thin film samples were analyzed using several electrical and physical measurement techniques. The dielectric properties (virgin and poled capacitance and dissipation factor) were measured on bulk and thin film samples using a Leader LCR meter at a measuring frequency of 1 kHz. Polarization (P) vs. electric field (E) hysteresis loops were also measured for both materials. The bulk samples were measured using a Sawyer-Tower circuit with a dc applied voltage of ±1400 V. The hysteresis loops were plotted with a Goerz Metrawatt X-Y plotter. Hysteresis loops of the thin film samples were customarily measured using a 60 Hz Sawyer-Tower circuit and an oscilloscope readout; however, in order to more accurately compare measurement of bulk and film hysteresis loops, the thin films were also measured using a low voltage (±30-50 V) dc looper.

The Curie temperature of bulk samples was determined for several PLZT compositions. Bulk samples were placed in a stirred oil bath and heated while taking capacitance and loss tangent measurements at 5°C increments. The Curie temperature was indicated by a maximum in the measured capacitance. X-ray diffraction analysis was also performed on bulk and thin film samples using a Scintag XDS 2000 diffractometer with Cu K-alpha radiation.

CH3080-0-7803-0465-9/92$3.00 ©IEEE

Results and Discussion

Several compositions were chosen for study near phase boundaries in the PLZT system. The morphotropic phase boundary compositions consisted of 2/55/45, 2/53/47 and 2/51/49 which regularly exhibit ferroelectric memory behavior. Compositions approaching and entering the paraelectric phase region with 65/35 Zr/Ti ratios included those with 6, 7, 8, 9, 9.5 and 10% La. These materials typically are memory materials at 6% La and range toward slim-loop ferroelectric materials in the 9 to 10% La range. Hot pressed bulk ceramics and spin coated thin films on Ag foil substrates were fabricated, and a comparison of properties was established.

Dielectric Properties

Dielectric and ferroelectric properties are listed for bulk and thin film samples in Table 1 including virgin and poled dielectric constants for each. As expected, thin film dielectric constants were generally lower than their bulk counterparts. These effects have previously been reported to be due to several effects caused by the obvious differences between bulk and thin film configurations including small grain size of the thin films, mechanical clamping effects and voltage sensitivity of the dielectric measurement due to the high electric field applied to a <1 um thin film.[2] The difference in dielectric properties found in the present results, however, was not as significant as that reported earlier.

In comparing bulk 2% La samples to thin films, some similarities and differences were noted. Unsurprisingly, both bulk and thin film data showed maxima in K_{vir} and K_{pol} at the 2/53/47 composition indicating the existence of the morphotropic phase boundary near this composition, although the position of the boundary for the thin films seemed to be slightly different than that of the bulk samples. K_{pol} and K_{vir} for 2/51/49 thin films was essentially equal to that of 2/55/45 films, while bulk 2/51/49 had a much greater poled dielectric constant than bulk 2/55/45. This result suggested that thin films and bulk ceramics did not behave equivalently near the morphotropic phase boundary since the dielectric constant was expected to peak at this boundary. A comparable result occured for x/65/35 compositions when the paraelectric phase boundary was encountered. The dielectric constant was expected to reach a maximum at this phase boundary which was previously reported at the 9/65/35 composition for mixed oxide processes.[3] Though both bulk and thin film samples seemed to have maximum dielectric constants at the 9.5/65/35 compositions, the 9/65/35 thin films were closer to 9.5/65/35 than the bulk. Note the occurance of the high K_{pol} for the 8/65/35 bulk sample despite the lower K_{vir} shown by this sample. The bulk ceramics demonstrated a larger difference in dielectric constants between the 9 and 9.5/65/35 compositions. Additionally, the thin film 6/65/35 composition revealed a higher dielectric constant than the bulk 6/65/35. These results would suggest that bulk and thin film samples showed dissimilar behavior also near the paraelectric phase boundary.

As mentioned above, the expected maximum dielectric constant for x/65/35 bulk ceramics produced via mixed oxide processes was 9/65/35; however, the results in Table 1 for the chemical process generally indicate a maximum at the 9.5/65/35 composition. Furthermore, the dielectric constants for all of these compositions were higher than values reported for mixed oxide processes.[3] These results could possibly be explained by realizing the type of process used in this study for fabricating bulk ceramics and thin films; i.e, thoroughly mixed acetate precursor solutions to produce chemically derived powders and thin films. This process may provide improved mixing of components which could slightly alter stoichiometry in the bulk and thin film samples-- especially Zr/Ti ratio and dispersion of the La dopant in PLZT. This could have produced higher dielectric constants and shifted the maximum in dielectric constants of these materials to 9.5% La. In order to explore this supposition, Curie temperatures of bulk x/65/35 samples were measured and are shown in Table 2 and Figure 1.

	K_{pol}	tan d (pol)	K_{vir}	tan d (vir)	E_C (dc) [kV/cm]	P_R (dc) [uC/cm^2]	E_C (ac) [kV/cm]	P_R (ac) [uC/cm^2]
BULK CERAMICS								
2/55/45	1328	.029	1293	.033	8	46	--	--
2/53/47	1885	.025	1391	.028	10	40	--	--
2/51/49	1630	.024	1234	.034	16	33	--	--
6/65/35	1355	.036	1774	.056	6	33	--	--
7/65/35	2712	.033	2479	.036	5	31	--	--
8/65/35	5700	.055	4692	.050	3	20	--	--
9/65/35	5147	.054	5007	.050	0	0	--	--
9.5/65/35	5658	.048	5603	.046	0	0	--	--
10/65/35	5548	.036	5538	.033	0	0	--	--
THIN FILMS								
2/55/45	997	.122	1228	.133	27	34	43	32
2/53/47	1265	.132	1619	.160	28	47	44	45
2/51/49	972	.122	1237	.146	28	38	46	37
6/65/35	1871	.142	1995	.141	14	21	28	25
7/65/35	2499	.170	2460	.145	14	18	27	21
8/65/35	3211	.194	3172	.176	11	15	22	19
9/65/35	4221	.195	4001	.172	9	11	22	17
9.5/65/35	4234	.190	4092	.164	7	8	19	18
10/65/35	4157	.193	4157	.209	7	10	18	16

Table 1. Electrical properties of PLZT bulk ceramics and thin films.

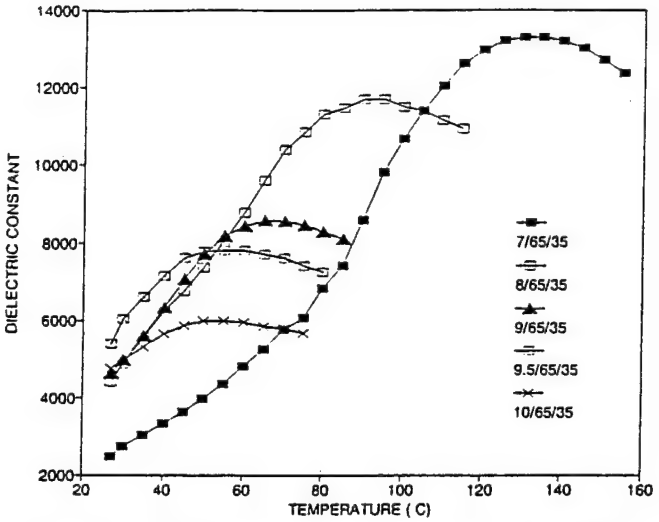

Figure 1. Curie temperature measurements of bulk x/65/35.

Table 2. Curie temperatures of PLZT x/65/35 bulk ceramics.

Composition	T_c
7/65/35	140
8/65/35	100
9/65/35	70
9.5/65/35	65
10/65/35	60

The Curie temperatures measured were consistently 10°C lower than previously reported for bulk samples produced by a mixed oxide process.[3] This result further emphasizes the possibility that the stoichiometries of the chemically prepared materials presented here were slightly different than the mixed oxide materials.

Crystallinity

X-ray diffraction patterns of thin film 8/65/35 and bulk 8/65/35 samples are shown in Figures 2a and 2b, respectively, and d-spacings are labeled for the PLZT peaks. Due to their greater intensities, the three Ag substrate peaks labeled on the thin film pattern masked three PLZT film peaks expected at the same angles. The thin film sample produced lower intensity PLZT peaks than the corresponding bulk sample. This could be a result of the thin film having either a lower degree of crystallinity than the bulk sample or simply a smaller quantitiy of material being analyzed by the

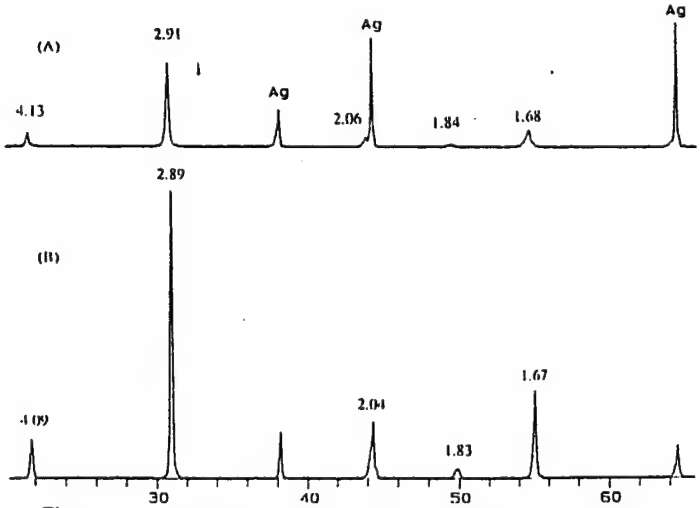

Figure 2. X-ray diffraction patterns of an 8/65/35 (A) thin film and (B) bulk ceramic. D-spacings are in angstroms.

diffractometer. In analyzing the lattice spacings of the materials, it was found that the thin film d-spacings were slightly larger than in the bulk material. Watanabe et al.[4] proposed that mechanical stress present in PZT thin films caused by lattice or thermal expansion mismatch between the film and the substrate can cause differences in lattice constant between bulk and thin film materials. This may be the cause of the difference in d-spacing observed here. The increase in d-spacing for the thin films is quite small--approximately 0.6 to 1% between the bulk and thin film samples. An absence of larger differences in d-spacings could be attributed to the Ag substrates used which are quite ductile and may allow the films to be relatively stress free compared to films fabricated on more rigid substrates (i.e. Si, sapphire, MgO).

Ferroelectric Properties

The ferroelectric properties calculated in Table 1 were taken from the P vs. E hysteresis loops shown in Figure 3. As stated above in the discussion of dielectric properties, both bulk and thin film materials indicated a transition across the morphotropic phase boundary. This transition was also evident in the hysteresis loops of the materials. In the bulk materials, the transition was obvious with a widening of the hysteresis loop signaling the emergence of the tetragonal phase in the 2/51/49 material. This phenomenon, however, did not occur in the thin film samples. The tetragonal phase was evident in the dc hysteresis loops of the thin films by a slightly more square hysteresis loop for 2/51/49 than for the rhombohedral 2/55/45 film. The phase transition was apparent in both ac and dc hysteresis loops of the films by a rise in remanent polarization in the 2/53/47 film. Previous work mentioned that thin films have a lower P_R and higher E_C than bulk materials for reasons similar to differences in dielectric properties mentioned above (grain size, clamping, voltage sensitivity).[2] Although the thin films presented here with 2% La had a higher E_C, the P_R of these films was not necessarily lower than for bulk materials. In fact, 2/53/47 and 2/51/49 films had a higher P_R than bulk samples of the same composition. Again, as with dielectric properties, the ferroelectric properties of the thin films seemed to be different across the phase boundary than the bulk ceramics. This was also the case for x/65/35 materials.

In PLZT bulk x/65/35 samples, the hysteresis loops obtained were similar to those expected for these compositions. The remanent polarizations and coercive fields calculated were lower than reported mixed oxide values[3], and this can possibly be attributed to the difference in processing between the coprecipitation and mixed oxide processes as discussed above. As anticipated, the 6, 7 and 8% La materials were memory materials, and the 9, 9.5 and 10% La materials were slim-loop materials. For the memory materials, E_C was higher and P_R was lower for thin films than for bulk materials which was similar to previously reported results.[2] Although both bulk and thin film memory materials experienced narrowing of their hysteresis loops with increasing %La, the bulk materials transformed to slim-loop materials at 9% La, while the thin films maintained ferroelectric memory hysteresis loops beyond 9% La. Research by Gu et al.[5] on quenched PLZT 9.5/65/35 ceramics showed that internal stresses induced in quenched samples can enhance polar region ordering and produce a more ferroelectric-like response. This produced higher remanent polarizations in quenched samples than in annealed samples. These findings could explain the memory behavior observed in the 9, 9.5 and 10/65/35 thin films in this study. Residual stresses in the thin films which could have produced the differences in d-spacings discussed above may have caused these films to retain ferroelectric memory hysteresis loops that were not observed in the bulk materials of the same compositions. Nevertheless, thin film behavior again differed from bulk ceramic behavior near the paraelectric phase boundary.

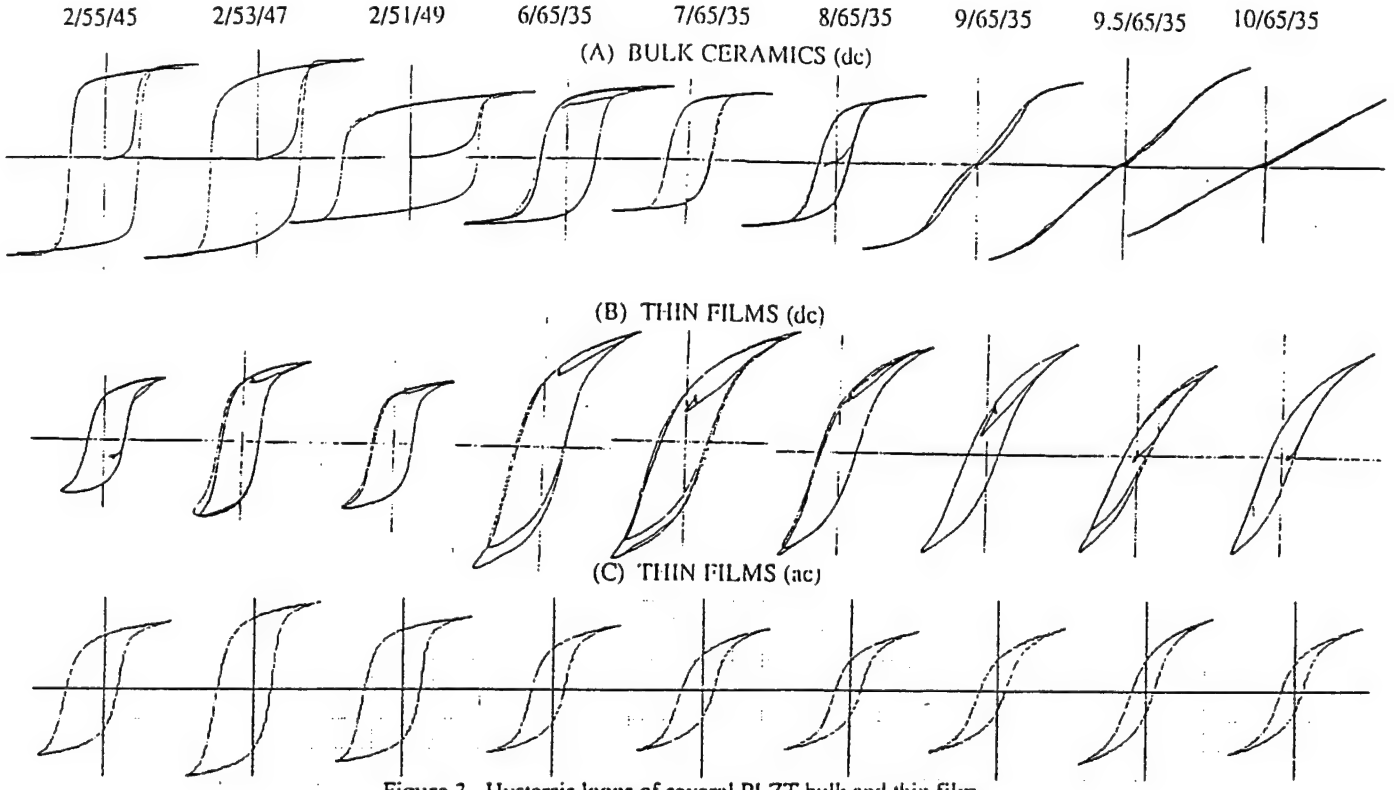

Figure 3. Hystersis loops of several PLZT bulk and thin film materials including (A) dc loops of bulk ceramics, (B) dc loops of thin films and (C) ac loops of thin films.

Summary and Conclusions

PLZT bulk ceramics and thin films were fabricated from the same acetate precursor solutions in order to minimize batching variations and accurately compare properties between bulk and thin film samples of the same compositions. It was found that materials near the morphotropic phase boundary with 2% La differed in behavior. Maximum dielectric constants were found at 2/53/47 for both materials; however, the bulk 2/51/49 had a proportionally higher dielectric constant than the thin film when compared to their respective 2/55/45 samples. The hysteresis loops of the bulk samples indicated a transition to a tetragonal phase with a widening of hysteresis loops (increased E_C, decreased P_R). Thin films also indicated a transition but with a maximum in P_R for the 2/53/47 composition.

Bulk x/65/35 materials behaved as expected with the exception of slightly lower Curie temperatures, coercive fields and remanent polarizations and slightly higher dielectric constants than previously reported. The 6, 7 and 8/65/35 materials produced memory hysteresis loops, and the 9, 9.5 and 10/65/35 materials produced slim hysteresis loops. The thin film memory loops were somewhat thinner than the bulk memory loops, and continual narrowing of the loops occurred toward the paraelectric phase boundary; however, slim-loop ferroelectrics were never completely achieved in the thin film materials. X-ray diffraction analysis showed that thin film lattice spacings were only slightly greater than the corresponding bulk spacings as indicated by diffraction peaks slightly shifted in diffraction angle between the two materials.

This comparison of bulk and thin film ferroelectrics is believed to be an accurate comparison of properties caused only by the inherent differences in configuration between bulk ceramics and thin films. It is believed that the current process used to fabricate these materials is one in which complete mixing of precursors and accurate batching of materials provided a minimization of batching differences that could cause serious variations in composition and properties of bulk and thin film PLZT ferroelectrics. Hence, this process provided a valid comparison between these materials.

Acknowledgement

This work was supported by ONR under contract #N00014-91-J-1508.

References

[1] L.M. Sheppard, "Advances in Processing of Ferroelectric Thin Films," Am.Cer.Soc.Bull., vol. 71(1), pp. 85-95, 1992.

[2] G.H.Haertling, "An Acetate Process for Bulk and Thin Film PLZT," in IEEE 7th International Symposium on Applications of Ferroelectrics, pp. 292-5, 1990.

[3] G.H.Haertling, "Electrooptic Ceramics and Devices," in Engineered Materials Handbook, vol. 4 (Ceramics and Glasses), ASM International, pp. 1124-30, 1991.

[4] H.Watanabe, T.Mihara and C.A.Paz De Araujo, "Device Effects of Various Zr/Ti Ratios of PZT Thin-Films Prepared by Sol-Gel Method," in Proceedings of the 3rd International Symposium on Integrated Ferroelectrics, pp. 139-50, 1991.

[5] W.Y. Gu, E.Furman, A.Bhalla and L.E.Cross,"Effects of Thermal Treatment on the Electrical Properties in Relaxor PLZT Ceramics," Ferroelectrics, vol. 89, pp. 221-30, 1989.

REFLECTIVE PLZT THIN FILM LIGHT MODULATOR
—— A PROTOTYPE DEVICE

(This device was constructed as one of the requirements for concluding the Office of Naval Research project "Intelligent Processing of Ferroelectric Thin Films" carried out at Clemson University, completed in March, 1994.)

The device adopts an ITO/PLZT/Pt thin film structure on a silicon substrate. The modulating medium is a ferroelectric/electrooptic PLZT thin film. A transparent indium-tin oxide (ITO) layer was deposited on the PLZT film as the top electrode. A reflected light of finite reflection angle is modulated in its polarization state by means of an voltage signal exerted to the ITO and Pt layers. The largest modulation depth is obtained near a Fabry-Perot interference peak located at an incident angle of approximately 57 degrees.

The packed assembly, shown in the photograph, consists of a wired ITO/PLZT/Pt thin film modulator, a polarizer and a photo-transistor. The orientation of the modulator and the photo-detector is arranged in specific angles to obtain a large modulation depth when a light beam of 633 nm wavelength (from a He-Ne laser) is incident through the input aperture. When desired, the photo-transistor may be removed to let the reflected light exit from the output aperture for external detection or visual monitoring. Driving voltage signal is applied to the modulator through a BNC connector. The photo-transistor is wired to an output jack.

The performance of the device as a light intensity modulator or a phase modulator is described in Section 5. The following summarizes the main features and advantages of the device:

1. **Integrated form.**
2. **Compatible with silicon or other semiconductor substrates**
3. **Reflection-mode — preferred for free-space optical interconnections.**
4. **Modulating visible and infrared light.**
5. **Operated at or near a Fabry-Perot peak.**
6. **High on/off signal ratio for intensity modulation — 20 at 10 volts pulses.**
7. **Large optical phase modulation — above 50 degrees at 10 volts pulses.**
8. **Capable of digital and analog modulations.**

9. High-frequency modulation*.
10. Simple design; easy to fabricate.
11. Large tolerance to the error of thickness and incident angle control.
12. Low cost.

*The bandwidth of the prototype is limited by the large rc constant that can be drastically reduced. The PLZT thin film material has proved to be able to modulate light at GHz frequencies.

The above listed features are favorable for the device to be incorporated in monolithic optoelectronic devices for light modulations, particularly for the implementation of free-space optical interconnections.

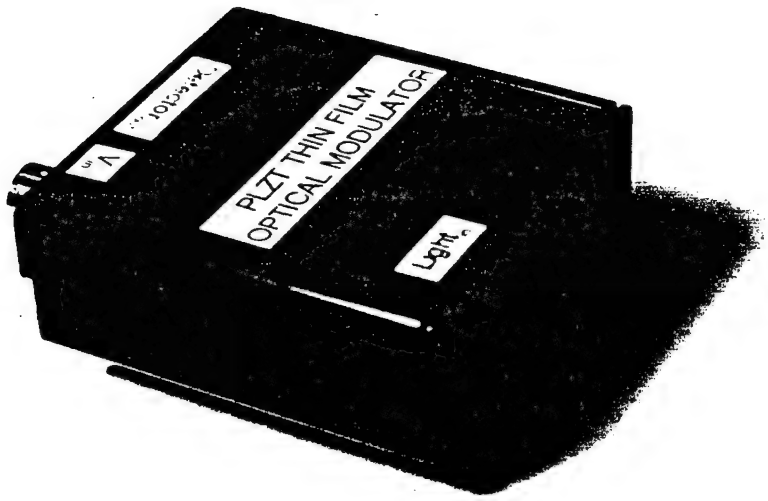

PLZT Thin Film Optical Modulator

Integrated Ferroelectrics, 1993, Vol. 3, pp. 207–215
Reprints available directly from the publisher
Photocopying permitted by license only

DIELECTRIC AND ELECTROOPTIC PROPERTIES OF ACETATE DERIVED PLZT X/65/35 THIN FILMS

GENE H. HAERTLING
Clemson University, Clemson, South Carolina, U.S.A.

(Received May 31, 1993)

PLZT solutions were prepared from the as-received acetate precursors by means of a simple mixing procedure which produced a stock solution of approximately 10% oxide solids. Films were fabricated via dip coating and heat treating at 700°C for two minutes per layer. As many as 150 layers were deposited with an automatic dip coating system. All of the resulting films were optically transparent and well crystallized in the perovskite phase. The films were evaluated with respect to dielectric and electrooptic properties. Shutter contrast ratios as high as 1000 to 1 were measured.

Keywords: thin films, PLZT films, electrooptics

INTRODUCTION

Thin films of ferroelectric (FE) compositions in the PLZT system are promising candidates for future devices involving memory and non-memory dielectrics, piezoelectric resonators, pyroelectric detectors and electrooptic modulators. A number of these applications necessitate films with thicknesses greater than those presently being designed for low voltage (1–3V) random access memories; i.e., 0.1–0.4 microns. A typical example of such an application is that of a transverse-mode spatial light modulator (SLM) which generally requires a film of several microns thick in order to generate the necessary optical retardation for sufficient optical contrast. Although much of the needed retardation can be produced via the direct electrooptic effect by simply increasing the electric field, there is a limit to this process since saturation of polarization or dielectric breakdown eventually occur. Consequently, for a given material composition, further gains in total retardation must be achieved by increasing the optical path length; i.e., the film thickness.

This investigation reports on work involved in the study of thicker films (0.5–6.5 μm of PLZT compositions composed of varying concentration of La (0–12 atom percent) at a constant Zr/Ti ratio of 65/35.

EXPERIMENTAL

The precursor materials used in the fabrication of the PLZT films consisted of lead subacetate (PbsubAc) powder with a PbO concentration of 78.6 wt.%, lanthanum acetate (LaAc) aqueous solution with an La_2O_3 content of 6.7 wt.%, zirconium acetate (ZrAc) aqueous solution containing 22.22 wt.% ZrO_2 and titanium acetylacetonate (TiAAc) chelated solution consisting of 16.96 wt.% TiO_2.

The various steps involved in the processing and fabrication of the films are

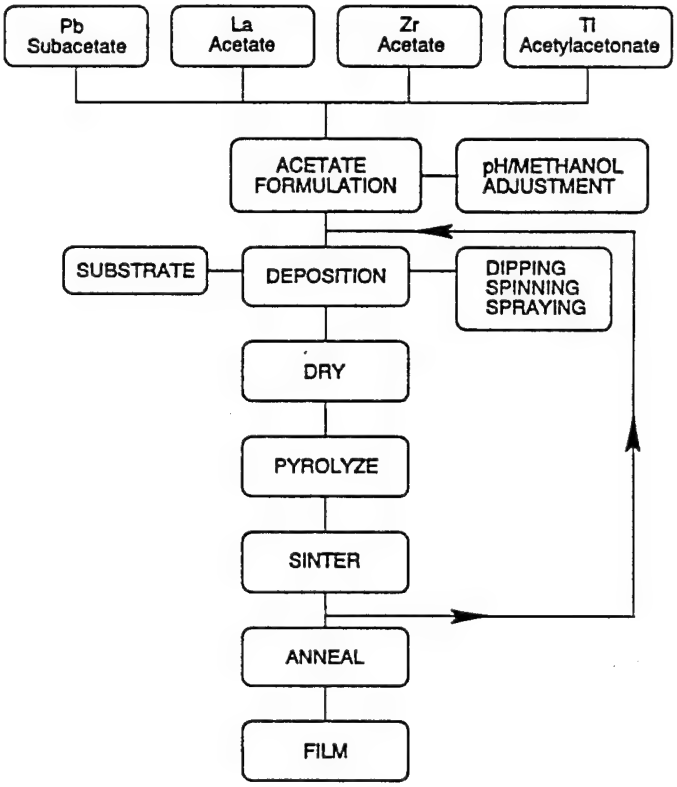

FIGURE 1 Flowsheet of the acetate process.

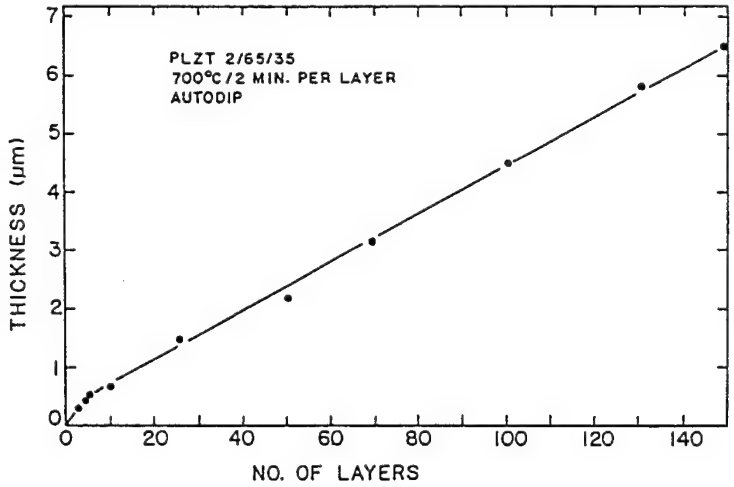

FIGURE 2 Relationship of film thickness to the number of layers.

shown in Figure 1. Compositions of various PLZT formulations ranging in La content from 0 to 12 atom % at a constant 65/35 Zr/Ti ratio were prepared by mixing the precursor ingredients in the proper proportions as they were received from the vendors. The solutions were then deposited via a dip coating process onto substrates consisting of either electrically conductive tin oxide coated (30 nm) PLZT (0.375 mm thick), randomly oriented sapphire (1.25 cm diameter × 0.5 mm thick) or Ag foil (0.127 mm thick). After drying for several seconds, the films were moved directly into the heating chamber and sintered at 700°C for two minutes per layer. An automatic, computer-controlled, dip coating apparatus was used to deposit and sinter the films.[1] As many as 150 layers were deposited, thus producing a total sintered thickness of 6.5 μm for the thickest films. A plot of the sintered film thickness as a function of the number of layers is given in Figure 2. As can be seen, the sintered film thickness is linearly related to the number of layers throughout the major portion of the deposition process. The slope of the plot in the linear region was calculated to be 415 angstroms (0.0415 μm) per layer; however, this value was less than half of the slope for the first few layers which was approximately 1000 angstroms (0.1 μm) per layer. The deposition behavior exhibited in this portion of the curve is believed to be due to the influence of the substrate surface.

A final anneal of the film, when performed, was carried out at 100°C below the sintering temperature for a period of 30 minutes with a slow cool in the furnace to room temperature; however, most of the films were not given an anneal in this study since the benefits of stress relief for these PLZT films on a PLZT substrate were considered to be marginal.

For the dielectric and hysteresis loop measurements, top copper electrodes, one mm diameter were deposited on the films through a mask via vacuum evaporation. Small signal dielectric measurements were carried out on a digital LCR meter at 1 kHz. Hysteresis loops (P vs. E) were measured on the films at frequencies of 1 kHz and near dc ($\frac{1}{8}$ Hz) at a driving voltage of <20 volts. Since PLZT substrates were inappropriate for use when determining the electrooptic characteristics of PLZT films, sapphire was chosen as an alternate substrate. Sapphire is highly transparent and readily available, however, it should be kept in mind that a thermal expansion mismatch between the film and substrate (i.e., 5.4 vs. 9 × 10^{-6}/°C, respectively) could lead to stresses in the film which may alter their properties.

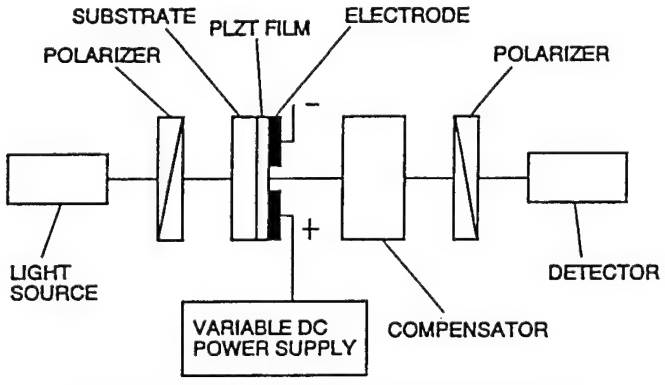

FIGURE 3 The setup for electrooptic measurements.

While it was felt that this could be the case with the films of less than one micron thickness, such a mismatch was not considered to be a significant factor in the measurements on the thicker films.

Electrooptic measurements were made on films dip coated on sapphire and elecroded with thermally evaporated aluminum. Several 50 μm gaps for producing the transverse electric field were photolithographically generated in the electrodes using a commercial aluminum etch which did not attack the PLZT film. The setup for the measurements is shown in Figure 3. An incandescent white light source along with a Babinet-Soliel compensator, crossed polarizers, a variable dc power supply and a United Detector Technology, Model S370, detector were used to make the birefringence measurements.

RESULTS AND DISCUSSION

Materials

Examples of the transparency of PLZT 2/65/35 films of various thicknesses ranging from 0.5 μm (5 layers) to 4.5 μm (100 layers) are shown in Figure 4. These specimens were autodip coated on PLZT substrates with a full sintering cycle for each layer. It was observed that all of the films were optically transparent and crack free, having a smooth, highly polished appearance. The grain sizes of these films ranged from 0.5–2 microns.

A typical optical transmission curve for a 5.5 μm thick PLZT film on sapphire is given in Figure 5. Overall, it may be observed that the transmittance of this film is very similar to that of the bulk material.[2] Additionally, it should be noted that the total transmission of the film is approximately the same as that of the bulk, i.e., 64% at 800 nm wavelength vs. approximately 67% for the bulk at the same wavelength. The onset of transparency was found to take place at approximately 360 nm, which is slightly lower than the 370 nm of the bulk.

An optical photomicrograph of a polished cross section and an SEM micrograph of a fractured surface are given in Figure 6. This figure shows the excellent thickness uniformity of the films after sintering as well as revealing the intimate growth between the many deposited layers. It also points out the fact that the thicker films are actually single, monolithic entities with bulk-like characteristics. X-ray diffraction patterns taken on several of the films indicated that the films possessed well developed, perovskite structures with little evidence for preferred orientation.

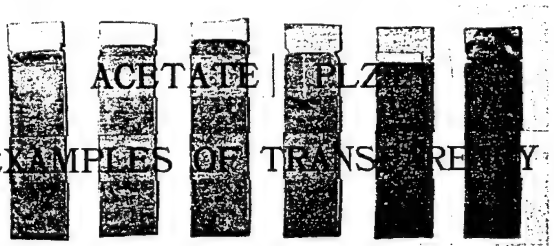

FIGURE 4 PLZT dip coated (2/65/35) on SnO_2/PLZT substrates illustrating optical transparency of the 5, 10, 25, 50, 69 and 100 layer samples (left to right).

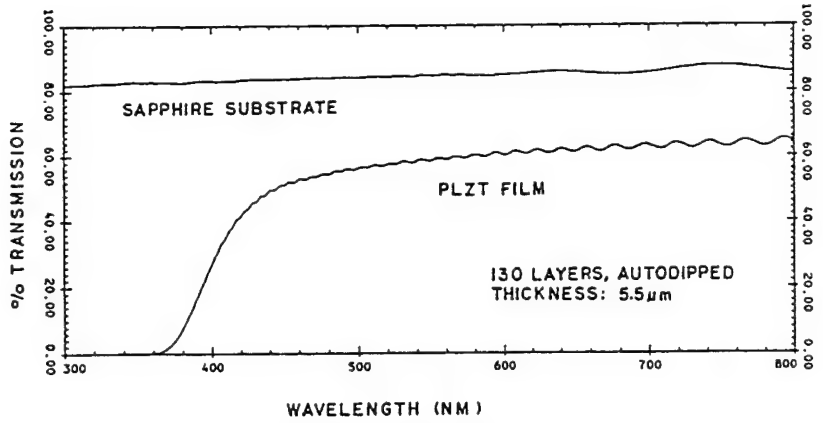

FIGURE 5 Optical transmittance of a 5.5 μm thick PLZT film on sapphire and the sapphire substrate without the film.

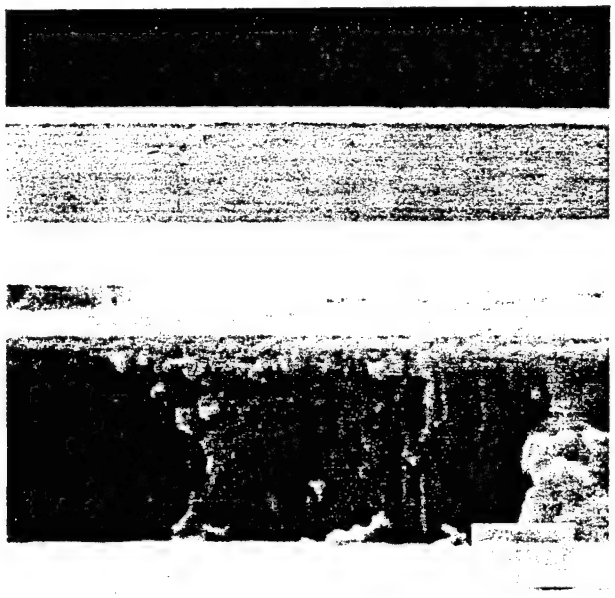

FIGURE 6 Cross section photomicrographs of 2.2 μm (50 layers) thick PLZT 2/65/35 film on PLZT substrate at x1250 magnification (top) and 3.2 μm (69 layers) thick PLZT film at x11,000 (bottom).

DIELECTRIC PROPERTIES

The dielectric properties of several of the PLZT films are listed in Table I as a function of thickness and in Table II as a function of composition. In Table I, it can be noted that the small signal relative dielectric constants (avg. = 702) and dissipation factors (avg. = 0.108) did not change significantly with increasing film thickness, however, this was not the case with the large signal properties taken from the hysteresis loops. Remanent polarization (P_R) increased with increasing

TABLE I

Electrical properties of PLZT 2/65/35 films of varying thickness

No. layer	Film thickness (μm)	Dielectric constant	Dissipation factor	P_R (μC/cm²)	E_c (kV/cm)
5	0.5	664	0.124	26	67
10	0.8	714	0.135	28	45
25	1.5	776	0.109	29	51
50	2.1	708	0.103	33	51
69	3.2	712	0.095	36	46
100	4.5	638	0.081	37	43

TABLE II

Dielectric properties of 0.6 μm thick PLZT films dip coated on Ag foil; (r_c values were obtained on sapphire substrates)

Comp.	T_c	Dielectric constant	Tangent delta-%	P_R μC/cm²	E_c kV/cm	r_c × 10^{-10}m/V
0/65/35	235	455	0.095	43	96	1.08
2/65/35	205	500	0.110	41	95	—
6/65/35	145	685	0.104	29	80	0.79
8/65/35	125	790	0.092	19	62	0.53
9/65/35	120	875	0.095	10	40	0.44
9.5/65/35	—	860	0.090	—	—	0.37
10/65/35	118	845	0.080	8	35	—
11/65/35	115	730	0.063	5	25	—
12/65/35	—	700	0.056	4	20	—

thickness, and coercive field (E_c) decreased with increasing thickness. These results again point out that the thicker films generally possessed properties more closely associated with bulk materials.

Dielectric data on compositions with La concentrations ranging from 0 to 12 atom % at a constant Zr/Ti ratio of 65/35 are given in Table II. The trends noted in these results generally follow those of the bulk materials; however, their absolute values, in some cases, were significantly different. For example, (1) the Curie temperatures (T_c) for all of the films were lower than the bulk by 50 to 80°C; (2) the dielectric constants were also lower, but the deviation from the bulk only became significant at La contents greater than 6%; (3) P_Rs were higher (more remanence) than the bulk for La contents of 9% or higher and (4) E_cs were substantially higher than the bulk for all compositions. The curves showing the temperature dependence of dielectric constant and the hysteresis loops for this series of compositions are given in Figures 7 and 8, respectively.

ELECTROOPTIC PROPERTIES

Using the setup shown in Figure 3, birefringence measurements were made on several of the films (5.5 μm thickness) deposited on sapphire. These data are given in Figure 9. It can be seen that the PLZT composition 0/65/35 at the top of the

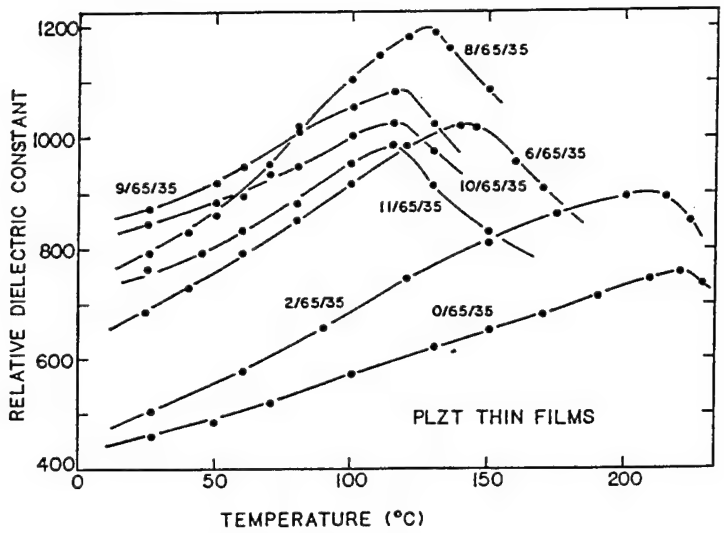

FIGURE 7 Temperature dependence of dielectric constant for various PLZT compositions.

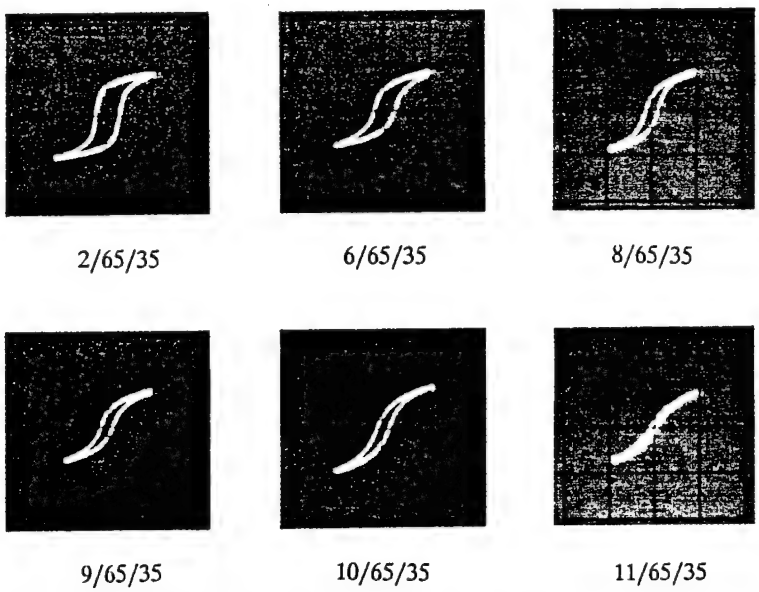

FIGURE 8 Hysteresis loops of selected films (0.6 μm thick) of PLZT dip coated on Ag foil.

figure is ferroelectric with definite remanent birefringence and switching characteristics, whereas, all of the other compositions (6, 8 and 9% La) appear to have very little remanent birefringence. The birefringences in these latter compositions appear to be primarily of the electrically-induced, quadratic nature which is similar to that of the bulk PLZT relaxor materials but only within the range from 9 to 12% La. The reason for the lack of remanence in compositions 6/65/35 and 8/65/35 is not understood at this time; but it is believed to be due, at least in part, to

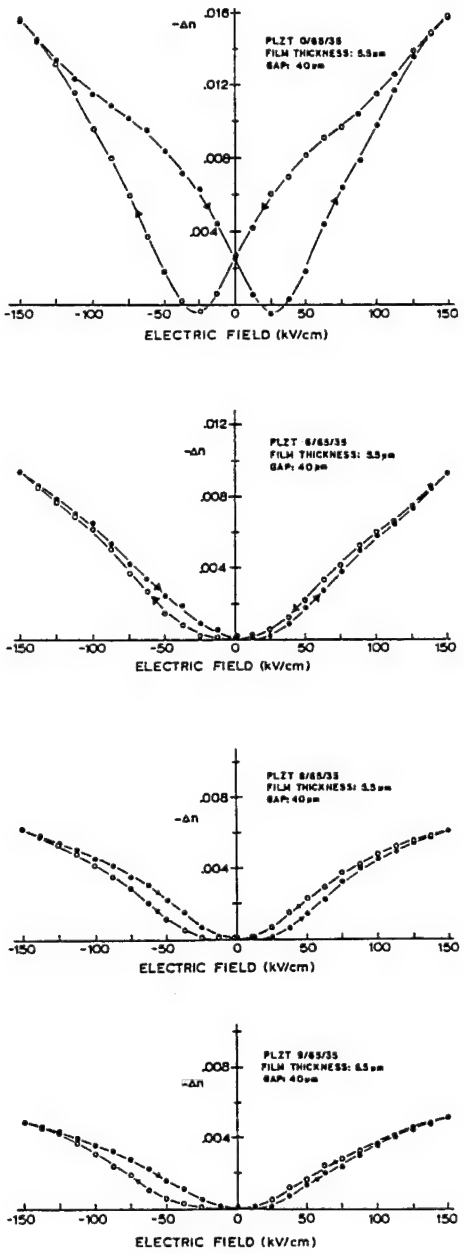

FIGURE 9 Electrooptic transverse-mode birefringence data on films of selected PLZT compositions.

stresses in the film from thermal mismatches or substrate clamping during activation when the film is constrained from moving piezoelectrically.

A closer examination of the non-remanent birefringence curves of Figure 9 reveals that at lower electric fields (<50 Kv/cm) the dependence is quadratic, however, "saturation effects" at higher fields causes the overall curve to be approximately linear. The saturation effect is, in all likelihood, the normal approach

FIGURE 10 Transverse-mode PLZT thin film device with one gap activated (right) and one gap inactive; (thickness = 5.5 μm and gap = 40 μm).

toward the half-wave retardation condition as experienced in bulk material, but spread out over much higher values of electric field. It was not possible in any of the films to actually achieve half-wave retardation, and this again, is believed to be due to the clamping effects of the substrate. Such effects were similarly noted by Wang *et al.* for compositions in the PLZT system.[3]

Although the required electrical fields for the films were substantially higher than the bulk materials (15 kV/cm vs. 150 kV/cm), it should also be noted that the birefringence values achieved were quite competitive with the bulk; i.e., -0.004 to -0.016 at 150 Kv/cm for a 5.5 μm thick film. The electrooptic r_c coefficients, calculated as a linear coefficient across the useable range of electric fields from 0 to 150 Kv/cm, were determined for the various compositions and are given in Table II. As seen, the values range from 1.08×10^{-10} m/V for 0/65/35 to 0.37×10^{-10} m/V for 9.5/65/35. A comparison of these values with similar ones for bulk material shows that the films at the 5 μm thick level possess bulk-like electrooptic properties.

Further evidence for the bulk-like character of these films is given in Figure 10. This figure is a photograph of one of the measured films (0/65/35) with one of the gaps activated while the other gap was held in the inactive state. To date, contrast ratios of up to 1000 to 1 have been obtained.

ACKNOWLEDGEMENTS

The author wishes to gratefully acknowledge the assistance of Kewen K. Li and Kimberly D. Preston for the preparation of some of the PLZT thin and thick film samples. This work was supported by the Office of Naval Research under contract No. N0014-91-J-1508.

REFERENCES

1. K. K. Li, G. H. Haertling and W. Y. Howng, *Integrated Ferroelectrics* (to be published).
2. G. H. Haertling, *Ferroelectrics*, **75**, 1 (1987).
3. F. Wang and A. Y. Wu, *Proceedings of 1990 Intl. Sym. Appl. Ferroelectrics*, Urbana, 131 (1992).

Electro-optic measurements of thin-film materials by means of reflection differential ellipsometry

Feiling Wang, Eugene Furman, and Gene H. Haertling
Gilbert C. Robinson Department of Ceramic Engineering, Clemson University, Clemson, South Carolina 29634-0907

(Received 14 November 1994; accepted for publication 11 March 1995)

Electro-optic properties of thin-film materials grown on opaque substrates are determined utilizing the principles of reflection differential ellipsometry. The scheme of the measurement involves the detection of the field-induced phase shift in a probing light beam reflected from thin-film samples. To quantitatively determine the field-induced indices change or birefringence and the field-induced strain it is essential to model the differential ellipsometric process in the stratified structure. The modeling reveals that the field-induced changes of the ordinary and the extraordinary indices contribute to the measured phase shift with different incident-angle dependences. The field-induced strain gives yet another unique incident-angle distribution. By means of an incident-angle-varying technique, therefore, the field-induced changes of ordinary index and extraordinary index in a thin-film material may be determined separately. Detailed descriptions of the measuring technique and the modeling work are presented. © *1995 American Institute of Physics.*

I. INTRODUCTION

The primary role of electro-optic thin-film materials in photonic devices is to modulate light waves with respect to their optical phase or amplitude. Such modulations may be achieved by means of the electric-field-controlled indices of refraction in the thin-film materials via their electro-optic effects. The characterization of the electro-optic properties of the thin-film materials is of obvious importance. For many device applications the thickness of the electro-optic films is usually smaller or comparable to the light wavelength. Accurate and reliable detection of the electro-optic effects in these films has remained a difficult and sometimes a challenging task, particularly so when films are grown on opaque substrates. In terms of the configuration of the electrodes and the propagation mode of the light, the reported detection methods may be summarized under the following three categories:

(1) the transmission-mode measurement for thin films grown on transparent substrates;
(2) the reflection-mode measurement for thin films grown on opaque substrates; and
(3) waveguide-mode measurement.

Under the first two categories, an either intensity- or phase-sensitive detection scheme can be adopted.

The transmission-mode measurement with either intensity- or phase-sensitive detection is the easiest to implement, and it has been the most widely used technique.[1–5] Its applicability is restricted to films deposited on transparent substrates while integration of electro-optic devices with opaque semiconductor substrates is becoming increasingly desirable. In addition, because of the planar structure of the electrodes in the transmission-mode detection, the distribution of the electric field in the electrode gap may be significantly nonuniform;[6] thus, the accuracy of the measurements is unsatisfactory. To measure the electro-optic properties of thin films deposited on opaque substrates waveguide refractometry was employed.[7] An advantage of waveguide refractometry is its capability of separating the field-induced change of the ordinary index from that of the extraordinary index. Some successes were reported in measuring the electro-optic properties of thin films by using reflection-mode measurement with an intensity-detection approach.[8,9] In these measurements it was often necessary to manually adjust the optical compensator in order to calibrate the phase shift under an applied electric field; direct measurements of the film indices change corresponding to varying applied fields cannot be obtained. Furthermore, light scattering limited the sensitivity and the accuracy of the measurement, a problem suffered by all intensity-detection approaches.

A reflection-mode measurement in conjugation with a phase-sensitive detection scheme has been used successfully to characterize the electro-optic effects of various thin films grown on opaque substrates.[10,11] The measuring technique is a variation of the polarization-modulation ellipsometry.[12] For the electro-optic characterizations, the measuring system is configured to directly measure the differentiation in the ellipticity of the probing light beam generated by the field-induced changes in the indices of refraction and the thickness of the films. Thus, the measuring method may be termed "reflection differential ellipsometry." Since the phase-sensitive detection excludes the scattered light from the detected signal, sensitivity of the measuring method is much higher than intensity-sensitive approaches.

To correctly extract the field-induced changes of the indices (ordinary and extraordinary) and the field-induced change of the film thickness (field-induced strain) from the measurements, it is essential to model the differential ellipsometric process in the stratified structure. Because of the multiple reflection of the light in the electro-optic film and the electrode layer(s), each field-induced change produces a unique phase-shift dependence on the incident angle. Based on a recently developed model, an incident-angle-varying

 0021-8979/95/78(1)/1/7/$6.00

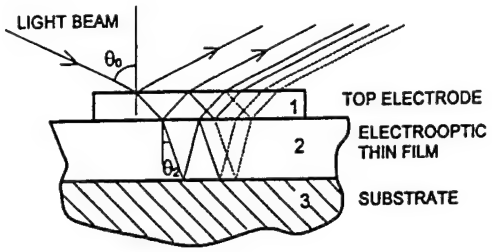

FIG. 1. Schematic diagram for the arrangement of the electrodes. The probing light is obliquely incident on the sample with an incident angle of θ_0.

technique has been utilized to determine separately the field-induced changes of the extraordinary and the ordinary indices and the change of film thickness. In this article both the techniques of the reflection differential ellipsometry and the modeling work are discussed in detail. Applications of the measuring method in electro-optic characterizations of ferroelectric thin films are also given.

II. PRINCIPLES OF THE MEASUREMENT

A. Phase detection in the reflection mode

In reflection differential ellipsometry the field-induced change in the ellipticity of the reflected light is measured. An electro-optic thin film is sandwiched between a transparent or semitransparent top electrode and a reflective bottom electrode, as shown in Fig. 1. Presence of the electric field in the electro-optic film, which is otherwise assumed to be isotropic, makes it optically uniaxial with its c axis in the normal direction of the surface as a result of the birefringent electro-optic effect. It is desirable to measure the field-induced change in the extraordinary index Δn_e and that of the ordinary index Δn_o or the field-induced birefringence, i.e., $\Delta n \equiv \Delta n_e - \Delta n_o$. Field-induced strain may also be present due to the piezoelectric or electrostrictive effect. The optical arrangement of the reflection differential ellipsometer is depicted in Fig. 2. Two polarizers are inclined 45° with respect to the incident plane, clockwise and counterclockwise, respectively. The polarization state of the probing laser beam is modulated in a periodic manner by means of an optical phase modulator M. The purpose of the inserted optical compensator C is to adjust the phase angle of the probing beam and to calibrate the detected signal.

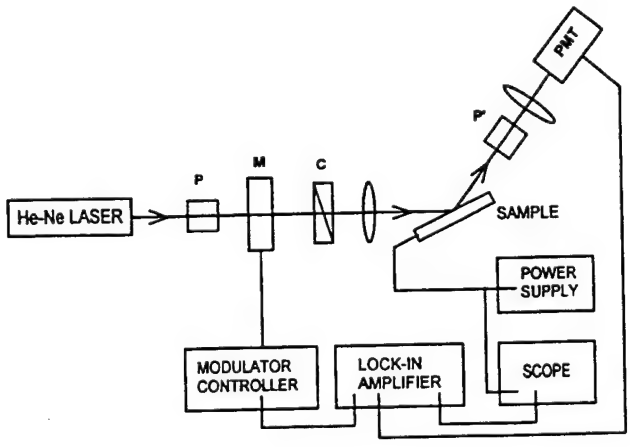

FIG. 2. Schematic diagram for the reflection differential ellipsometer. PMT denotes photomultiplier tube; M is the optical phase modulator; C the optical compensator; P and P′ polarizers.

The changes of the principal indices, caused by the electro-optic effects of the thin films, for the probing light propagating along the refraction angle θ_2 are calculated first. We designate the light component polarized in the incident plane as the p polarization and the component polarized perpendicularly to the incident plane as the s polarization. In the following calculation whenever p or s appears as a subscript the referred quantity is associated with p or s polarization, respectively. For differential changes of the extraordinary index n_e and that of the ordinary index n_o in the electro-optic films, the changes in the principal indices for light propagating along the refraction angle θ_2 are given by[13]

$$\Delta n_p(\theta_2) = \sin^2 \theta_2 \Delta n_e + \cos^2 \theta_2 \Delta n_o, \quad \Delta n_s = \Delta n_o. \quad (1)$$

The above field-induced changes of the refractive indices cause an optical phase shift $\Delta\Gamma_p$ for the reflected p-polarized light and $\Delta\Gamma_s$ for the reflected s-polarized light. The field-induced relative phase shift (phase retardation), defined by $\Delta\Gamma \equiv \Delta\Gamma_p - \Delta\Gamma_s$, is to be directly measured by using the following scheme.

Let us assume that the phase modulation provided by the optical phase modulator M is exerted upon the p component relative to the s component and is expressed by a sinusoid function $M \cos \Omega t$. The reflection of the probing light beam is governed by the complex reflectance $\tilde{R}_p \equiv R_p e^{-j\Gamma_p}$ for the p component and $\tilde{R}_s \equiv R_s e^{-j\Gamma_s}$ for the s-polarized component, respectively. Upon reflection the complex amplitudes of the two orthogonal light components can be expressed as (assuming unity amplitude for both components prior to reflection)

$$E_s = R_s e^{-j\Gamma_s}, \quad E_p = R_p e^{-j(M \cos \Omega t + \Gamma_c + \Gamma_p)}, \quad (2)$$

where Γ_c is the phase shift imposed by the adjustable optical compensator. Therefore, the detected intensity of the reflected light takes the following form:

$$I = -R_p R_s \cos(M \cos \Omega t + \Gamma_c + \Gamma_p - \Gamma_s) + \tfrac{1}{2}(R_p^2 + R_s^2). \quad (3)$$

The phase shift Γ_p consists of a zero-field part $\Gamma_p(0)$ and a field-induced part $\Delta\Gamma_p$ (the same applies to Γ_s),

$$\Gamma_p = \Gamma_p(0) + \Delta\Gamma_p, \quad \Gamma_s = \Gamma_s(0) + \Delta\Gamma_s. \quad (4)$$

If the optical compensator is adjusted so that $\Gamma_c + \Gamma_p(0) - \Gamma_s(0) = 0$, the intensity of the detected light may be rewritten as

$$I = -R_p R_s \cos(M \cos \Omega t + \Delta\Gamma) + \tfrac{1}{2}(R_p^2 + R_s^2). \quad (5)$$

By setting the internal reference signal of the lock-in amplifier as $\cos \Omega t$, the output signal of the lock-in amplifier S is proportional to the Fourier amplitude of the light intensity associated with $\cos \Omega t$, which is found to be given by

$$S = CJ_1(M)\sin \Delta\Gamma, \tag{6}$$

where J_1 is the Bessel function of the first order; C is a system constant. In many practical cases the phase retardation is sufficiently small so that the following approximation may be used:

$$S = CJ_1(M)\Delta\Gamma. \tag{7}$$

The proportionality constant C in the above equation and in Eq. (6) can be calibrated using the adjustable optical compensator by reading the output signal S associated with a known phase change $\Delta\Gamma_c$ of the compensator.

In this phase detection scheme, incoherent scattering of the light beam does not contribute to the measured phase retardation. This can be deduced from Eq. (5), where incoherent scattering may be represented by an additional constant term. Such a constant term does not alter the output signal of the lock-in amplifier given by Eq. (6). On the other hand, field-induced scattering of the light may cause errors in the calibration of the detected signal; however, such a situation only happens when very severe field-induced scattering causes the amplitude of the reflected light to become substantially field dependent. In the electro-optic measurement of thin-film materials these situations are rare.

B. Multiple-reflection model

Now we attempt to derive the relationship between the measured phase retardation $\Delta\Gamma$ and the field-induced changes in the ordinary index and the extraordinary index, as well as the thickness of the electro-optic films. First we need to derive the complex reflectance, resulting from the interference of the multiple reflection of light in the thin-film structure, for both polarization components. The problem of concern is the overall reflectance for the structure of two thin films sandwiched between a semi-infinite ambient and an effectively semi-infinite conducting substrate. From the theory of light interference in thin-film systems[14] it is found that in such a stratified structure the complex reflectance $\tilde{R}$ is given by

$$\tilde{R} \equiv Re^{-j\Gamma}$$

$$= \frac{(\tilde{r}_{01}+\tilde{r}_{12}e^{-j2\tilde{\beta}_1})+(\tilde{r}_{01}\tilde{r}_{12}+e^{-j2\beta_2})\tilde{r}_{23}e^{-j2\beta_2}}{(1+\tilde{r}_{01}\tilde{r}_{12}e^{-j2\tilde{\beta}_1})+(\tilde{r}_{12}+\tilde{r}_{01}e^{-j2\tilde{\beta}_1})\tilde{r}_{23}e^{-j2\beta_2}}, \tag{8}$$

where $\tilde{r}_{01}$, $\tilde{r}_{12}$, and $\tilde{r}_{23}$ are the individual Fresnel reflection coefficients for boundaries between media {0,1}, {1,2}, and {2,3}, respectively. Because media 1 and 3 are conducting materials, all the Fresnel reflection coefficients are complex quantities. In other words, reflection of light from these interfaces involves continuous phase shift.[15] The phase thicknesses $\tilde{\beta}_1$ and β_2 for layer 1 and layer 2 are given by

$$\tilde{\beta}_1 = \frac{2\pi h_1 \tilde{n}_1}{\lambda}\cos\theta_1, \quad \beta_2 = \frac{2\pi h_2 n_2}{\lambda}\cos\theta_2, \tag{9}$$

where h_1 and h_2 are the thickness of layers 1 and 2, respectively. The complex index of refraction of the top electrode $\tilde{n}_1$ produces a complex phase thickness $\tilde{\beta}_1$, characterizing the optical absorption. The scattering loss of the light in the electro-optic layer, characterized by a loss coefficient α, may be incorporated in the Fresnel coefficient $\tilde{r}_{23}$. As Eqs. (8) and (9) apply to both polarizations the subscripts associated with all the quantities have been omitted. It is important to note, however, that since the Fresnel reflection coefficients are different for the two orthogonal polarizations, Eq. (8) represents two different mathematical forms for the p and s polarizations as functions of the material properties and the incident angle.

All the Fresnel reflection coefficients and phase thicknesses involved in Eq. (8) can be expressed in terms of the thicknesses of the films, the indices of all the media, scattering loss, and the incident angle. The overall reflection coefficient $\tilde{R}$ then may be expressed in terms of the incident angle and these material parameters. In particular, the overall phase angles Γ_p and Γ_s, may be written in the following form:

$$\Gamma_p = f_p(\tilde{n}_1, n_2, \tilde{n}_3, \alpha, h_1, h_2, \theta_0),$$
$$\Gamma_s = f_s(\tilde{n}_1, n_2, \tilde{n}_3, \alpha, h_1, h_2, \theta_0). \tag{10}$$

The partial derivatives of the above functions with respect to n_2 determine the change of the measured phase shifts $\Delta\Gamma_p$ and $\Delta\Gamma_s$ caused by differential field-induced index changes, Δn_p and Δn_s, respectively. Formally, these derivatives can be written as

$$\left.\frac{\partial f_p}{\partial n_2}\right|_{n_2(0),h_2(0)} \equiv w_p(\tilde{n}_1, n_2, \tilde{n}_3, \alpha, h_1, h_2, \theta_0),$$
$$\left.\frac{\partial f_s}{\partial n_2}\right|_{n_2(0),h_2(0)} \equiv w_s(\tilde{n}_1, n_2, \tilde{n}_3, \alpha, h_1, h_2, \theta_0), \tag{11}$$

where $n_2(0)$ and $h_2(0)$ are the index and the thickness of the electro-optic layer under zero external field, respectively. In general, a small thickness change accompanies the field-induced birefringent change in electro-optic films through a piezoelectric or an electrostrictive effect. The following two quantities relate the thickness change to the measured phase shift:

$$\left.\frac{\partial f_p}{\partial h_2}\right|_{h_2(0),n_2(0)} \equiv v_p(\tilde{n}_1, n_2, \tilde{n}_3, \alpha, h_1, h_2, \theta_0),$$
$$\left.\frac{\partial f_s}{\partial h_2}\right|_{h_2(0),n_2(0)} \equiv v_s(\tilde{n}_1, n_2, \tilde{n}_3, \alpha, h_1, h_2, \theta_0). \tag{12}$$

With the help of Eq. (1) the detected phase shift is found to be given by

$$\Delta\Gamma = w_p \sin^2\theta_2 \Delta n_e - (w_s - w_p\cos^2\theta_2)\Delta n_o + (v_p - v_s)\Delta h_2. \tag{13}$$

The above equation shows that the measured phase retardation contains contributions from three sources, namely, the field-induced change of extraordinary index Δn_e, of ordi-

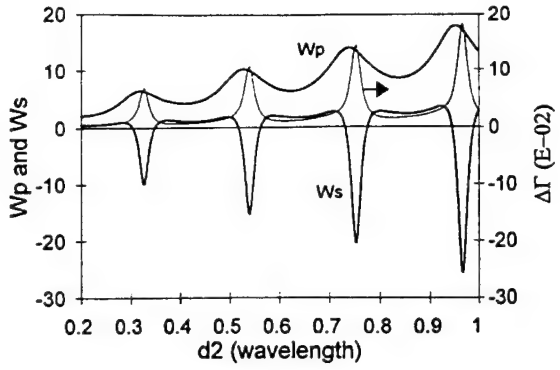

FIG. 3. The calculated coefficients w_p and w_s as functions of the thickness of the electro-optic layer. The thickness of the top electrode layer is chosen to be 0.5 wavelength of the light beam; the incident angle is assumed to be 60°.

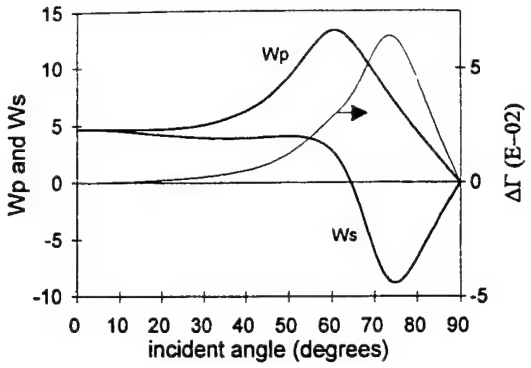

FIG. 4. The calculated coefficients w_p and w_s for p and s components as functions of the incident angle. The thicknesses of the electro-optic layer and the top electrode are chosen to be unity wavelength and 0.5 wavelength of the probing light beam.

nary index Δn_o, and the field-induced thickness variation Δh_2. Since the changes in the Fresnel coefficients and in the refraction angle under external electric fields cause second-order corrections to the phase retardation, it is often a good approximation to relate the two pairs of derivatives shown in Eqs. (11) and (12) through $n_2 w = h_2 v$ (subscripts omitted), as implied by Eq. (9). Therefore, to examine how each of the three field-induced changes contributes to the phase retardation at various incident angles, the values of the derivatives w_s and w_p as functions of the incident angle need to be determined. It can be seen that unless w_s and w_p happen to have the same value at certain incident angles the measured phase retardation $\Delta\Gamma$ is not proportional to the field-induced birefringence $\Delta n = \Delta n_e - \Delta n_o$.

To evaluate the field-induced changes, i.e., Δn_e, Δn_o, and Δh, of a thin-film sample from the measured quantity $\Delta\Gamma$, it is necessary to calculate the values of w_p and w_s for the sample. The explicit functional forms of w_p and w_s can be derived from Eq. (8). The derivations are straightforward, however, lengthy expressions arise. These calculations may be performed with the help of a computer. In general, because of the changing phase relation between the adjacent reflected light waves, the values of w_p and w_s oscillate as functions of the film thickness. For example, w_s and w_p are computed for a typical perovskite electro-optic thin film grown on a platinum bottom electrode with an indium-tin-oxide (ITO) top electrode. The thickness of the ITO layer is assumed to be 0.5 wavelength. The incident angle of the probing beam is assumed to be 60°. The calculated w_p and w_s as functions of the thickness of the electro-optic layer are shown in Fig. 3. The thin line in Fig. 3 represents the detected phase shift $\Delta\Gamma$ of the sample by assuming $\Delta n_e = -0.01$ and $\Delta n_o/\Delta n_e = -0.5$. The oscillations of w_p and w_s are apparently from the alternating phase relation between adjacent reflected light waves with the change of film thickness. The thickness variation of the top electrode causes similar oscillations. Such oscillations of w_p and w_s with the changing thicknesses represent the characteristics of a Fabry–Pérot interferometer.

The incident angle dependence of w_s and w_p deserves our special attention. By using the same material parameters as in the previous calculation and choosing the thickness of the electro-optic layer to be a unit wavelength, the calculated w_s and w_p as functions of the incident angle are shown in Fig. 4. Because the reflection of the p-polarized light obeys different rules from s-polarized light, the Fresnel reflection coefficients in Eq. (8) possess different incident angle dependences for the two orthogonally polarized components. It is not surprising to see in Fig. 4 that w_s and w_p possess their respective incident-angle dependences. In this example, except in the range of small incident angle, where $w_s \approx w_p$, the measured phase shift $\Delta\Gamma$ given by Eq. (13) is not proportional to the field-induced birefringence $\Delta n_e - \Delta n_o$.

Different incident-angle dependences for w_p and w_s greatly complicate the interpretation of the measured phase retardation, however, they permit the resolution of Δn_e, Δn_s, and Δh_2 from the experimental data. To determine the values of Δn_e, Δn_s, and Δh_2 in a thin-film material in the presence of certain applied field, phase retardation of the sample is measured for the applied field at various incident angles. If the thicknesses and the indices of each layers are known to a good precision, reliable values for w_p and w_s can be calculated as functions of the incident angle. The scheme of least-squares fitting may be employed in fitting the calculated phase retardation as a function of the incident angle, from Eq. (13), to the measured values at various angles using Δn_e, Δn_s, and Δh_2 as fitting variables. The values of Δn_e, Δn_s, and Δh_2 are thus determined to yield the best fitting.

The theory presented in this article has been utilized in the design of electro-optic light modulator using ferroelectric thin films. Taking advantage of the interference-enhanced modulation peak, as for example shown in Fig. 3, large phase modulation and high on/off signal ratios were achieved in a ferroelectric reflective light modulator using a lead lanthanum zirconate titanate (PLZT) thin film on a silicon substrate.[16]

III. DETECTION TECHNIQUES AND APPLICATIONS

A schematic diagram of the reflection differential ellipsometer is shown in Fig. 2. The light source is a He-Ne laser. The phase modulation of the laser beam is generated by a photoelastic modulator which provides variable modulating

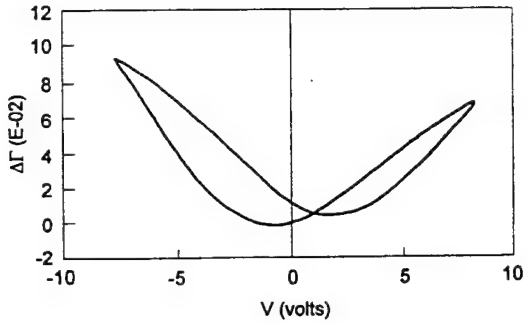

FIG. 5. Field-induced phase retardation vs electric-field loop for a 8/65/35 PLZT thin film sputter deposited on a Pt-coated silicon substrate.

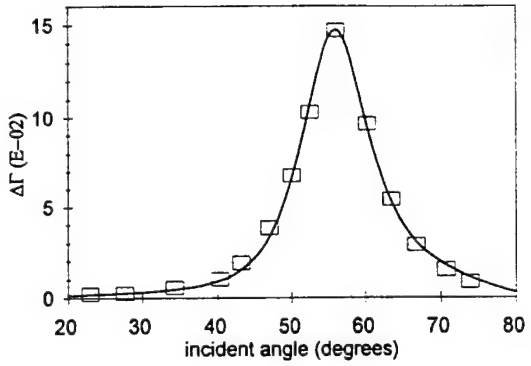

FIG. 6. Incident angle dependence of the field-induced phase retardation under voltage of −8.0 V for the PLZT thin-film sample measured in Fig. 5. The discrete points are experimental data. The solid line is the theoretical curve from least-squares fitting Eq. (13) to the experimental data.

depth at a frequency of 50 kHz, suitable for the lock-in amplifier. As has been discussed in the previous section, it is preferred to adjust the optical compensator under zero applied field so that

$$\Gamma_c+\Gamma_p(0)-\Gamma_s(0)=0. \tag{14}$$

From Eq. (5) we see that under the above condition the oscillation of the light intensity at frequency Ω is absent. Therefore, the above condition, i.e., Eq. (14), may be reached by observing the wave form of the light on an oscilloscope while adjusting the optical compensator. When an external electric field is applied to the sample, an modulating component at frequency Ω is created in the light intensity due to the field-induced phase shift. In order to detect this phase shift, the internal reference signal of the lock-in amplifier must be set as $\cos \Omega t$. To obtain the best sensitivity of detection, the modulating amplitude M in Eq. (6) should be adjusted to $\pi/2$.

To obtain the phase retardation versus applied voltage loops, a low-frequency cyclic voltage is applied to the sample between the top and the bottom electrodes. The frequency of the applied voltage must be much lower than the modulation frequency of the light provided by the optical phase modulator (50 kHz) in order for the lock-in amplifier to reach a steady output at any instantaneous voltage. For the experiments described in this article, the cycling frequency of the applied voltage is typically around 1 Hz.

The present reflection differential ellipsometer has been used to characterize various electro-optic thin films. Figure 5 shows measured phase retardation versus electric-field curve for an 8/65/35 PLZT (Ref. 17) thin film sputter deposited on a Pt/Ti-coated silicon substrate. The thickness of the PLZT film is approximately 1.1 μm. The top electrode is a 0.4-μm-thick ITO layer deposited by sputter deposition. The phase retardation versus electric-field loop was measured at an incident angle of 60° for the probing laser beam.

The PLZT thin film is a polycrystalline ferroelectric material. Along with the field-induced changes in the index of refraction, Δn_e and Δn_o, a field-induced strain is expected to be present in the thickness direction, i.e., Δh_2, caused by the piezoelectric effect of the material. As has been mentioned previously, all three field-induced changes contribute to the measured phase retardation through the relation established by Eq. (13). When the indices and thicknesses of the stratified structure are known to a good precision, the values of the two pairs of derivatives, defined by Eqs. (11) and (12), can be calculated for any given incident angle. Because v_p and v_s are related to w_p and w_s through the multiplification of a constant (as mentioned in the previous section), the formers are omitted in the following discussion. In order to determine each individual change under certain electric field, at least three measurements need to be performed at three different incident angles while keeping other variables constant. With the calculated w_p and w_s for the three chosen incident angles, all three field-induced changes can be solved simultaneously using Eq. (13). To obtain reliable values for the three field-induced changes under certain external field, however, it is preferred to measure the phase retardation at multiple incident angles while keeping the cycling voltage constant. The unknowns are determined from the least-squares fitting of Eq. (13) to the experimental profile of phase retardation versus incident angle. An example is described below.

The phase retardation versus cycling voltage (±8 V) curves for the 8/65/35 PLZT thin-film sample were successively taken with varying incident angles. The phase retardation of the film at −8.0 V are plotted in Fig. 6 as a function of the incident angle, shown by the discrete points. A computer program was used to calculate the values of w_p and w_s at each experimental incident angles and to fit Eq. (13) to the experimental data by using Δn_e, Δn_o, and Δh_2 as the fitting variables in a least-squares-fitting scheme. The resultant values are

$$\Delta n_e=-1.1\times10^{-2},$$
$$\Delta n_o/\Delta n_e=-0.27, \tag{15}$$
$$\Delta h_2=0.43 \text{ nm}.$$

The above results give a field-induced birefringence of $\Delta n_e-\Delta n_o=-0.014$. The solid line in Fig. 6 is the theoretical curve of Eq. (13) using the calculated w_p and w_s.

Another example is the detection of the electro-optic effect of antiferroelectric lead zirconate thin films on a Pt/Ti-coated silicon substrate. The films were deposited by using a

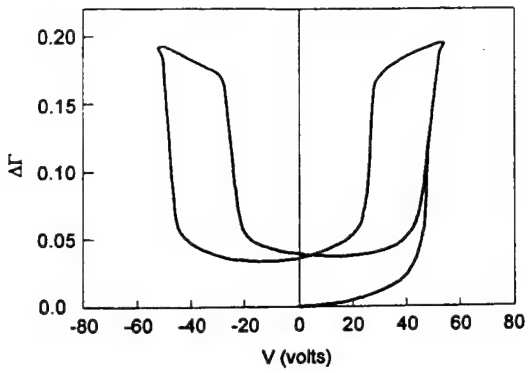

FIG. 7. Field-induced phase retardation vs applied voltage loop for an antiferroelectric lead zirconate thin film grown on a Pt-coated silicon substrate.

dip-coating process. The thickness of the film is approximately 0.8 μm. An incident angle of 67° was used during the measurement. A phase retardation versus electric-field loop is presented in Fig. 7. At this incident angle the values of w_p and w_s, calculated from the model, are 13.7 and -1.92, respectively. According to the model [Eq. (13)], the field-induced change of the ordinary index gives the greatest contribution to the measured phase retardation. The digital type of electro-optic response shown in Fig. 7 is a result of the field-induced antiferroelectric-ferroelectric structural transition.[8] Such response can only be observed in a reflection-mode electro-optic measurement where the sandwich structure creates a very uniform electric field inside the thin-film material.

Because the sandwich electrode configuration is used in the reflection-mode differential ellipsometry, one can simultaneously measure the field-induced phase retardation and the electric polarization from the same sample. This enables the direct measurement of the relationship between the field-induced index change and the electric polarization of thin-film materials. Figure 8 shows the field-induced phase retardation versus polarization loop of a 8/65/35 PLZT thin film, obtained by simultaneously detecting the field-induced birefringence and the polarization of the thin film during a voltage cycle. This type of loop cannot be easily obtained in a transmission-mode electro-optic measurement because of the geometry of planar electrodes.

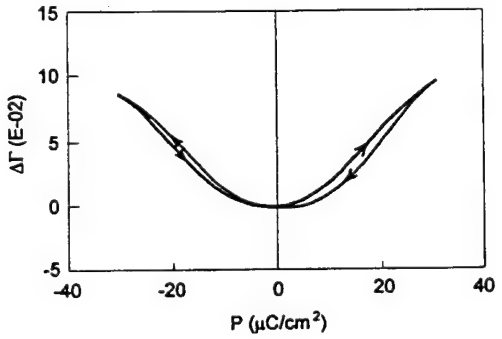

FIG. 8. Field-induced phase retardation vs polarization loop measured from an 8/65/35 PLZT thin film grown on a Pt-coated silicon substrate.

IV. CONCLUSIONS

The principles of reflection differential ellipsometry for electro-optic measurement of thin-film materials are presented. The scheme of the measurement involves a phase-sensitive detection of the field-induced phase retardation in a probing light beam reflected from thin-film samples. Scattering of light does not contribute to the detected signal.

The occurrence of multiple reflection in the stratified structure causes the reflection of light to exhibit characteristics of a Fabry–Pérot interferometer. Theoretical calculation of the overall phase change corresponding to the differential changes in indices of refraction and thickness of the electro-optic films resulted in a realistic model for the quantitative description of the process. An incident-angle-varying technique enables us to separate the field-induced changes in extraordinary index, in ordinary index, and in film thickness. Such separation is based on the fact that each field-induced change contributes to the overall phase retardation (measured quantity) with their distinct incident-angle dependences.

Electro-optic properties of various thin films grown on opaque substrates were characterized by means of the reflection differential ellipsometry. Using the incident-angle-varying technique and a data fitting scheme, the field-induced changes of the extraordinary index, of the ordinary index, and of the field-induced strain of a PLZT thin-film material grown on PT-coated silicon substrates were successfully determined. The reflection differential ellipsometry also provides a means of directly measuring the relationship between the field-induced index change and the polarization of thin-film materials.

ACKNOWLEDGMENTS

F. W. would like to thank Dr. C. Bustamante and C.-B. Juang for introducing him to the differential polarization microscopy, from which the technique of transmissive differential ellipsometry for electro-optic measurements was developed. Dr. K. K. Li produced the antiferroelectric thin-film samples used in the measurements. This work was partially sponsored by the U.S. Office of Naval Research under Contract No. N00014-91-J508.

[1] C. E. Land, J. Am. Ceram. Soc. **72**, 2059 (1989).
[2] G. H. Haertling, Ferroelectrics **75**, 25 (1987).
[3] H. Adachi, T. Kawahuchi, K. Sentsune, K. Ohji, and K. Wasa, J. Appl. Phys. **42**, 867 (1983).
[4] K. Carl and K. Geisen, Proc. IEEE **61**, 967 (1973).
[5] F. Wang, C. B. Juang, C. Bustamante, and A. Y. Wu, in Proceedings of the 4th International SAMPE Electronics Conference, Albuquerque, NM, June 12–14, 1990, p. 712.
[6] G. W. Farnell, I. A. Cermak, P. Silverster, and S. K. Wong, IEEE Trans. Sonics Ultrasonics **SU-17**, 188 (1970).
[7] B. G. Potter, Jr., M. B. Sinclair, and D. Dimos, Appl. Phys. Lett. **63**, 2180 (1993).
[8] M. Ishida, H. Matsunami, and T. Tanaka, Appl. Phys. Lett. **31**, 433 (1977).
[9] D. Dimos, C. E. Land, and R. W. Schwartz, Ceram. Trans. **25**, 323 (1992).
[10] F. Wang, K. K. Li, E. Furman, and G. H. Haertling, Opt. Lett. **18**, 1615 (1993).
[11] F. Wang and G. H. Haertling, Appl. Phys. Lett. **63**, 1730 (1993).
[12] S. N. Jasperson and S. E. Schnatterly, Rev. Sci. Instrum. **40**, 761 (1969).
[13] A. Yariv and P. Yeh, in *Optical Waves in Crystals* (Wiley, New York, 1984).

[14]For theories of reflection of light from stratified structures references can be found in M. Born and E. Wolf, *Principle of Optics*, 6th ed. (Pergamon, Oxford, 1980), and R. M. A. Azzam and N. M. Bashara, *Ellipsometry and Polarized Light* (North-Holland, Amsterdam, 1977).
[15]For theories of light reflection from conducting materials references can be found in A. Vasicek, *Optics of Thin Films* (North-Holland, Amsterdam, 1960), and J. Lekner, *Theory of Reflection* (Martinus Nijhoff, Dordrecht, 1987).
[16]F. Wang and G. H. Haertling, in Proceedings of the 9th IEEE International Symposium on the Application of Ferroelectrics, University Park, PA, 7–10 August 1994.
[17]G. H. Haertling and C. E. Land, J. Am. Ceram. Soc. 54, 1 (1971).

Birefringent bistability in $(Pb,La)(Zr,Ti)O_3$ thin films with a ferroelectric-semiconductor interface

Feiling Wang and Gene H. Haertling
Department of Ceramic Engineering, Clemson University, Clemson, South Carolina 29634-0907

(Received 29 March 1993; accepted for publication 16 July 1993)

We report a birefringent bistability exhibited in ferroelectric thin films with a ferroelectric-semiconductor interface. Such birefringent bistability is observed in $(Pb,La)(Zr,Ti)O_3$ (PLZT) thin films which are sandwiched between a platinum and a semiconducting indium-tin oxide (ITO) electrode. The magnitude of the birefringence between the two remanent states is approximately 0.9×10^{-3}. The Pt/PLZT/ITO structure features a nonvolatile electro-optic memory operation, i.e., the switching between the two remanent birefringent states with bipolar electric pulses.

Ferroelectric polarization reversal, which has facilitated a nonvolatile memory mechanism for electric signals,[1,2] has not proved to be able to perform a nonvolatile electro-optic memory function for optical signals due to the fact that the two remanent polarization states in normal ferroelectric materials are optically indistinguishable. The symmetry in the optical properties under polarization reversal may be broken if one of the polarization directions is made more favorable than the other under the influence of certain electrode combinations. The asymmetric polarization in ferroelectric thin films on semiconductor substrates has been observed,[3] however, its implications for the electro-optic properties of the thin films have not been studied. The purpose of this letter is to report the phenomenon of a birefringent bistability associated with the polarization reversal in ferroelectric $(Pb,La)(Zr,Ti)O_3$ (PLZT)[4] thin films which are electroded with a metal and a semiconducting layer.

The birefringent bistability in PLZT thin films was observed to exist in a thin film metal/ferroelectric/semiconductor (MFS) structure shown in Fig. 1. Polycrystalline PLZT thin films of composition 8/65/35(La/Zr/Ti) were deposited on Pt-coated silicon substrates by means of magnetron sputtering. The thickness of the PLZT films was approximately 750 nm. Indium-tin oxide (ITO) films of about 350 nm in thickness were then deposited on the PLZT films also by sputtering. A post-deposition annealing process was used to obtain a perovskite crystalline structure of the PLZT material.

With dc voltage or electric pulses applied to the platinum and the ITO layers, a sandwiched PLZT film becomes birefringent with its c axis along the normal of the film surface as a result of the transverse electro-optic effect. A phase-detection scheme in the reflection mode, with the experimental setup shown in Fig. 2, was used to measure the field-induced birefringence, $\Delta n=n_e-n_0$, in the PLZT thin film. The modulation of the incident light was provided by a photoelastic modulator. At a finite incident angle, the reflected light polarized in the incident plane acquires a phase retardation with respect to the component polarized perpendicularly to the incident plane due to the birefringence of the PLZT thin films. Such phase retardation is associated with a modulating component of the light received by the photodetector. With a proper setting of the reference signal, the output of the lock-in amplifier is proportional to the birefringence, Δn, of the PLZT thin films.

The birefringence in the PLZT films as a function of the slowly varying dc voltage exhibited severe asymmetry as revealed by a typical loop shown in the insert of Fig. 3. The voltage shown in the figure is measured with respect to the platinum electrode. An important feature of Fig. 3 is that there are two distinguishable remanent birefringent states dependent on the polarity of the voltage from which the zero voltage is reached. The occurrence of the two distinguishable remanent birefringent states is not a result of accidental poling of the material during the initial application of an electric field, since all samples reproduced the same features as in Fig. 3 regardless of the polarity of the initial electric field. To further verify the inherent nature of these two distinguishable birefringent states, a series of plots were successively taken from a small to a large field scan range. As shown in Fig. 3, with the increase of the scan range, the two remanent birefringent states approach their saturation values, Δn_A and Δn_B, respectively.

The interswitching of the two remanent birefringent states with electric signals was achieved by applying bipolar electric pulses to the MFS devices. With the detection system shown in Fig. 2, the output voltage of the lock-in amplifier (proportional to the birefringence of the thin film) was recorded versus time when bipolar electric pulses were fed to the device. Figure 4 represents the birefringent signal forms of the PLZT film responding to bipolar elec-

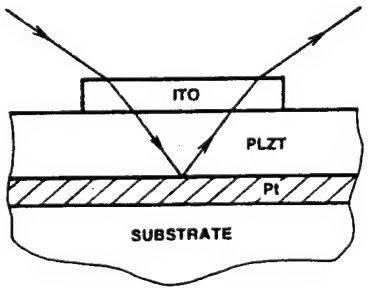

FIG. 1. Structure of the Pt/PLZT/ITO thin film device. The propagation of the light beam in the phase-detection measurement is shown by the line with arrows.

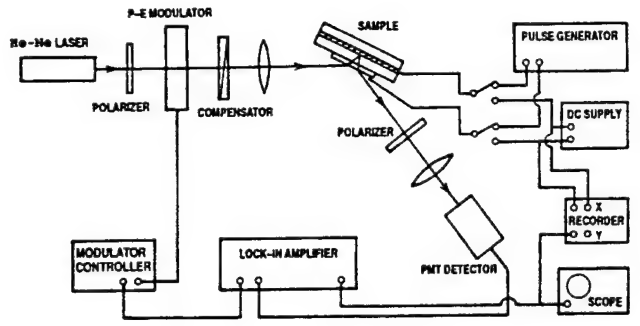

FIG. 2. Schematic diagram for the phase-detection scheme in the reflection mode.

tric pulses of 0.1 ms in pulse width and peak voltage ranging from 5 to 30 V. The interval between the pulses was 5 s. The dashed line schematically denotes the polarities and positions of the bipolar pulses.

It is shown in Fig. 4 that bipolar electric pulses switch the PLZT thin film between two distinguishable birefringent states, which correspond to the two remanent states for each dc cycle in Fig. 3. The magnitude of the birefringence between the two remanent states (birefringent spacing) substantially increases with increasing peak voltage of the pulse until saturation behavior takes place. The saturated birefringent spacing is approximately 0.9×10^{-3}. Such saturation is consistent with the dc response of the devices shown in Fig. 3. The nonvolatile nature of the birefringent switching is obvious in that after a positive pulse, the thin film remains in a low birefringent state until the following negative pulse switches the material to a high birefringent state. Because of the detection method, the response speed of the measuring system was determined by the integration time of the lock-in amplifier. The transient behavior of the switching, therefore, cannot be directly observed with this measurement.

Figure 5 shows the birefringent spacing of the device as a function of the pulse width while keeping the peak voltage constant. Although the intrinsic switching speed of the PLZT thin film is essentially determined by the domain switching process, the response time of the device, however, may be predominated by the rc constant of the device, which was approximately 2.5 μs. It is shown in Fig. 5 that when the pulse width becomes comparable to the rc constant of the device, the birefringent spacing between the two states is significantly reduced, indicating an incomplete switching of the ferroelectric domains. When the pulse width becomes much larger than the rc constant, the birefringent spacing is no longer dependent on the pulse width.

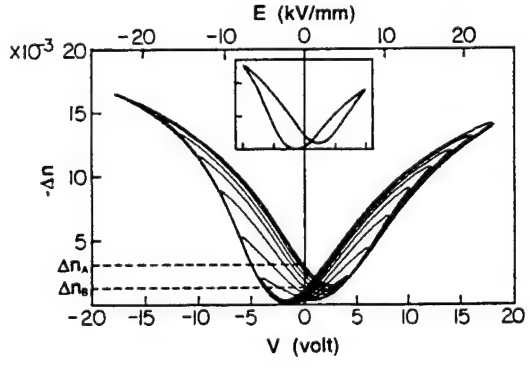

FIG. 3. Measured birefringence Δn in the PLZT thin film as a function of the slowly varying dc voltage, taken successively from a small to a large dc field scan range. A single cycle is shown in the insert. The horizontal and the vertical scales of the insert are 5×10^{-3} per division and 5 V per division, respectively.

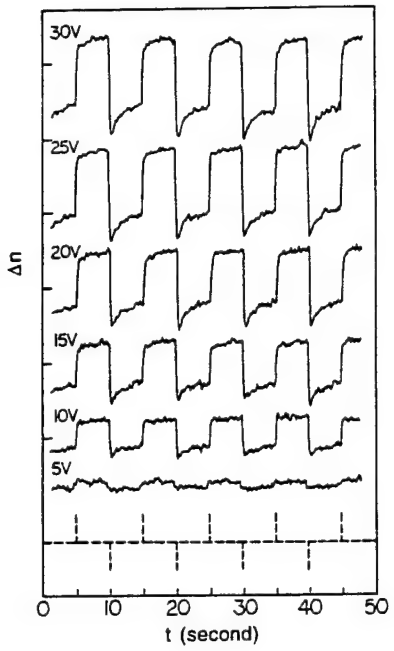

FIG. 4. Interswitching between the two remanent birefringent states with bipolar electric pulses. The peak voltage of the switching pulses are marked on each curve. The dashed line schematically denotes the positions and the polarities of the bipolar pulses. The vertical scale for the birefringence is 10^{-3} per division.

The occurrence of the birefringent bistability in the device may be explained by the polarity sensitive polarization of the PLZT thin films with a ferroelectric-semiconductor interface. It was recognized that electrodes in contact with a ferroelectric material play an important role in sustaining polarizations in the ferroelectric material.[5] In particular, the compensation of surface charges by electrodes is sometimes crucial in determining the remanent polarization in thin film ferroelectrics. Experimental evidence has shown that the birefringent bistability in the

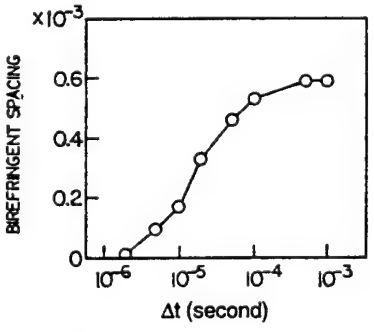

FIG. 5. Birefringent spacing between the two remanent states as a function of the pulse width with a fixed peak voltage of 15 V.

MFS structure was a result of the unequal remanent polarizations of opposite polarities caused by the PLZT/ITO interface. Being an *n*-type semiconductor,[6] an ITO film is expected to form a *p-n* junction with the PLZT thin film that usually exhibits *p*-type conduction properties.[7] Under the short-circuit condition, the band bending in the *p-n* junction creates a built-in bias (inside the PLZT film) that enhances the polarization in the direction of the ITO layer and suppresses the polarization in the direction of the Pt electrode. As a result, the PLZT thin films possess a higher remanent polarization when the zero voltage is reached from a negative polarity than a opposite polarity. A higher remanent polarization, in turn, produced a higher remanent birefringence in the PLZT thin films. It should be pointed out that the mechanism of the birefringent bistability is yet to be fully understood.

The birefringent bistability in the MFS structure is a potential mechanism for realizing a nonvolatile programmable spatial light modulator. It is also suitable for integrated devices in waveguide architectures. The Pt/PLZT/ITO device presented here is actually a complete electrically addressable nonvolatile electro-optic memory unit.

The authors would like to thank E. Furman for many helpful discussions. This study was sponsored by the Office of Naval Research under Contract No. N00014-91-J508.

[1] J. T. Evans and R. Womack, IEEE J. Solid-State Circuits **23**, 1171 (1988).
[2] G. H. Haertling, J. Vac. Sci. Technol. A **9**, 414 (1991).
[3] Y. Xu, C. Chen, R. Xu, and J. D. Mackenzie, J. Appl. Phys. **67**, 2985 (1990).
[4] G. H. Haertling and C. E. Land, J. Am. Ceram. Soc. **54**, 1 (1971).
[5] D. Wurfel and I. P. Batra, Phys. Rev. B **8**, 5126 (1973).
[6] K. S. Sree Harsha, K. J. Bachmann, P. H. Schmidt, E. G. Spencer, and F. A. Thiel, Appl. Phys. Lett. **30**, 645 (1977).
[7] Z. Wu and M. Sayer, *Proceedings of the 1990 IEEE 7th International Symposium on the Applications of Ferroelectrics* (IEEE, Service Center, Piscataway, NJ, 1991), p. 677.

Transverse electro-optic effect of antiferroelectric lead zirconate thin films

Feiling Wang, Kewen K. Li, and Gene H. Haertling

Department of Ceramic Engineering, Clemson University, Clemson, South Carolina 29634-0907

Received March 16, 1992

The transverse electro-optic effect in antiferroelectric lead zirconate thin films grown on fused quartz is observed. The birefringence shift as a function of the external electric field exhibits a characteristic response that is related to the electric-field-induced antiferroelectric-to-ferroelectric structural transition.

Dielectric properties of lead zirconate ($PbZrO_3$) ceramic have been extensively studied.[1–5] The appeal of lead zirconate is its antiferroelectric (AFE) crystal structure at room temperature. It is well known that a transition to a ferroelectric (FE) or paraelectric phase occurs in lead zirconate when it is subjected to a sufficiently high external electric field or elevated temperatures; however, the electro-optic properties of lead zirconate have not yet been explored in either bulk or thin-film form. The recent success in depositing lead zirconate thin films[6] has opened up the possibility of new integrated devices for utilizing its unique electro-optic response. This Letter is mainly concerned with the transverse electro-optic effect detected from lead zirconate thin films.

Lead zirconate thin films were deposited onto optically polished fused quartz by a dip-coating technique from an acetate precursor solution.[7] Room-temperature x-ray diffraction patterns showed a peak at $2\theta \cong 16.9$ deg, which is characteristic of the AFE double-cell crystal structure. Copper electrode pairs with a gap width of 50 μm were fabricated on top of the films by a photolithography process. The transverse electro-optic properties were measured by means of a phase-detection technique[8] in the transmission mode. The light source was a He–Ne laser of 632.8-nm wavelength. The modulation of the laser beam was provided by a photoelastic modulator. Since in the phase-detection schemes the amplitude of the lock-in frequency is proportional to the phase retardation generated by the thin film, the possible electric-field-induced scattering effect[9] did not contribute to the output signal. The system was calibrated with an optical compensator.

A typical room-temperature birefringence shift of the lead zirconate thin film as a function of the applied dc electric field is shown in Fig. 1. The film thickness was 0.65 μm. As seen from the figure, the hysteresis loop shows characteristic differences from the normal response of ferroelectric materials, e.g., lead lanthanum zirconate titanate (PLZT) of composition 8/65/35.[10] The most characteristic feature is represented by the enhanced hysteretic behavior in the high-electric-field region (10–20 kV/mm) and the rapid increase of the slope when the increasing external electric field exceeds 17 kV/mm. The raggedness of the curve was caused by the system noise.

The observed birefringence curve can be related to the electric-field-induced AFE–FE phase transition in the lead zirconate thin films. It is known that an AFE–FE phase transition can be induced by an external electric field at temperatures slightly below the Curie point. The dielectric property corresponding to such a phase transition is the occurrence of the double hysteresis loop.[1] To demonstrate that such a field-induced phase transition can also occur in a lead zirconate thin film at room temperature, thin films were also deposited on silicon substrates coated with a conductive Pt/Ti metallization layer. Figure 2 shows typical room-temperature dielectric hysteresis of the films measured under dc and ac conditions. Compared with that of the double hysteresis loop obtained by Shirane *et al.*[1] at a temperature of 228°C, the critical electric field E_f for the AFE $\rightarrow$ FE phase transition in the thin-film lead zirconate at room temperature is approximately an order of magnitude higher (at roughly 25 kV/mm). A possible reason for the large difference is that the farther the temperature is below the Curie point, the higher the external field that is required to cause the phase transition.

A model of the transverse electro-optic effect of polar materials shows that the change of refractive index along the polar direction can be in general described by a quadratic effect, whereas the linear electro-optic effect can be considered as a quadratic effect biased by an additional local electric field created by the spontaneous polarization.[11,12] If we assume that this view point applies when an AFE–FE phase transition occurs, the dependence of the field-induced birefringence shift Δn on the low-frequency external electric field E and the polarization $P(E)$ should obey roughly the following relation:

$$\Delta n \propto \left[E + \frac{4\pi}{3}P(E)\right]^2, \tag{1}$$

where the local electric field is approximated by the Lorentz formula for cubic materials. The solid

0146-9592/92/161122-03$5.00/0

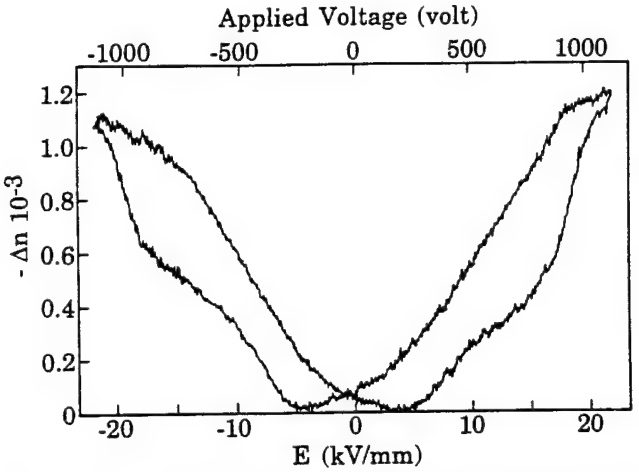

Fig. 1. Measured birefringence shift Δn as a function of the applied electric field E in a lead zirconate thin film on fused quartz.

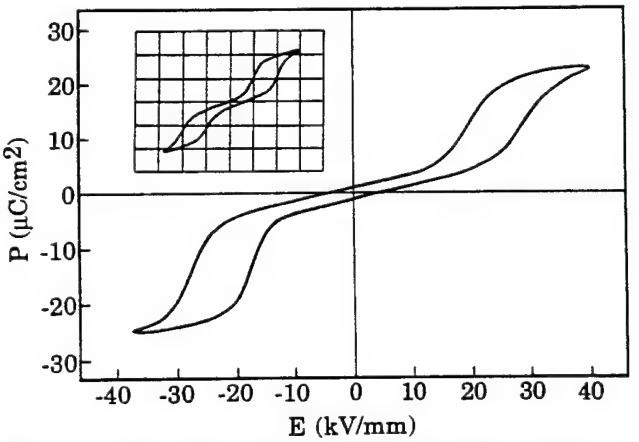

Fig. 2. Measured dc and ac (inset) dielectric property of a lead zirconate thin film on a Pt/Ti-coated silicon substrate. The direction of the electric field is perpendicular to the thin film. The horizontal and vertical scales for the ac loop are 15.4 kV/mm per division and 15.1 $\mu C/cm^2$ per division, respectively.

curve in Fig. 3 is a prediction of the birefringence curve calculated from a double hysteresis loop (dashed curve) by using relation (1). Although Fig. 1 indeed reveals some of the main features predicted by relation (1), a quantitative correlation between the dielectric hysteresis loop and the electro-optic hysteresis loop was not possible. As can be seen, the dielectric loop of Fig. 2 indicates that a rapid increase of the slope for the field-induced birefringence curve should occur near $E = 25$ kV/mm when approached from below. The experimental result (Fig. 1) shows that this transition actually occurs at an external field of approximately 18 kV/mm for the film on fused silica. The discrepancy may be caused by the following three main reasons: (1) the measurements of the dielectric properties and electro-optic properties involved thin films deposited onto two different types of substrate, i.e., fused quartz and Pt/Ti-coated silicon, owing to the requirements of the experimental methods; (2) in the two measurements, the external fields were applied in two different directions to the thin-film materials, which were generally anisotropic; and (3) in the electro-optic measurements, the distribution of the applied field in the film was nonuniform and possessed the general feature that the field strength at the edge of the electrodes was considerably higher than at the central region of the gap.[13] The electric-field strength as marked on the x axis in Fig. 1 is actually the average lateral field across the gap, which is given by $E = V/g$, where V is the applied voltage and g is the gap width. The distribution of the electric field implies that the AFE–FE phase transition does not occur simultaneously across the gap.

Both dielectric and electro-optic measurements suggest that the lead zirconate thin films possess a certain amount of FE crystal structure at room temperature in addition to the AFE phase. The FE phase is indicated by the hysteretic behavior in the low-electric-field region of the hysteresis loops. This mixed phase may be related to the stress and strain produced by the film–substrate interface.

Assuming that the lead zirconate thin film possesses the same nonlinear polarizability at optical frequencies as its isomorphs (as implied by Miller's rule[14]), e.g., PLZT thin films of composition 8/65/35, we estimate the birefringence shift in the polarization saturation region to be of the order of 10^{-3}, which is consistent with the measured value at an electric-field strength near 20 kV/mm. As in other nonlinear-optical materials, the transverse electro-optic effect in the lead zirconate thin films consists of an electronic contribution and an ionic contribution. Although the ionic response is not essential for some applications, the characteristic electro-optic response in the lead zirconate thin films can be observed only when the electric-field-induced AFE–FE phase transition occurs. The response time for the AFE–FE phase transition in the lead

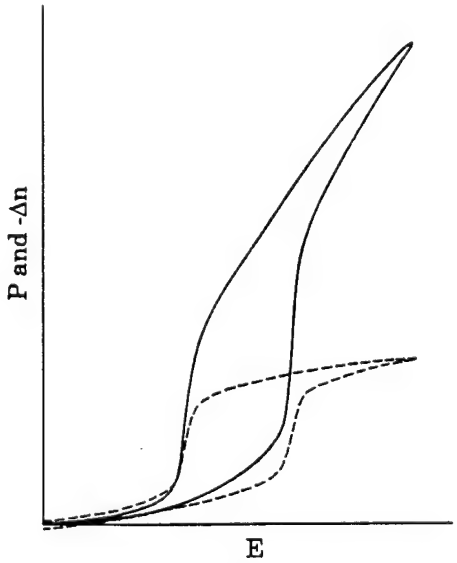

Fig. 3. Prediction of the transverse electro-optic property of a material under AFE–FE phase transition. The solid curve for Δn versus E is calculated from the dashed curve for P versus E by using relation (1).

zirconate thin films is still unknown; however, we may speculate that the time scale for such a process is a microsecond, as observed in related materials.[15]

The authors acknowledge the participation of R. Owens in this research.

References

1. G. Shirane, E. Sawaguchi, and Y. Takagi, Phys. Rev. **84,** 476 (1951).
2. F. Jona, G. Shirane, F. Mazzi, and R. Pepinsky, Phys. Rev. **105,** 849 (1957).
3. B. A. Scott and G. Burns, J. Am. Ceram. Soc. **55,** 331 (1972).
4. O. E. Fesenko, R. V. Kdesova, and Yu G. Sindeev, Sov. Phys. Solid State **21,** 668 (1979).
5. M. T. Lanagan, J. H. Kim, S.-J. Jang, and R. E. Newnham, J. Am. Ceram. Soc. **71,** 311 (1988).
6. K. K. Li, F. Wang, and G. H. Haertling, "Antiferroelectric lead zirconate thin films derived from an acetate precursor system," J. Mater. Sci. (to be published).
7. G. H. Haertling, Ferroelectrics **116,** 51 (1991).
8. F. Wang, C. B. Juang, C. Bustamante, and A. Y. Wu, in *Proceedings of the 4th International SAMPE Electronics Conference* (Society for the Advancement of Material and Process Engineering, Covina, Calif., 1990), p. 712.
9. C. E. Land, IEEE Trans. Electron Devices **ED-26,** 1143 (1979).
10. G. H. Haertling and C. E. Land, J. Am. Ceram. Soc. **54,** 1 (1971).
11. S. K. Kurtz and F. N. H. Robinson, Appl. Phys. Lett. **10,** 62 (1967).
12. M. DiDomenico, Jr., and S. H. Wemple, J. Appl. Phys. **40,** 720 (1969).
13. G. W. Farnell, I. A. Cermak, P. Silvester, and S. K. Wong, IEEE Trans. Sonics Ultrason. **SU-17,** 188 (1970).
14. R. C. Miller, Appl. Phys. Lett. **5,** 17 (1964).
15. W. Pan, Q. Zhang, A. Bhalla, and L. E. Cross, J. Am. Ceram. Soc. **72,** 571 (1989).

Discrete electro-optic response in lead zirconate thin films from a field-induced phase transition

Feiling Wang, Kewen K. Li, Eugene Furman, and Gene H. Haertling

Department of Ceramic Engineering, Clemson University, Clemson, South Carolina 29634

Received May 4, 1993

A discrete transverse electro-optic response associated with a field-induced antiferroelectric–ferroelectric phase transition has been observed to exist in lead zirconate thin films grown on Pt/Ti-coated silicon substrates. The magnitude of the birefringence jump from the antiferroelectric to the ferroelectric state is approximately 2.5×10^{-2}. Quantitative correlation between the field-induced birefringence and the polarization was also experimentally studied. The discrete birefringent change in the thin films may be a desirable property for applications in optical switches or other integrated-optical devices.

The field-induced antiferroelectric (AFE)–ferroelectric (FE) phase transition has been utilized to produce discrete strain for applications in actuators and shape memory.[1,2] To exploit optical usefulness of AFE materials, one can ask questions as to whether a field-induced AFE–FE phase transition is accompanied by a discrete change in optical properties of the materials. In a recent Letter the transverse electro-optic effect in AFE lead zirconate (PZ) thin films was reported.[3] It was found that the field-induced birefringence in the PZ films exhibited a characteristic response different from that of ferroelectric materials; this response was attributed to the field-induced AFE–FE structural transition. However, because of the field nonuniformity created by the planar electrodes, the measured birefringence did not clearly show the discrete change under the field-induced AFE–FE phase transition predicted by a phenomenological model. The electro-optic measurement in the transmission mode also made it unfeasible to study experimentally the correlation between the birefringence of the thin film materials and their polarization because (1) the electro-optic properties and the dielectric properties had to be measured from thin films deposited onto two different types of substrate, and (2) the direction of the external electric field was different for the two types of measurement owing to the requirements of the measuring methods.

With a newly developed measuring method that uses a phase-detection scheme in the reflection mode, it has become possible to measure the electro-optic effect of thin films deposited onto opaque substrates. Both dielectric and electro-optic properties of the thin films therefore can be measured from the same sample with the same configuration of electrodes. The purpose of this Letter is to report what is to our knowledge the first observation of the discrete birefringent change in PZ thin films under field-induced AFE–FE phase transitions and the direct measurement of the correlation between the field-induced birefringence and the polarization of the materials.

Polycrystalline PZ films were deposited onto Pt/Ti-coated silicon wafers by using an automated dip-coating technique from an acetate precursor.[4,5] Indium tin oxide (ITO) layers were deposited onto the films as top electrodes by means of magnetron sputtering for both dielectric and electro-optic measurements. The dielectric properties of the films were measured by means of a Sawyer–Tower circuit. When a voltage is applied to the ITO and the Pt electrodes, a sandwiched PZ thin film becomes birefringent, with its c axis along the normal of the film surface as a result of the transverse electro-optic effect. A reflection-mode phase-detection technique, a modification of the transmission-mode phase-detection technique,[6] was used to measure the field-induced birefringence, $\Delta n = n_e - n_o$, in the PZ thin films. The arrangement of the optics and the electrodes is illustrated in Fig. 1. A He–Ne laser of 632.8-nm wavelength was utilized as the light source. The polarizers, P and P′, are inclined 45° with respect to the incident plane and mutually crossed. The polarization state of the light beam was modulated in a periodic manner by means of a photoelastic modulator, M. At a finite incident

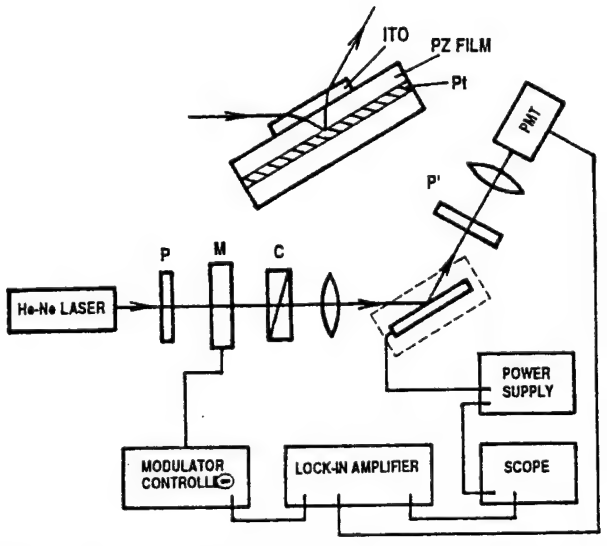

Fig. 1. Measuring system for the field-induced birefringence of the PZ films. Also shown is the arrangement of the electrodes. PMT, photomultiplier tube.

0146-9592/93/191615-03$6.00/0

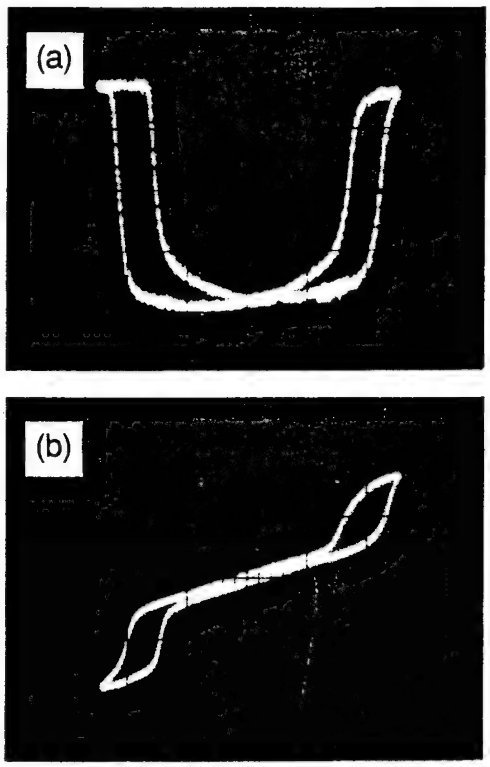

Fig. 2. (a) Field-induced birefringence as a function of the applied low-frequency voltage, (b) polarization as a function of the applied low-frequency voltage. The horizontal scale is 20 volts per division. The vertical scales are -0.7×10^{-2} and 20 $\mu C/cm^2$ for (a) and (b), respectively.

angle, the reflected light polarized in the incident plane acquires a phase retardation with respect to the component polarized perpendicularly to the incident plane as a result of the birefringence of the PZ thin film. Under a properly chosen reference signal in the lock-in amplifier at the modulation frequency (synchronized with the photoelastic modulator), the output signal of the lock-in amplifier is proportional to the phase retardation generated by the thin film. The proportional constant was calibrated by using the adjustable optical compensator, C.

A typical response of the birefringence in the PZ films versus low-frequency (~0.2-Hz) voltage is shown in Fig. 2(a). The voltage was measured with respect to the bottom electrode, i.e., platinum coating. The thickness of the PZ film was approximately 1 μm. A clear transition is manifested with an abrupt increase of the birefringence as the increasing external field reaches approximately 40 kV/mm (40 V). The enhanced birefringence is sustained until the field is reduced below approximately 30 kV/mm (30 V). In order to relate the observed electro-optic response of the PZ thin film with its dielectric properties, we measured a polarization-versus-voltage loop, shown in Fig. 2(b), from the same sample. Figure 2(b) exhibits a typical double-hysteresis loop for AFE materials under a field-induced AFE–FE structural transition. Comparing Figs. 2(a) and 2(b), it is clear that the transition behavior in the electro-optic response occurs precisely at the electric field where the field-induced AFE–FE transition occurs. Such an electro-optic response is consistent with an earlier prediction.[3] The reason for the discrete change in the birefringence to be observed in this measurement was that the electric field in the thin-film material during the reflection-mode phase-detection measurement was uniform. The magnitude of the birefringent difference between the AFE state (Δn_A) and the FE state (Δn_F) is approximately $\Delta n_A - \Delta n_F = 2.5 \times 10^{-2}$, which is similar to that of perovskite thin film in ferroelectric phase, i.e., 8/65/35 lead lanthanum zirconate titanate, under polarization saturation.[7]

Although the main features of the electro-optic response shown in Fig. 2 are consistent with the theoretical prediction, the quantitative correlation between the birefringence Δn and the polarization of the thin-film materials possesses a more complicated behavior. In Fig. 3, the field-induced birefringence is plotted as a function of the polarization by detecting both quantities simultaneously in a low-frequency voltage cycle. Portion A of the curve corresponds to the AFE state of the material; portions F and F′ correspond to the field-induced FE state, while portions B and B′ of the curve correspond to the phase transition, which occupies a small portion of the time duration in the voltage cycle. In the field-induced FE state the birefringence exhibits a different polarization dependence from that in the AFE state. Detailed measurements showed that within the AFE region the birefringence of the thin films can be described by a quadratic function of the polarization as expected by using a phenomenological model similar to that for FE materials. In the field-induced FE region, however, the birefringence exhibits a saturation behavior that is not fully understood at present. The splitting of the curve in the phase-transition region indicates that a single order parameter, namely polarization, is not sufficient for determining the birefringence of the material during the phase transition. The asymmetry shown in both Figs. 2 and 3 may be attributed to a ferroelectric–semiconductor contact behavior in the presence of ITO electrodes.[7]

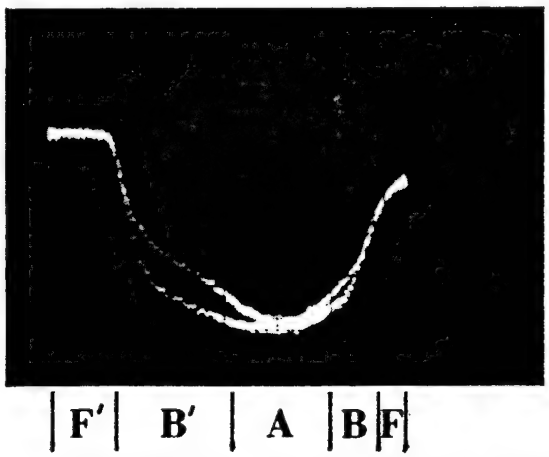

Fig. 3. Birefringence as a function of the polarization. The horizontal and vertical scales are 10 $\mu C/cm^2$ per division and -0.7×10^{-2}, respectively.

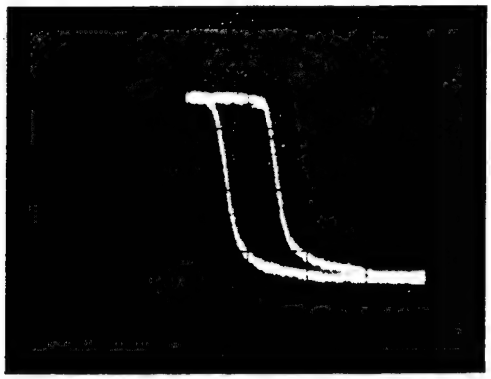

Fig. 4. Birefringence-versus-applied-voltage curve under a bias of −20 V. The horizontal and vertical scales are 10 volts per division and -0.7×10^{-2} per division, respectively.

The quadratic electro-optic R coefficient for the PZ thin film in the AFE phase is evaluated from the experimental data to be approximately 3×10^{-19} $(m/V)^2$, which is 2 orders of magnitude smaller than that of a typical FE perovskite thin-film material. Because the low-frequency linear susceptibility of the PZ films is an order of magnitude smaller than that of FE perovskite materials, the quadratic polarization-optical g coefficient defined by

$$\Delta n = -\frac{1}{2} n^3 g P^2, \tag{1}$$

where P is the polarization of the material, yields $g = 0.05$ m^4 C^{-2}, which is close to the typical value for perovskite materials in the FE phase.[8] This result seems to extend the boundary of Miller's rule[9] into AFE materials. An explanation of the constancy of the polarization-optical g coefficient is that the field-induced birefringence in a perovskite material is determined by the (low-frequency) local bias field that is dominated by the linear susceptibility of the materials at the low frequency, provided that the nonlinear polarizability at optical frequencies is similar for all perovskite materials, including AFE materials. The nonlinear polarizability of the materials at optical frequencies is known to be dominated by the electronic polarization determined by a structure common to all perovskites, namely, oxygen octahedra.[10,11]

The observed discrete change of the field-induced birefringence at the AFE–FE phase transition field may be utilized in optical switches or spatial light modulators. With a bias field, the thin-film materials exhibits a birefringent bistability, as shown by the biased Δn-versus-voltage loop in Fig. 4. Such bistability may be used to realize programmable spatial light modulators, in which on/off status of a pixel can be interswitched by bipolar electric pulses.

This study was sponsored by the U.S. Office of Naval Research under contract N00014-19-J-508.

References

1. K. Uchino, Jpn. J. Appl. Phys. **24** (Suppl. 2), 460 (1985).
2. W. Pan, C. Q. Dam, Q. Zhang, and L. E. Cross, J. Appl. Phys. **66,** 6014 (1989).
3. F. Wang, K. K. Li, and G. H. Haertling, Opt. Lett. **17,** 1122 (1992).
4. K. K. Li, F. Wang, and G. H. Haertling, "Antiferroelectric lead zirconate thin films derived from an acetate precursor system," J. Mater. Sci. (to be published).
5. G. H. Haertling, Ferroelectrics **116,** 51 (1991).
6. F. Wang, "Electro-optic properties of (Pb,La)(Zr,Ti)O_3 thin film and related materials," Ph.D. dissertation (University of New Mexico, Albuquerque, N.M., 1991), p. 12.
7. F. Wang and G. H. Haertling, "Birefringent bistability in (Pb,La)(Zr,Ti)O_3 thin films with a ferroelectric–semiconductor interface," Appl. Phys. Lett. (to be published).
8. P. D. Thacher, J. Appl. Phys. **41,** 4790 (1970).
9. R. C. Miller, Appl. Phys. Lett. **5,** 17 (1964).
10. M. DiDomenico, Jr., and S. H. Wemple, J. Appl. Phys. **40,** 720 (1969).
11. F. Wang and A. Y. Wu, Phys. Rev. B **46,** 3709 (1992).

Large Electrooptic Modulation Using Ferroelectric Thin Films in a Fabry-Perot Cavity

Feiling Wang and Gene H. Haertling
Gilbert C. Robinson Department of Ceramic Engineering
Clemson University
Clemson, South Carolina 29634-0907

Abstract — We report a reflective thin film ferroelectric light modulator which has exhibited optical phase modulation as large as fifty degrees and on/off signal ratio of twenty for intensity modulation. The large optical modulation was achieved by means of multiple reflection. A ferroelectric (FE) PLZT thin film material, deposited on Pt-coated silicon substrate, was used as the modulating medium. An indium-tin oxide (ITO) thin layer was deposited on the ferroelectric films as the top electrode. A He-Ne laser beam was obliquely incident on the ITO/FE/Pt structure. The light modulation was detected in the laser beam reflected from the thin film structure when a voltage signal was applied to the ITO and Pt electrodes. Unlike transmission-mode modulators, the sandwich of the ferroelectric films between the air-ITO and FE-Pt interfaces exhibited characteristics of a Fabry-Perot etalon. Near a Fabry-Perot peak, drastically enhanced light modulation than transmission devices was obtained. Design principles and the performance of the modulator are discussed.

Introduction

A number of thin film ferroelectric materials, including lead lanthanum zirconate titanate (PLZT), barium titanate, lithium niobate, strontium barium niobate and lead magnesium niobate, have exhibited attractive birefringent electrooptic effect when deposited on suitable substrates [1]-[4]. Using these materials for optical modulation has been the focus of many studies. Integrated optical modulators using ferroelectric media may adopt three different designs, namely, transmission devices, waveguide devices and reflection devices. Transmission modulators are not compatible with opaque substrates; their usage are thus limited. They also suffer from shallow modulation depth because of the rather short optical path. Waveguide devices, such as total internal reflection (TIR) switch, using PLZT thin films grown on sapphire substrate have been successfully demonstrated [5].

With the advances in high-performance optoelectronic devices, it has become increasingly desirable to realize the integration of thin film optical modulators with semiconductor substrates to form hybrid devices [6]. Ferroelectric optical modulators in these devices may perform such functions as electrical-optical signal interface through spatial light modulation, intra- and inter-chip optical interconnections. The same ferroelectric media in these device may also perform all-optical operations, such as frequency doubling and optical logic, by using their outstanding optical nonlinearities. Combined with the more traditional task for ferroelectrics, namely, nonvolatile memory capability, ferroelectric thin films may become multifuctional media in various integrated optoelectronic devices. Using ferroelectric/electrooptic thin film for optical interconnection has been proposed by Lee and Ozguz [7],[8]. Enhanced phase retardation by means of interference has been observed in PZT films by Dimos *et al* [9], however, incoherent light scattering has prevented a sufficient signal-to-noise ratio for intensity modulation.

In this paper we will report a reflection thin film ferroelectric spatial light modulator constructed on silicon substrates. By adopting a low finesse Fabry-Perot cavity, the modulator can achieve large phase modulation and high signal-to-noise ratio for intensity modulation. The device may be used as an implementation of free-space optical interconnections.

Device Design and Theory of Modulation

The thin film light modulator was constructed on oxidized and Pt/Ti-metallized silicon wafers. Fine grain ferroelectric PLZT thin films were deposited on the metallized silicon substrates by using magnetron sputtering. An indium-tin oxide (ITO) layer was then sputter deposited on the ferroelectric thin films as top electrode. Figure 1 shows the schematic cross-section of the thin film modulator.

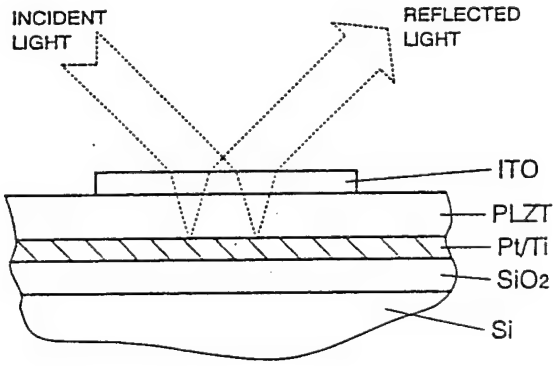

Figure 1. Schematic cross-section of the ferroelectric thin film reflection light modulator.

Linearly polarized light beam with equal amplitude for p-polarization (parallel to the incident plane) and s-polarization (perpendicular to the incident plane) was obliquely incident on the modulator as shown in Figure 1. Because of the polycrystalline nature of the ferroelectric thin films, the materials are optically uniaxial defined by the normal of the substrates. With an external electric field exerted through a voltage across the ITO and Pt layers, the extraordinary index n_e and ordinary index n_o experience field-induced changes, Δn_e and Δn_o, respectively. The corresponding changes in the indices for the p- and s-polarized light components are given by

$$\Delta n_p(\theta_2) = \sin^2\theta_2 \Delta n_e + \cos^2\theta_2 \Delta n_o \ ,$$
$$\Delta n_s = \Delta n_o \ . \qquad (1)$$

where θ_2 is the refraction angle of the light beam inside the ferroelectric thin film material. As the ferroelectric films are bounded by the Pt and ITO layers, the light beam experiences multiple reflections. Although all three interfaces, namely, air-ITO, ITO-FE and FE-Pt interfaces, cause light reflection, the air-ITO and FE-Pt boundaries dominates the characteristics of the reflected light beam because of the moderate difference between ITO and FE in refractive index. The device therefore can be characterized as a low finesse Fabry-Perot reflector. Under an external electric field, the optical length of the Fabry-Perot etalon becomes different for p- and s-polarized light components because of the field-induced birefringence in the ferroelectric thin films according to Equation (1). The polarization state of the reflected light, therefore, can be modulated with an voltage signal. As expected from any Fabry-Perot etalon, the modulation of the light can be greatly enhanced when a critical optical length of the etalon is satisfied. In the present devices, the critical optical length is determined by the thickness of the films and the incident angle of the light. Theoretical modeling has resulted in an accurate prediction for the light modulation as a function of the thickness of the films and incident angle [10]. The following equation can be used to formally describe the phase difference $\Delta\Gamma \equiv \Delta\Gamma_p - \Delta\Gamma_s$, between the field induced phase change in p-polarized light $\Delta\Gamma_p$ and s-polarization light $\Delta\Gamma_s$:

$$\Delta\Gamma = w_p \sin^2\theta_2 \, \Delta n_e - (w_s - w_p\cos^2\theta_2) \, \Delta n_o \ . \qquad (2)$$

where w_p and w_s are complicated functions of indices and thickness of all the layers involved as well as the incident angle. Figure 2 shows the calculated w_p and w_s as functions of the thickness of the ferroelectric layer with other parameters given. The oscillation of w_p and w_s is caused by the alternating phase relation between the neighboring reflected partial light beams with the thickness change. Consequently the total phase retardation of the device, $\Delta\Gamma$, exhibits similar oscillation. A phase retardation maximum occurs as neighboring reflected partial beams differ in optical phase by 180 degrees. Under this condition, partial light is forced to remain in the ferroelectric films for a much longer average path, experiencing accumulated phase retardation.

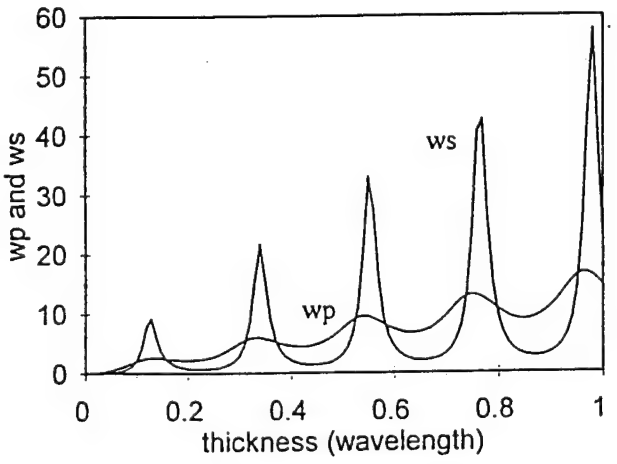

Figure 2. Calculated coefficients, w_p and w_s, as functions of the thickness of the electrooptic layer.

In order to characterize the ferroelectric thin film modulator, a reflection differential ellipsometer [11] was employed to measure the field-induced phase retardation of the reflected light. The intensity modulation of the light beam was measured with the optical setup shown in Figure 3. Linearly polarized He-Ne laser beam of 632.8 nm wavelength was obliquely incident on the thin film modulator, upon which electric signals were applied. A light sensor is located after a polarizer to detect the light reflected from the modulator.

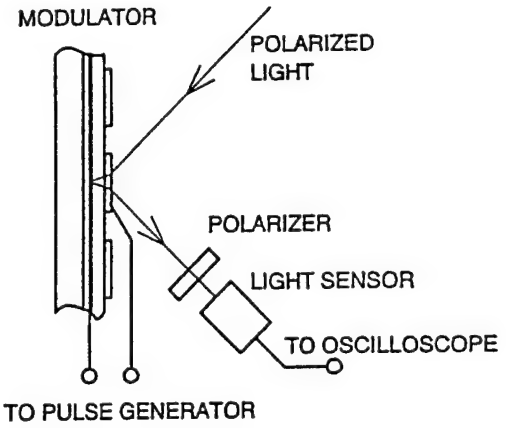

Figure 3. Light intensity modulation detecting system.

Experimental Results

Lead lanthanum zirconate titanate (PLZT) of composition 2/55/45 (La/Zr/Ti) was deposited on Pt/Ti-coated silicon substrate as the modulating medium. A post-deposition annealing process was employed to acquire the perovskite structure of the deposited thin films. Thickness of the PLZT films was approximately 480 nm. Indium-tin oxide layer of thickness approximately 350 nm was also sputter deposited on the PLZT films.

The phase shift of the reflected light beam as a function of the applied voltage, measured with the reflection differential ellipsometry, is shown in Figure 4. The measured phase shift roughly represented the birefringence, $\Delta n = \Delta n_e - \Delta n_o$, of the film when a proper incident angle was chosen for the measurement. As shown in the figure, the field-induced birefringence of the PLZT film exhibits a slightly asymmetric butterfly-shaped loop, typical for ferroelectric thin films. Field-induced phase shift loops were taken at various incident angles. A phase-shift peak was located at approximately 57 degrees, where phase shift reaches approximately 50 degrees. This peak is consistent with the model calculation, from which the thickness of the films was designed.

The performance of the device as a light intensity modulator was examined using the measuring system shown in Figure 3. Electric pulses were applied to the devices with 2 mm diameter ITO dots as top electrodes. Light intensity modulations, sensed by a photo-multiplier tube, were recorded by an oscilloscope. Figure 5 shows a light intensity modulation responding to electric pulses of 10 volts in peak height and 5 ms in pulse width. An on/off signal ratio of 12 was measured during this

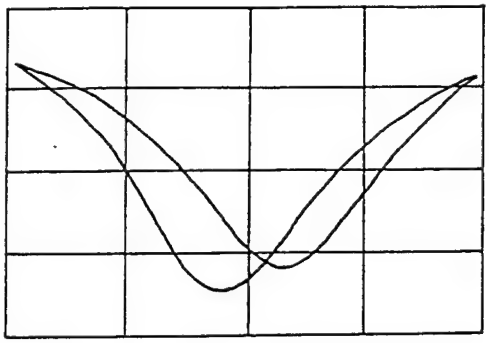

Figure 4. Field-induced relative phase shift (phase retardation) of the reflected light beam measured by using the reflection differential ellipsometer. The horizontal and vertical scales are 7.9 volts per division and 0.28 per division respectively.

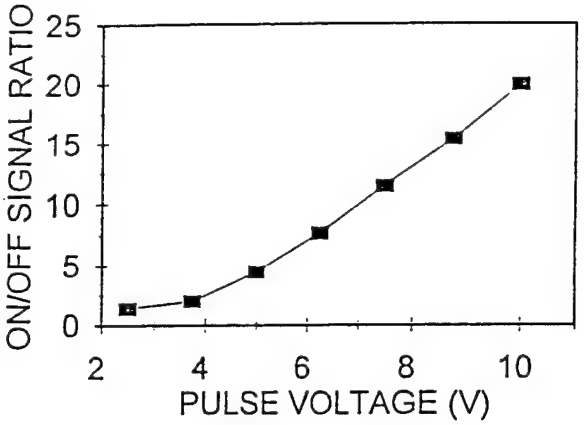

Figure 6. Light on/off ratio as a function of the pulse voltage.

operation. Higher on/off signal ratio may be acquired by further reducing the light in the off state. The on/off signal ratio as a function of the peak height of the pulses is shown by Figure 6. Light modulation remained substantial under pulses of peak height less than 5 volts, while modulation at 10 volts peak height was very visible.

Because of the large area of the top electrode for the convenience of the experiments, the rc constant limited the operation bandwidth of the devices. Under this limitation, intensity modulation at a frequency of 100 kHz was still detectable, although with much shallower modulation depth. The rc constant may be drastically reduced with reduced electrode area and wiring impedance, which will ultimately results in a material response limited operation bandwidth.

Because of the large field-induced birefringence in ferroelectric thin films, $\Delta n_e - \Delta n_o \approx 0.02$ under a moderate external field, the modulator remained a substantial on/off signal ratio for intensity modulation even when the incident angle is a few degrees away from the Fabry-Perot peak. This property gives the ferroelectric modulator a great tolerance to the error of thickness control of the films, vital for practical fabrications.

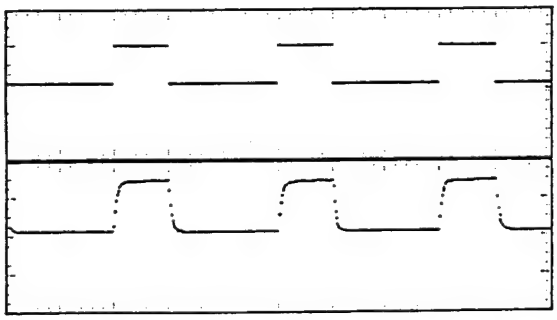

Figure 5. Light intensity modulation with electric pulses. The upper trace is the voltage signal applied to the modulator. The lower trace is the recorded light intensity reflected from the modulator. The horizontal scale is 5 ms per division. The vertical scale for the upper trace is 10 volts per division.

CONCLUSION

A thin film ferroelectric reflection spatial light modulator has been constructed on semiconductor substrates. The device consists of an ITO/PLZT/Pt thin film structure on oxidized silicon substrate. With the help of interference of multiple reflection, larger than 50 degrees phase shift in the reflected light from an obliquely incident light beam has been achieved. Using the device as an intensity light modulator, on/off signal ratio of twenty has been obtained with electric pulses of 10 peak voltage. This device may be used in various optoelectronic devices as an implementation of free-space optical interconnections.

ACKNOWLEDGMENTS

The authors benefited greatly from numerous discussions with E. Furman concerning this subject. This work was sponsored by the Office of Naval Research under Contract No. N00014-91-J508.

REFERENCES

[1] K. D. Preston and G. H. Haertling, "Comparison of electro-optic lead-lanthanum zirconate titanate films on crystalline and glass substrates," *Appl. Phys. Lett.* vol. 60, pp.2831-33, June 1992.

[2] A. Wegner *et al*, "Integrated PLZT thin film waveguide modulators'" *Ferroelectrics*, vol. 116, pp. 195-204, 1991.

[3] H. Adachi *et al*, "Electro-optic effects of (Pb,La)(Zr,Ti)O_3 thin films prepared by rf planar magnetron sputtering," *Appl. Phys. Lett.* vol. 42, pp. 867-68, May 1983.

[4] F. Wang and G. H. Haertling, "Birefringent bistability in (Pb,La)(Zr,Ti)O_3 thin films with a ferroelectric-semiconductor interface," *Appl. Phys. Lett.* vol. 63, pp. 1730-32, Sep. 1993.

[5] H. Higashino *et al*, "High speed optical TIR switched using PLZT thin-film waveguides on sapphire," *Japan. J. Appl. Phys.*, vol. 24, suppl. 24-2, pp. 284-86, 1985.

[6] C. H.-J. Huang and T. A. Rost, presented at the 6th Interna-

tional Symposium on Integrated Ferroelectrics, March 14-16, 1994, Monterey, California

[7] S. H. Lee et al, "Two-dimensional silicon/PLZT spatial light modulator: design considerations and technology," *Optical Engineering*, vol. 25, pp. 250-60, Feb. 1986

[8] V. H. Ozguz, S. Krishnakumar and S. H. Lee, "Ferroelectric thin films for smart spatial light modulator applications," manuscript.

[9] D. Dimos, C. E. Land and R. W. Schwartz, "Electrooptic effects and photosensitivities of PZT thin films," *Ceramic Transactions*, vol. 25: Ferroelectric Film, (American Ceramic Society, Westerville, OH, 1992), pp. 323-39

[10] F. Wang *et al*, to be published.

[11] F. Wang *et al*, "Discrete electro-optic response in lead zirconate thin films from a field-induced phase transition," *Opt. Lett*,. vol.18, pp. 1615-17, Oct. 1993.

1. Ulrich, Ankele, Appl. Phys. Lett. 27, 337 (1975).
2. Pennings, Deri, Bhat, Hayes, Andreadakis, IEEE Photon. Technol. Lett. 5, 701 (1993).
3. Thoen, Molter, Donnelly, in *Proc. International Symposium on Guided-Wave Optoelectronics*, October 26-28, 1994, New York.

CThI22

Integrated reflection light modulator using ferroelectric films on silicon

Feiling Wang, Gene H. Haertling, *Gilbert C. Robinson Department of Ceramic Engineering, Clemson University, Clemson, South Carolina 29634-0907*

Reflection light modulators using integrated metal-oxide ferroelectrics on semiconductor substrates have demonstrated the potential to bgh-performance and low-cost devices.[1,2] In previously reported works, modulation systems using thin-film ferroelectrics were based on phase modulation utilizing the birefringent electro-optic effect of the materials. In this paper, we report what we believe to be the first reflection intensity light modulator using a metal-oxide thin-film material on a silicon substrate.

The structure of the modulator and the propagation direction of the light are schematically shown in Fig. 1. A ferroelectric lead lanthanum zirconate titanate (PLZT[3]) thin film was deposited on a Pt/Ti-coated silicon substrate as the modulating medium. An indium-tin oxide (ITO) layer was deposited on the PLZT film as the top electrode.

A helium–neon laser beam with a wavelength of 633 nm was obliquely incident on the device. The light beam was polarized perpendicularly to the incident plane. The reflected light was directly received by a photomultiplier tube (PMT). This modulator structure formed a low-finesse asymmetric Fabry–Perot interferometer. Absorption of the light drastically increased if the incident angle coincided with the Fabry–Perot peak. In the presence of a moderate external electric field exerted by a voltage between the ITO and Pt electrodes, the electro-optic effects of the PLZT film caused the ordinary index of the material to change by an increment of approximately 0.003. This field-induced index change served as a tuning mechanism for the light modulation in an absorption mode. A normally-off modulation was observed when the incident angle of the light was smaller than the angle for the Fabry–Perot peak, whereas a normally-on modulation was achieved when the incident angle was greater than the peak position.

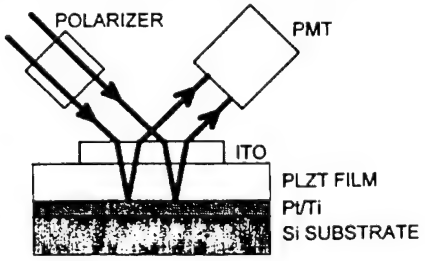

CThI22 Fig. 1. Schematic cross-section of the reflection ferroelectric light intensity modulator.

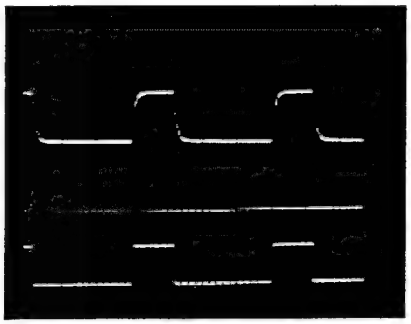

CThI22 Fig. 2. Normally-off intensity modulation. The upper trace is the detected light intensity responding to the voltage pulses, shown by the lower trace. The intermediate trace is the zero-intensity position of the PMT. The horizontal scale is 5 ms/div.

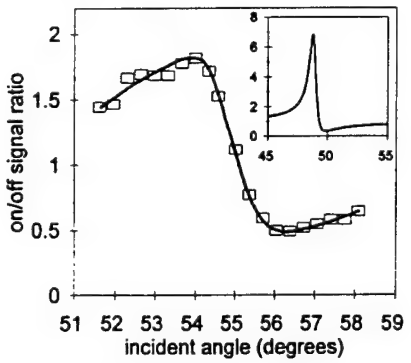

CThI22 Fig. 3. Measured on/off signal ratio vs. incident angle. The insert is the calculated distribution from the mode.

Figure 2 shows the normally-off modulation of the light with a voltage signal of 10 μV across a 0.48-μm-thick PLZT film . The incident angle was approximately 54°. An on/off-signal ratio of approximately 1. 8 was obtained in this measurement. A greater on/off ratio (>2. 5) was achieved with higher-voltage pulses. The on/off-signal ratio as a function of the incident angle was measured with 10-V electric pulses. Figure 3 shows that normally-off modulation was observed for incident angles smaller than 55°, whereas normally-on modulation was obtained for incident angles greater than 55°, semiquantitatively in agreement with a model prediction.[4] Because of the poor control of the film thickness during the deposition, the experimentally achieved on/off-signal ratio was smaller than the design value. Nevertheless, a greater tolerance to the detuning of the incident angle resulted as a tradeoff. The response speed of the modulator was *RC*-time-constant limited in spite of the much faster inherent response speed of the PLZT material.

The modeling predicted that modulators of this kind, utilizing the large electro-optic coefficients in some metal-oxide ferroelectrics, may tolerate much greater error margin for thickness control than can multiple-quantum-well based modulators, when operated with the on/off-signal ratio and light throughput described.

1. D. Dimos *et al*, Ceramic Transactions, in *Ferroelectric Films*, Vol. 25 of (American Ceramic Society, Westerville, Ohio, 1992), p. 323.
2. F. Wang, G. H. Haertling, in *Proc. 1994 International Symposium on Applications of Ferroelectrics*, (Institute of Electrical and Electronics Engineers, New York), in press.
3. G. H. Haertling, C. E. Land, J. Am. Ceram. Soc. 54, 1 (1971).
4. F. Wang, E. Furman, G. H. Haertling, submitted to J. Appl. Phys.

CThI23

All-optical quantum-well-modulator device based on strong carrier separation in piezoelectric layers

N. T. Pelekanos, *Max Planck Institute for Solid State Research, Heisenbergstrasse 1, 70569 Stuttgart, Germany*

We describe a novel contact-free quantum-well (QW) light modulator. It is designed to operate all optically in the sense that an incident write laser beam strongly modulates a second read beam resonant to a QW exciton. Essential to this device is the fact that in strained semiconductor heterostructures grown along a polar axis, such as, for example, [111], the lattice-mismatch-induced strain generates a large piezoelectric field along the growth axis.[1] The magnitude of the piezoelectric field can exceed 10^5 V/cm for rather moderate lattice-mismatch strains of $\varepsilon \sim 0.7\%$.[2]

In Fig. 1, we show a schematic diagram of one period of the heterostructure grown along a polar axis. The period consists of three QWs, where QW_1 and QW_3 are the electron- and hole collection QWs, respectively, and QW_2 has its exciton resonance modulated by the presence of stored carriers in QW_1 and QW_3. The key feature of the device is the presence of piezoelectric field in the barrier layers between QW_1 and QW_2 (barrier B_1) and between QW_2 and QW_3 (barrier B_2).

The principle of operation of the device is as follows: A control optical beam λ_{write}, with photon energy larger than the band gap of the barrier layers, photogenerates electrons and holes at the barrier layers. There they experience the piezoelectric field and separate on either side of the barrier layer. For instance, the electrons generated in barrier B_1 of Fig. 1 will relax in QW_1, whereas the holes will relax in QW_2. Similarly, electrons and holes from B_2 will pour into QW_2 and QW_3, respectively. Thus, in QW_2 we find equal populations of electrons and holes at all times, a fact that allows them to deplete rapidly by radiative

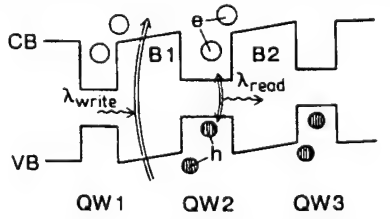

CThI23 Fig. 1. Schematic band diagram of one period of the heterostructure and photogeneration of electric field by photocarrier separation in the piezoelectric barriers.

ACerS - Boston 1994

RAINBOWS AND FERROFILMS - SMART MATERIALS FOR HYBRID MICROELECTRONICS

Gene H. Haertling
Gilbert C. Robinson Department of Ceramic Engineering
Clemson University, Clemson, SC 29634-0907

ABSTRACT

This review paper describes the materials, processing, properties and applications of the newly developed ultra-high displacement Rainbows and thick/thin ferroelectric Ferrofilms. Their applicability to hybrid and fully integrated microelectronics is discussed in regard to each of these areas of concern.

INTRODUCTION

Current trends have shown that industrial and commercial hybrid microelectronic components designed for the automobile, home, office and factory are becoming an increasingly more important segment of present-day automation. The materials for such applications are required to be more sophisticated in that they must be able to perform more than one function (e.g., actuation and sensing) during operation or provide a unique combination of highly specialized properties. These materials are now commonly known as smart or intelligent materials and are exemplified by such general groups as ferroelectrics, piezoelectrics, pyroelectrics, electrooptics, electrostrictive materials and composites.

Key factors in the application of these materials to hybrid circuits and microelectronics are (1) their ability to be scaled down in size (i.e.,miniaturized or fully integrated) without loss of bulk properties, (2) their capability of achieving the proper form factor for the substrate and (3) their processing compatibility with other components on the substrate. Recent research and development work has shown that significant progress has been made in the last several years in each of these areas.[1-5] A new processing technique has recently led to the development of ultra-high displacement

ceramic actuators which have been coined as RAINBOWS (Reduced And INternally Biased Oxide Wafers), an acronym for the chemical reduction process used to transform ordinary planar piezoelectric and electrostrictive wafers into domed, high displacement, two-dimensional bending actuators of moderate load-bearing capability.[6-7] Rainbow devices such as speakers, pumps, switches, deflectors and linear actuators have been made in sizes as large as 10 cm. in diameter and as small as 2 mm. in diameter or length.

An assessment of the present-day ceramic actuator technologies for bulk materials is given in Table 1. As seen from the table, a variety of direct extensional configurations, composite flextensional structures and bending mode devices are used to achieve an electromechanical output. Trade-offs between stress generating/loading capability and displacement are commonly made when designing for particular applications. Maximum displacement can be seen to be achieved with composite or bender structures; however, this is usually accomplished at the expense of less load bearing capability, greater complexity and higher cost. The recent introduction of the Rainbow bender to this family of actuators has served to either extend the stress capability of the bender technologies without sacrificing displacement or extending the displacements achievable with equal load-bearing capacity. Additionally, because of their unique dome or saddle-type structure, small discrete Rainbow elements for hybrid circuits can be fabricated from larger, bulk processed wafers.

For the fabrication and integration of actuator/sensors and other devices at the microelectronic (micron) level, one must consider different technologies than those previously mentioned. Among these techniques are vacuum deposition, spinning, dipping, chemical vapor deposition and laser ablation; however, those which have been reported to successfully produce both thin (0.02 - 5 um in this paper) and thick (5 - 30 um in this paper) films of the above mentioned materials are considerably fewer in number, and the most promising of these, in the near term, is dipping. Using an automated dipping apparatus, Li, et.al.,[8] were successful in fabricating thin and thick films of PLZT ferroelectric and electrooptic compositions on Ag, Si, sapphire and glass substrates. Films as thick as 15 microns have yielded properties quite similar to those of the bulk material and show excellent promise for future devices.

It is the object of this review paper to describe the materials, processing and properties of two types of recently developed smart materials; i.e., Rainbows for discrete and hybrid structures and thick/thin ferroelectric films (Ferrofilms)

for hybrid and integrated structures. Examples of typical applications are discussed.

Table 1. Present-Day Ceramic Actuator Technologies

Type	Configuration	Max. Stress* (MPa)	Actuator Movement (w/Voltage)	Actuator Type (P or E)	Actuator Displacement (%)+
Monolithic (d_{33} mode)	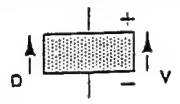	40	Expansion	P	0.40
Monolithic (d_{31} mode)	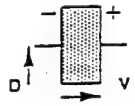	40	Contraction	P	-0.15
Monolithic (s_{11} mode)	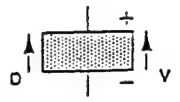	40	Expansion	E	0.24
Monolithic (s_{12} mode)	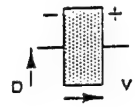	40	Contraction	E	-0.08
Composite Structure (d_{33} mode) (flexten.)	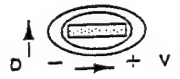	10	Contraction	P	-1.0
Composite Structure (d_{33}/d_{31}) (Moonie)	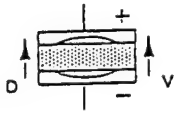	0.028	Expansion	P/E	1.3
Unimorph (bender)		0.002	Expansion/ Contraction	P/E	10
Bimorph (bender)	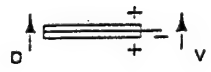	0.002	Expansion/ Contraction	P/E	20
Rainbow Monomorph (bender)	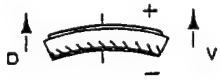	0.020	Expansion/ Contraction	P/E	35-500

Notes: V = Voltage; D = Actuator Displacement; P = Piezoelectric; E = Electrostrictor
* = Max. generated stress; + = Displacement at ± 10 kV/cm based on thickness

MATERIALS

Although a number of different compositions have been successfully prepared as Rainbows and Ferrofilms, those most compatible to the specific processes used and most amenable to achieving the desired properties are in the PLZT solid solution family. Typical high displacement ferroelectric compositions are 1/53/47 (La/Zr/Ti) and 5.5/56/44 for low and high dielectric constant applications, respectively; whereas, the usual compositions for the electrooptic, electrostrictive-type applications are 9/65/35 or 8.6/65/35.[9] These specific compositions are pointed out in the PLZT phase diagram given in Figure 1. As may be noted, the ferroelectric materials are morphotropic phase boundary compositions and the non-memory, electrostrictive materials are compositionally located along the ferroelectric-to-paraelectric phase boundary.

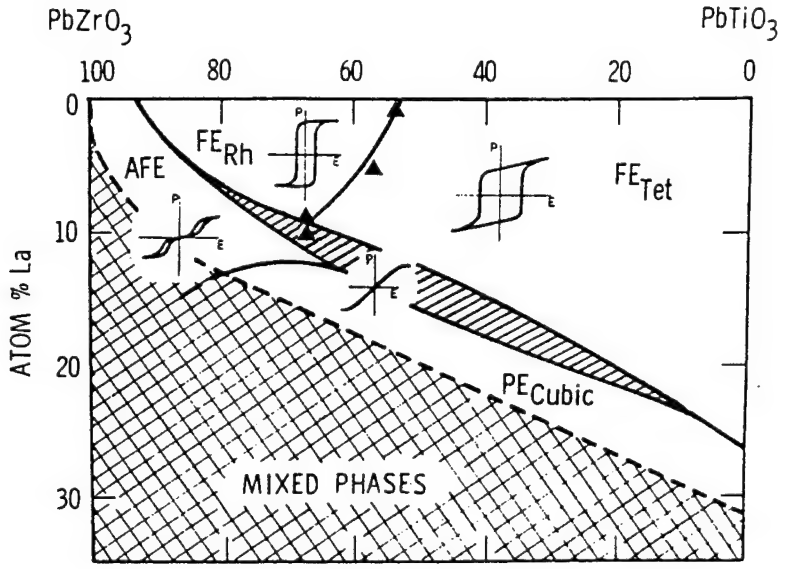

Figure 1. Room Temperature Phase Diagram of the PLZT System
Compositions are indicated by triangular markers

PROCESSES

In this section, the specific processes which have been reported for both the Rainbows and the Ferrofilms are described. Since Rainbows are produced via a bulk-type process and the Ferrofilms are fabricated with a thick/thin film technique, they are distinctly different, by nature, and thus, are discussed in

separate sections.

Rainbow Process

The Rainbow technology fundamentally consists of a new processing method that is applied to standard, high lead-containing ferroelectric, piezoelectric and electrostrictive ceramic wafers which are transformed by the process into a monolithic, composite structure consisting of a stressed dielectric and a chemically reduced, electrically conductive layer which acts as the stressing element as one of the electrodes for the final device. Since all of the materials are ferroelectric or electrically-enforced ferroelectric materials, they are multifunctional and smart, by nature, and are thus capable of performing both actuator and sensor functions, simultaneously.

The high temperature chemical reduction process involves the local reduction of one surface of a planar ceramic plate, thereby achieving an anisotropic, stress-biased, dome or saddle-shaped wafer with significant internal tensile and compressive stresses which act to increase the overall strength of the material and provide its unusually high displacement characteristics. According to previously reported work, the chemical reduction process proceeds via simple reactions consisting of the oxidation of the solid carbon (graphite) block to carbon monoxide and further oxidation of the carbon monoxide gas to carbon dioxide with the associated loss of oxygen from the PLZT oxide in contact or in near contact with the graphite block.

Rainbow ceramics are produced from conventionally sintered or hot pressed ceramic wafers by means of a few simple steps requiring approximately two hours of additional time as shown in the process flowsheet of Figure 2. A Rainbow is produced from an as-received wafer by placing it on a flat graphite block, placing a protective zirconia plate of the same size on top of the wafer and introducing the assembly into a furnace held at temperature in a normal air atmosphere. The part is treated at a temperature of 975°C for one hour, removed from the furnace while hot and cooled naturally to room temperature in about 45 minutes. A reduced layer approximately 150 um thick is produced in the wafer under these treatment conditions, When cool, the dome shaped wafer is lifted from the graphite block, brushed lightly on the reduced (concave) side to remove any metallic lead particles and to expose the reduced layer, and then electroded for test and evaluation. A variety of electrodes can be used such as epoxy silver, fired-on silver and vacuum deposited metals. After depositing appropriate electrodes, the Rainbow is completed and ready for operation.

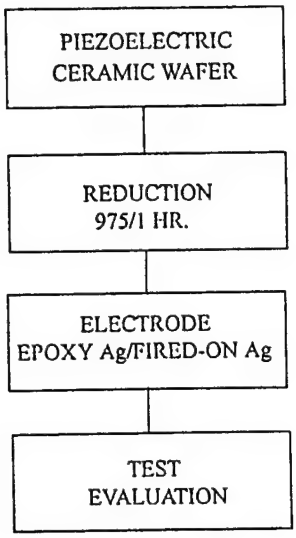

Figure 2. Process Flowsheet for PLZT Rainbow Ceramics

In regard to operation, a Rainbow is similar to a device known in the industry as a unimorph bender. A unimorph is composed of a single piezoelectric element externally bonded to a flexible metal foil which is stimulated into action by the piezoelectric element when activated with a ac or dc voltage and results in an axial buckling or displacement as it opposes the movement of the piezoelectric element. However, unlike the unimorph, the Rainbow is a monolithic structure with internal compressive stress bias on the piezoelectric element; thus producing the dome structure, rendering it more rugged and able to sustain heavier loads that normal. The integral electrode (usually the bottom electrode) consists of metallic lead intimately dispersed throughout the semiconductive oxide layer. The change in shape of the wafer after reduction is believed to be due to the reduction in volume of the bottom reduced layer (largely metallic lead) compared to the unreduced material, as well as the differential thermal contraction between the reduced and unreduced layers on cooling to room temperature.

Like other piezoelectric devices, Rainbows may be operated with a dc, pulse dc, or ac voltage; however, when driven with ac, the largest displacements are usually achieved at 100 Hz or less. In operation, the dome height of the Rainbow varies as a function of the magnitude and polarity of the voltage. When a given polarity of voltage is applied, the dome decreases in height depending on the magnitude of the voltage; and alternatively, when the polarity is reversed, the dome increases. The large axial motion of the dome

is largely due to contributions from a lateral contraction produced in the material via the d_{31} coefficient and a stress-directed domain switching process.

It should be noted that although Rainbows are processed in bulk wafer form, after heat treatment they may be diced or scribed into smaller elements for a pick-and-place operation onto a hybrid substrate. This technique is possible since each individually diced element possesses a smaller but similar dome structure with a radius of curvature identical to the larger wafer. Even though the displacements of the smaller individual elements are proportionately less than the parent wafer, they nevertheless, are large enough (5 - 50 microns) to be useful in some devices. Some typical examples of sizes and shapes of Rainbows are shown in Figure 3.

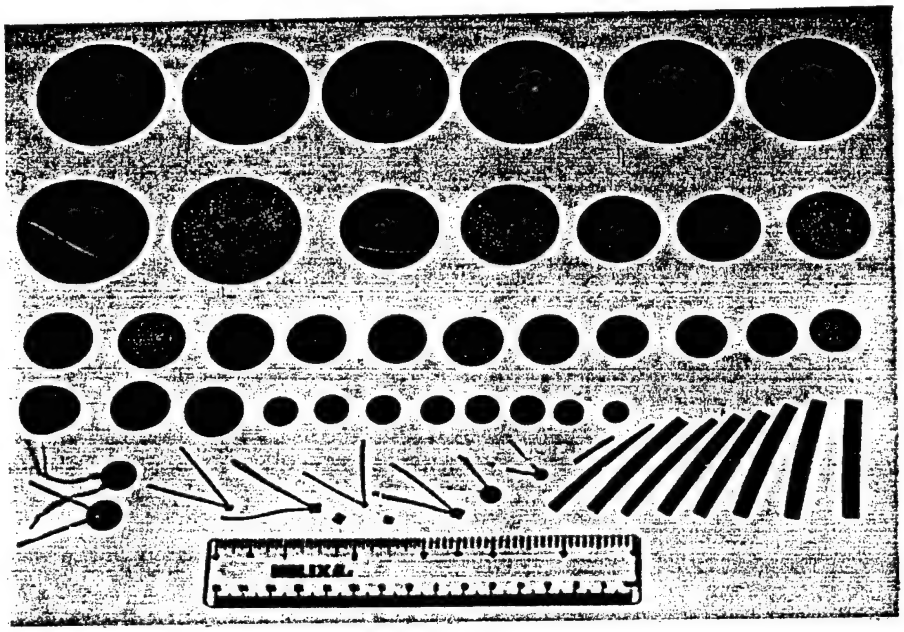

Figure 3. Typical Examples of Sizes and Shapes of Rainbows

Ferrofilm Process

Thick and thin films of ferroelectrics, piezoelectrics and electrostrictive materials are presently being fabricated from a water-soluble, acetate-precursor, liquid chemical system (Metal Organic Decomposition type) using an automated dipping process. An operational flowsheet for this process is given in Figure 4; however, the details of the process and the apparatus have

previously been reported as part of a overall effort involving the intelligent processing of ferroelectric films.[10]

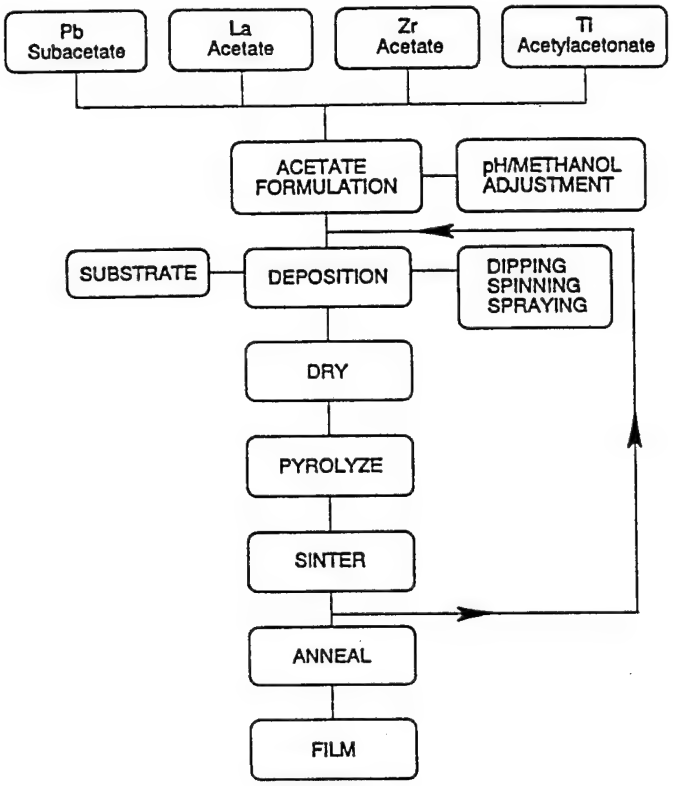

Figure 4. Process Flowsheet for PLZT Acetate MOD Process

Briefly, the process consists of formulating the stock solution from as-received precursors of Pb (lead subacetate), La (lanthanum acetate), Zr (zirconium acetate) and Ti (titanium acetylacetonate) by mixing them together in the requisite amounts along with the appropriate amount of methyl alcohol for viscosity control. This simple, five minute operation yields a clear, light yellow solution which is water soluble and stable for long periods of time. The solution is then deposited on the selected substrate via automatically controlled dipping and withdrawal operations. Drying occurs in a matter of a few seconds, and the coated substrate is subsequently sintered very quickly by introducing it directly into a furnace pre-heated to the sintering temperature. Multiple dipping, drying, sintering and cooling cycles are required in order to build up the necessary film thickness for the specific device. Depending on the dilution ratio of the solution, individually dipped layer thicknesses may vary from approximately 0.05 to 0.3 um, yielding films

as thick as 12 um for a 40 layer device. For a cycle time of three minutes, the total time required to dip a 40-layer device is about two hours.

The final sintered film deposited on a suitable substrate such as a 0.125 mm thick Ag foil is usually transparent and crack-free with a smooth, shiny surface. After applying suitable electrodes such as air dried Ag, epoxy Ag or vacuum deposited metals, the film is ready for operation; however, it should be remembered that poling may be required if it is a ferroelectric thick film. Some examples of electroded and unelectroded thick films on Ag substrates are shown in Figure 5.

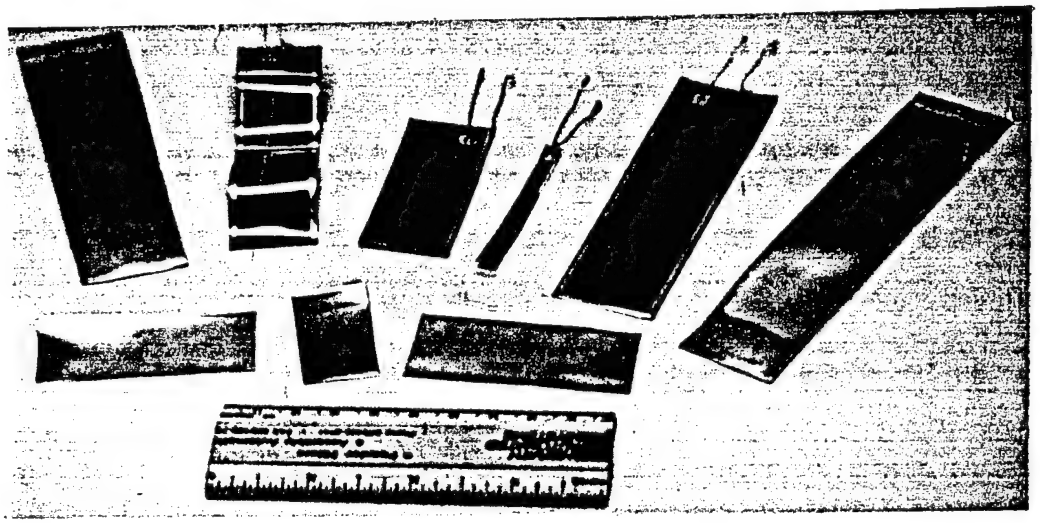

Figure 5. Typical Examples of Unelectroded and Electroded Ferrofilms

Although Ferrofilms lend themselves well to a number of different fabrication processes at the totally integrated level, for discrete components at the hybrid microelectronics level the dipping technique has been found to be reliable and predictable and can easily be implemented in a totally hands-off environment. In addition, industrial equipment is readily available to dip very large as well as small, discrete parts at minimal cost. The acetate process, being water insensitive, is especially suitable for the dipping process since the open solution is usually exposed to the atmosphere for long periods of time and during this period must withstand chemical interactions as well as minimal evaporation of solution.

PROPERTIES

In the last two years since the Rainbow ceramics were first developed at

Clemson University, there has been a considerable on-going effort to (1) understand the details of the reduction process in the PLZT materials, (2) measure their properties and characterize their unusually high displacement and load bearing capabilities as benders, (3) model their electromechanical behavior and frequency dependent properties and (4) construct working models illustrating various proof-of-principle applications. Some of this data for the Rainbow ceramics will be presented in this section, along with the limited amount of data available, to date, for the Ferrofilms. In most instances, a standard Rainbow size of 31.75 mm diameter and 0.5 mm thick was used to obtained the data. Additional technical data on the Rainbow ceramics has been reported in a document prepared by Sherrit, et.al., of the Royal Military College of Canada.[11]

Rainbows Characteristics

Dielectric Properties - The temperature dependent dielectric behavior for two PLZT compositions; i.e., 1/53/47 and 8.6/65/35, are shown in Figures 6 and 7, respectively. It can be seen from Figure 6 that a gradual rise occurs in the relative dielectric constant (1 kHz) of 1/53/47 from a room temperature value of approximately 1100 to about 2700 at 200°C. No peak is observed in this range for this composition because its Curie point is 330°C. On the other hand, composition 8.6/65/35 in Figure 7 shows a change in K from 3200 to 5700 over this same temperature range with a peak occurring at 105°C, which is its usual Curie point as determined from small signal measurements. Since this composition is an electrostrictive, relaxor-type material, this Curie point does not coincide with its loss in polarization which occurs at about 20°C; thus, making it one of the most sensitive, high displacement, electrostrictive Rainbow materials. It may be noted that the dielectric constants and dissipation factors for both compositions are comparable to previously reported values, and this indicates that the Rainbow reduction process does not change the dielectric properties of the unreduced part of the structure.

Hysteresis Loops - Typical examples of dc hysteresis loops for compositions 1/53/47 and 9/65/35 are given in Figure 8. The loop in Figure 8(A) was taken on the ferroelectric Rainbow element (1/53/47) in its virgin condition before any other measurements were made. It should be noted that on the initial application of positive voltage to +450V there was approximately 60% of the total remanent polarization switched rather than the usual 50% one ordinarily observes in a virgin, randomly oriented ceramic.. This behavior is highly unusual and indicates that the Rainbow ceramic was partially poled before testing. Additional audio and piezoelectric tests of other virgin parts also

indicated that the elements were partially poled to varying degrees; i.e., some very little and others as high as 75%.

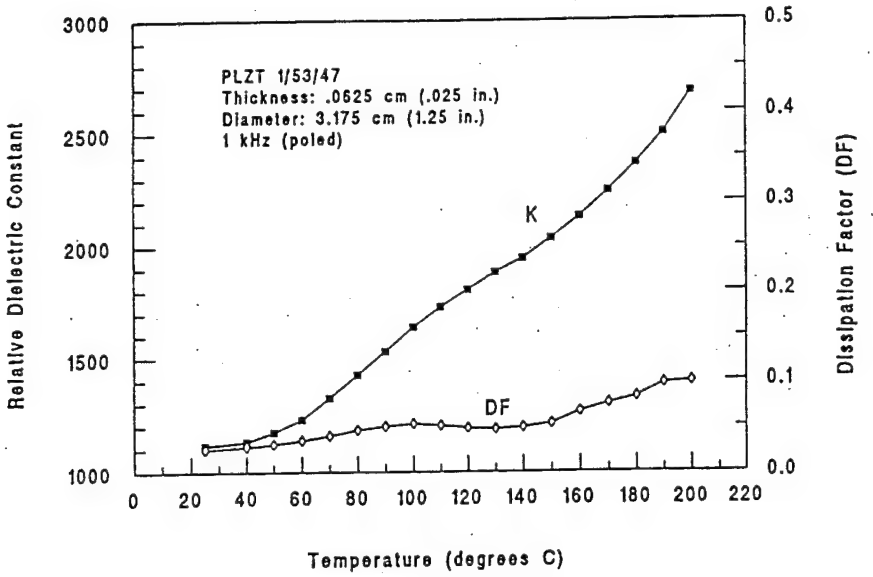

Figure 6. Temperature Dependent Dielectric Properties of PLZT Rainbow 1/53/47

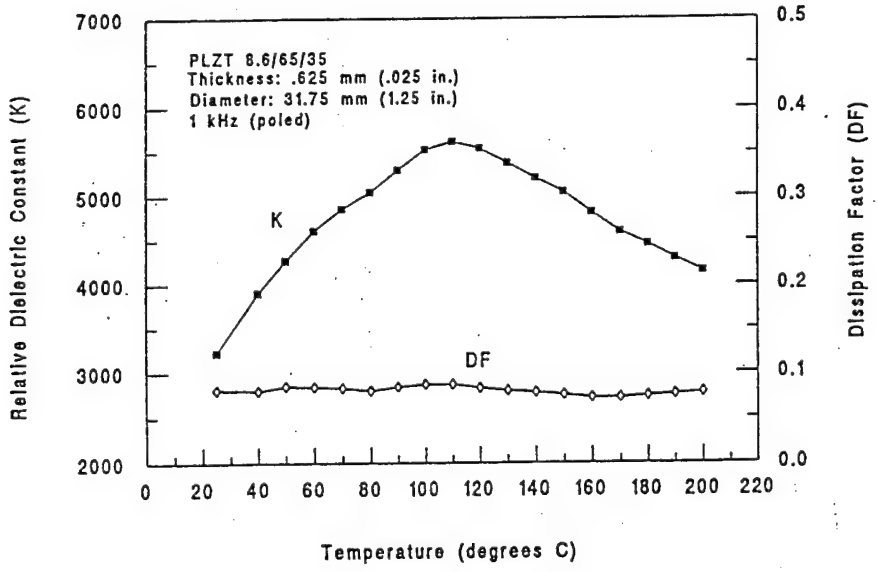

Figure7. Temperature Dependent Dielectric Properties of PLZT Rainbow 8.6/65/35

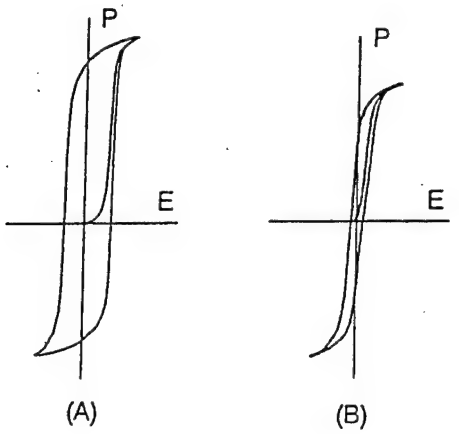

Figure 8. Virgin Hysteresis Loops for Rainbow PLZT Compositions (A) 1/53/47 and (B) 9/65/35

One explanation for this condition occurring in the electrically virgin state is that the mechanical compressive and tensile stresses produced in the Rainbow wafer during processing are acting together to switch some of the domains in this soft ferroelectric/ferroelastic material. Since uniform stress is a symmetrical quantity, it is recognized that it alone is insufficient to produce a net polarization in a given direction even though it may be of sufficient magnitude to switch domains; however, a stress gradient such as produced by the Rainbow bending process is a vector quantity and can, indeed, produce the observed effect. This non-uniform stress is believed to be responsible for the partial poling of the Rainbow wafers. Measured properties on the above wafer were: P_R = 44.8 uC/cm^2, E_C = 7.5 kV/cm, dielectric constant = 1210 and dissipation factor = 0.047.

The virgin loop of Figure 8(B) is a typical one for the electrostrictive (9/65/35) type of Rainbow materials and is very similar to that obtained on bulk electrooptic material. Measured properties on this wafer were: $P_{10kV/cm}$=28.3 uC/cm^2, dielectric constant = 3142 and dissipation factor = 0.085. As a matter of course, no unsymmetrical hysteresis loops were observed in the electrostrictive materials, and none was expected, since there are no stable domains in these materials at zero electric field. Conceivably, a high enough stress could precipitate stable domains in a very near-ferroelectric material, however, this was not experimentally confirmed

Displacement Loops - Displacement vs. electric field (butterfly) loops for the Rainbow wafers described above are shown in Figure 9. As before, Figure

9(A) illustrates the Rainbow axial motion as the sample is electrically switched from zero to +450V, to -450V and back to zero, however, in this case this loop was not taken on the virgin wafer. It may be noted that this loop is remarkably similar to that observed when measuring the direct extensional (longitudinal, lateral) displacements via the piezoelectric d_{33} or d_{31} coefficients. The value of displacement in the + voltage direction was measured at 190.5 um, and the total amount of displacement (+/-) was 432 um.

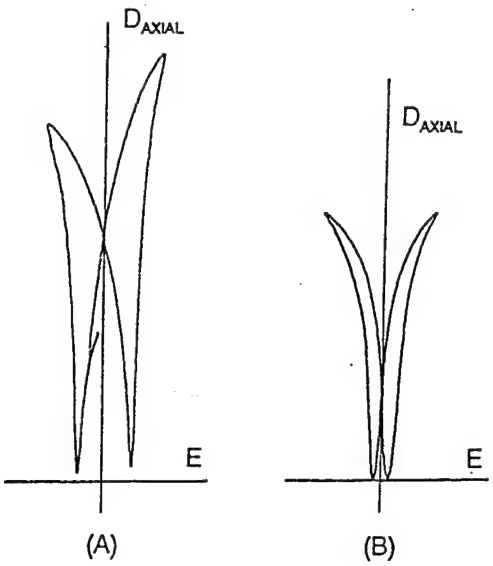

Figure 9. Axial Displacement Loops for Rainbow PLZT Compositions (A) 1/53/47 and (B) 9/65/35

Figure 9(B) shows the displacement loop of the electrostrictive Rainbow material (9/65/35) mentioned above. Since 9/65/35 is a relaxor material there should be little or no memory, and the same value and sign of displacement should be obtained whether a + or a - voltage is applied. One can see by switching this sample through a full voltage loop that a small amount of remanent displacement (strain) is present which is probably due to the close proximity of this composition to a FE phase. A further indication of this incipient FE phase is the higher than normal value of P_{10} (P_{10} = 28.4 vs. 18.0 uC/cm^2) as given above. Measured value of total displacement for this wafer was 178 um.

Displacement Characteristics - The displacement characteristics as a function of applied voltage are given in Figure 10 for some selected compositions. One of the most striking features of this figure is the very high displacements

achieved by these Rainbow ceramics at moderate electric fields; e.g., 400 volts is equivalent to an electric field of 10 kV/cm. Composition 8.6/65/35 is noted to possess the highest displacement of 210 um at a maximum voltage of 600 volts, however, its displacement is characteristically non-linear because of its electrostrictive nature. Compositions 1/53/47 and 5.5/56/44 are ferroelectric materials, and thus, are more linear in behavior. As a general rule, the displacements of the ferroelectric materials are lower than those of the electrostrictive compositions, particularly when operated at higher voltages and one polarity; however under bipolar operation, the displacement values of theferroelectric materials will commonly be double the values shown in Figure 10.

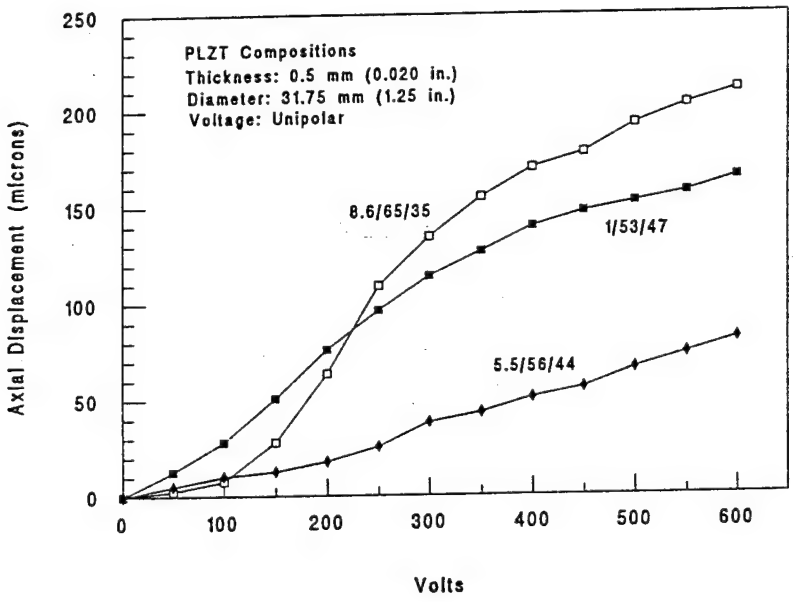

Figure 10. Axial Displacement Characteristics of Rainbow PLZT Compositions as a Function of Voltage

A measure of the difference in displacement between the planar (lateral extensional mode) direction and the orthogonal axial (Rainbow bender mode) direction is given in Figure 11 for PLZT 8.6/65/35, which also shows the temperature dependence of these two modes. This figure clearly demonstrates the very large displacement amplification of the bending phenomenon when one considers the data showing a change in displacement from approximately 0.07% to 22% at 25°C; i.e., an amplification of 315%. Although not shown on the figure, both displacements are negative (i.e., a contraction) when voltage is applied.

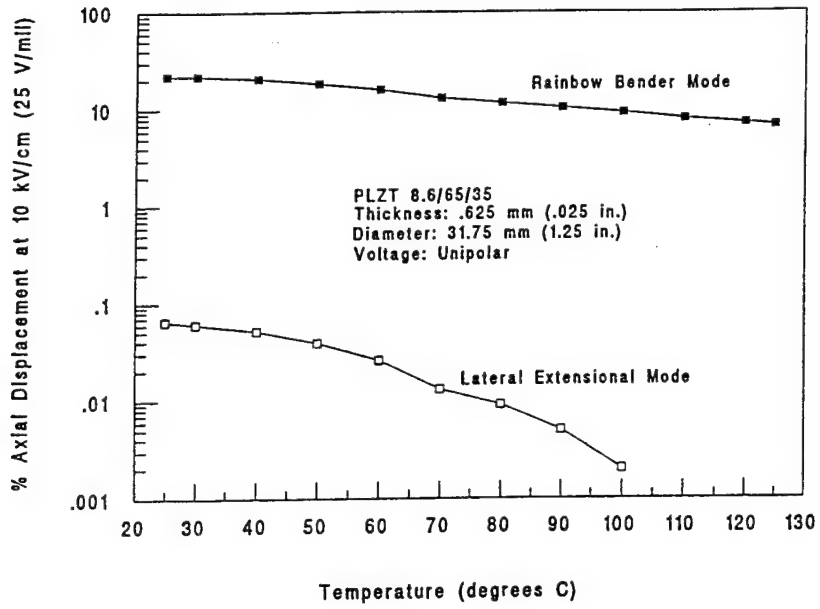

Figure 11. Temperature Dependence of Electrostrictive Lateral and Rainbow Bending Displacements in PLZT 8.6/65/35 Ceramics

Figure 12 illustrates the profile of the vertical bending displacement across the diameter of a Rainbow wafer during activation at 10 kV/cm. As might be anticipated, the highest displacement is in the center of the wafer, dropping off to zero at the circumference. This zero displacement at the edge of the wafer is beneficial because a Rainbow can be conveniently placed on a planar surface and operated as a linear actuator device or its circumference can be sealed off, and it can be operated as a cavity-mode pump.

The variation of a Rainbow's axial displacement as a function of wafer diameter is given in Figure 13. For a 0.5 mm thick wafer of composition 1/53/47, the values of displacement can be seen to vary from 170 um for a diameter of 31.75 mm (1.25 inch) to approximately 3 um at 6.5 mm diameter. Thus, a discrete 15 mm diameter Rainbow component on a hybrid substrate could be expected to have a displacement of about 40 um when operated with a single polarity and about 80 um when operated bipolar.

Wafer thickness has been found to have a significant effect upon axial displacement primarily because of the change in motional mode; i.e., from dome to saddle-type, as the wafer thickness is reduced to approximately one one-hundredth of the diameter. For example, a 31.75 mm (1.25 inch) diameter wafer usually develops a saddle-mode configuration when its

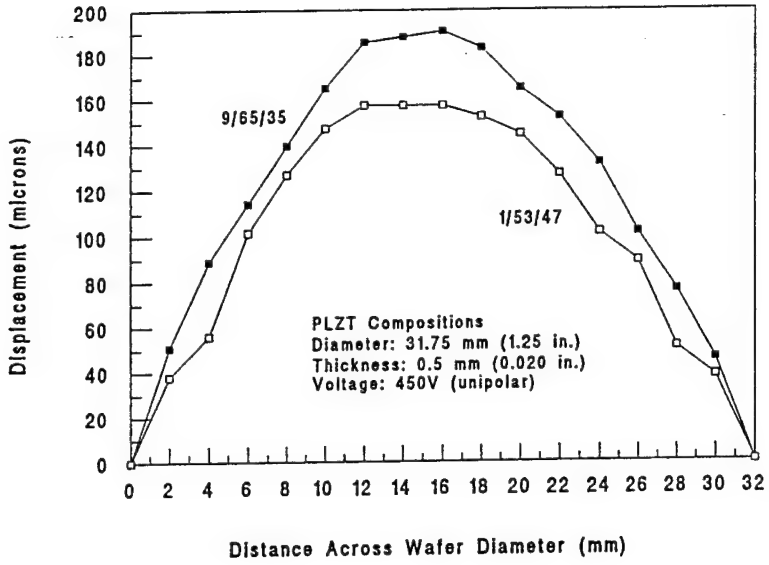

Figure 12. Profile of Displacements Measured Across Rainbow Wafer Diameter for PLZT 1/53/47 and 9/65/35

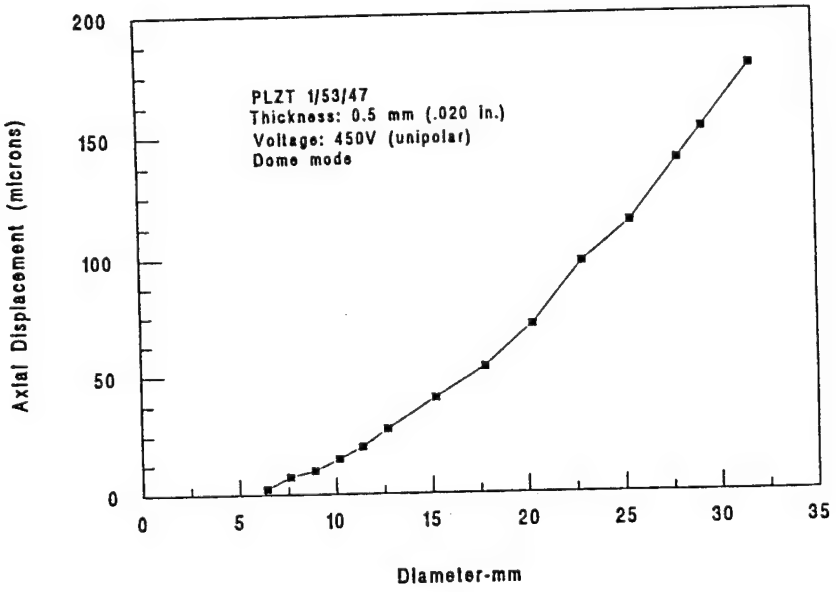

Figure 13. Variation of Axial Displacement as a Function of Rainbow Wafer Diameter for PLZT 1/53/47

thickness is less than 0.32 mm (0.013 inch). Saddle-mode operation provides maximum displacement with minimum load bearing capability; and therefore,

should only be considered for special applications. Figure 14 illustrates the unusually large range of displacements obtained for Rainbows as a function of thickness. Please note that the displacement axis is a log scale.

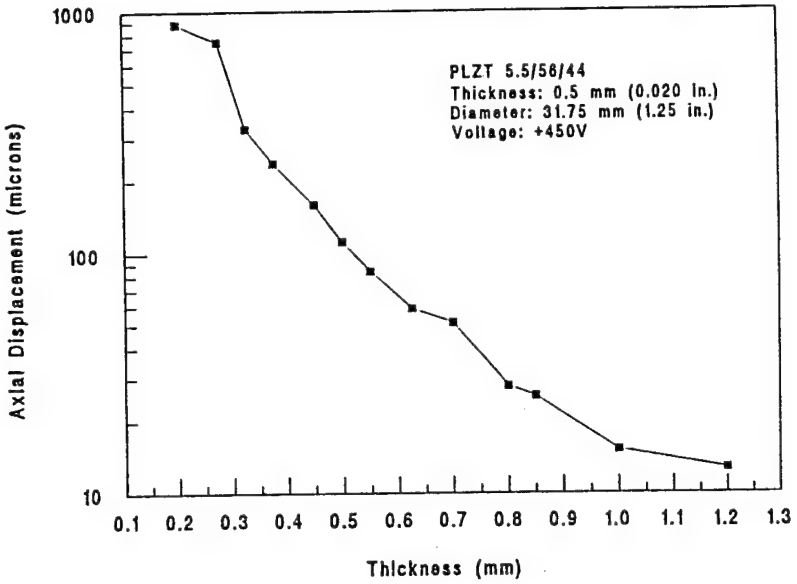

Figure 14. Effect of Thickness on Axial Displacement for PLZT 5.5/56/44

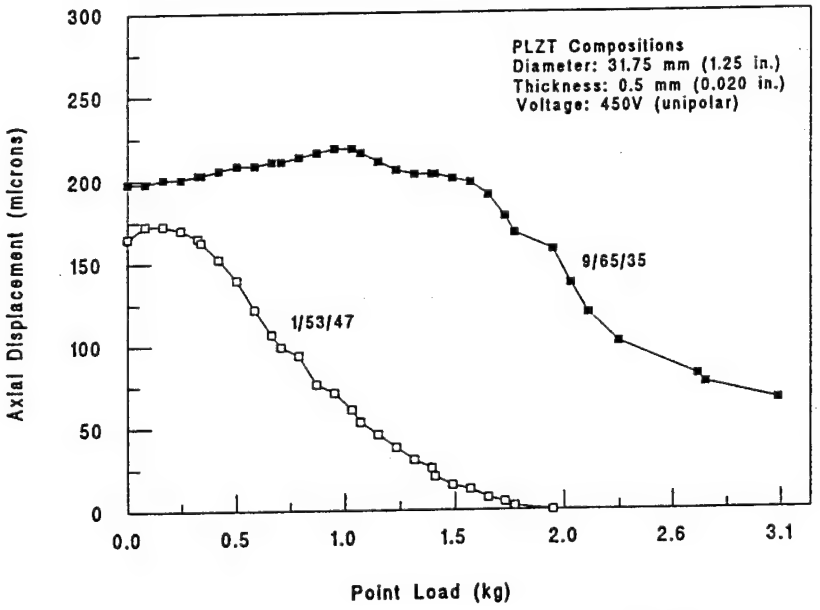

Figure 15. Point Load-Bearing Properties of Rainbow PLZT Compositions

The effect of an unconstrained point load on the displacement of an activated Rainbow is given in Figure 15 for compositions 1/53/47 and 9/65/35. PLZT 1/53/47 can be seen to be relatively ineffective when loaded with a dead weight of 1.5 kg (3.3 lbs), whereas, composition 9/65/35 is still effective at a load of over 3 kg. This result is not too surprising since the elastic modulus of 9/65/35 (10.9 x10^4 MPa) is noticeably higher than that of 1/53/47 (5.7 x 10^4 MPa). Another point to note from the figure is the increase in displacement with the introduction of a finite amount of load on the device. This effect was previously reported by Furman, et. al.[12] The tradeoff between thickness and maximum sustainable point loading is given in Figure 16 for 1/53/47.

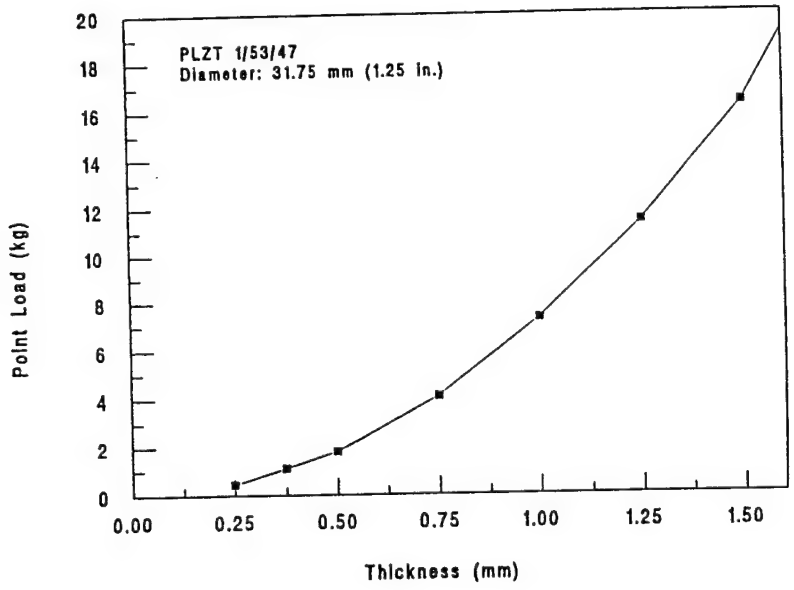

Figure 16. Maximum Sustainable Point Load for Rainbow PLZT 1/53/47 as a Function of Thickness

Another concern of actuator designers is the amount of force that can be generated by an actuator when voltage is applied. This is shown in Figure 17 for a 1/53/47 Rainbow of standard size. As can be seen, the force generated is a linear function of voltage until the onset of saturation for this particular configuration. A maximum force of 1.3 kgf was achieved at 450 volts.

Finally, displacement and sustainable overpressure data for PLZT 5.5/56/44 as a function of wafer thickness are presented in Figure 18. The left ordinate scale represents the maximum allowable pressure differential across the wafer thickness before the wafer contacts the planar surface and stops flexing

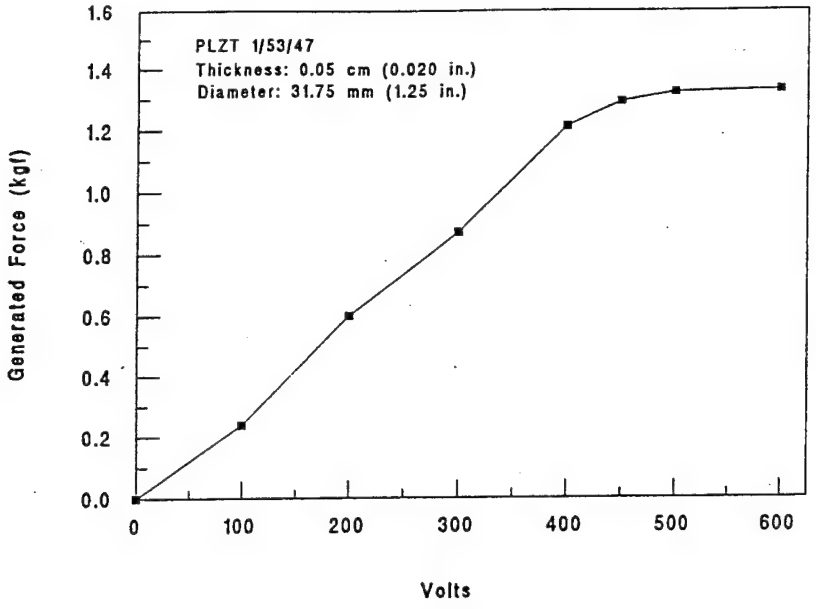

Figure 17. Effect of Applied Voltage on the Force Generated by a PLZT 1/53/47 Rainbow Wafer

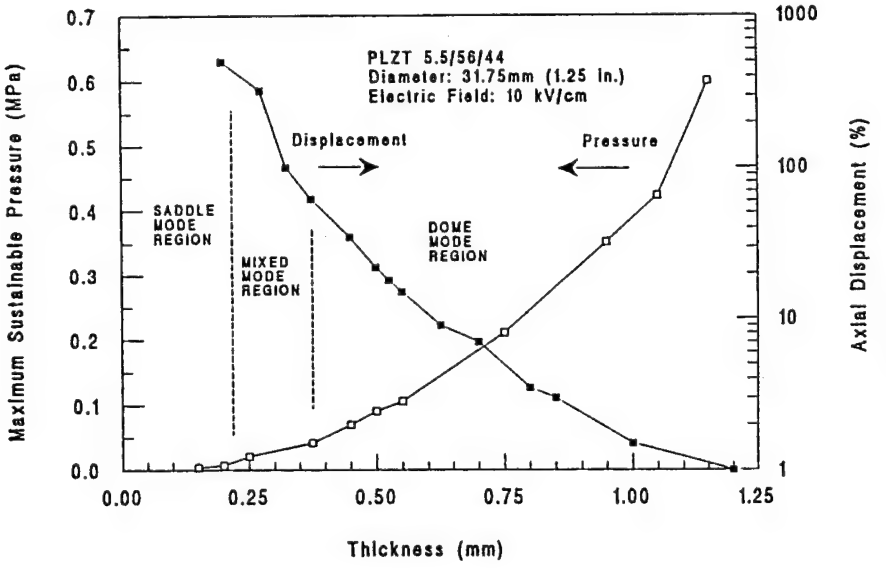

Figure 18. Sustainable Pressure and Displacement Characteristics for Rainbow PLZT 5.5/56/44 as a Function of Thickness

usually <0.5 mm thickness) or the wafer mechanically fractures (>0.5 mm thickness). The right ordinate log scale is the percent displacement (based on wafer thickness) of the device when operated at 450 volts dc while only under

the loading of the dial gage (80 grams). Also indicated on the figure are the wafer thickness regions where the saddle and dome modes of operation are dominant for a wafer 31.75 mm (1.25 in.) in diameter. The data shown in the figure indicate that Rainbow displacements span an unusually large range from near zero to at least 500% with actual displacements of up to 1 mm (0.040 in.) for a 0.2 mm (0.008 in.) thick wafer. Of course, such large displacements are not possible when operating under significant pressure differentials or under moderate point loading situations near its capacity.

Resonance Characteristics - The resonant, frequency dependent properties of a standard Rainbow wafer is given in Figure 19 which displays both impedance and phase angle as a function of frequency. Some outstanding features of this figure are the large radial resonance anomaly at 70 kHz and the several bending resonances between 1 to 20 kHz. Other resonances not shown in this figure are (1) overtone resonances of the fundamental radial resonance in the range from 100 kHz to 1 MHz, (2) thickness resonances in the low megahertz range around 4 and 8 MHz for the fundamental and first overtone and (3) very low frequency structurally-dependent resonances in the range of 25 to 500 Hz which can be noted when a Rainbow is operated as part of a working device.

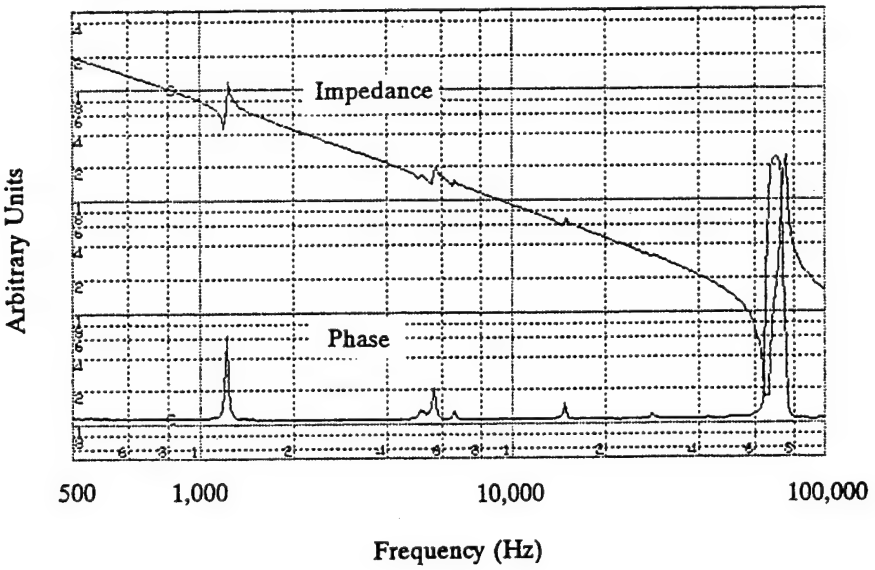

Figure 19. Resonance Characteristics of a Rainbow PLZT 1/53/47 Wafer

Table of Properties - A summary of selected properties which have been determined, to date, for the Rainbow ceramics are given in Table 2. In

addition to these, a number of advantages and features of the Rainbows are: (1) simplicity, (2) solid-state type, (3) monolithic, (4) pre-stressed for greater strength and durability, (5) can sustain/generate moderate loads, (6) mechanical overload protection, (7) medium fast response, (8) very high axial displacement, (9) surface mountable, (10) above-the-plane displacement, (11) no bonding layers, (12) temperature compensation possible, (13) can be stacked to multiply strain, (14) easy to fabricate and (15) cost effective.

Table 2. Some Selected Properties of Rainbow Ceramics

Thermal Expansion	-	10.0×10^{-6}/°C (reduced layer) 5.4×10^{-6}/°C (oxide layer)
Modulus of Rupture	-	1.58×10^{2} MPa (22,500 psi)
Modulus of Elasticity	-	5.7×10^{4} MPa (8.1×10^{6}psi)(bending)(1/53/47) 10.9×10^{4} MPa (15.5×10^{6} psi)(bending)(8.6/65/35) 6.9×10^{4} MPa (reduced layer)(acoustic)(5.5/56/44) 7.8×10^{4} MPa (oxide layer) (")(")
Acoustic Velocity	-	4015 m/sec (reduced layer) 4248 m/sec (oxide layer)
Poisson's Ratio	-	0.38 (reduced layer) 0.38 (oxide layer)
Resistivity	-	3.8×10^{-4} ohm-cm
Effective $d_{33\ (saddle)}$	-	2.5×10^{-6} m/V (bending mode)
$d_{33\ (dome)}$	-	2.8×10^{-7} m/V (bending mode)
Hysteresis	-	5 - 35%
Displacement (31.8 mm)	-	178 microns (0.007 inch)(0 - 450V)(dome mode) 381 microns (0.015 inch)(+/- 450V)(dome mode) 1143 microns (0.045 inch)(0 - 450V)(saddle mode)
(102 mm dia.)	-	3175 microns (0.125 inch)(0 - 450V)(saddle mode) 1016 microns (0.040 inch)(0 - 450V)(dome mode)
Capacitance (1.25" dia.)	-	15 nF (PLZT composition 1/53/47) K = 1200 30 nF (PLZT composition 5.5/56/44) K = 2400 60 nF (PLZT composition 9/65/35) K = 3800

Ferrofilms

The properties of Ferrofilms were determined from PLZT composition 2/53/47 prepared via the acetate process and automatically dip coated for 40 layers onto Ag substrates ranging in thickness from 0.025 to 0.25 mm, yielding an overall film thickness of approximately 12 um. Standard, 1-mm diameter, vacuum evaporated Cu electrodes were deposited on the surface of the films for testing.

Dielectric Properties - The small-signal dielectric measurements of the PLZT thick films revealed that they possess properties very similar to bulk material of the same composition. For the particular composition evaluated, relative dielectric constants (1 kHz) ranged from 1400 to 1800 and dissipation factors from 3.5% to 4.6%.

Hysteresis Loops - Hysteresis loops (1 KHz) were obtained with an ac looper constructed in-house because thick films require higher voltages (>100 V) than normally available from standard thin film testers. An example of a typical loop is shown in Figure 20. As can be seen, the loop (polarization vs. electric field) is very square with sharp, saturated loop tips at maximum field, indicating a high degree of domain switching and good, insulating characteristics well into saturation at 100 kV/cm. The loop of Figure 20 displays typical properties for these films; i.e., that of: P_R = 42 uC/cm^2 and E_c = 15.7 kV/cm (40 V/mil). It should be recognized that this low value for E_c is more typical for bulk material than for thin films which characteristically possess E_cs of 75 kV/cm or higher.

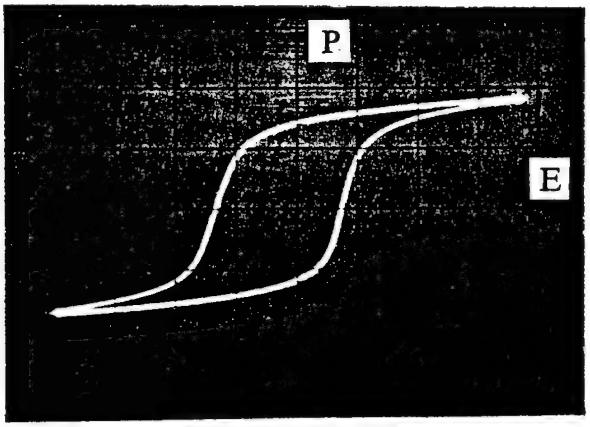

Figure 20. Typical Hysteresis Loop of Ferrofilm PLZT 1/53/47 on Ag

APPLICATIONS

A number of examples of applications are given in this section in order to demonstrate the versatility of the Rainbow and Ferrofilm technologies. These working models are essentially discrete, proof-of-principle devices which require further engineering design, miniaturization and modification in order for them to be suitable for hybrid microelectronics or integrated structures. In any case, it is believed that the Rainbow technology best serves the application range from macroelectronics to millielectronics, whereas the thick/thin Ferrofilms are best suited for the range from millielectronics to microelectronics.

The Rainbow devices shown in Figures 21 and 22 are typical examples of a number of applications envisioned for this technology. As can be seen, they range from actuators to sensors, and speakers to pumps. A more extensive list of applications include (1) linear actuators, (2) cavity/piston pumps, (3) loud speakers, (4) reciprocating motors, (5) relays/switches/thermostats, (6)

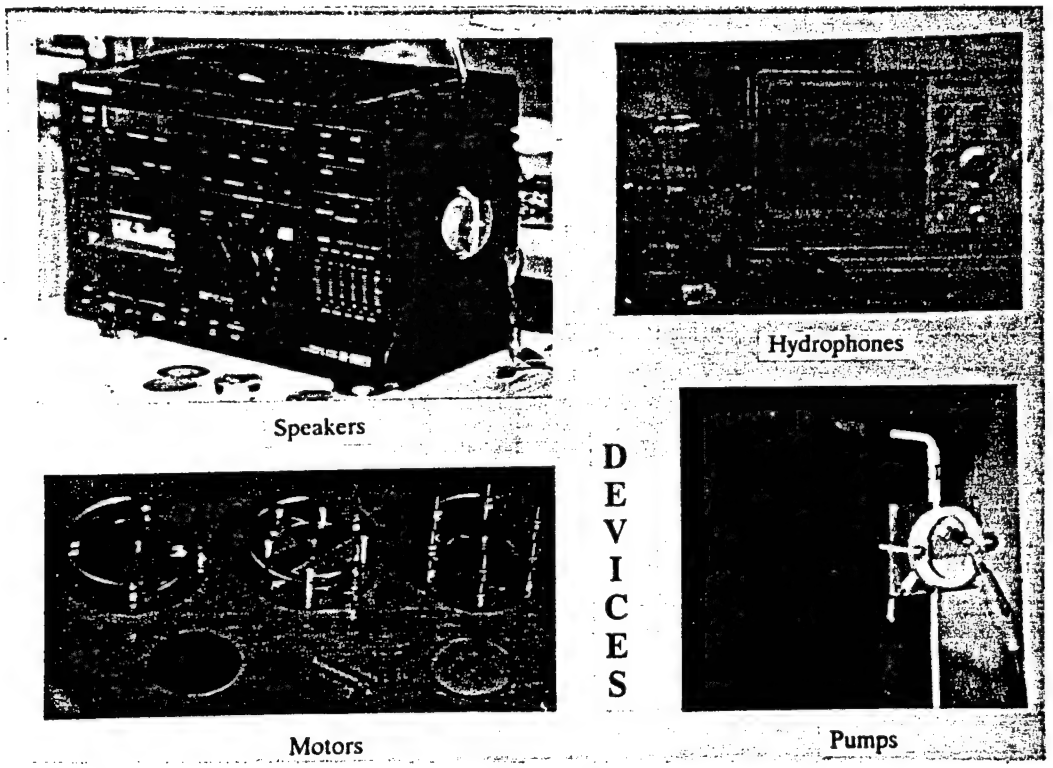

Figure 21. Examples of Working Model Devices Using Rainbow Ceramics as Actuators

sensors, (7) hydrophones/hydroprojectors, (8) variable-focus mirrors/lenses, (9) optical deflectors/scanners, (10) vibrating delivery systems, (11) liquid delivery systems, (12) antivibration/noise cancelling devices, (13) displays, (14) sonic and ultrasonic devices and (15) auto-leveling platforms.

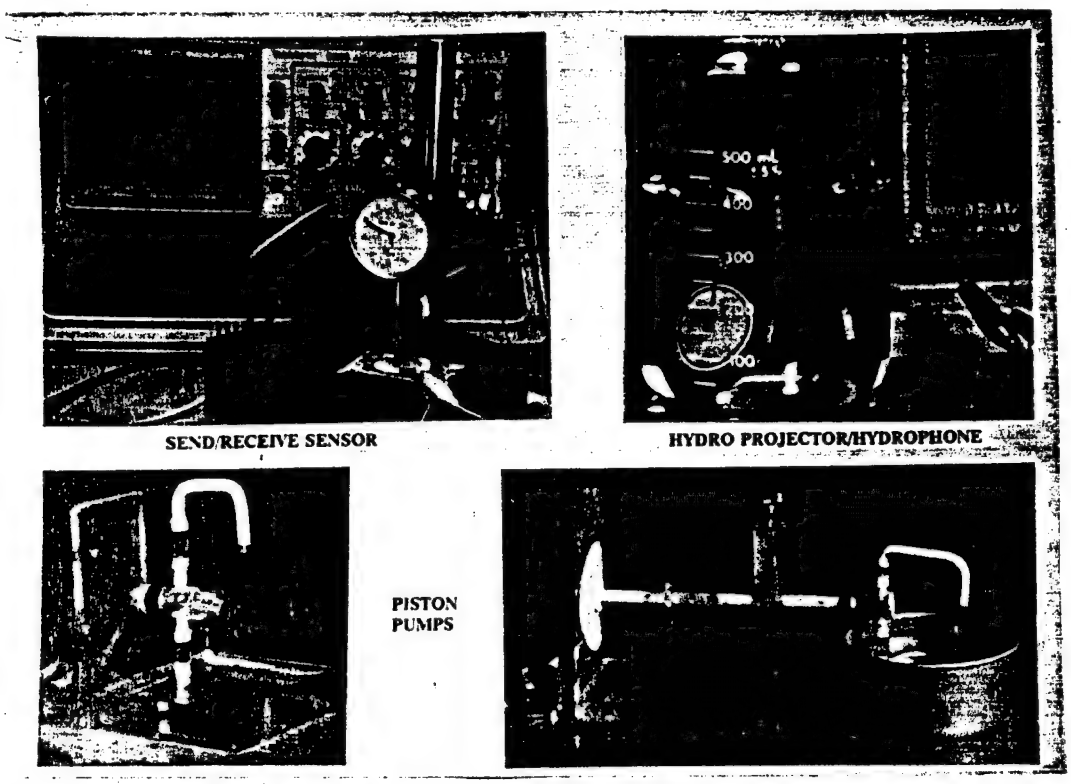

Figure 22. Additional Examples of Working Models Using Rainbow Ceramics as Actuators and Sensors

A single Ferrofilm device is shown in Figure 23. It simply consists of a 25 x 50 mm x 12 um thick film which was dip coated onto a 0.125 mm thick Ag substrate and electroded on the top major surface with vacuum-deposited Cu. After poling the film at 70 volts, the film/substrate is mounted to a resonating enclosure (in this case the enclosure is a cardboard box) and connected to the output of a radio. As with most ferroelectric/piezoelectric audio devices, the quality of the audio is only moderate, at best, when operated over the full audio range of the radio.

CONCLUSIONS

The prospects for utilizing Rainbows and Ferrofilms in discrete hybrid and

totally integrated microelectronics are promising for future applications involving smart ceramics such as ferroelectrics, piezoelectrics, pyroelectrics, electrooptics and electrostrictive materials. Rainbows have opened up a new dimension in ultra-high displacement actuators while Ferrofilms have now bridged the gap from bulk materials to thin films. The key to adapting these materials to specific devices and applications is the manner in which answers are found to questions concerning their reproducibility, reliability, longevity and cost effectiveness. Further development and design work are obviously needed in order to answer these questions.

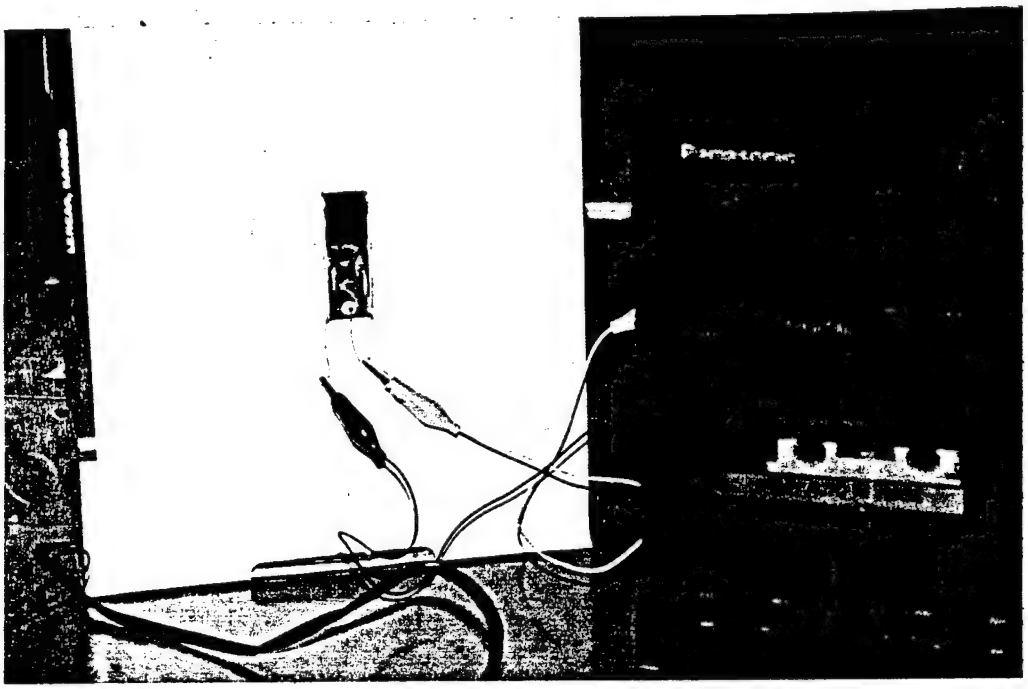

Figure 23. A Ferrofilm Speaker for a Stereo System

REFERENCES

1. L.H. Sheppard, "Advances in Processing of Ferroelectric Thin Films, Bull. Am. Ceram. Soc., 71, No. 1, 85-95 (1992)

2. P.C. Fazan, "Trends in the Development of ULSI DRAM Capacitors," Integrated Ferroelectrics, 4, 247-256 (1994)

3. R. Watton, "Ferroelectric Materials and IR Bolometer Arrays: From Hybrid Arrays Towards Integration," Integrated Ferroelectrics, 4, 175-186 (1994)

4. E.M. Lenoe, W.N. Radicic and M.S. Knapp, "Implications of Smart Materials in Advanced Prosthetics," Proceedings SPIE on Smart Structures and Materials, 2189, 84-104 (1994)

5. C.C. Hsueh, T. Tamagawa, C. Ye, A. Helgeson and D.L. Polla,"Sol-Gel Derived Ferroelectric Thin Films in Silicon Micromachining," Integrated Ferroelectrics, 3, 21-32 (1993)

6. G.H. Haertling, "Rainbow Ceramics - A New Type of Ultra-High Displacement Actuator," Bull. Am. Ceram. Soc., 73, No. 1, 93-96 (1994)

7. G.H. Haertling, "Chemically Reduced PLZT Ceramics for Ultra-High Displacement Actuators," Ferroelectrics, 154, 101-106 (1994)

8. K.K. Li, G.H. Haertling and W-Y Howng, "An Automatic Dip Coating Process for Dielectric Thin and Thick Films," Integrated Ferroelectrics, 3, 81-91(1993)

9. G.H. Haertling, "Dielectric and Electrooptic Properties of Acetate Derived PLZT X/65/35 Thin Films," Integrated Ferroelectrics, 3, 207-215 (1993)

10. G.H. Haertling, "Intelligent Processing of Ferroelectric Films," Bull. Am. Ceram. Soc., 73, No. 8, 68-73 (1994)

11. S. Sherrit, H.D. Wiederick and B.K. Mukherjee, "Evaluation of PLZT Based RAINBOW Ceramic Samples Developed by Dr. Gene Haertling at Clemson University," Report No. DREA CR/94/436, Royal Military College of Canada, Kingston, Ontario, Canada, June (1994)

12. E. Furman, G. Li and G.H. Haertling, "Electromechanical Properties of Rainbow Devices," Proceedings of the 9th ISAF Meeting, State College, June (1994)

Antiferroelectric Lead Zirconate Thin Films Derived from Acetate Precursors

Kewen K. Li, Feiling Wang and Gene H. Haertling

Department of Ceramic Engineering

Clemson University, Clemson, SC 29634-0907

Antiferroelectric lead zirconate ($PbZrO_3$) films derived from acetate precursors have been fabricated on Pt/Ti-coated silicon wafers and fused silica at 700°C with an automatic dip coating process. Films formed directly on the metallized silicon wafer showed the coexistence of perovskite and pyrochlore phases. A pre-coated titania layer of about 100Å facilitated the formation of the desired perovskite phase. Films deposited on fused silica exhibited interactions between lead and silica which inhibited the crystallization of the films. In this case, a pre-coated titania layer in the range of 500-750Å acted as a diffusion barrier layer, allowing the formation of the perovskite phase. Antiferroelectricity in the films was confirmed by x-ray superstructure, dielectric double hysteresis loops and dc bias behavior at room temperature. The corresponding transverse electrooptic properties were also measured for films deposited on fused silica.

1. Introduction

Lead zirconate (PZ) is a typical antiferroelectric (AFE) material at room temperature [1,2], from which the ferroelectric (FE) state can be induced when subjected to a sufficiently large electric field. However, this transition field usually exceeds the material breakdown strength, and consequently, the field-enforced AFE→FE transition is usually carried out at a few degrees centigrade below its Curie point (~230°C) [2]. Owing to the antiparallel arrangement of the spontaneous polarization directions, its unit cell is a superstructure of orthorhombic symmetry consisting of eight perovskite units [3,4]. Although lead zirconate has been well studied in the bulk form, its thin film properties have rarely been reported.

Preparation of the PZ films was first motivated by a mixed-phase problem encountered in the solution-derived FE lead zirconate titanate (PZT) or La-modified PZT (PLZT) thin films. The coexistence of the perovskite and the pyrochlore phases was commonly observed in these films [5-8] fabricated from different precursor systems, and the amount of the pyrochlore phase increased as the film composition approached the Zr-rich side [5,8]. Thus, PZ was expected to be the most difficult composition in the PZT family to obtain with the desired perovskite phase. Moreover, studying the formation of the PZ films benefits the overall knowledge about microstructure evolution mechanisms as well as providing a proper processing technique which could be applied to other PZT or PLZT compositions.

Remedies to the mixed-phase problem in the PLZT films have been proposed by forming a buffer layer of either lead titanate (PT) [9] or La-modified lead titanates (PLTs) [8] prior to the PLZT film deposition. These PT-based compositions were found to crystallize readily into the perovskite structure at lower temperatures, and PLZT films isostructurally grown on these buffer layers showed enhanced perovskite phase formation. Similar conclusions were noted for sol-gel $LiNbO_3$ films [10] in which the perovskite phase was formed at a much lower temperature when deposited on top of an existing perovskite layer.

AFE materials possess unique dielectric, piezoelectric [11,12] and electrooptic properties [13] which make them suitable for devices such as micro-displacement transducers. Since PZ is the base composition for some AFE compounds [14]; for example, Sn-modified PZT, preparation of the PZ films provided a starting point for other PZ-based AFE films. Further incentive to prepare PZ films on transparent substrates resulted from the theoretical interest in studying the electrooptic behavior associated with the field-induced AFE→FE phase transition [13].

The purpose of this paper is to overview the processing aspects of the PZ films prepared from the acetate precursor system and to study their microstructure evolution. Preliminary results on the electric/dielectric and electrooptic properties of the AFE PZ films are also discussed.

2. Experimental Procedure

The specific precursors used in the preparation of the PZ films and the TiO_2 pre-coats were previously reported in a paper describing the acetate solution system for PLZTs [15]. For the PZ composition, lead subacetate powder, $Pb(OOCCH_3)_2 \cdot 2Pb(OH)_2$, and aqueous zirconium acetate solution (ZAA) were used. The oxide contents of the precursors were assayed beforehand. Lead subacetate was first dissolved into the ZAA and continuously stirred for 20 min. Methanol was then added into the mixture as a solvent and stirred for another 10 min. The final coating solutions contained 6 to 8.5wt.% oxide.

The TiO_2 pre-coats were derived from titanium diisopropoxide biacetylacetonate (TIAA), 75wt.% in isopropanol. It was mixed with methanol at a weight ratio of 1 to 5 to form the coating solution containing about 3wt.% TiO_2.

Films were deposited on Pt/Ti-coated Si wafers and optically polished fused SiO_2 for measuring their dielectric and electrooptic properties, respectively; however, Ag foils were also occasionally used as substrates. All films were formed by an automatic dip coating process which involved a multiple dipping and firing approach [16]. Substrates were withdrawn from the solutions at a speed of 18.7cm/min. The coating cycle was repeated 15 to 30 times which gave a final film thickness ranging from 0.6 to 1μm. Each coating layer was fired at 700°C for 2 minutes.

Pulverized solid samples obtained by drying the coating solution at 60°C were subjected to thermogravimetry analysis (TGA) and differential thermal analysis (DTA) in air. The dried samples were also heated in a furnace at various temperatures for 1 hour for x-ray diffraction (XRD) and other analyses.

Dielectric measurements were made at 1kHz. Hysteresis loops were measured with a modified Sawyer-Tower circuit. The transverse electrooptic properties were measured by means of a phase-detection technique in the transmission mode [17]. Evaporated Cu was used as the electrodes.

3. Results and Discussions

3.1 *Thermal Decomposition and Crystallization Behavior*

XRD patterns of the pyrolyzed powder are shown in Fig. 1 as a function of the firing temperatures. Powders heated below 400°C (not shown) had a very broad amorphous peak centered around ~30° 2θ (CuKα). Metallic Pb appeared at 400°C, and was subsequently oxidized at higher temperatures. A small amount of the perovskite PZ phase started to form at 600°C and became the only phase at 700°C. Formation of metallic Pb and PbO_x during the thermal decomposition process was not uncommon for it has also been reported in sol-gel systems for PZT [18] and PZ [19]. The pyrochlore phase, however, was not appreciable in these XRD results.

Fig. 2 shows the TGA and DTA results of dried solid samples heated from room temperature to 800°C at a rate of 10°C/min. The sample lost about 30% of its weight during pyrolysis, and this corresponded to approximate 2 moles each of OAc^- and OH^-(or H_2O) per mole of PZ. By comparing the results with Fig. 1 and other infrared spectra data, the dried solid first underwent dehydroxylation(or dehydration) at temperatures below 200°C. The endothermic peaks between 250 and 400°C were attributed to the decomposition of the acetate group and possibly the melting of Pb. The broad exothermic peak between 400 and 600°C accompanied by about 5% weight loss was the oxidation of residual carbonaceous material and Pb. The small exothermic peak at about 660°C corresponded to the crystallization of the perovskite PZ. From these results it was decided to set the processing temperature for the PZ films at 700°C.

3.2 *Film Microstructure and Phase Formation*

3.2.1 *Pt/Ti-coated Si substrates.* Fig. 3 shows a scanning electron microscope (SEM) photograph of a 10-layer PZ film deposited on the Pt/Ti-coated Si substrate and treated afterwards with a dilute HF-HCl etching solution. The presence of two distinct phases in the film, also detected by XRD, was a phenomenon similar to that found in PLZT films [5-8]. The pyrochlore phase region appeared darker than the perovskite one owing to their differences in Pb content.

From Fig. 1 and 2, the appearance of metallic Pb during the decomposition process and the large temperature difference between the

formation of Pb (~375°C) and the crystallization of the perovskite phase (~660°C) suggests that: (1) the loss of Pb and (2) segregation of the Pb species during the firing process might be responsible for the observed microstructure. The absence of the pyrochlore phase in powdered samples indicated that the loss of Pb was more significant in thin films. These arguments are also supported by the fact that a faster heating rate, which would shorten the time to reach the crystallization temperature, improves the film microstructure [5].

Using PT or PLT buffer layers proved to be as effective in modifying the microstructure of the PZ film as those of the PLZT films. However, a TiO_2 layer was also found to be capable of improving the perovskite phase formation. Results from XRD and TGA/DTA experiments on composition PT indicated that Pb had a much greater tendency to combine with Ti; i.e. no Pb was detected by XRD and perovskite PT could be formed at ~470°C which was almost 200°C lower than that of PZ. A relatively thin TiO_2 layer, dip-coated onto the Pt/Ti-coated Si substrate and fired at 700°C for 30sec, was estimated [16] to be in the range of 100Å and possessed a rutile structure. The etched microstructure of a PZ film processed at the same conditions as in Fig. 3 but with a pre-coated TiO_2 layer is shown in Fig. 4. The pyrochlore phase was not discernible in this picture and the film morphology has been improved dramatically with the TiO_2 pre-coat. The reasons for the improved microstructure of the PZ films deposited with a TiO_2 pre-coat are presently under study.

For Pt/Ti-coated Si substrates, growing films on PT or PLT layers was more easily controlled than on a TiO_2 layer. However, TiO_2 has proved to be very useful for films deposited on fused SiO_2 substrates. On both types of sublayers, however, the PZ films were found to retain a small amount of the pyrochlore phase when examined by XRD, therefore, excess Pb (as much as 20at.%) has been added in the preparation of subsequent films in order to compensate for the loss of Pb.

3.2.2 *Fused silica substrates.* PZ films deposited directly onto fused SiO_2 substrates and fired at 600-700°C were colorless and showed no crystallinity under XRD. Large cracks were present throughout the films and also the substrate surfaces, suggesting a film-substrate interaction. Films could be crystallized into the perovskite structure with the PT or PLT buffer layers but regions of imperfections still could be found. This indicated that in these Pb-containing layers, Pb was responsible for the film-substrate interactions. This effect was not unexpected since it was well known that PbO reacts easily with SiO_2 to form low melting silicates. The TiO_2 sublayer was found to be the better choice in this case, yet it required a layer thickness of 500-750Å to inhibit such interactions. Similar uses of TiO_2 layers have been reported for PLZT films deposited on glass substrates [20] and in CMOS devices integrated with PLZT ferroelectrics [21].

The crystallized PZ films were transparent, light yellow in color and suitable for transmission electrooptic properties measurements. Fig. 5

shows the morphology of a 1μm PZ film deposited on a fused SiO_2 substrate pre-coated with a TiO_2 layer. As can be seen in Fig. 6 its XRD pattern that this film was highly crystallized into a single perovskite phase. The superstructure orthorhombic {110} peak at about 16.9° 2θ confirmed the multiple cell structure of this film.

3.2.3 *Microcracks.* All PZ films deposited on the above two types of substrates had a certain degree of microcracks as can be seen in Fig. 3 to 5. While this phenomenon was not observed in other FE PLZT films deposited on the same substrates under similar processing conditions, their formation was attributed particularly to the extra volume shinkage which occurred at the phase transition from the higher temperature paraelectric state to the lower temperature AFE state [14] during the film cooling stage. On the other hand, microcracks were not seen in PZ films deposited on substrates such as Ag, which possessed a higher thermal expansion coefficient ($22x10^{-6}°C^{-1}$) than those of the Pt-coated Si ($2.6x10^{6}°C^{-1}$) and fused SiO_2 ($0.5x10^{-6}°C^{-1}$). Since the general PLZT films were in a compressive state when deposited on Ag foils [22], it suggested that the microcracks could be avoided by a residual compressive stress. These microcracks, however, did not prevent the measurements of the electrical and optical properties, yet they affected somewhat the optical quality of the films on fused SiO_2.

3.3 *Dielectric and Electrooptic Properties*

All the PZ films had a dielectric constant at 1kHz in the range of 200 to 250. Dissipation factors were 0.02 to 0.03 and dc resistivities were greater than $10^{10}\Omega$-cm. A typical polarization versus electric field (P-E) double hysteresis loop measured at room temperature was shown in Fig. 7 for a 0.8μm PZ film deposited on a Pt/Ti-coated Si substrate with a TiO_2 sublayer. The AFE→FE transition field was about 40kV/mm and the reverse FE→AFE was about 20kV/mm. The FE phase saturated at about 60kV/mm with a polarization between 0.3 to 0.4μC/mm^2.

The success in observing the double hysteresis loop of PZ film at room temperature was attributed to the superior dielectric strength usually found for thin film materials. For example, the AFE→FE transition field found for these PZ films was an order of magnitude greater than the reported values for bulk materials [2]. Such a large field would certainly cause breakdown in bulk PZ.

Inasmuch as the slope of the P-E hysteresis loop indicates the permittivity of the sample, this parameter would be expected to increase sharply as the sample passed through the AFE→FE and FE→AFE phase transitions. Fig. 8 shows the variation of the permittivity of a virgin PZ film recorded as a function of a slowly varying dc bias applied first in the positive direction. The permittivity sharply increased by 40 to 60% of its original value at the AFE→FE transition field and dropped as the loop

saturated. The increase in permittivity at the FE→AFE transition was slightly smaller than at the AFE→FE transition.

Weak ferroelectricity was usually observed in these PZ films and was best illustrated in Fig. 8. As the varying dc field just completed one half cycle and switched to the negative direction, the permittivity started to increase slightly and then dropped before the AFE→FE transition. A possible ferroelectric interface between the Ti-containing layer and the PZ film might explain this phenomenon, however, earlier results on pure PZ films also showed some ferroelectric behavior at low fields. This effect will require further detailed study.

Fig. 9 demonstrates the dc bias-induced hysteresis behavior obtained in the antiferroelectric films. As expected, this film behaved like a linear capacitor when the alternating field (±24.6kV/mm) was below the AFE→FE transition field (~32.3kV/mm). When biased with a dc voltage at 16V (24.6kV/mm), the P-E hysteresis loop behaved like a normal ferroelectric material with two polarization states. This was originated from the hysteresis in the AFE↔FE phase transitions.

The films deposited on fused SiO_2 substrate were electroded with an interdigital pattern having a gap width of 10 μm. The birefringence curve shown in Fig. 10 again showed the ferroelectric behavior at small fields. The AFE→FE transition was accompanied by a steep increase in the birefringence. A detailed description of this transverse electrooptic behavior has been given elsewhere [13].

4. Summary

AFE $PbZrO_3$ films derived from acetate precursors were deposited on several substrates by an automatic dip coating process. The phase inhomogeneity observed in these films was attributed to the volatility of the Pb species formed during the precursor decomposition process. A thin TiO_2 layer was able to facilitate the formation of the perovskite $PbZrO_3$ and also inhibit the interactions between Pb and SiO_2 at the processing temperature. X-ray diffraction revealed the superstructure characteristic of the antiferroelectric phase in these films. The antiferroelectric properties, along with the dc bias behavior, were measured for $PbZrO_3$ films at room temperature.

References

1. E. Sawaguchi, G. Shirane and Y. Takagi, *J. Phys. Soc. Japan* **6** (1951) 333.
2. G. Shirane, E. Sawaguchi and Y. Takagi, *Phys. Rev.* **84** (1951) 476.
3. E. Sawaguchi, H. Maniwa and H. Hoshina, *Phys. Rev.* **83** (1951) 1078.
4. H. Fujishita, Y. Shiozaki, N. Achiwa and E. Sawaguchi, *J. Phys. Soc. Japan* **51** (1982) 3583.
5. L.N. Chapin and S.A. Myers, *Mater. Res. Soc. Symp. Proc.* **200** (1990) 153.
6. C.-C. Hsueh and M.L. Mecartney, *ibid*, p. 219.
7. A.H. Carim, B.A. Tuttle, D.H. Doughty and S.L. Martinez, *J. Am. Ceram, Soc.* **74** (1991) 1455.
8. K.D. Preston and G.H. Haertling, *Integrated Ferroelectrics* **1** (1992) 89.
9. S.L. Swartz, S.J. Bright, P.J. Melling and T.R. Shrout, *Ferroelectrics* **108** (1990) 71.
10. S. Hirano and K. Kato, *J. Non-Cryst. Solids* **100** (1988) 538.
11. B. Jaffe, *Proc. Inst. Radio Engrs.* **49** (1961) 1264.
12. K. Uchino and S. Nomura, *Ferroelectrics* **50** (1983) 191.
13. F. Wang, K.K. Li and G.H. Haertling, *Opt. Lett.* **17** (1992) 1122.
14. D. Berlincourt, H.H.A. Krueger and B. Jaffe, *J. Phys. Chem. Solids* **25** (1964) 659.
15. G. H. Haertling, *Ferroelectrics* **116**, 51 (1991).

16. K.K. Li, G.H. Haertling and W.-Y. Howng, *Integrated Ferroelectrics*. **3** (1992) to be published.

17. F. Wang, C.B. Juang, C. Bustamante and A.Y. Wu, in Proc. of the 4th Intern. SAMPE Electronic Conf., Albuquerque, New Mexico, June, 1990 (Soc. Advancement of Mater. & Process Engr., Covina, Calif.) p.712.

18. Y. Takahashi, Y. Matsuoka, K. Yamaguchi, M. Matsuki and K. Kobayashi, *J. Mater. Sci.* **25** (1990) 3960.

19. K.D. Budd, S.K. Dey and D.A. Payne, *Brit. Ceram. Proc.* **36** (1985) 107.

20. Y. Takahashi and K. Yamaguchi, *J. Mater. Sci.* **25** (1990) 3950.

21. B.A. Tuttle, private communication.

22. K.K. Li, G.H. Haertling and W.-Y. Hwong, presented at the Am. Ceram. Soc. 94th Ann. Meeting, Minneapolis, MN, April 1992. (Abstr.45-E-92)

Figure Captions

Fig. 1. XRD patterns of dried powder pyrolyzed at different temperatures. (#: Pb, ○: oxidized Pb, ∗: perovskite $PbZrO_3$.)

Fig. 2. TGA and DTA curves of dried $PbZrO_3$ powder heated in air at a rate of 10°C/min.

Fig. 3. SEM photograph of a 10-layer $PbZrO_3$ film deposited on a Pt/Ti-coated Si substrate.

Fig. 4. SEM photograph of a 10-layer $PbZrO_3$ film formed on a Pt/Ti-coated Si substrate with a thin TiO_2 pre-coat.

Fig. 5. A 1μm $PbZrO_3$ film formed on fused SiO_2 pre-coated with a TiO_2 layer.

Fig. 6. XRD pattern of the $PbZrO_3$ film shown in Fig. 5 and its super-structure peak characterizing the antiferroelectricity.

Fig. 7. A typical dielectric double hysteresis loop of $PbZrO_3$ film deposited on Pt/Ti-coated Si substrate with a TiO_2 layer.

Fig. 8. Variation of the $PbZrO_3$ film permittivity as a function of the dc bias.

Fig. 9. P-E hysteresis loop of a $PbZrO_3$ film with and without a dc bias when the alternating field is lower than the AFE→FE transition field.

Fig. 10. Birefringence shift, Δn, versus electric field, E, plot of an anti-ferroelectric $PbZrO_3$ film on fused SiO_2.

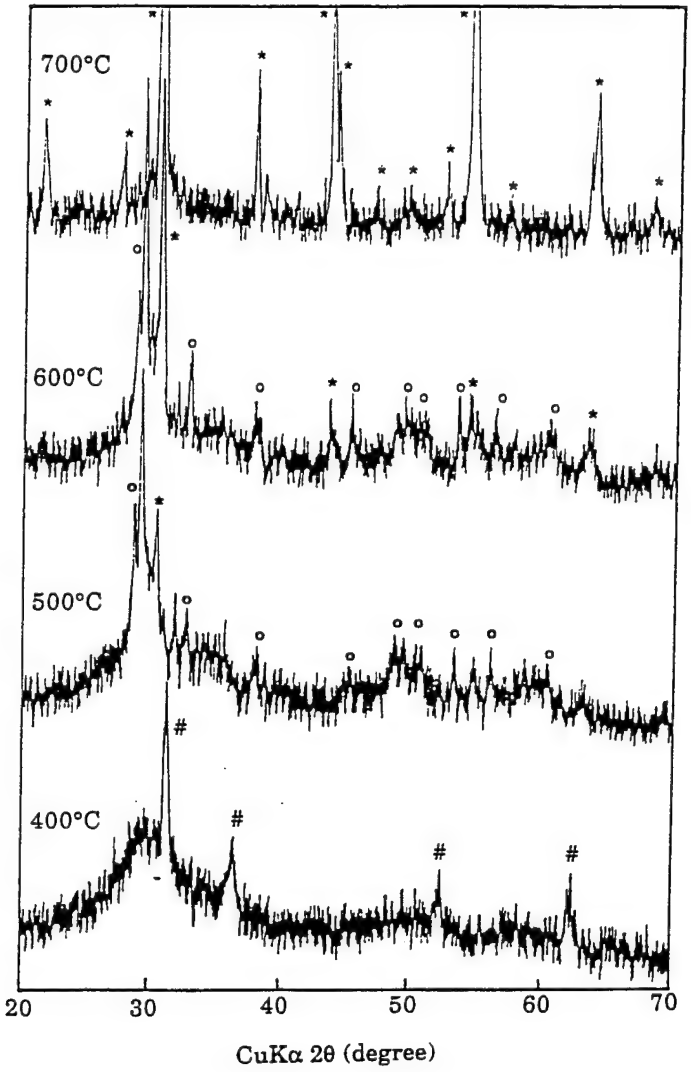

Fig. 1. XRD patterns of dried powder pyrolyzed at different temperatures. (#: Pb, ○: oxidized Pb, ∗: perovskite $PbZrO_3$.)

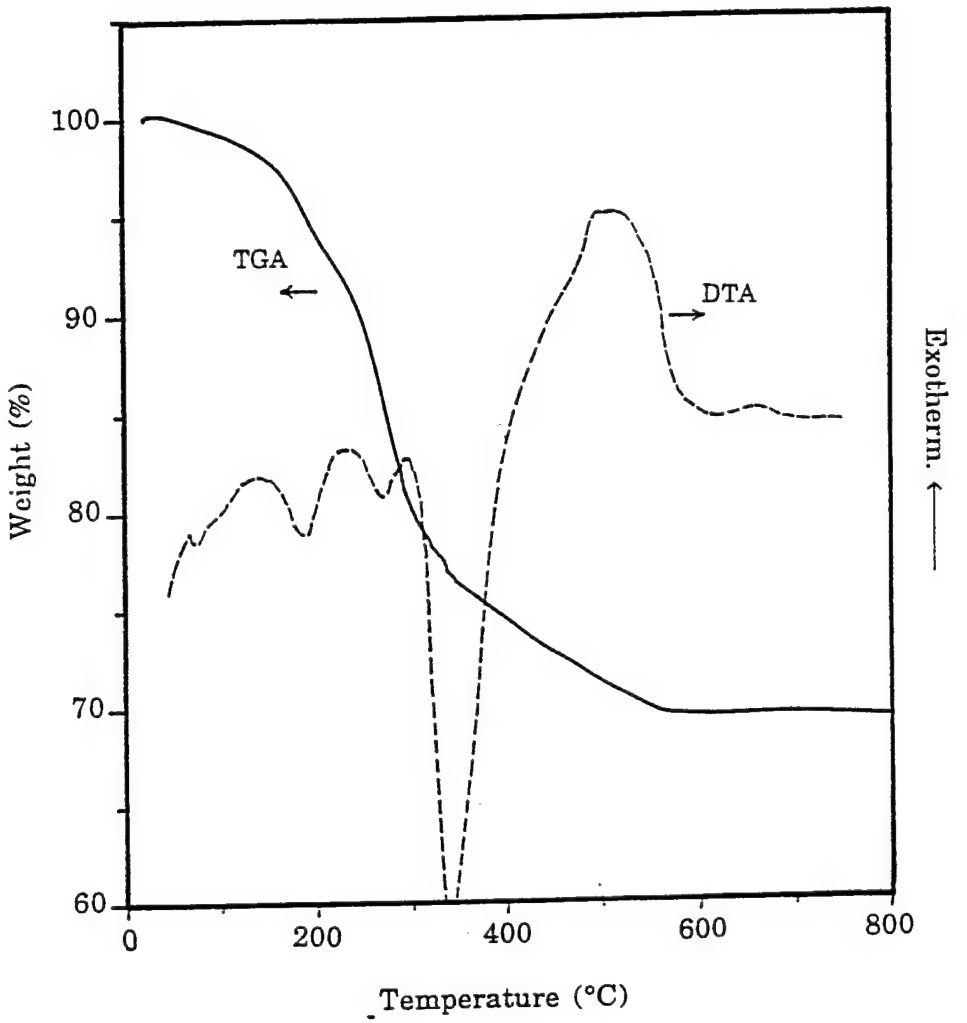

Fig. 2. TGA and DTA curves of dried $PbZrO_3$ powder heated in air at a rate of 10°C/min.

Figure 3. (K.K. Li, F. Wang and G.H. Haertling)

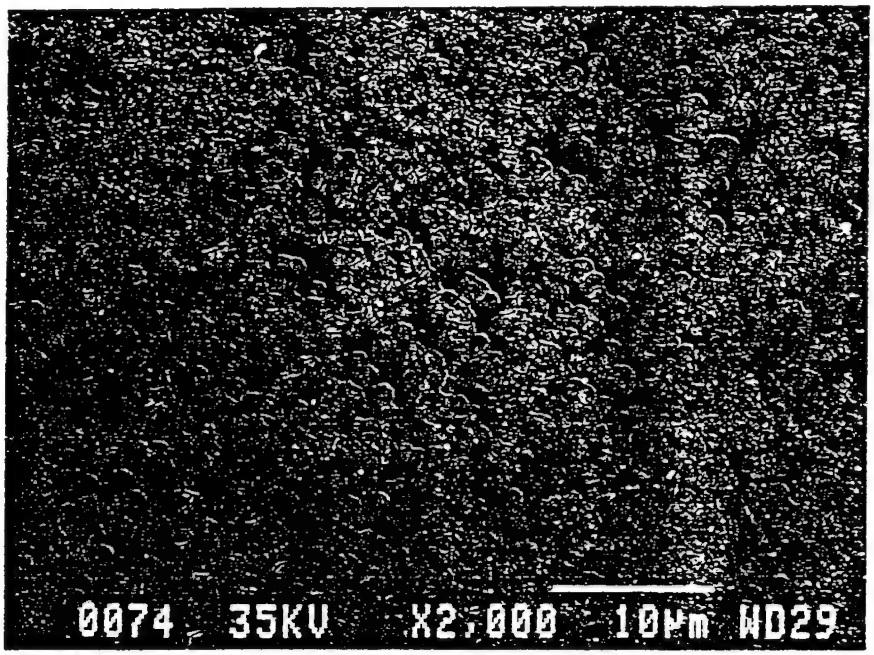

Fig. 3. SEM photograph of a 10-layer $PbZrO_3$ film deposited on a Pt/Ti-coated Si substrate.

Figure 4. (K.K. Li, F. Wang and G.H. Haertling)

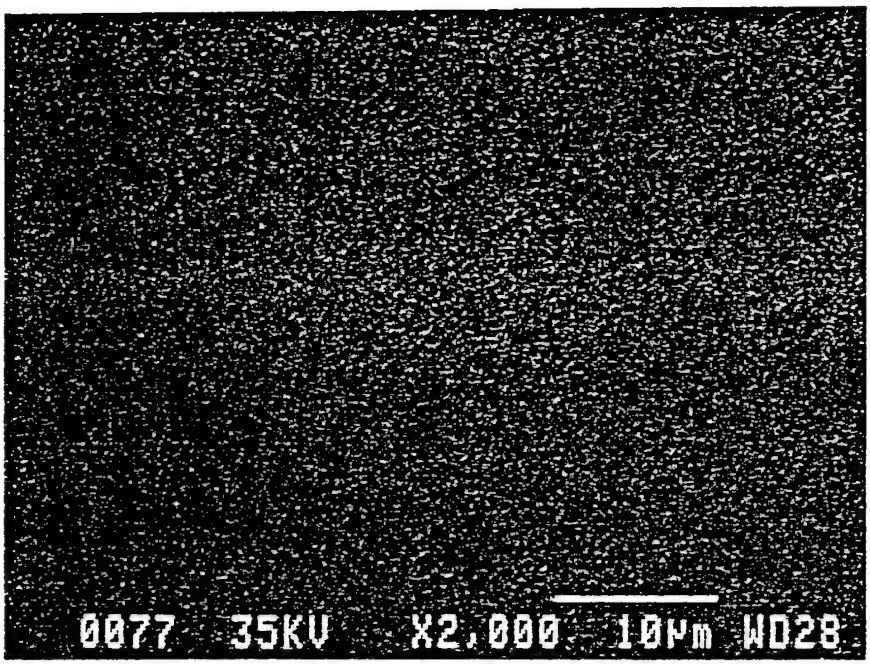

Fig. 4. SEM photograph of a 10-layer $PbZrO_3$ film formed on a Pt/Ti-coated Si substrate with a thin TiO_2 pre-coat.

Figure 5. (K.K. Li, F. Wang and G.H. Haertling)

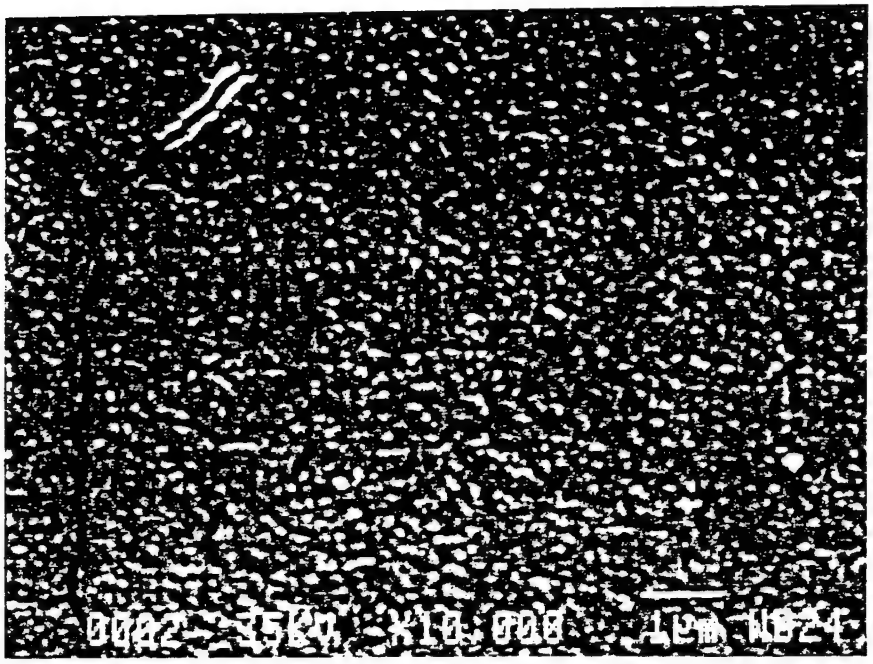

Fig. 5. A 1μm $PbZrO_3$ film formed on fused SiO_2 pre-coated with a TiO_2 layer.

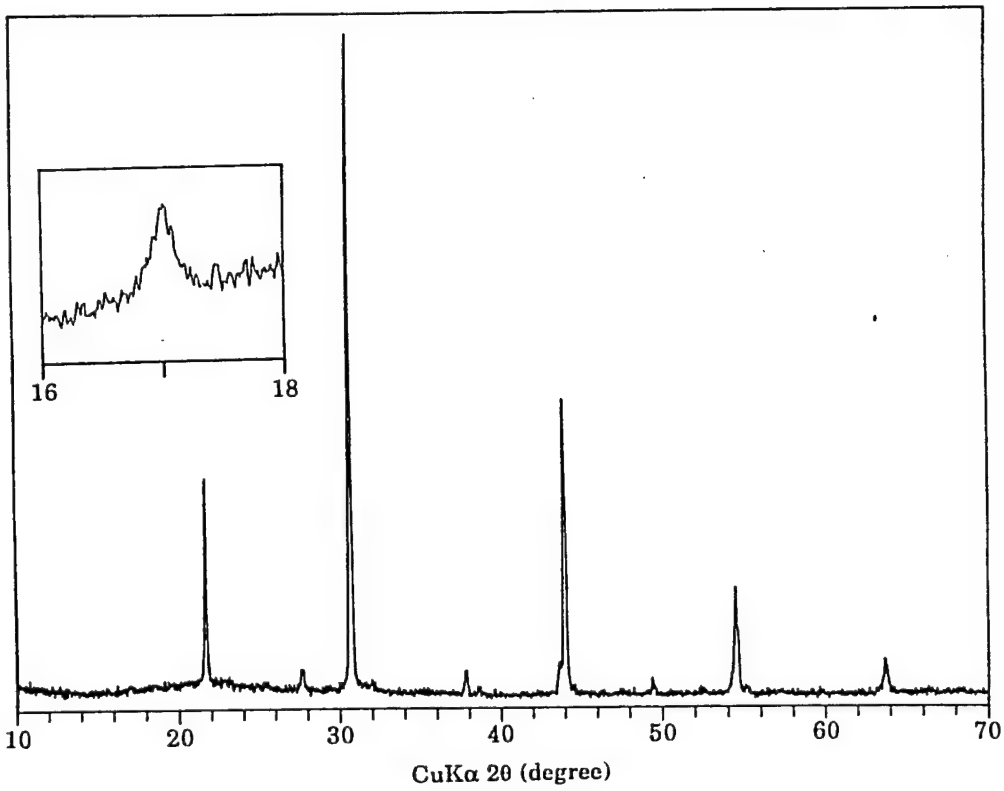

Fig. 6. XRD pattern of the $PbZrO_3$ film shown in Fig. 5 and its superstructure peak characterizing the antiferroelectricity.

Figure 7. (K.K. Li, F. Wang and G.H. Haertling)

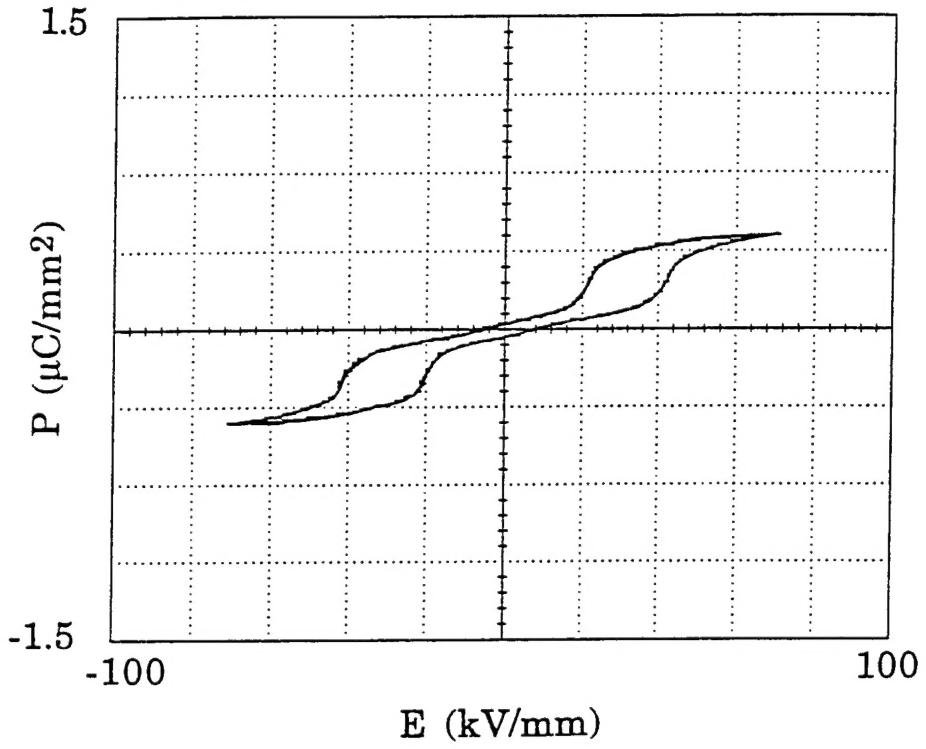

Fig. 7. A typical dielectric double hysteresis loop of $PbZrO_3$ film deposited on Pt/Ti-coated Si substrate with a TiO_2 layer.

Figure 8. (K.K. Li, F. Wang and G.H. Haertling)

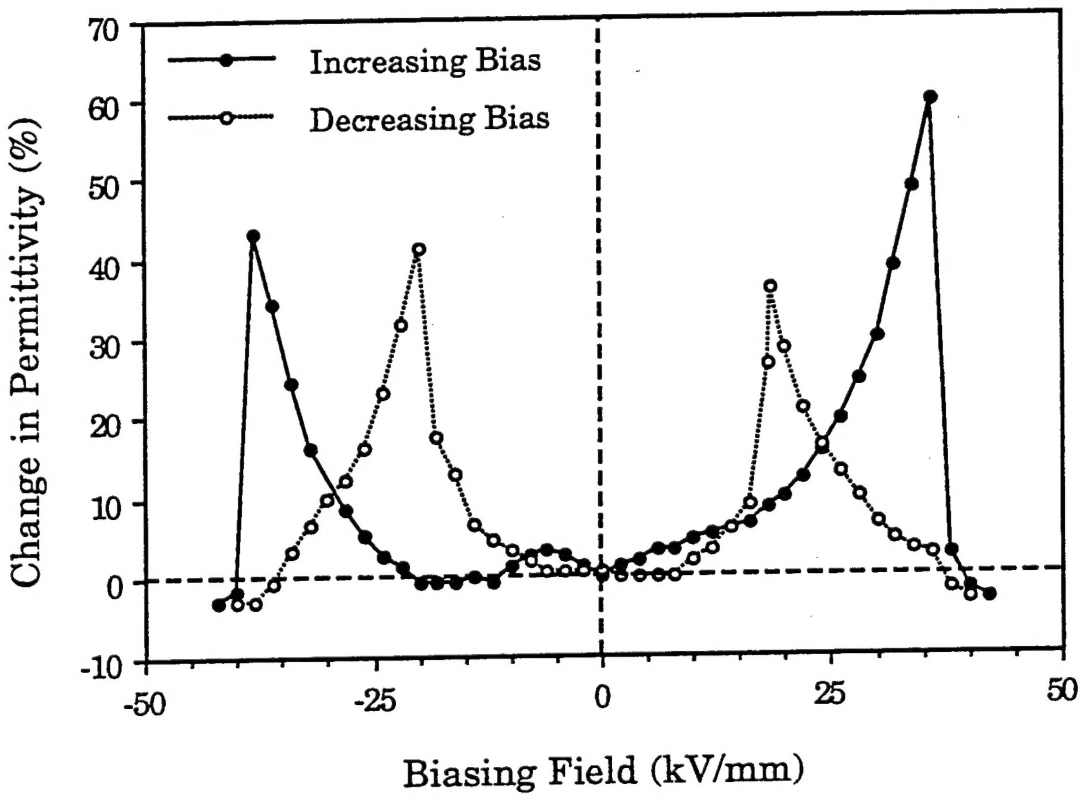

Fig. 8. Variation of the $PbZrO_3$ film permittivity as a function of the dc bias.

Figure 9. (K.K. Li, F. Wang and G.H. Haertling)

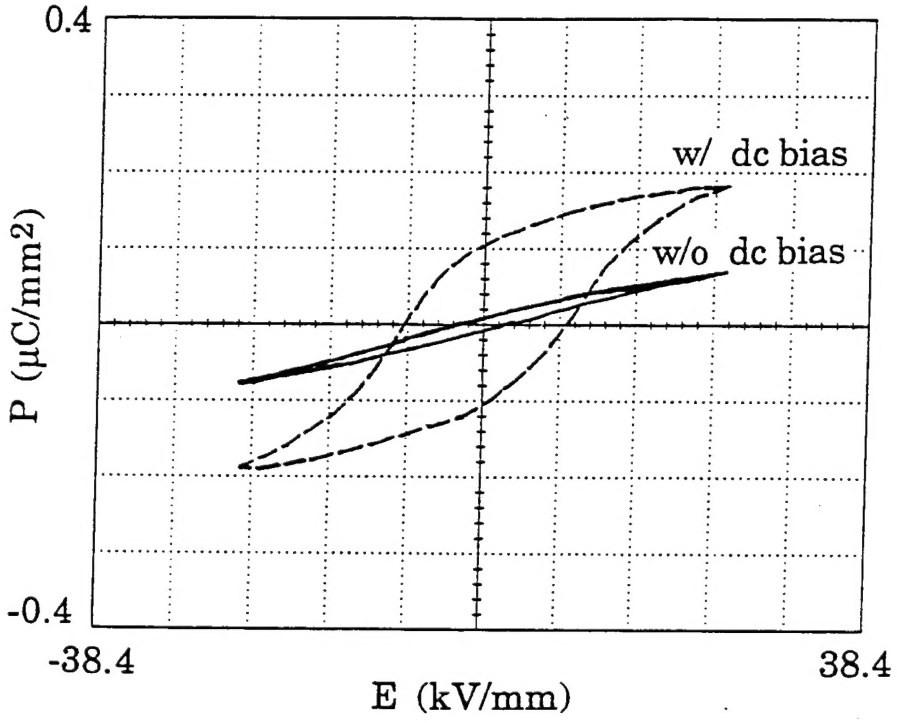

Fig. 9. P-E hysteresis loop of a $PbZrO_3$ film with and without a dc bias when the alternating field is lower than the AFE→FE transition field.

Figure 10. (K.K. Li, F. Wang and G.H. Haertling)

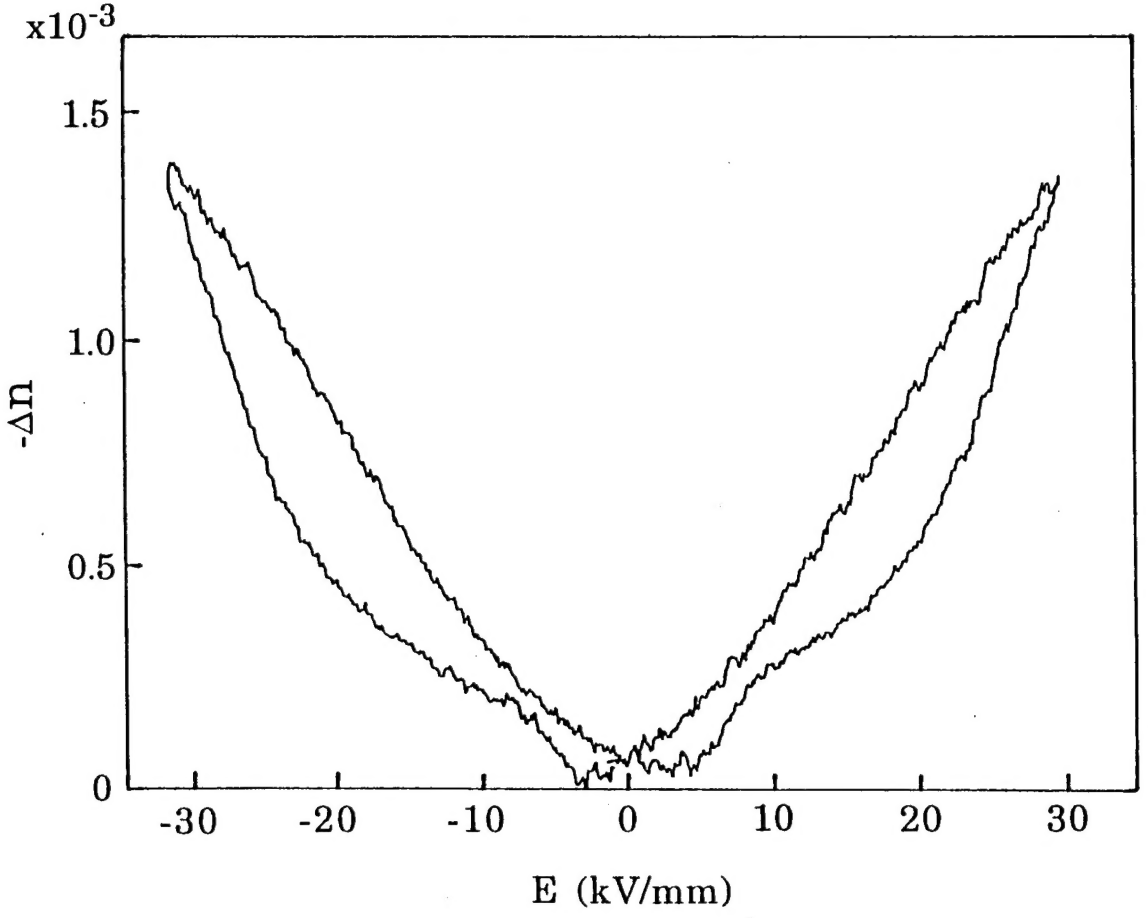

Fig. 10. Birefringence shift, Δn, versus electric field, E, plot of an anti-ferroelectric $PbZrO_3$ film on fused SiO_2.